DYNAMIC PERFORMANCE OF TRANSMISSION POLE STRUCTURES UNDER BLASTING INDUCED GROUND VIBRATION

by

Kaoshan Dai

A dissertation submitted to the faculty of
The University of North Carolina at Charlotte
in partial fulfillment of the requirements
for the degree of Doctoral of Philosophy in
Infrastructure and Environmental Systems

Charlotte

2009

Approved by:

_____
Dr. Shen-En Chen

_____
Dr. Brian Anderson

_____
Dr. David Boyajian

_____
Dr. Qiuming Wei

_____
Dr. Kingshuk Bose

DISCLAIMER OF LIABILITY

With respect to the current document, neither Southern Company, Duke Energy, Sauls Seismic, Inc. nor University of North Carolina at Charlotte nor any of their employees, makes any warranty, express or implied, including the warranties of fitness for a particular purpose, or assumes any legal liability or responsibility for the accuracy, completeness, or usefulness of any information or process disclosed, or represents that its use would not infringe privately owned rights. The research findings in the current document should not be used as a design or analysis standards and should not be used as legal evidence in court.

ABSTRACT

KAOSHAN DAI. Dynamic performance of transmission pole structures under blasting induced ground vibration. (Under the direction of DR. SHEN-EN CHEN)

Structural integrity of electric transmission poles is crucial for the reliability of power delivery. In some areas where blasting is used for mining or construction, these structures are endangered if they are located close to blasting sites.

Through field study, numerical simulation and theoretical analysis, this research investigates blast induced ground vibration and its effects on structural performance of the transmission poles. It mainly involves: (1) Blast induced ground motion characterization; (2) Determination of modal behavior of transmission poles; (3) Investigation of dynamic responses of transmission poles under blast induced ground excitations; (4) Establishment of a reasonable blast limit for pole structures; and (5) Development of heath monitoring strategies for the electric transmission structures.

The main technical contributions of this research include: (1) developed site specific spectra of blast induced ground vibration based on field measurement data; (2) studied modal behavior of pole structures systematically; (3) proposed simplified but relatively accurate finite element (FE) models that consider the structure-cable coupling; (4) obtained dynamic responses of transmission pole structures under blast caused ground vibration both by spectrum and time-history analysis; (5) established 2 in/s PPV blast limit for transmission pole structures; (6) developed two NDT techniques for quality control of direct embedment foundations; and (7) described an idea of vibration-based health monitoring strategy for electric transmission structures schematically.

ACKNOWLEDGMENTS

The author first would like to acknowledge Dr. Shen-En Chen for his supervision since the beginning of the author's study at the University of North Carolina at Charlotte (UNC Charlotte). Appreciation also goes out to Dr. Brian Anderson, Dr. David Boyajian, Dr. Qiuming Wei and Dr. Kingshuk Bose for sitting on my doctoral committee.

It has been the author's honor to learn from many knowledgeable faculty members and to work with diligent students here at the Department of Civil & Environmental Engineering (CEE), UNC Charlotte. Thanks are owed to the Infrastructure and Environmental Systems (INES) Ph.D. program and CEE Department for the financial support throughout the author's study. Special thanks are given to Dr. David Young, Director of the INES program and Chair of CEE Department, and Dr. Hilary Inyang, Duke Energy Distinguished Professor and Director of the Global Institute for Energy and Environmental Systems, for their guidance and help from the first day the author came to UNC Charlotte. The author also recognizes the contributions of his peers, Eric Conner, Wen-ya Qi, Antoaneta Koleva and Wanqiu Liu for their involvement in the author's research. The author would like to acknowledge the financial and technical supports from Southern Company, Sauls Seismic, Inc., and Duke Energy. Colby Galloway and Luke Stafford of Alabama Power, Eddie Sheffield of Georgia Power, Charles Munden and Dennis Mize of Southern Company Transmission System Design Committee, Bill Kitchens of the Alabama Department of Surface Mines, Mac Sauls and Randall Franklin of Sauls Seismic, Inc., Jeff Erdle of Duke Energy are specially thanked. Additionally, this acknowledgement would not be complete without thanks to friends and family. Their continuous support, encouragement, and love have been greatly appreciated.

TABLE OF CONTENTS

LIST OF TABLES

LIST OF FIGURES

LIST SYMBOLS

W:	charge weight per delay
R:	distance from blast to structure
ρ:	rock density
$\dot{u}$:	peak particle velocity
SD:	scaled distance
D:	energy released from the explosion
V:	the volume of the chamber
Q:	the TNT charge weight
f_s:	fundamental frequency for the guyed tower
f_b:	fundamental bending frequency of the mast
$x(n)$:	original signal
$y(n)$:	filtered signal
$h(n)$:	filter function
$H(\omega)$:	transfer function
Δt:	time step
f_d:	lower cut-off frequency
f_u:	upper cut-off frequency
Δf:	frequency interval
m:	mass of SDOF
c:	damping of SDOF
k:	stiffness of SDOF
$x(t)$:	displacement time history

$\dot{x}(t)$: velocity time history

$\ddot{x}(t)$: acceleration time history

ξ: damping ratio

ω: circular frequency

$S_d(\omega)$: displacement spectrum

$S_v(\omega)$: velocity spectrum

$S_a(\omega)$: acceleration spectrum

E_c: concrete modulus of elasticity

f_c': concrete compressive strength

w_c: concrete density

[K]: stiffness matrix of the entire system

$[\mathrm{K_p}]$: pole structure stiffness matrix

$[\mathrm{K_s}]$: soil spring stiffness matrix

{R}: boundary reaction

{φ}: mode shape vector

$\mathrm{k_h^s}$: spring constant for translational springs

$\mathrm{k_\theta^s}$: spring constant for rotational springs

$\mathrm{E_S}$: modulus of elasticity of the backfill-material/soil

$\mathrm{H_B}$: buried depth

$\mathrm{D_B}$: average diameter of the buried portion of the pole

$[M]$: mass matrices of the coupled system

$[K]$: stiffness matrices of the coupled system

Δm: additional mass

$\emptyset$:	phase difference
f:	frequency
V_s:	surface wave velocity
L:	distance between the two geophones in SASW testing
λ:	wavelength
$\overline{V_s}$:	mean shear wave velocity
d_i:	thickness of each layer of soil
V_{si}:	shear wave velocity for each soil layer
l:	horizontal distance between two poles
q:	conductor mass of a unit length
l_0:	limit span
$\lvert\{x(t)\}\rvert_{max}$:	maximum displacement response
$\{\Phi\}_r$:	mode shape of the *r*th mode
$(S_d)_r$:	spectral displacement for the *r*th mode
Γ_r:	participation factor
R_{max}:	maximum value of a particular response
R_r:	peak value of a particular response for the *r*th mode
p:	number of the modes involved in the mode combination
R_s:	peak value of a particular response for the *s*th mode
η:	ratio of circular frequencies between *s*th mode and *r*th mode
$[C]$:	structural damping matrix
$\{F\}$:	excitation vector
M_{cr}:	cracking moment

f_r:	modulus of rupture of concrete
I_g:	gross moment of inertia of the pole section
A_g:	gross area of the cross section
P:	prestress force
A:	cross-sectional area
I:	moment of inertia of the cross section
M_c:	bending moment
F_y:	yield stress
w:	flat width of a side
t:	wall thickness
f_c':	compressive strength of concrete
f_{ct}:	tensile strength of concrete
f_{ct}:	modulus of rupture of concrete
F_t:	tensile stress permitted
F_a:	compressive stress permitted
F_v:	shear stress permitted
σ_x:	stress in *x* direction
σ_y:	stress in *y* direction
σ_z:	stress in *z* direction
$\sigma_{combined}$:	stress in combination

LIST OF ACRONYMS

PPA:	peak particle acceleration
PPV:	peak particle velocity
PPS:	peak particle displacement
FE:	Finite Element
PF:	principal frequency
PGA:	peak ground acceleration
FIR:	finite impulse response
FRF:	frequency response function
SASW:	spectral analysis of surface waves
SSI:	soil structure interaction
SRSS:	square-root-of-the-sum-of-the-square
CQC:	complete-quadratic-combination
NDT:	nondestructive testing
MT:	modal testing
FRF:	frequency response function
MAC:	modal assurance criterion
MSHA:	Mining Safety and Health Administration

CHAPTER 1: INTRODUCTION

1.1 Problem outline and motivation

Electric transmission structures are unique civil structures used to support conductors and shield wires of a transmission line. They are either lattice type or pole type structures. Transmission poles can be wood, steel or concrete. Prestressed concrete pole and tubular steel pole structures are commonly used in the power industry mainly due to their construction efficiency.

In areas where blasting is used for mining or construction, these transmission structures are endangered if they are located too close to the blasting operation sites (Figure 1.1). Structural integrity of these poles is critical to the reliability of power supply. Common practice in the power industry is to limit ground motion by specifying maximum peak particle velocity. So far, there is a lack of industry-wide recognized guidelines on how the blast limits should be set for the transmission pole structures. Some empirical criteria employed by power company engineers or blasting consultants are borrowed from the observation results of residential structure damages and human annoyance (i.e. blast peak particle velocity not exceeding 2 in/s). While these limits may yield prudent protection for these low-rise houses, whether they are the reasonable option for these non-residential structures is a question.

With increased requests for possible relaxation of current blast limits near electric transmission structures in order to cut costs and increase coal mining production, a research project was conducted to study the dynamic responses of these structures under blasting effects.

In this research phase, the focus is placed on transmission pole type structures. Through field monitoring and numerical simulation, this research attempts to address the following questions:

(1) What are the characteristics of blast induced ground vibration?

(2) What are the dynamic behaviors of typical transmission pole structures?

(3) What are structural responses of the transmission poles under blast induced ground excitations?

(4) What are necessary recommendations for setting a blast limit?

(5) What are possible health monitoring strategies for protecting transmission structures during severe loading?

The answers to these questions become the basis leading to a comprehensive blast design guideline for transmission structures. They benefit both mining and power industries.

1.2 Objectives and scope

Through field study, numerical simulation and theoretical analysis, this study is mainly to investigate medium to high frequency blast induced ground vibration and its effects on structural integrity of the transmission poles (Figure 1.1). The author also intends to provide readers with some information regarding possible protection strategies

for power transmission structures by exploring relevant health monitoring techniques. The specific objectives to be accomplished in this study include:

(1) Characterize blast induced ground vibration at specific sites.

(2) Determine modal behavior of typical transmission pole structures.

(3) Obtain dynamic responses of transmission poles under blast induced ground motions.

(4) Investigate structural integrity of transmission pole structures under different blasting levels.

(5) Propose blast limit recommendations for transmission structures.

(6) Explore health monitoring strategies relevant to transmission line protection.

Working towards these objectives, several tasks were performed, which include: blast monitoring in two coal mines and one rock quarry, full-scale modal testing on four prestressed concrete poles and two tubular steel poles, and a systematic numerical computation of pole dynamic responses using the finite element (FE) method. The detailed scope of work is shown in the following:

(1) Literature review

Existing codes and guidelines for transmission structures were first reviewed, which then was extended to review of publications of dynamic studies of various types of transmission structures. It was believed that such a detailed state-of-the-art literature review would give more insights toward the proposed topic.

(2) Blast-induced ground motion characterization

A comprehensive field monitoring work was conducted at three mining sites. Blast induced ground vibration was measured both by traditional seismographs and by innovative wireless triaxial sensing units. Characteristics of blast induced ground motions

were obtained by analyzing the records both in time and frequency domains. Vibration parameters, like peak particle velocity (PPV), were further quantified through data mining. Based on statistical analysis, spectra of blast caused local ground motions were generated for FE analysis.

(3) Determination of modal behaviors of transmission pole structures

Modal behavior of transmission poles, including eigenvalues and eigenvectors, represents dynamic characteristics of this unique type of structure. The free vibration results can be used to ensure the validity of FE models of transmission poles. Natural frequencies and mode shapes of structural vibration are also essential information for seismic analysis. Modal characteristics of the transmission poles were obtained by impact excitation modal tests combined with FE modal analysis. Simple but relatively accurate FE models for transmission pole structures were then derived based on modal results.

(4) Investigation of dynamic responses of transmission poles under blast induced ground vibration

Both time-history and response spectrum analyses were conducted on valid FE models with blasting induced ground motions as input excitations. The target ground vibration spectra were established from blast monitoring records; while ground vibration time-history data included both direct measurements and artificially modified acceleration time histories. Structural responses of the poles, in the form of deformations, reactions, and stress states, were obtained through FE analysis.

(5) Structural integrity analysis of the transmission poles under blasting effects

Designs of transmission pole structures are based on corresponding codes and guidelines. These design requirements are compared with structural response results from

dynamic analysis. A reasonable blast limit was established based on structural performance analysis. This criterion is the basis of a comprehensive blast design plan, which should also include other recommendations such as those of dealing with flying rock issues, which was discussed in a previous study (Conner 2007).

(6) Development of health monitoring strategies for the electric transmission structures

Pilot work aiming at developing structural inspection as well as health monitoring strategies for the transmission structures was performed. State-of-the-art nondestructive technologies as well as health monitoring strategies were explored. Multi-discipline knowledge that is relevant to power transmission structure reliability, including monitoring scheme design, sensing technology, etc. is summarized.

1.3 Research significance and original contributions

This research was anticipated to provide a comprehensive integrity evaluation for both prestressed concrete poles and tubular steel pole structures under blast induced ground vibration. It represents the first open publication of study on the blasting effects on electric transmission structures. The blast limit derived from this research can provide a reference for both mining industry and power industry engineers for the design of a reasonable blast plan or establishing blast restriction criteria. The knowledge learned through this study is also a valuable supplement for the future design of transmission poles.

The original contributions of the dissertation as follows:

(1) An innovative ground vibration measurement technique was implemented in field monitoring work. Triaxial wireless sensing units were used to record blast induced

ground movements. Acceleration time histories of ground vibration were directly obtained using this technology. The remote sensing feature of the wireless accelerometers meets the safety requirements of blast monitoring.

(2) Site specific spectra of blast induced ground vibration were developed based on field measured data. Empirical relations were established between peak particle acceleration (PPA), peak particle velocity (PPV), and peak particle displacement (PPS). Response spectrum amplification factors were obtained through data analysis. Response spectra based on different levels of PPV criteria can be used as the input ground excitations in numerical response spectrum analysis.

(3) Modal behavior of transmission pole structures was systematically studied. Full-scale impact modal tests were performed on both prestressed concrete poles and tubular steel poles. FE modeling of transmission pole structures was optimized based on free vibration behaviors of these poles. Simple but relatively accurate FE models that take structure-cable coupling issue into account were proposed.

(4) Dynamic responses of transmission pole structures under blast induced ground vibration were obtained both by spectrum analysis and by time-history analysis. These analytical works yielded structural responses of both concrete and steel poles under blast induced ground motions. The study provides engineers valuable information for pole structure design under dynamic loading beyond wind load considerations.

(5) Although based on site specific blast records, a reasonable blast limit for transmission pole structures was established. Following the methodology presented in this study, practical blast criteria can be easily established with blast data and structural

information. It can be easily extended when more experimental results are available. A comprehensive blast design plan for the transmission structure can be developed with additional considerations besides the blast limit established in this research.

(6) An in-depth review regarding transmission line inspection as well as structural health monitoring techniques was performed. This study explored state-of-the-art multi-discipline knowledge relevant to power transmission structure reliability, including monitoring schematic design, nondestructive techniques, sensing technology, etc. A conceptual health monitoring strategy was proposed. This is a pilot work that is expected to lead to a health monitoring system specifically for the power transmission line.

1.4 Organization of the dissertation

Figure 1.2 shows the outline of the dissertation organization, which is presented in eight key chapters.

In Chapter 2, an in-depth literature review is presented. Existing codes and guidelines for transmission structures, as well as publications of dynamic loads effects on various types of transmission structures are reviewed.

In Chapter 3, blast field monitoring and resultant records are introduced. The instrumentation and experimental procedures are described in detail. Through data analysis, blasting induced ground vibrations are characterized. Response spectra used for FE analysis are developed from blast records.

In Chapter 4, results of modal behavior of transmission poles obtained from physical modal testing and numerical analysis are presented. FE modeling of the transmission line system considering cable coupling issues is discussed. Simplified FE models for

transmission pole structures are derived based on studying on free dynamic vibration behaviors of these poles.

In Chapter 5, spectral analysis of transmission poles is presented. Both the FE models used in the analysis and spectra developed for different levels of PPV are explained. Structural responses of pole structures at different levels of ground movements are obtained.

In Chapter 6, time history analysis results of the transmission poles are shown. Original records and modified acceleration time histories are used as ground excitations in the FE analysis. Dynamic responses of the pole structures at corresponding levels of ground excitations are derived.

In Chapter 7, comparisons are made between the pole design requirements and the structural dynamic behaviors obtained from the spectrum and time history analyses. Structural integrity of pole structures under various blasting levels is examined. A reasonable blast limit is proposed based on the study.

In Chapter 8, in-depth reviews related to transmission line inspection as well as structural health monitoring techniques are performed. A conceptual health monitoring strategy is developed.

In Chapter 9, research results are summarized. Important findings as well as conclusions are presented. Discussions and recommendations extended from the current study are also given in this chapter.

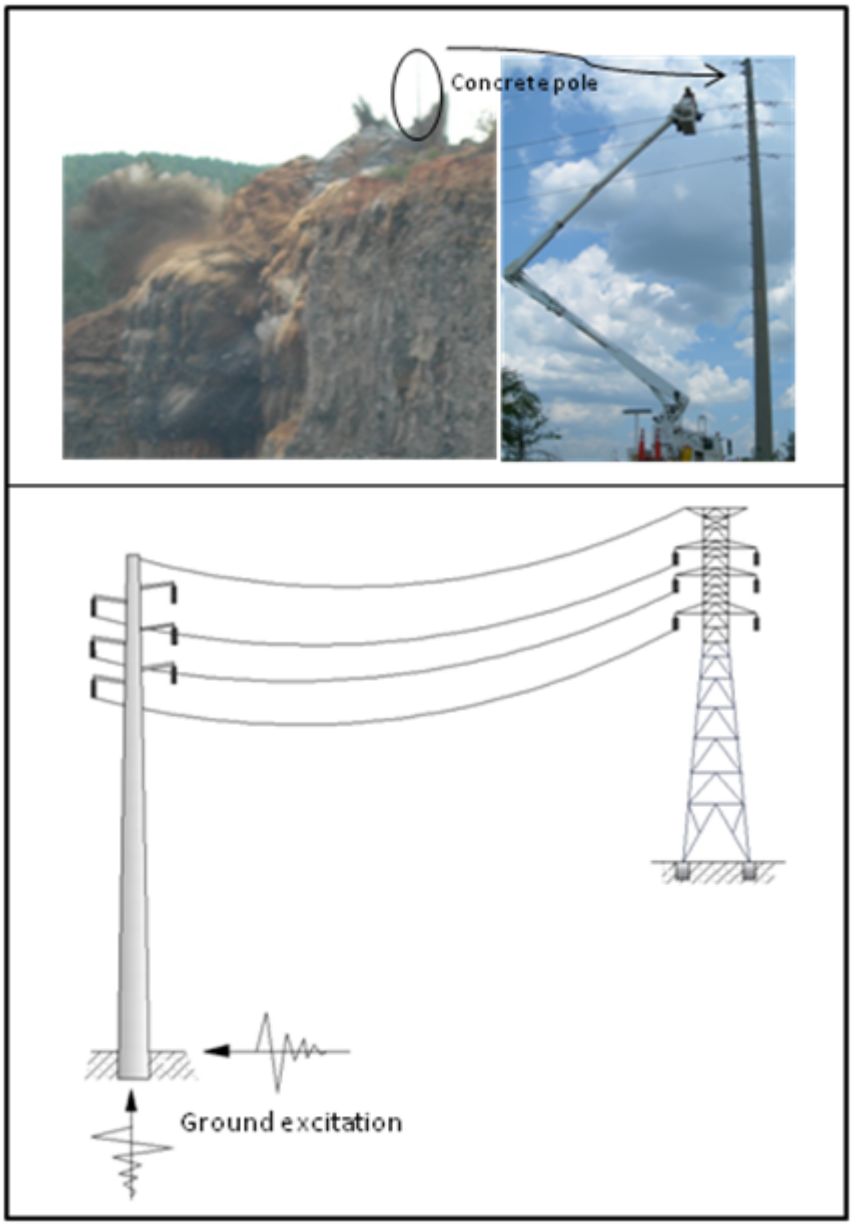

Figure 1.1: Blast effects on transmission structures

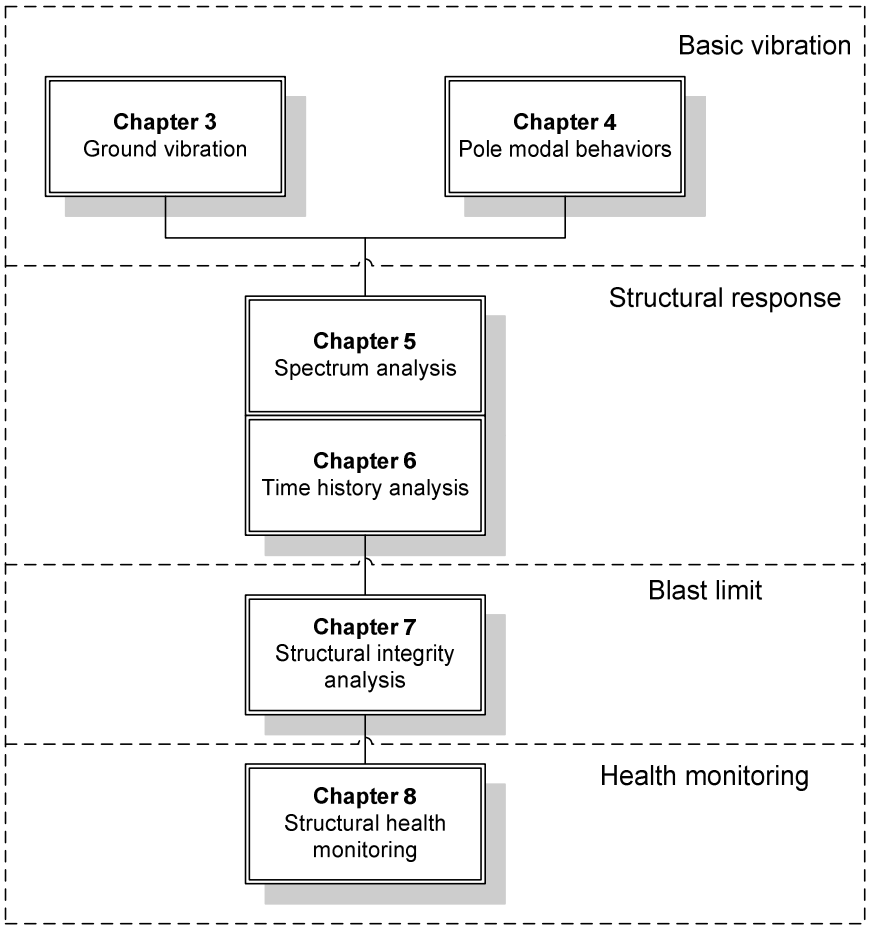

Figure 1.2: Organization of the text

CHAPTER 2: LITERATURE REVIEW

2.1 Transmission structure design

Design of transmission structures is primarily based on codes and guidelines (ANSI 1979; ANSI/ASCE 1991; ASCE 1987; ASCE 1990; ASCE 1991; ASCE/PCI 1997; ASCE/SEI 2006; Fang et al. 1999; IEEE 1991; RUS 2005; Southern Company 1992; Southern Company 2006). Prevailing practices use reliability-based procedures by analyzing the transmission line for weight, wind/ice loading, and effects either due to conductors/insulators breaking or due to collapse of an adjacent structure. This dissertation focuses on two specific transmission structure types: prestressed spun-cast concrete poles (Figure 2.1) and tubular steel poles (Figure 2.2).

Prestressed spun-cast concrete poles are extensively used as support structures in power transmission and distribution lines in the southeastern United States. They are fabricated by centrifugal casting method. The design of prestressed concrete poles is a complex process that mainly involves considerations of the ultimate flexural strength, cracking strength, shear and torsion capacities, and pole deflection. Buckling of a concrete pole is unusual under normal circumstances (ASCE/PCI 1997). Besides normal design procedures, Kocer and Arora (1996) formulated and solved prestressed concrete transmission pole design as an optimization problem, which provided more economical designs.

Tubular steel poles can be self-supporting or guyed structures. Design of steel pole is also based on the ultimate strength method using factored design loads. General stability and local buckling are the main design concerns for the pole subjected to compressive forces. Tension, shear, bending and combined stresses caused by all types of loads should not be beyond specified allowable values (ASCE/SEI 2006).

Typically, transmission structures are not designed for ground vibration because loading influences caused by wind/ice combinations and broken wires usually exceed earthquake effects (ASCE 1991). However, this may change as a result of the increasing demands on wider transmission line spans – which increase the criticality of the overall stability of a single structure (Ghobarah et al. 1996; Li et al. 2005). To date, effects on transmission systems due to ground-induced vibrations, such as blasting, have not been addressed by the design codes or guidelines.

2.2 Blasting induced ground vibration

2.2.1 Characteristics of blast induced ground motions

Explosion-generated ground motions can be described by three perpendicular components: longitudinal, vertical and transverse (Figure 2.3). The longitudinal vibration is usually oriented along the explosion radius while the other two components are vertical and transverse to the radial direction. Generally, blasting induced ground motion is measured in particle vibration time history. The important vibration parameters are peak amplitude, principal frequency and duration. Peak particle velocity (PPV) and principal frequency (PF) are the most commonly used parameters to describe a typical blasting record. PPV was found to be well correlated with structural damages (Duvall and Fogelson 1962; Nicholls et al. 1971; Wiss 1968). Ground vibration caused by blast loads

is different from earthquakes with its characteristics of higher frequencies and shorter durations (Dowding 1985; Siskind et al. 1980).

Ground vibration characteristics usually depend on parameters such as transmission medium and distance, dynamite charge weight and other blast design considerations (Conner et al. 2007). Project-specific attenuation relations for ground motion are geology-sensitive (Dowding 1985). Site investigation is a fundamental work for determination of ground motion characteristics under blasting practices. There are three main types of waves generated by explosions: compressive, shear, and surface waves. Shear and surface waves travel slower than the compressive wave. However, most blasting is detonated as a series of explosions, which greatly complicates wave-type identification (Dowding 1985).

Blasting induced ground motions are usually recorded using geophones in terms of particle velocity, which is believed to be the best single ground motion descriptor (Siskind et al. 1980). It is related to displacement and acceleration by integration and differentiation. The recorded ground motion data are valuable for statistical analysis of ground vibration characteristics in terms of response spectra, which are necessary for structural spectrum analysis. For critical structures, a step-by-step time history analysis is preferred. The accelerogram data can be used as direct external excitation inputs in structural time history analysis.

Different methodologies have been utilized to predict blasting induced ground motions. Empirical expressions based on the collection of blast data are most commonly found in publications:

Dowing (1985) in his book gives equations to predict displacement, particle velocity and acceleration based on cube root scaling relationships derived from field measurements. Assuming that charge weight per delay is W; distance from blast to structure is R; rock density is ρ; then peak particle velocity is:

$$\dot{u} = 0.72\left(\frac{100}{R}\right)^{1.46}\left(\frac{W}{10}\right)^{0.48}\left(\frac{4.66}{\rho}\right)^{0.48} \quad (2.1)$$

Herrell (1996) collected 4,700 data points and plotted the relation between peak particle velocity and scaled distance. Typical design envelope line proposed to predict maximum particle velocity is as the following:

$$PPV = 10.245 * SD^{-0.5682} \quad (2.2)$$

where PPV is peak particle velocity; and SD is scaled distance and is derived from distance from the explosion D, and energy released from the explosion W by $SD = (D/W)^m$.

Herrell (1996) pointed out that the data used to establish this relation may only be accurate at this specific geologic site where the study was conducted.

By designed explosion experimentation, Hao et al. (2001) investigated the rock joint effects on blast stress wave propagation. Ground accelerations on rock surface were measured and analyzed. The authors gave the attenuation equations both for peak ground acceleration (PGA) and for peak particle velocities (PPV). The following is the best fitted function of PPV paralleling with the rock joint orientation:

$$PPV = 442.48 * \left(\frac{R}{\frac{1}{W^3}}\right)^{-1.359} \quad (2.3)$$

in which R is distance between the shot and the measurement and W is charge per delay.

Kahriman (2004) proposed an empirical relationship between peak particle velocity and scale distance through statistical evaluation of 73 blast events at a limestone quarry located in Istanbul, Turkey. The equation with 95% confidence level is given below:

$$PPV = 340 * \left(\frac{R}{\sqrt{W}}\right)^{-1.79} \quad (2.4)$$

where R is distance between the shot and the station (m) and W is charge per delay (kg).

Considering that Fourier analysis cannot provide time durations of blast waves, Aldas (2005) used Stockwell transform to study time duration of blasts besides the amplitude versus frequency shown in Fourier spectra. The purpose of this study was to help determine delay intervals in a blast design. The research results were drawn from actual field measurements.

Ground vibration time history has been successfully generated through FEM simulation. Wu and Hao (2005) realized that limited studies were devoted to discuss differences of blast motions on ground surface and in free field. They used a validated numerical model to simulate motions on ground surface and in free field caused by explosions. Attenuation formulas for PPV, PPA, and PF were obtained. The averaged empirical attenuation relations for surface ground vibration was proposed as:

$$PPV = 2.981 f_1 \left(\frac{R}{Q^{1/3}}\right)^{-1.3375} \quad (2.5)$$

in which

$$f_1 = 0.121 \left(\frac{Q}{V}\right)^{0.2872} \quad (2.6)$$

$$\mathrm{PF} = 198 \mathrm{h}_1 \left(\frac{\mathrm{R}}{\mathrm{Q}^{1/3}}\right)^{-0.6620} \quad (2.7)$$

and

$$h_1 = 3.497\left(\frac{Q}{V}\right)^{-0.1768} \quad (2.8)$$

where R is the distance in meters measured from charge center, V is the volume of the chamber in cubic meter and Q is the TNT charge weight in kilograms.

Toraňo et al. (2006) developed a FEM model to predict ground vibrations due to blasting. All the factors that are known to have influence on vibrations were introduced in the model. Randomness factor was also introduced.

The neural network approach was proposed by Khandewal and Singh (2005) in blasting study, which through training datasets, can predict ground vibration with various influencing parameters including rock mass, explosive characteristic and blast design.

From the review of previous work, it can be found that, to date, empirical relations obtained from blast measurements are still the dominant approach to predict blast induced ground vibration.

2.2.2 Blast effects on structural integrity

Explosions can generate high air pressure as well as strong ground vibration. Hao et al. (2002) employed the numerical simulation method to study two-storey reinforced concrete frames with or without infill masonry. Damage indicators were put forward to define structural damages. It was concluded that infill masonry affected both the damage level and the damage pattern of the frames. In this research, ground motion induced by underground explosion was generated by numerical simulation. Through comparison of spectra between seismic motions and blast induced ground motions, the authors showed in the paper that the energy of blast caused ground vibration was distributed along a wide frequency band. The paper also indicated that structures might not respond primarily at their global modes due to high frequency features in blasting induced ground vibration.

Distributed concrete damage induced by high-frequency responses is also reported by Ma et al. (2002). Their research indicated that current design codes based on ground motion peak particle velocity alone is conservative. In the research, Ma et al. (2002) employed a commercial software AUTODYN to study two-story concrete frames under explosion induced ground motions and gave the conclusion that damage assessment at the material level could obtain local failure of components while common earthquake engineering methods based on story drift could not effectively describe structural damages caused by high-mode vibration.

A lab test was conducted by Lu et al. (2002a) to study structural responses of scaled reinforced concrete frame models under ground shock generated by an electromagnetic shaker. The experimental results indicated that, at high frequency blast loading, local-mode response was significant and this prompts the need to investigate material level damages rather than the overall displacements. Lu et al. (2002b) summarized both numerical study and laboratory testing results of the concrete frame structure. Again the authors noted that local mode resonance could occur when ground vibration was sufficiently high, rendering the conventional displacement-based criteria inapplicable and more emphasis on the stress-strain responses were necessary. Lu et al. (2005) employed the smooth particle hydrodynamics technique combined with the normal FEM to simulate responses of a buried concrete structure under subsurface blast. They compared 2D and 3D modeling schemes and found that the maximum acceleration and velocity responses took place around the center of the front wall for a side burst scenario. Wu et al. (2005) studied a masonry structure and masonry infilled RC frames through the 3D modeling technique. The research results verified the conclusions that structural responses and

damages to high-frequency blast ground motions were primarily dominated by structural high vibration modes. A typical blast induced ground vibration and its modified signals by scaling amplitude in the form of peak particle velocity were used in the research. Hao and Wu (2005) studied responses of RC frame structures with numerically simulated underground blast-induced ground motions as the input excitation. The authors again pointed out that the overall structural response and damage were highly ground motion frequency dependent. They noted the importance of local modes in governing dynamic structural responses when ground motion frequency was high. Wu and Hao (Wu and Hao 2005; Hao and Wu 2005) studied influences of simultaneous ground shock and airblast forces on structural responses. This research found that at certain conditions, ground motions have great contributions to structural damages.

Equipment foundation responses to ground-transmitted excitations were studied by Naggar (2003) though four different cases. The author pointed out the importance of a vibration-monitoring program for a vibration-sensitive equipment foundation. The author also found that the widely used half-space model might lead to overestimation of damping and underestimation of soil stiffness.

Ma et al. (2004) studied the effect of soil-structure interaction of a five storey frame under blast-induced ground excitation in plane. They found that soil showed the ability to serve as a low pass filter and would affect top displacements of a building. It was also found that increasing base mass would significantly affect the base shear and axial force. They concluded that higher shear wave velocity (V_s) of the underlying soil was associated with stiffer soil and had decreasing soil-structure interaction.

Although studies about blasting effects on electric power transmission structures are not found in public literatures, research results from blasting effects on buildings indicated special characteristics of structural responses under blast induced ground motions as compared to other types of loads.

2.2.3 Current blast regulations

A lot of research has been implemented to establish relations between vibration parameters (displacement, velocity, acceleration and frequency) and observed structural damages. Most current blast criteria to date are based on studies on effects of residential buildings.

The most widely known blast limit, 2 in/s peak particle velocity is based on a 10-year study by U.S. Bureau of Mines (Nicholls 1971). The criterion for ground vibrations does not take frequency into consideration. A further work conducted by Bureau of Mines developed frequency-based safe limits in RI 8507 (Siskind et al. 1980). Figure 2.4 is a typical blast monitoring report based on RI 8507(Nomis 2003).

Office of Surface Mining modified 2 in/s PPV into a regulation as the following: 0.03 in for 1-3.5 Hz, 0.75 in/s for 3.5-12 Hz, 0.01 in for 12-30 Hz, and 2.0 in/s for 30-100 Hz. These criteria considered both displacement and velocity for wide range of dominant frequencies (Svinkin 2003).

Siskind et al. (1980) proposed a distance-dependent set of the PPV blast limit: 1.25 in/s for distance from 0 to 300 ft, 1.0 in/s for 300 to 5000 ft, and 0.75 in/s for distances greater than 5000 ft.

These blast limits are obtained on the basis of correlation between intensity of ground vibrations and damage of low-rise houses. Structural conditions, i.e. how old of the structure, are not included in these regulations.

Federal Highway Administration (FLHP 2008) summarized a more comprehensive recommendation regarding vibration-related engineering problems, such as settlement, motions due to blasting, strains due to motions, etc. The type of sensors used in the monitoring work and some application examples were provided in its website.

For power transmission systems, some power companies set their blast safety regulations based on previous US Bureau of Mines research results on low-rise residential structures. For instance, Southern Company requires that the maximum ground vibration limit as 2.0 in/s PPV (Chen et al. 2007). There is so far no systematic study on blast limits for electric transmission structures. Conner (2007) reviewed existing blast regulations and developed a qualitative blast plan for transmission structures by schematically considering many aspects of blast effects. It is necessary to develop a quantitative criterion, which when combined with the all-aspect schematic considerations of Conner's work (2007), yields a comprehensive blast design guidelines for both power company engineers and blast consultants.

2.3 Free vibration behaviors of the transmission structure

2.3.1 Modal study in civil engineering

Many applications of structural dynamics rely their success upon having a faithfully representative model. Modal analysis is an effective technique of system identification by determining inherent dynamic characteristics of a system. It is based upon the philosophy that the vibration response of a linear time-invariant (LTI) system can be expressed as the

linear combination of a set of vibration modes. Modal testing is an experimental technique to obtain modal data representative of a physical model in reality. Based on the concept that error-free measurements truly represent a structure, the mathematical model can be verified or updated (He and Fu 2001).

Based on the assumption that the ambient vibration is a random white noise, standard time domain curve-fitting procedures can be applied to the cross-correlation functions to estimate resonant frequencies and modal damping of the structure. In this way, system identification can be performed from ambient vibration measurements. Farrar and James III (1997) employed this method to study a highway bridge. Resonant frequencies and modal damping were identified.

Full-scale testing of a six-story steel frame building was performed by Memari et al. (1999) using ambient and forced vibration methods. Through the test, the authors studied effects of Autoclaved Cellular Concrete (ACC) block infill partition walls on dynamic properties and stiffness of the building. It was concluded that the ACC light-weight material could result in larger than expected damping ratios for the fundamental lateral modes, stiffening effect and minimized building weight, and therefore had advantages for the building in seismic regions.

Natural frequency and associated mode shape data were used in parameter estimation of civil structures. The modal stiffness-based error function was developed by Sanayei et al. (1999) and successfully used in capturing complicated foundation system and connection behaviors, thereby improving the accuracy of the FE models.

Through minimization of eigensolution residuals, the model updating technique based on modal analysis was employed to identify material properties of a system, such as elastic constants of composite materials (Cunha and Piranda 1999).

Optimization problems involved in identification of civil engineering structures is the focus of Teughels (2003). Minimization between the finite element model and experimental modal data is solved by adjusting unknown model parameters.

Two output-only time-domain system identification methods (the Random Decrement Method combined with Ibrahim Time Domain method and the Natural Excitation Technique combined with Eigensystem Realization Algorithm) were employed by Siringoringo and Fujino (2008) to identify a suspension bridge using ambient vibration response. The results from the study demonstrated that using both methods, ambient vibration measurement can provide reliable information on dynamic characteristics of the bridge.

Thus far, system identification based on modal analysis is widely applied to various civil structures including dams (Loh and Wu 2000), bridges (Ren et al. 2004), buildings (Ivanovic et al. 2000), and structure members (Pavic and Reynolds 2003).

Beyond system identification application and parameter estimation, modal testing also supplies information for FE model verification, damage detection, structural optimization design, etc. Brownjohn et al. (2001) described the sensitivity-analysis-based FE model updating method and its application to structure condition assessment. Although the finite element model updating method has been successfully used for condition assessment of bridges, the authors pointed out that the success of applications

depended on a well-designed and controlled modal test and an integration of analytical and experimental arts.

With the idea that the variation of dynamic characteristics can be an indicator of structural health conditions, Rahman (2003) explored different techniques for identifying linear structures. Three system identification methods, including Fourier transform approach, discrete-time filter method with Least Squares solver, and Discrete-time filter method with Instrumental Variables solver, were studied.

Dynamic experiments were conducted on an all-FRP composite pedestrian bridge by Bai and Keller (2008). The influence of the joint types on dynamic behavior of this truss bridge was studied and it was concluded that the lowest natural frequency resulted from the first lateral mode was 26-28% smaller for the bolted span than for the bonded span.

2.3.2 Vibration of transmission structures

Dynamic behaviors of transmission structures are of concerns since wind loads are predominant in structural design considerations. Hence, vibrational characteristics of power lines as well as the support structures have been studied extensively.

Simplified numerical procedures were introduced by Ozono et al. (1988) to study characteristics of in-plane free vibration. The tower-conductor coupled system was considered in their model. It was found that at higher frequencies, a group of natural frequencies of the coupled model was observed close to each natural frequency of the same freestanding tower. Ozono et al. (1992) examined the in-plane dynamic interaction between a tower and conductors and explained mechanism of the in-plane free vibration of transmission line system. They found that the contribution of a conductor to the

dynamic tension force transmitted to a tower was more significant among transverse-wave modes.

To answer the question that how cable oscillation initiates, Venkatasubramanian (1992) investigated the galloping of electric power transmission lines. The coupling between axial modes and torsional modes and its influence on natural frequencies of cable vibrations were studied through theoretical analysis as well as numerical modeling. It was found that the sag-to-span ratio did not have a significant effect on torsional frequencies although it caused great changes of vertical oscillation frequencies. The author pointed out that galloping might be initiated in a purely vertical mode, purely torsional mode or a combination of these two. But the torsional mode was more likely to be the initiating mode for transmission line galloping.

Field measurements of transmission line vibration were conducted by Momomura et al. (1997). They collected data of tower vibration under wind in a mountainous area. The vibration characteristics of the tower indicated that conductors had strong influence on tower dynamic behaviors. The research results also showed that tower responses, in forms of acceleration, strain of the tower with conductors, and conductor tensile forces, increased in proportion to wind speed and power. The authors concluded that mode shapes of the tower with conductors in a frequency range of 1 Hz or less were similar to the fundamental mode shape of the tower without conductors attached.

Natural frequencies of guyed masts were determined by Madugula et al. (1998) through modeling in ABAQUS with both truss elements and beam-column elements. The natural frequencies from these models agreed closely with each other. The numerical results were also verified by scaled lattice tower model tests. The influence of ice

accumulation, guy initial tensions and torsion resistors on dynamic behaviors of the guyed tower was discussed. It was found that ice on guyed masts results in reduction of natural frequencies and iced guyed masts were vulnerable to dynamic wind effects. It was also concluded that the mast height had greatest effect on the lowest natural frequency and an increase in the initial tension of the guys leaded to an increase of its natural frequencies.

Both theoretical and experimental studies were performed by Rao et al. (2004) to evaluate natural frequencies of the towers. An equation was derived by the authors to predict natural frequencies of the tower. The paper also introduced a non-dimensional parameter to take into account effects of increased transmission tower deformations.

Murtagh et al. (2004) developed simple approximate methods to obtain natural frequencies and mode shapes of tower supporting utilities based on lumped mass models. The first three natural frequencies yielded by using this method were accurate. A further simplified analysis using the approximate cantilever system, on the other hand, could yield accurately fundamental natural frequency and mode shape only, which might be sufficient to predict the response of a lattice tower in wind.

Post-buckling behaviors and collapse modes of guyed towers under extreme wind loading conditions were simulated based on the proposed advanced Spectral Element method and the Computational Fluid Dynamics by Horr et al. (2004). Free vibration modes of the guyed tower structures were obtained by using the general purpose finite element program ANSYS. Eigenvalues were found to range from 1.77 Hz to 8.48 Hz for the first six global modes.

Vibration of transmission structures is a complex problem especially when considering coupling issues between cables and support structures. There is so far little published research discussing the free vibration of transmission pole structures with the effects of conductors. Lantrip (1995) and Chen et al. (2006) reported modal tests and FE analysis on different size concrete poles. Polyzois et al. (1998) used the finite element method to obtain natural frequencies of composite poles. All of the above studies were based on free-free or cantilevered beam models. The relevant study in this research project is valuable for understanding dynamic behaviors of transmission poles and therefore improves their structural design.

2.4 Dynamic responses of transmission structures

Forced vibration of electric power transmission structures is one of the main concerns for structural design considering that large span characteristics of the transmission lines. These power grids, mainly composed of conductors and towers/poles, are vulnerable to wind or ice loads when they are in cold regions. The complexity caused by the coupling between cables and supported structures increases the difficulty in studying dynamic responses of transmission systems.

Chang (1985) employed the computer simulation to study galloping of transmission lines and it was found that torsional motion could cause vertical motion for a sagged and coupled transmission line. The simulation program developed by the author was capable of handling the complex cable vibration problems.

Loredo-Souza (1996) examined the behavior of transmission lines under severe winds through wind tunnel tests. Theoretical comparison was made between current design and the statistical method proposed by the author. It was found that aerodynamic damping

had a significant effect on dynamic behaviors of cables. With increasing separation between cables, correlation and coherence between cable forces diminished. The study also concluded that dynamic responses of transmission structures were strongly dependent on turbulence intensity and sensitive to design parameters.

Yasui et al. (1999) studied wind-induced power transmission tower vibration coupled with power lines. They found that differences in the way of how the power transmission tower supports the power line had an influence on response characteristics. It was shown that peak factors computed from a time series response were greater than those computed from power spectrum density. For the same support types, the peak factors of member axial forces were greater than those of transverse direction displacements.

Structural analysis of transmission towers under wind loads were performed by Battista et al. (2003) through the finite element method. Fundamental frequency of the transmission tower, useful in early design stages, could be estimated by a simplified two degree-of-freedom analytical model. To reduce the tower top horizontal along-wind displacements in the cross-line direction, nonlinear pendulum-like dampers were developed.

Transmission lines subject to high intensity wind loads, such as downbursts, were studied by Shehata et al. (2005). Through comparisons between structural performance under downburst winds and normal winds, the authors showed the importance of considering high intensity winds in structural design of transmission towers. In numerical models, three-dimensional linear elastic frame elements were used to model the members of the tower while two-dimensional curved beam elements with geometric non-linearity included were used to model conductors and ground wires.

Kudzys (2006) adopted probability-based approaches, treating wind and ice storms as persistent design situations, to reveal effects of these extreme climatic events on the time-dependent safety of power transmission lines. The time-dependent performances of some structural members were presented in terms of their random safety margin sequences.

Park et al. (2007) proposed two types of friction-type reinforcing members (FRM), dissipating energy in slotted bolted connections, to enhance wind resistant performance of a transmission tower. The proposed FRMs were verified though cyclic loading tests.

Savory et al. (2008) compared wind-induced foundation loads measured on a transmission line tower in the field with those calculated using design codes. The comparison indicated that existing design codes provided reliable transformation of the local wind effects to tower foundations.

Due to the lack of research in the area of seismic analysis of transmission lines, El-Attar (1997) realized the significance of studying the response of transmission lines under earthquakes in order to evaluate current design codes. Both power lines and steel towers were modeled and seismic responses were calculated and compared with the effects of wind and ice loads. Research results showed that displacements and internal forces in transmission lines were substantial under ground vibration and it was suggested that cable motion during earthquakes should be included in the design of line clearances. The studies also indicated that forces in tower members due to earthquakes might exceed those caused by the wind loads.

Transmission towers subjected to spatially incoherent seismic ground motions were also described in the same study (Ghobarah et al. 1996). Artificial ground displacement records were developed and were used in the finite element analysis. It was found that

seismic wave propagation velocity had significant effects on lateral displacements of transmission lines.

Li et al. (2005) proposed simplified models for transmission tower-lines that include tower-line interaction. The validity of simplified models was examined through shaking-table experiments on scaled coupled transmission line systems. A simplified analysis method was proposed for seismic response calculation of the coupled tower-conductor system. It was found that the models yielded better results for out-of-plane vibrations than those under in-plane vibrations.

Scenarios such as broken conductors, insulator rupture, as well as other types of dynamic loads play an important role in the transmission line design. To enhance the design, a software, DYNTRN, was developed by Nafie (1997) to analyze a transmission line with conductors, support structures, and insulators subjected to different dynamic loading conditions. The stiffness method was used to calculate deformations and forces in transmission line components. Geometric nonlinearities were accounted and were solved by using the Newton-Raphson method. This program was tested for several dynamic loading. Results showed reasonable agreement with experimental works.

Dynamic analysis was performed by McClure and Lapointe (2003) with consideration of shock load effects on overhead power lines, caused by conductor rupture. The authors successfully applied a macroscopic modeling approach to a case study, which could capture salient features of shock load propagation. The approach could be used to study other loading scenarios, such as sudden ice-shedding effects from conductors or sudden failure of other components like towers or suspension strings. Using ADINA, Tucker (2007) studied dynamic effects of broken suspension insulator and multiple tower failures

on power transmission lines. The numerical model for the scenario of a broken insulator failure was compared with the published full-scale test data. Numerical analysis of tower failure was validated through a small-scale test. The study provided a better understanding of cascade failure of transmission lines.

Literatures that report dynamics of other structure types similar to power transmission structures, such as telecommunication towers, have also been reviewed. These research results provide some insights about electric transmission structures subjected to blast induced seismic loads.

Khedr (1998) studied self-supporting lattice telecommunication towers using modal superposition method as well as response spectrum technique. Structural response was obtained and earthquake amplification factors for the base shear and the total vertical reaction were proposed for design estimation. A simplified static method was developed to estimate member forces in self-supporting lattice towers based on the assumption that: 1) the lowest three flexural modes of vibration were sufficient to describe structural responses to horizontal excitations and 2) first axial mode was enough to reflect the dynamic responses to vertical excitations. The author also extended the study to include transmission line towers by replacing the cables as equivalent masses. However, the proposed simplification could not include significant tower-cable interaction that was often observed.

Seismic performances of guyed telecommunication towers were studied by Meshmesha (2005) using ABAQUS. Based on studies on nine towers with 24 earthquake records, the research yielded valuable information about dynamic behaviors of steel towers. Some empirical equations were proposed to calculate the equivalent shears, axial

loads, and bending moments, etc. for quick design check. The research also indicted that periods from 0.1 to 2.3 seconds had the most significant influence on responses of guyed towers. The author gave empirical equations to predict the fundamental frequency of the guyed tower vibration:

$$f_s = 28.5H^{-0.86} \quad (2.10)$$

$$f_b = 132.43H^{-0.92} \quad (2.11)$$

where f_s (Hz) is the fundamental frequency for the guyed tower when guy modes are not suppressed; f_b is fundamental bending frequency of the mast in Hz; and H is the height of the mast in meters.

Seismic performance of a 120-m-tall guyed mast was examined using the finite element method by Hensley (2005). The guyed tower model was subjected to two ground motion records and three orthogonal earthquake components were input for each record. The results, such as deflections, bending moments, guy tensions, and base shears were obtained and structural responses were examined. The effects of snap loads introduced by the guys were also studied with the aim of analyzing the potential use of Snapping-Cable Energy Dissipators to minimize lateral responses.

Although there is a variety of research regarding transmission structure responses to dynamic loads, there is lack of a systemic study on the forced vibration of transmission pole structures.

2.5 Structural health monitoring in civil engineering

The concept of structural health monitoring is put forward based on the idea that civil infrastructure has its own aging process. Many methods have been developed for diagnosis of structural health. Yan et al. (2007) presented a review of state-of-the-art of

vibration-based structure damage detection methods. Peeters (2000) developed a damage detection technique for an experimental model with output-only measurements, where structural damages under varying environmental conditions were detected through a statistical system identification solution. This method was proved by the Z24 bridge case study including both long-term monitoring and with different damage scenarios.

Two damage detection techniques have been proposed by Maeck (2003): the direct stiffness calculation technique and the sensitivity based updating technique. The basic idea is that structural damage is well correlated with the changes of structural dynamic properties (eigenfrequencies, mode shapes and/or transfer functions). Test programs including laboratory testing on reinforced concrete beams as well as experiments on two prestressed concrete bridges proved that the proposed dynamic analysis method was a helpful tool in structural health monitoring.

Two types of full-scale concrete structures, including concrete pavements and a simply-supported prestressed concrete beams, were subjected to fatigue loads to investigate the effectiveness of two vibration-based damage detection methods: Fast Fourier transform (FFT) and continuous wavelet transform (CWT) by Melhem and Kim (2003). The study concluded that the wavelet analysis had a great potential in the damage detection of concrete.

A gradually damaged prestressed concrete beam was diagnosed through the FE model updating technique using experimental modal information (Unger et al. 2005). Modal curvatures were found to be more sensitive to local changes of bending stiffness than eigenfrequencies and mode shapes.

Based on the multiple damage location assurance criteria, Koh and Dyke (2007) performed damage detection study for long-span, cable stayed bridges. Through iteratively searching for the maximum level of correlation between variations in measured and analytically synthesized natural frequencies, the locations of damage were determined. A cantilevered beam model and a cable-stayed bridge model were used for simulating in the study.

Besides damage detection, health monitoring also means tracking a structure's health by measured data and analytical simulations (Aktan et al. 2003), which now involves a broad concept of assessing in-service performance of structures using a variety of measurement techniques. Although there is a long history of power transmission performance monitoring, the concept of structural health monitoring has not been caught on by the power industry. Common practices to ensure structural health in the power industry are based on periodic visual inspections along electric grids. Considering the geographic dispersed nature of electric power grids, this kind of inspection is both expensive and time consuming. León et al. (2007) realized the advantages of wireless sensor networks and presented a conceptual design scheme for an application of wireless sensor technology to assess structural health of transmission lines. Selected sensors and their responses to any mechanical event were summarized in a matrix (Table 2.1). It was proposed tension and strain sensors to be mounted at all conductor attachments of all strain structures. Accelerometers were proposed to be installed in the support structure body for vibration and tilt monitoring. Installation of temperature sensors were also considered for the purpose of detecting over-heating. The two-layer communication model was developed for the wireless mechanical sensor network, including

communication ranges not greater than 100 feet for a local sensor group with a local data and communication processor installed at each support, and interaction between local data communication processors and the collaboration layer. The second layer handled all message processing and delivered the mechanical status information to substations. This two-layer architecture overcame the range limitation for communication. Four different failure modes were classified. For different failure modes, different actions need to be taken. The integrated power system security program that could perform real-time assessment of the mechanical/electrical situation was developed. The simulation studies showed that the proposed monitoring scheme could help power engineers make fast and appropriate decisions based on mechanical failure modes.

It is obvious that there are many research needs for electric power facilities assessment. It remains promising to introduce structural health monitoring strategies into the transmission systems. These modern technologies are expected to save labors and money. Such modernization relies on a systematic research, which might include studies on structural dynamic characteristics of various transmission structures, development of sensing techniques and data acquisition systems, data management and interpretation methods, and structural condition assessment and health prediction models.

2.6 Summary

Electric power transmission lines are critical civil infrastructure. The reliability of these structures is sometimes endangered by extreme events. Typical structural designs, however, do not include extreme loading such as blasting. Current blast limits are mostly based on the observation of residential housing damages, which may not be suitable for power transmission structures. Developing protection strategies for transmission facilities

requires the study of dynamic responses of these structures as well as the characteristics of blast induced ground motions. Vibrational behaviors of transmission poles, widely used as support structures in power transmission grids, received little attentions. Experiences obtained from studying on communication towers provide additional references for dynamic analysis of transmission poles. With more understanding of transmission structure dynamic behaviors, health monitoring design is a promising approach to ensure our power delivery safety. Valuable information was derived from health monitoring strategies for other structure types and latest research on wireless sensor based health monitoring for the power transmission system.

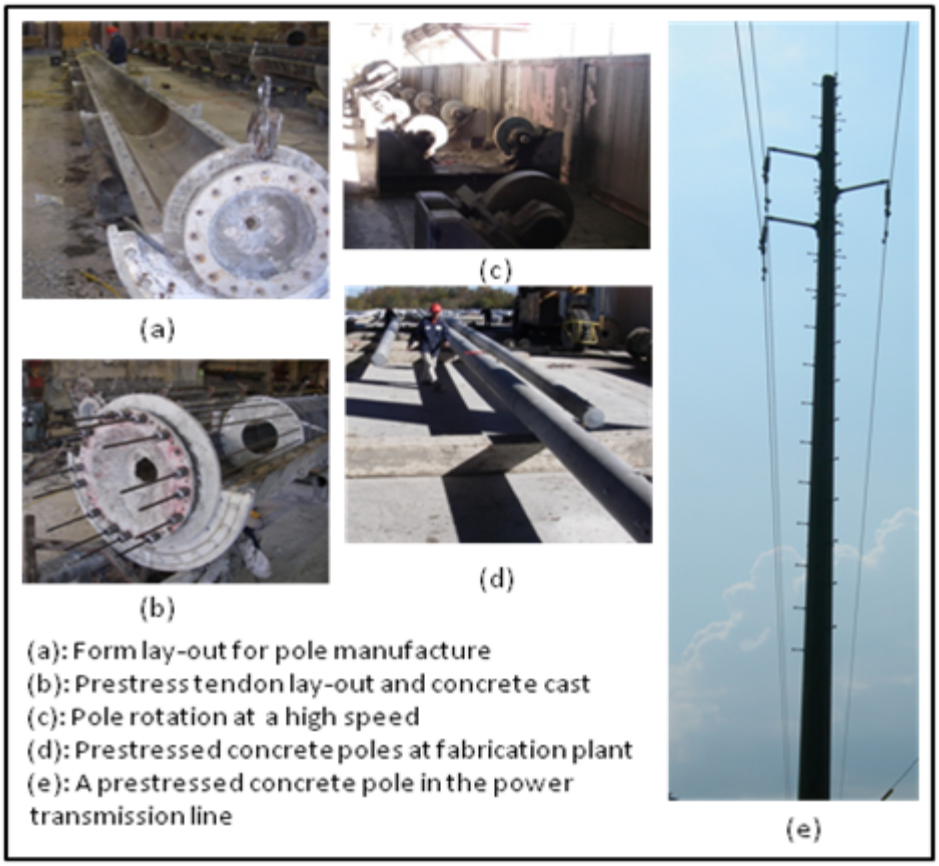

Figure 2.1: Pole fabrication and a typical prestressed concrete pole

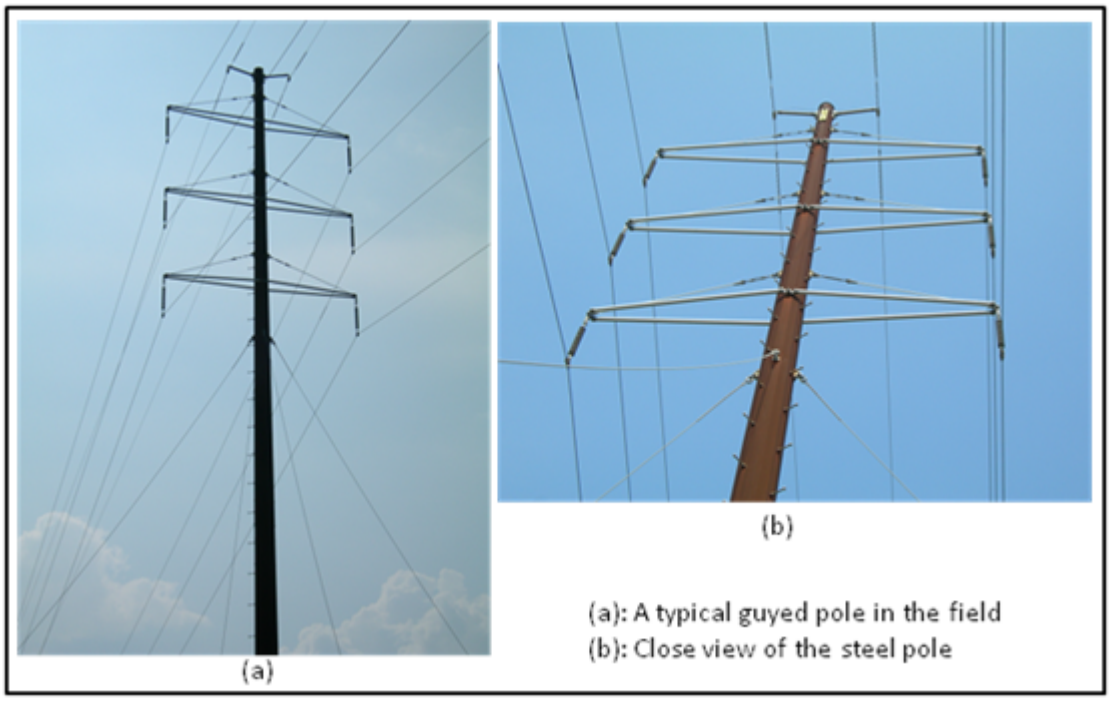

Figure 2.2: A typical steel pole

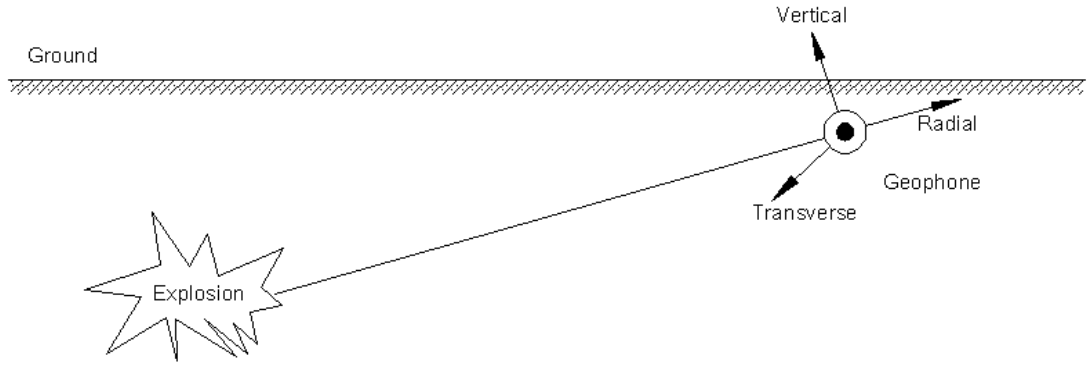

Figure 2.3: Blast explosion and ground vibration

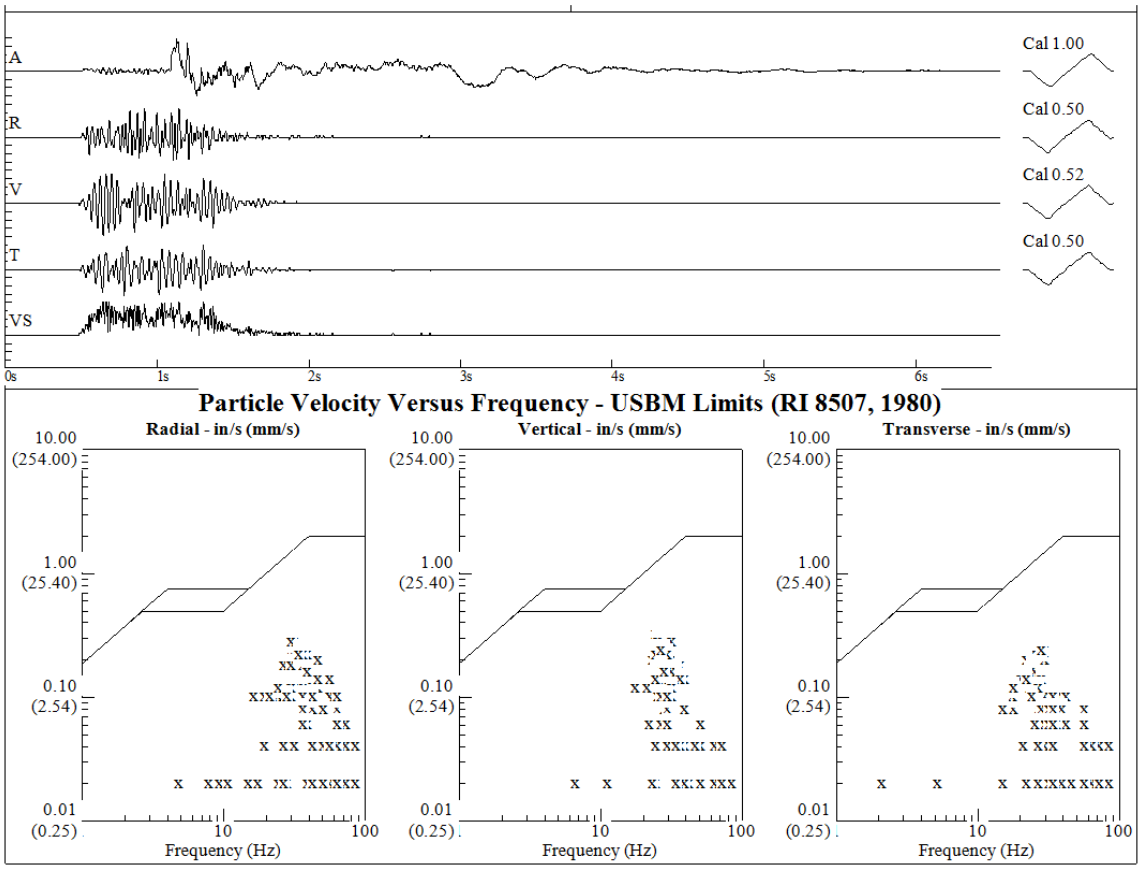

Figure 2.4: Typical blast monitoring report (Nomis 2003)

Table 2.1: Sensor application matrix (León et al. 2007)

	Tension/Strain	*Vibration*	*Tilt*	*Temperature*
Normal conditions	Normal values	Normal values	Normal values	Normal values
Ice accretion low wind	Increased, inside	Normal values	Normal values Very small angle	Normal values
Medium-high wind Bare conductor	Increased, inside limits	High frequency inside limits	Normal values Very small angle	Normal values
Medium-high wind Uniform ice	Increased, inside Limits	High Frequency Inside limits	Normal Values Very small angle	Normal values
Galloping	Increased, at limit values	Low frequency High amplitude	Oscillating values	Normal values
Explosion blast	Sharp increase	Sharp amplitude increase	Oscillating values	Temporary rise
Compromised structure	Increased in strain support Loss of equilibrium in suspension supports	No information	Appreciable tilt 0-90 degrees	Normal values
Collapse structure	Sharp increase, then goes to zero	No information	Appreciable tilt ~90 degrees	Normal values
Hot spots	Normal values	Normal values	Normal values	Isolated high temperature
Overheating	Increased strain caused by sagging	Normal values	Normal values	Uniform between conductors and nearby supports

CHAPTER 3: BLAST INDUCED GROUND VIBRATION

3.1 Introduction

In this chapter, an extensive field monitoring work was performed. Results of blast induced ground motions were characterized for two blasting sites in the southeastern United States. Empirical design response spectra with expected peak particle velocity were generated based on collected records. These design spectra curves would be used for later transmission structure spectrum analysis to obtain structural response during ground vibration caused by blasting.

3.2 Blast monitoring

Ground motions induced by surface blasting were recorded both by traditional geophones and wireless accelerometer units. Sensors were buried at the location usually hundreds of feet away from the explosion but in the proximity of the foundation of the studied electric transmission structure, usually about one foot down the ground (Figure 3.1). Blasting was involved in a surface coal mine and a rock quarry. Site characterization was established by conducting geophysical testing and studying previous boring data. The results indicated that both sites can be described as shallow bedrocks with surface layer of stiff, silty sands. Such sites are characteristics of most Appalachian mountain regions with either carboniferous coal formations or mineral quarry.

While the general site horizons are similar, the site geometries involved in the blasting for two sites are quite different: Site A represented a surface ground blast that travels through a continuous surface to the transmission structure; whereas Site B involved a gapped area between the blast site and the subject structure (Figure 3.1). The difference in site geometries can result in different wave propagation phenomena. The site geometries associated with the transmission structures are typical of commercial surface mining in south-eastern US. Table 3.1 lists the selected data from the entire blasting database based on preliminary signal observation.

Equipments used in monitoring included wireless accelerometers and seismographs, both of which are commercially available. The wireless sensor unit is a tri-axial MEMS accelerometer (MicroStrain 2007) (Figure 3.2). It has three channels (Channel 1, 2 and 3) representing three directions of vibration measurements. The MicroStrain G-Link wireless sensor features 2 KHz sweep rates, combined with 2 Mbytes of flash memory. Accompanied with the bi-directional RF communications antenna, real-time data can be transmitted to the host PC. The seismograph used in the blasting monitoring is a geophone product of Sauls Seismic, Inc. It has three perpendicular components of velocity described as radial, transverse and vertical directions. Recoding duration for seismographs is about 6 seconds. It was buried side by side with the wireless sensor during blast monitoring. Compaction efforts were made while burying the sensor to reduce impacts of disturbed soil around the sensor. Since the main objective of this monitoring work was to collect ground vibration data to use as foundation excitations during the later dynamic response analysis, detailed studies of explosion distance, charge weight, wave propagation and attenuation was not included in the scope of this project.

3.3 Ground motion records

The ground vibration signals obtained by the wireless accelerometer are acceleration time histories, which have amplitude in g's and time unit in seconds. The recording duration was set first around 12 seconds and later about 8 seconds, which is sufficient to catch ground motions induced by the blasting. Most recorded data usually lasted around one second. A trigger was set to instruct the wireless sensor unit to begin streaming data at a specified level determined on site. After blasting, acceleration data was then downloaded for later analysis.

Wireless sensor units used in this monitoring work were relatively sensitive and picked up ambient noises. Filters were then programmed to reduce the noise from recorded signals. The implementation of such a filter function can be expressed as a convolution operation (Jenkins et al. 2000):

$$y(n) = h(n) * x(n) = \sum_{m=-\infty}^{\infty} h(n)x(n-m) \qquad \text{in time domain} \qquad (3.1)$$

$$Y(\omega) = H(\omega)X(\omega) \qquad \text{in frequency domain} \qquad (3.2)$$

where $x(n)$ is the original signal, $y(n)$ is the filtered signal, and $h(n)$ is the filter function; $X(\omega)$, $Y(\omega)$, and $H(\omega)$ are the Fourier Transform of $x(n)$, $y(n)$ and $h(n)$. $h(n)$ in frequency-domain is often called the transfer function ($H(\omega)$). Its theoretical form can be written as the following (Jenkins et al. 2000):

$$H\left(e^{j\omega}\right) = \sum_{n=-\infty}^{\infty} h(n)e^{-j\omega n} \qquad -\pi \le \omega \le \pi \qquad (3.3)$$

$$h(n) = \frac{1}{2\pi}\int_{-\pi}^{\pi} H\left(e^{j\omega}\right)e^{j\omega n}d\omega \qquad -\infty \le n \le \infty \qquad (3.4)$$

A Finite Impulse Response (FIR) filter was developed in this paper. It is a frequency-selective filter. The original record within certain range is blocked by the filter function or transfer function in the frequency-domain. The windowing technology was used in the

FIR filter design. Typical windows include Rectangular window, Hanning window, Hamming window, Kaiser window, etc. The simple rectangular window was selected to design the FIR filter, which is defined as (Kumar 2005):

$$w(m) = \begin{cases} 1, & 0 \le m \le N \\ 0, & otherwise \end{cases} \tag{3.5}$$

The output signal ($y(n)$) can be calculated by input signal ($x(n)$) from the following equation (Karam 1999):

$$y(n) = \sum_{m=N_1}^{N_2} h(m)x(n-m) \tag{3.6}$$

Corresponding expression in frequency domain is obtained from the following (Karam 1999):

$$Y(m) = H(m)X(m) \qquad m = 0, \dots, N_{DFT} \tag{3.7}$$

where $X(m), H(m)$ and $Y(m)$ are the Discrete Fourier transform of $x(n)$, $h(m)$ and $y(n)$. N_{DFT} is the size of the DFT. $h(m)$ is the impulse response of the filter and can be obtained from multiplication of an ideal filter function ($h_d(m)$) as a high-pass truncation with a selected window ($w(m)$):

$$h(m) = h_d(m)\, w(m) \tag{3.8}$$

A typical blasting signal recorded by the wireless sensor is shown in Figure 3.3, for which the FIR filter was applied. A simple square low-pass filter was used. More raw blast records can be found in Appendix A.

The geophone data is the velocity time history in unit of in/s (Figure 3.4). The geophone used in monitoring has remote communication ability. The measurement instruments were left underground for weeks to collect sufficient ground vibration data. Neglecting pre-triggered data, a blasting event from the velocity time history also has

about one second duration, which is less than that of a typical natural earthquake (Figure 3.5). More blast records by geophones can also be found in Appendix A.

Transferring recorded signals from time domain to frequency domain, characteristics of blasting induced ground vibration were further examined. As shown in the spectral form, the frequency range is between 0.5 Hz to 200 Hz with dominant modes below 120.0 Hz for the accelerometer (Figure 3.6) and the frequency range for the blasting signal are from 0.2 Hz to 100 Hz with most sensitive range below 50 Hz for the geophone (Figure 3.7). This difference may be caused by different bandwidth characteristics of accelerometers and geophones. Other measurement related issues can also contribute to frequency contents: sensor sensitivities and sensor placements. Compared with natural earthquake Fourier spectrum (Figure 3.8), ground motions caused by blasting occurred at relatively higher frequencies, which was consistent with other research (Dowding 1985).

It is noted that Hao and his colleagues' research (Hao et al. 2001; Hao et al. 2002; Hao and Wu 2005; Lu et al. 2002a; Lu et al. 2002b; Ma et al. 2000; Ma et al. 2002; Wu et al. 2004; Wu and Hao 2005; Wu et al. 2005; Wu and Hao 2007) indicated a relatively higher frequency at the peak ground motion than our findings. It is easy to understand since most of their results are based on idealized numerical work and ours are from actual field experimental measurements. Besides this research methodology difference, geological type, charge weight, explosion distance, site conditions, blast design and many other factors can affect the ground vibration characteristics.

3.4 Signal integration and differentiation

Numerical integration and differentiation were performed to generate target data that could not be obtained from direct measurement. Numerical integration scheme in time

domain is straightforward: assuming $\{x(n)\}$ $(n = 0,1,2 \dots N)$ is the measured signal, and Δt is integration time step, then the integral of $\{x(n)\}$ can be calculated using the Trapezoidal rule (MATLAB 2008; Manassah 2001; Wang and Hu 2006):

$$\{y(n)\} = \Delta t \sum_{k=1}^{n} \frac{x(k-1)+x(k)}{2} \quad (n = 1,2, \dots N) \tag{3.9}$$

Numerical differentiation is to estimate the derivative of a signal using recorded discrete values. A simple two-point estimation was used to compute the differentiation of input signal $\{x(n)\}$ $(n = 0,1,2 \dots N)$ with time step, Δt (MATLAB 2008; Manassah 2001; Wang and Hu 2006):

$$\{y(n)\} = \frac{x(n)-x(n-1)}{\Delta t} \quad (n = 1,2, \dots N) \tag{3.10}$$

Numerical integration can also be realized in frequency domain (Wang and Hu 2006):

$$y_1(n) = \sum_{k=1}^{N} \frac{1}{j2\pi k\Delta f} H(k)X(k)e^{\frac{j2\pi nk}{N}} \qquad \text{first order} \tag{3.11}$$

$$y_2(n) = \sum_{k=1}^{N} -\frac{1}{(j2\pi k\Delta f)^2} H(k)X(k)e^{\frac{j2\pi kn}{N}} \quad \text{second order} \tag{3.12}$$

The numerical differentiation in frequency domain is calculated as follows (Wang and Hu 2006):

$$y_1(n) = \sum_{k=1}^{N} j(2\pi k\Delta f)H(k)X(k)e^{j2\pi kn/N} \qquad \text{first order} \tag{3.13}$$

$$y_2(n) = \sum_{k=1}^{N} -(2\pi k\Delta f)^2 H(k)X(k)e^{j2\pi kn/N} \qquad \text{second order} \tag{3.14}$$

where $H(n) = \begin{cases} 1, & f_d \le n\Delta f \le f_u \\ 0, & other \end{cases}$, and f_d, f_u are lower and upper cut-off frequencies, respectively. $X(n)$ is the Fourier transform of the input signal $\{x(n)\}$ and Δf is the frequency interval. k and n here are sequence variables.

Codes for numerical integration and differentiation were developed in MATLAB® environment. The vertical direction vibration of signal R5 (Figure 3.9) recorded by the

seismograph was processed and shown here. Since the raw data is time domain velocity signal, it can be either integrated into displacement time history or differentiated into acceleration time domain data. The computation results were close enough between time and frequency domain methods (Figures 3.10-3.13).

3.5 Signal characterization

All the raw data were first gone through noise reduction. Then numerical integration or differentiation was performed to obtain expected time histories. The peak values of acceleration, velocity and displacement in time domain were identified. The frequencies at the peak amplitudes in frequency domain were also identified. Summary of peak particle acceleration (PPA), peak particle velocity (PPV) and peak particle displacement (PPS) were listed in the Tables 3.2 and 3.3. The frequency distribution for PPA, PPV and PPS is shown in Figure 3.14 (a), (b) and (c), respectively. A very wide scatter characteristic for these frequency distributions exists because the data were obtained from a variety of blast events. Frequencies for PPA, PPV, and PPS were averaged to give mean values for each of them. These average values yield the range for the principal frequency in spectrum design.

Maximum values of PPA, PPV and PPS for each blast were calculated and these maximum values were lineally fitted. Figure 3.15 shows relations between PPA, PPV and PPS. These empirical correlations can be used to predict maximum acceleration and displacement at a given peak particle velocity.

3.6 Development of response spectrum

The response spectrum is presented in the form of plots of maximum peak responses to an excitation versus natural frequencies. If dynamic characteristic of a SDOF under ground vibration is described as (Tedesco et al 1999):

$$m\ddot{x}(t) + c\dot{x}(t) + kx(t) = -m\ddot{x}_g(t) \tag{3.15}$$

where m, c, and k are mass, damping and stiffness of SDOF, respectively; while $x(t)$, $\dot{x}(t)$ and $\ddot{x}(t)$ are displacement, velocity and acceleration of SDOF relative to the ground; $\ddot{x}_g(t)$ is ground motion.

For a given damping ratio ξ, maximum values of relative displacement, relative velocity and absolute acceleration at different frequencies ω can be calculated as displacement spectrum $S_d(\omega)$, velocity spectrum $S_v(\omega)$ and acceleration spectrum $S_a(\omega)$ (Wang and Hu 2006):

$$S_d(\omega) = \left|\frac{1}{\omega_d}\int_0^t \ddot{x}_g(\tau)e^{-\xi\omega(t-\tau)}\sin\omega_d(t-\tau)d\tau\right|_{max} \tag{3.16}$$

$$S_v(\omega) = \left|\int_0^t \ddot{x}_g(\tau)e^{-\xi\omega(t-\tau)}\left[\cos\omega_{\mathrm{d}}(\mathrm{t}-\tau) - \frac{\xi}{\sqrt{1-\xi^2}}\sin\omega_d(t-\tau)\right]d\tau\right|_{max} \tag{3.17}$$

$$S_a(\omega) = \left|\omega_d\int_0^t \ddot{x}_g(\tau)e^{-\xi\omega(t-\tau)}\left[\left(\frac{1-2\xi^2}{1-\xi^2}\right)\sin\omega_{\mathrm{d}}(\mathrm{t}-\tau) + \frac{2\xi}{\sqrt{1-\xi^2}}\cos\omega_{\mathrm{d}}(\mathrm{t}-\tau)\right]d\tau\right|_{max}$$

(3.18)

The plot of maximum responses ($S_d(\omega)$, $S_v(\omega)$, and $S_a(\omega)$) against frequencies is the response spectrum curve. Assuming a damping ratio ξ of 0.02 for monitored structures (Loredo-Souza and Davenport 2003), response spectra of ground motion induced by blasting can be generated. Typical spectra are shown in Figures 3.16 to 3.18.

Pseudo peak ground vibration is defined as the peak value of these spectra. The amplification factors, the ratio of average pseudo peak ground motions at designated

frequency ranges via corresponding PPA, PPV and PPS can be obtained. Distribution of amplification factors is shown in Figure 3.19.

A target ground motion curve can be generated based on empirical criteria. By setting PPV to certain expected values, PPA as well as PPS can then be calculated following the empirical relations between PPA, PPV and PPS (Figure 3.15). The principal spectrum frequency can be estimated from frequency distributions (Figure 3.14). Plotting target velocity with predicted acceleration and displacement in a tripartite paper results in a target ground motion curve. A response spectrum for the blast limit with a certain PPV value can then be constructed by multiplying the target ground motion with the average amplification factor and drawn it as a tripartite plot, following the method proposed by Dowding (1985). This design response spectrum can be used in the spectrum analysis to investigate structural response of transmission facilities.

Take the empirical blast limit PPV=2 in/s for example: Figure 3.20 is the target ground vibration curve in tripartite format, in which PPA and PPS were obtained from relations in Figure 3.15; Figure 3.21 is the response spectrum designed through multiplying values in Figure 3.20 with the amplification factor. In the same way, other anticipated design spectral curves with different levels of PPV can be developed.

3.7 Summary

To protect electric power lines under strong ground motions caused by surface mining blasts, an extensive monitoring work was performed. This chapter introduced field experimental results. Ground movements were recorded using both traditional geophones and wireless tri-axial sensing units. Signal process technologies, including noise reduction, numerical integration/ differentiation, convolution integral were used to

analyze blast induced ground vibrations. Empirical relations between peak values of acceleration, velocity, and displacement were developed, which could be used to predict acceleration and displacement for a specific peak value of velocity. The design response spectra of blast induced ground vibrations were generated based on given PPV blast limits.

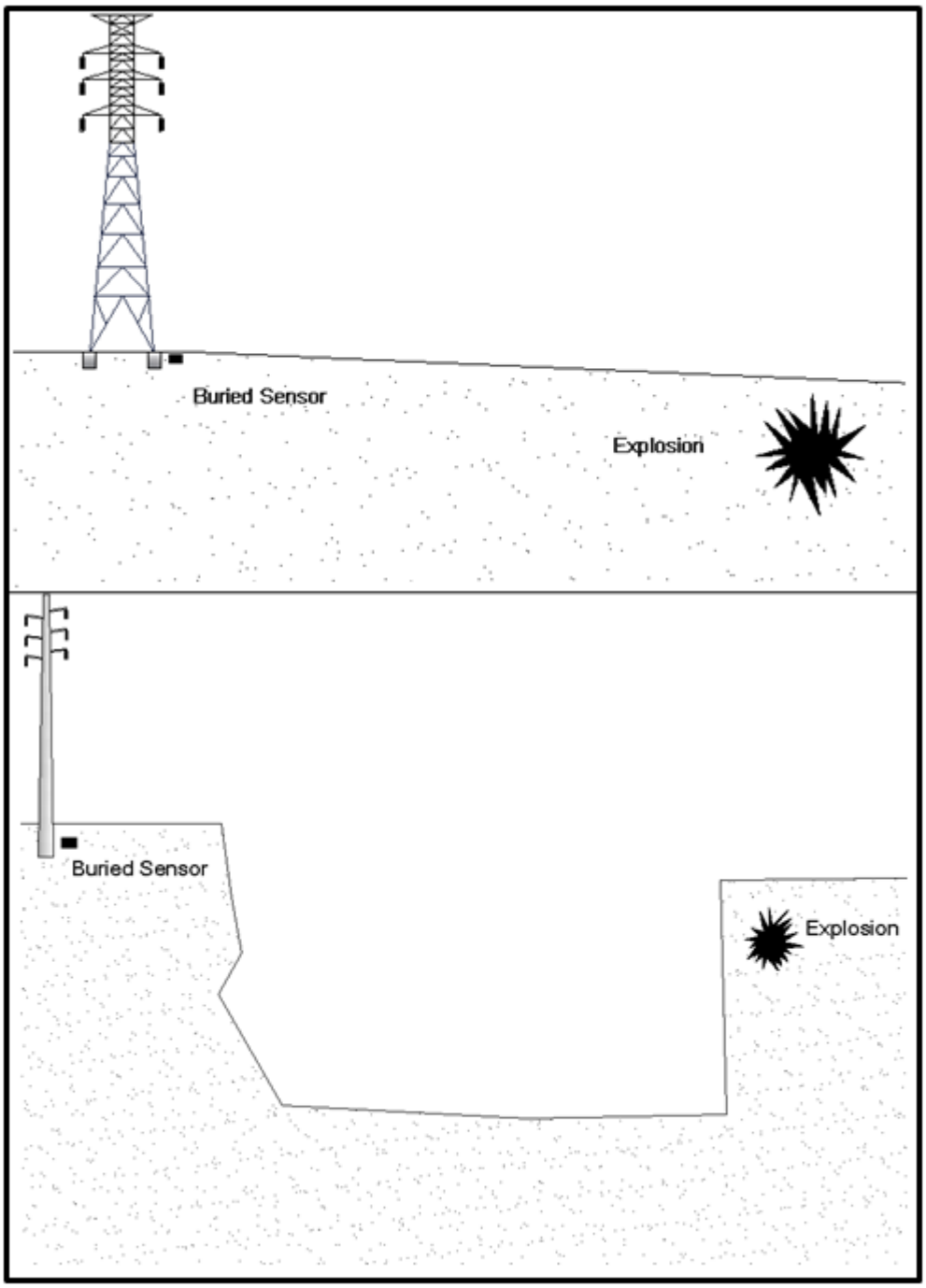

Figure 3.1: Sensor deployment during ground vibration monitoring

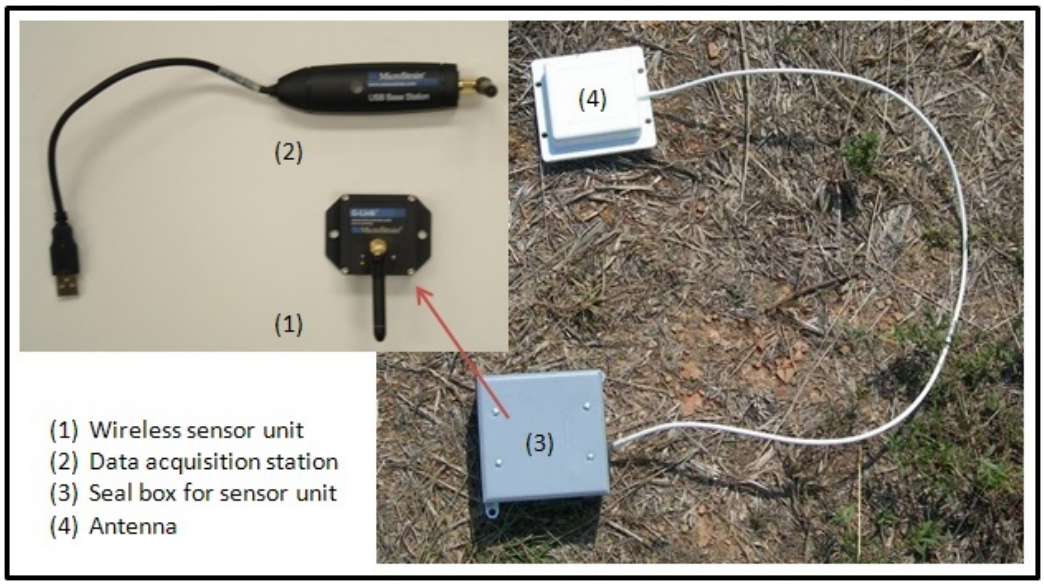

Figure 3.2: Wireless sensor used in blasting monitoring

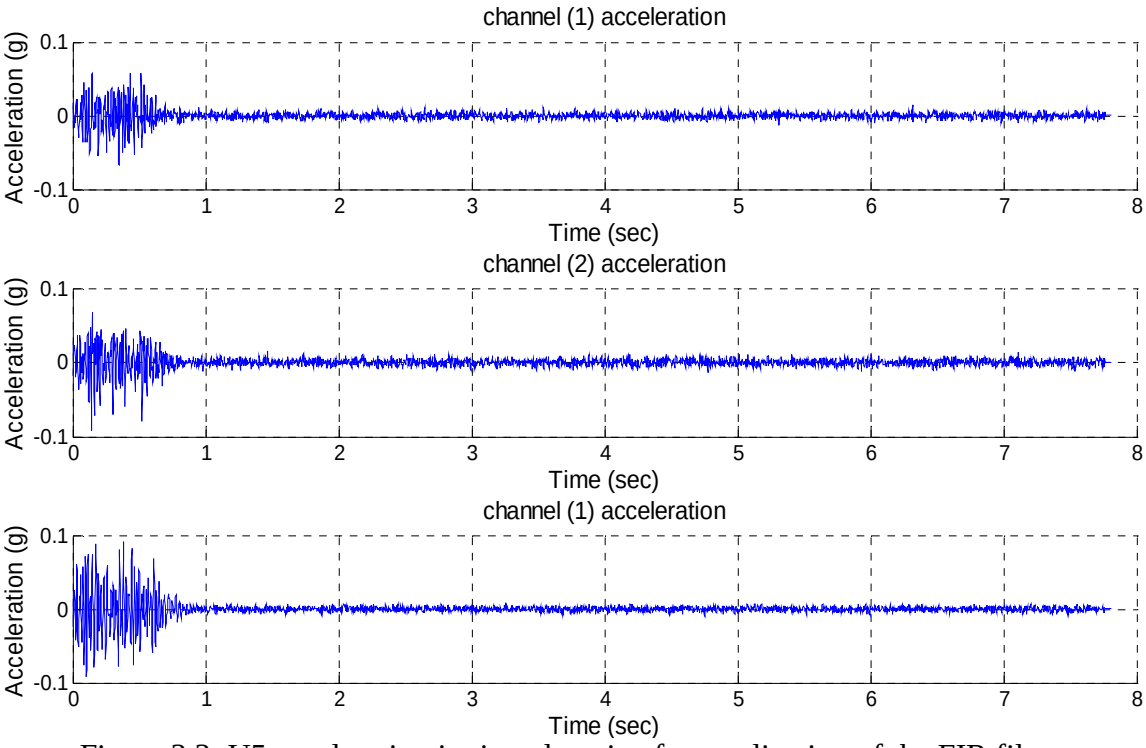

Figure 3.3: U5 acceleration in time domain after application of the FIR filter

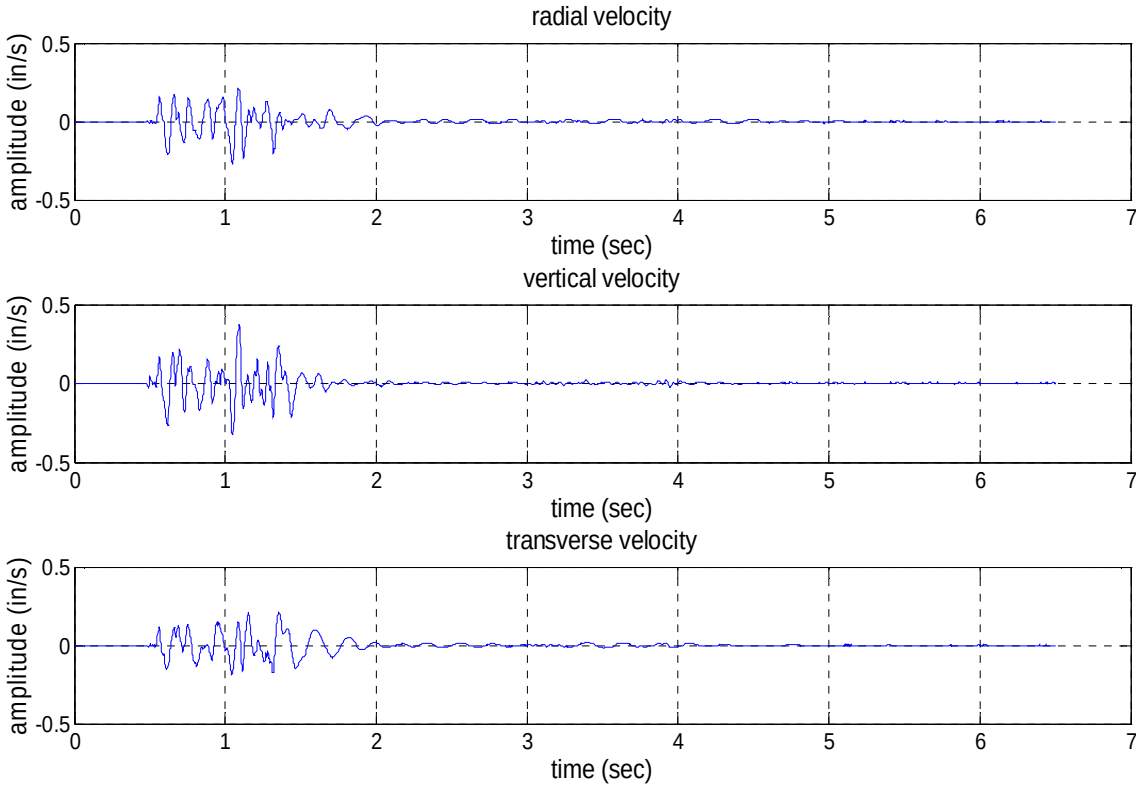

Figure 3.4: R5 velocity record

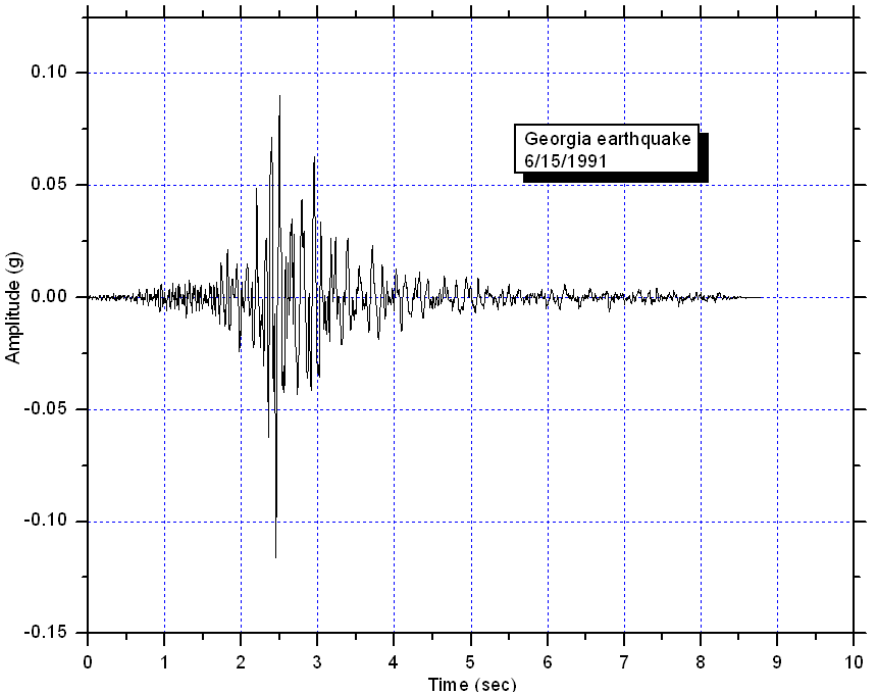

(a)

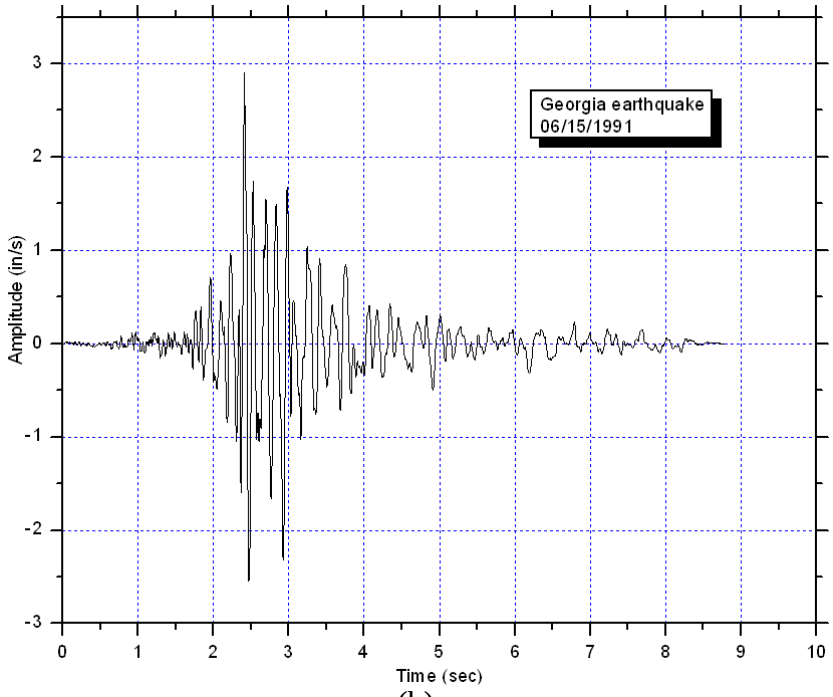

(b)

Figure 3.5: Time history of a natural earthquake at Georgia: (a) acceleration; (b) velocity (Data source: http://peer.berkeley.edu/smcat/)

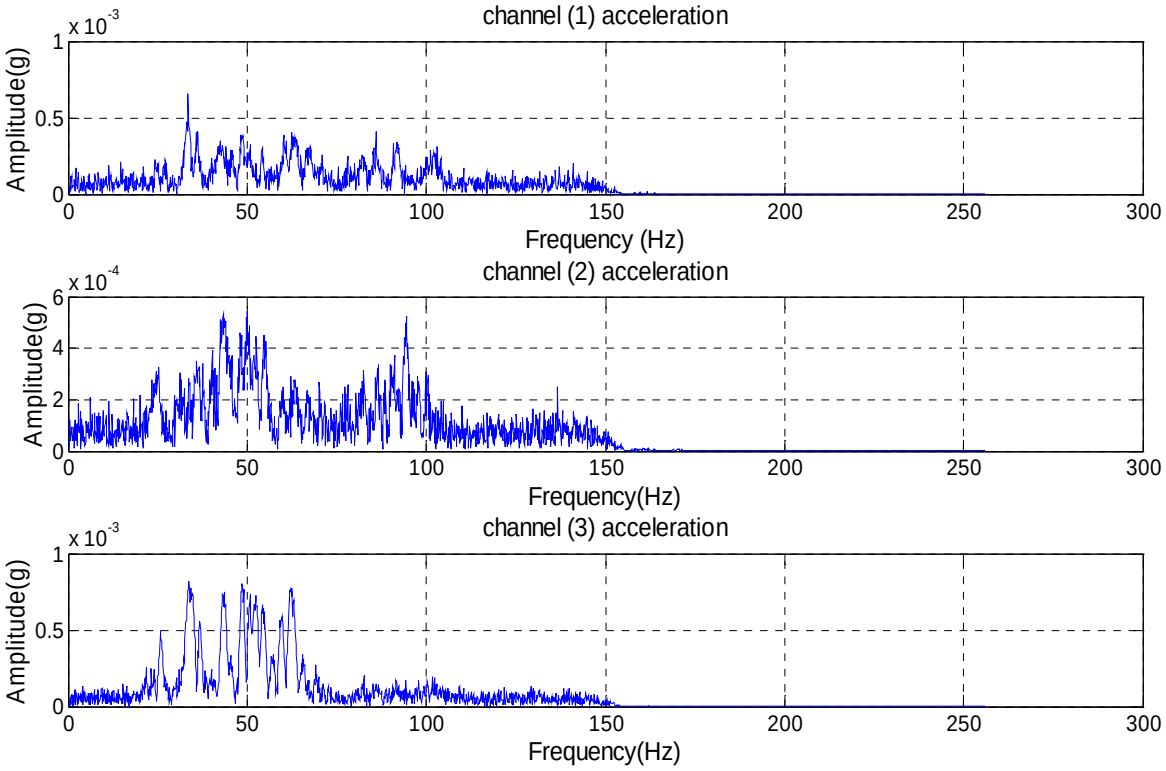

Figure 3.6: U5 acceleration in frequency domain after application of the FIR filter

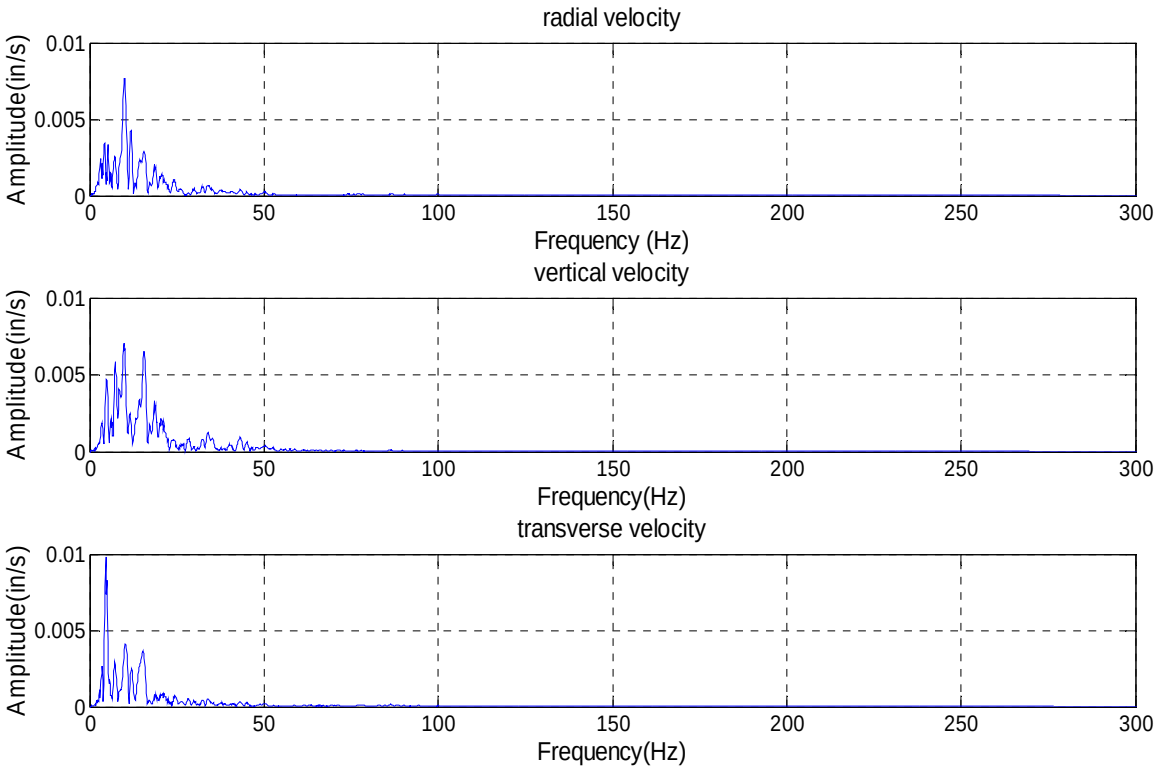

Figure 3.7: R5 velocity record in frequency domain

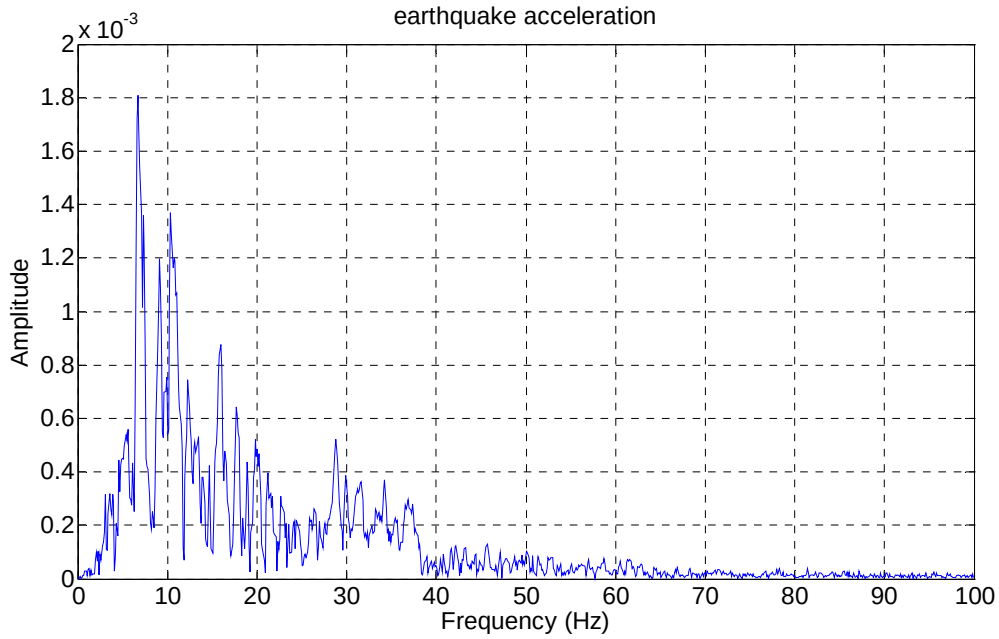

(a)

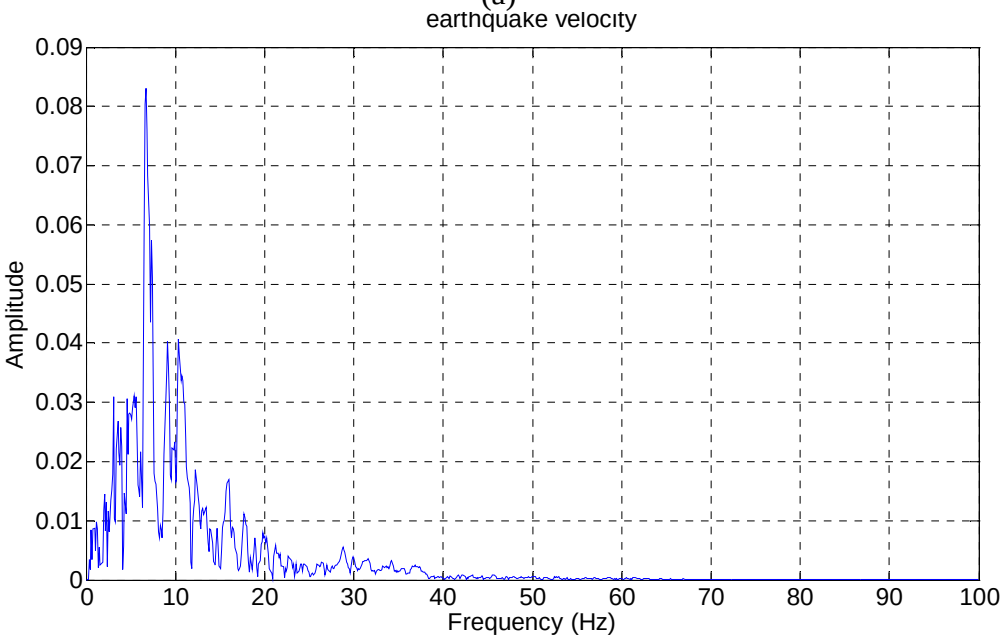

(b)

Figure 3.8: Spectrum of a natural earthquake at Georgia: (a) acceleration (g); (b) velocity (in/s)
(Data source: http://peer.berkeley.edu/smcat/)

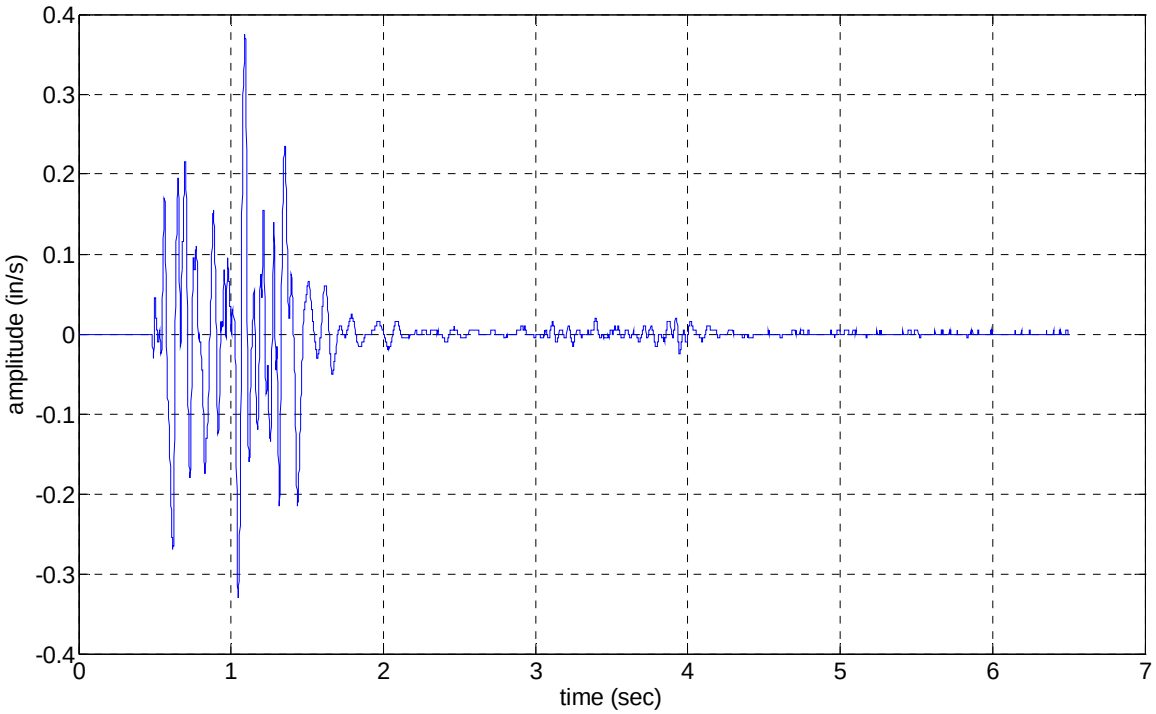

Figure 3.9: The vertical velocity signal of R5 record

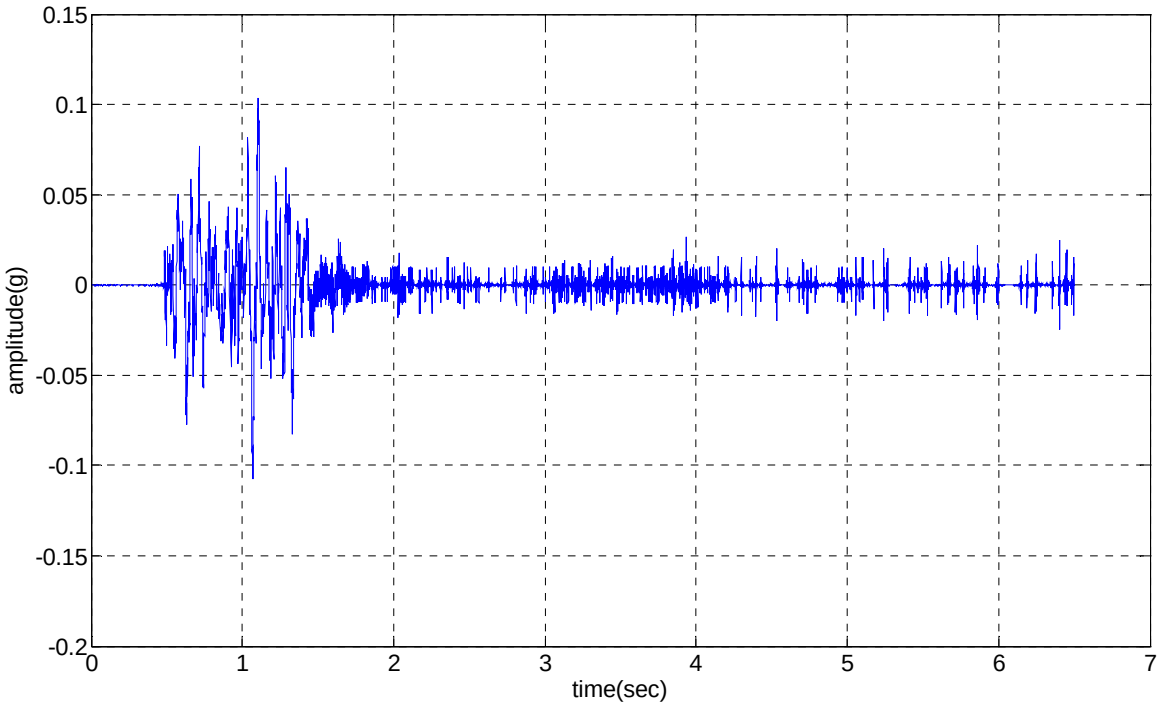

Figure 3.10: Differentiation of R5 velocity signal using time domain method

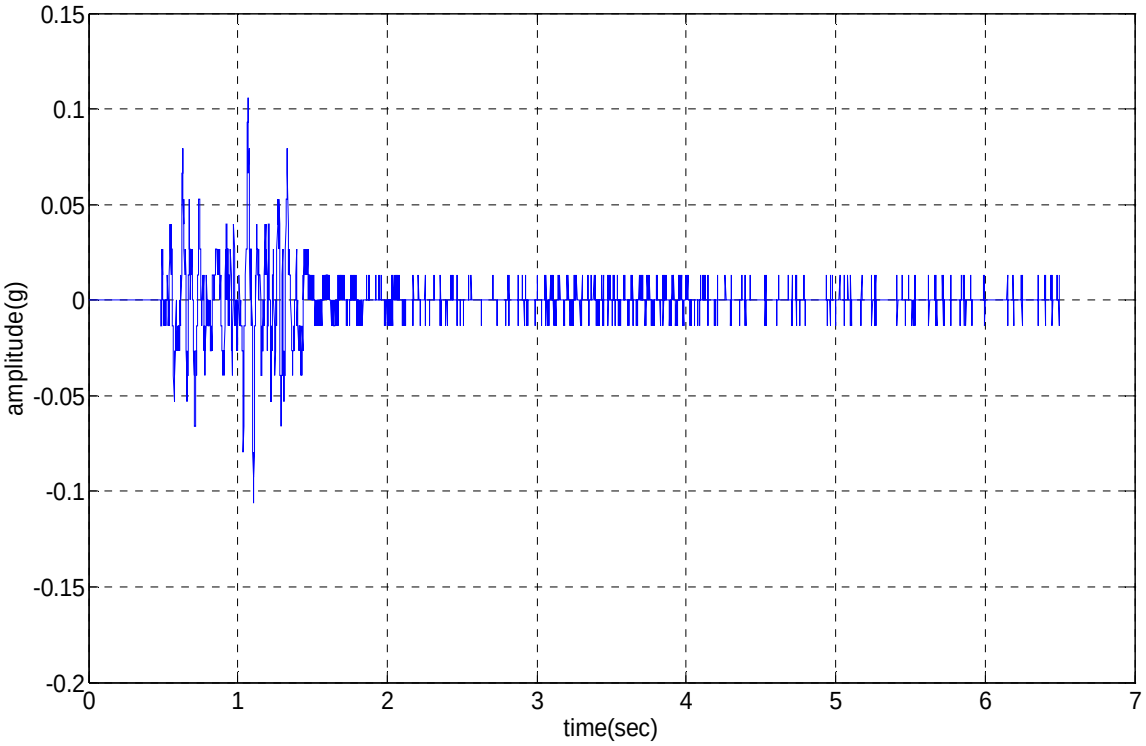

Figure 3.11: Differentiation of R5 velocity signal using frequency domain method

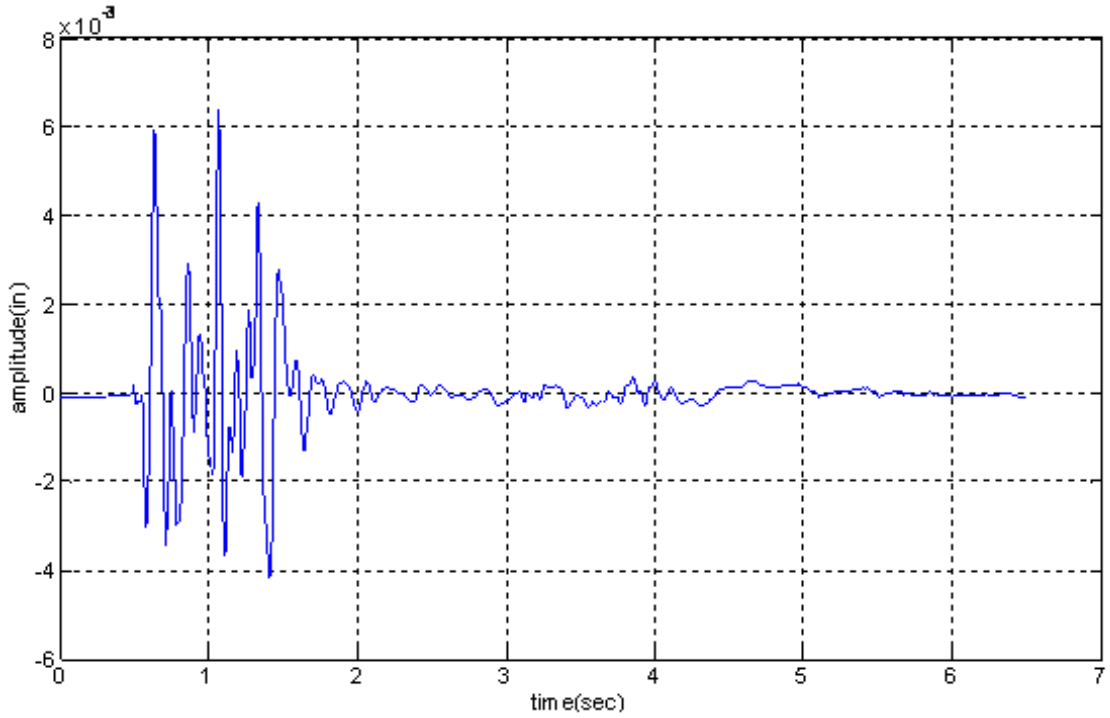

Figure 3.12: Integration of R5 velocity signal using time domain method

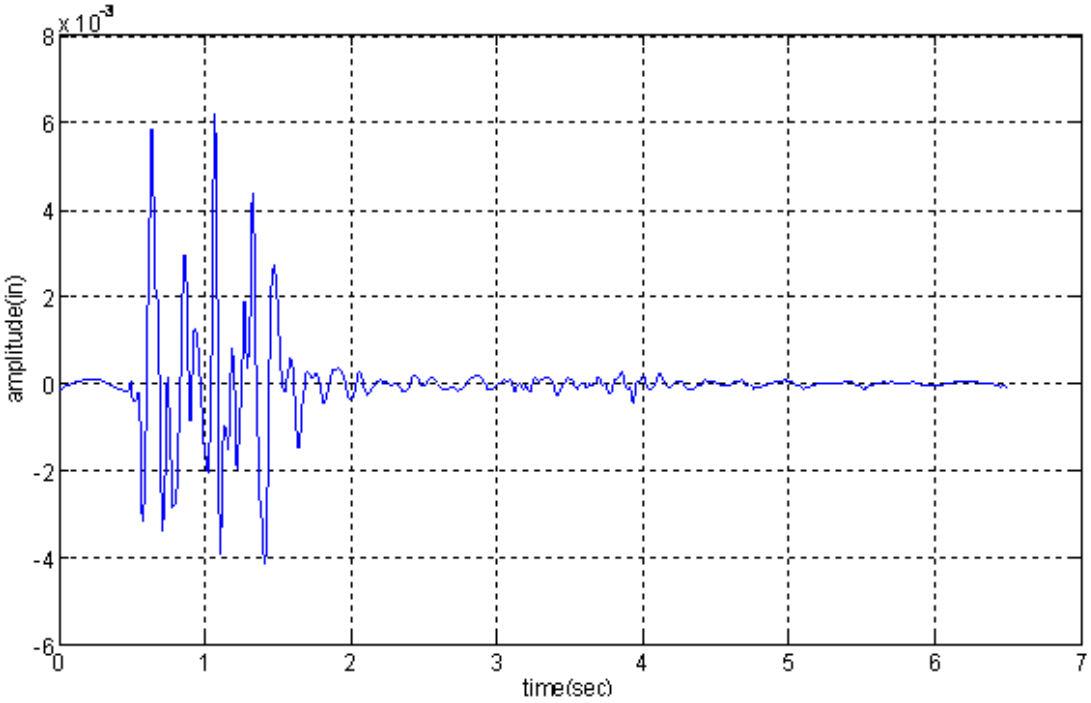

Figure 3.13: Integration of R5 velocity signal using frequency domain method

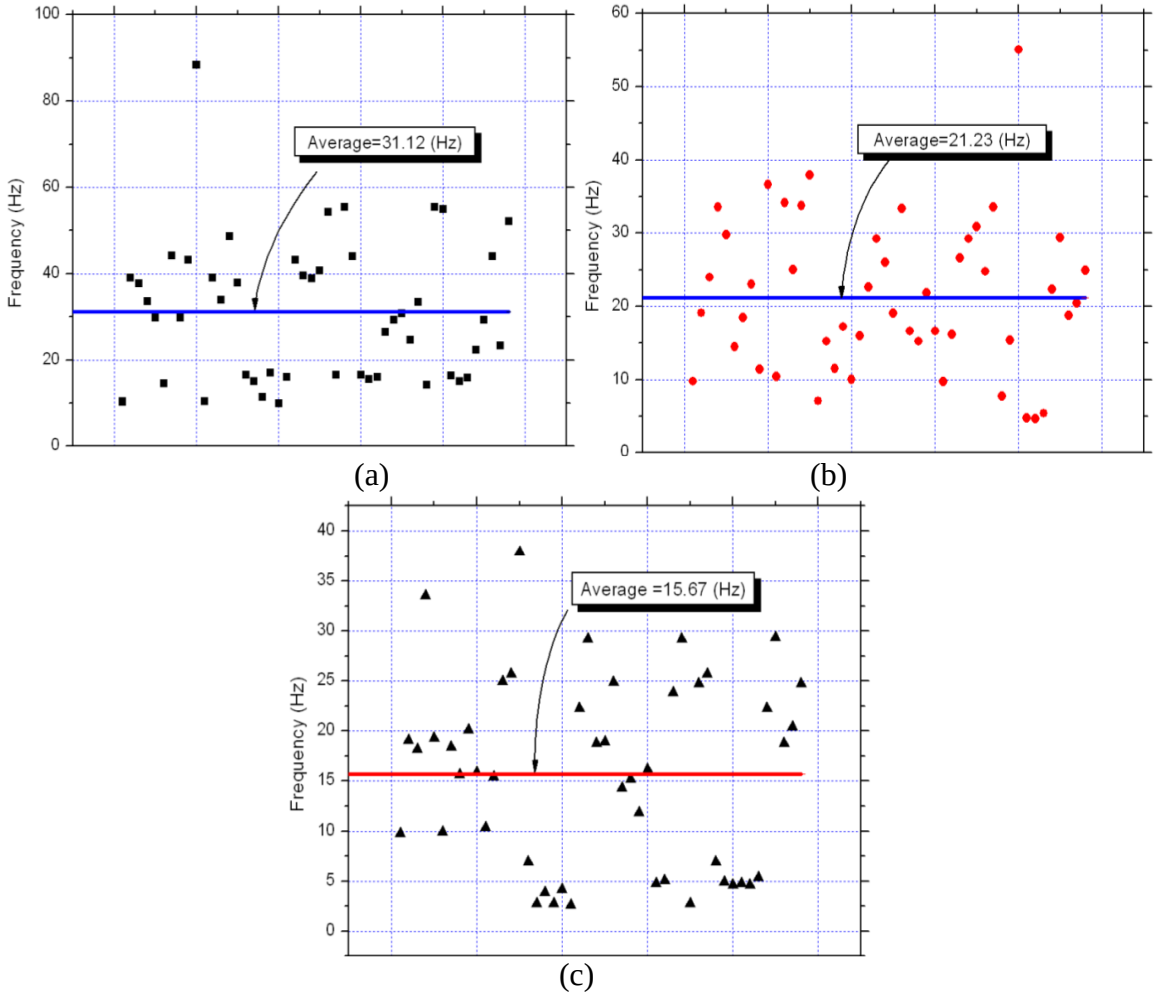

Figure 3.14: Frequency distribution for: (a) PPA; (b) PPV; and (c) PPS

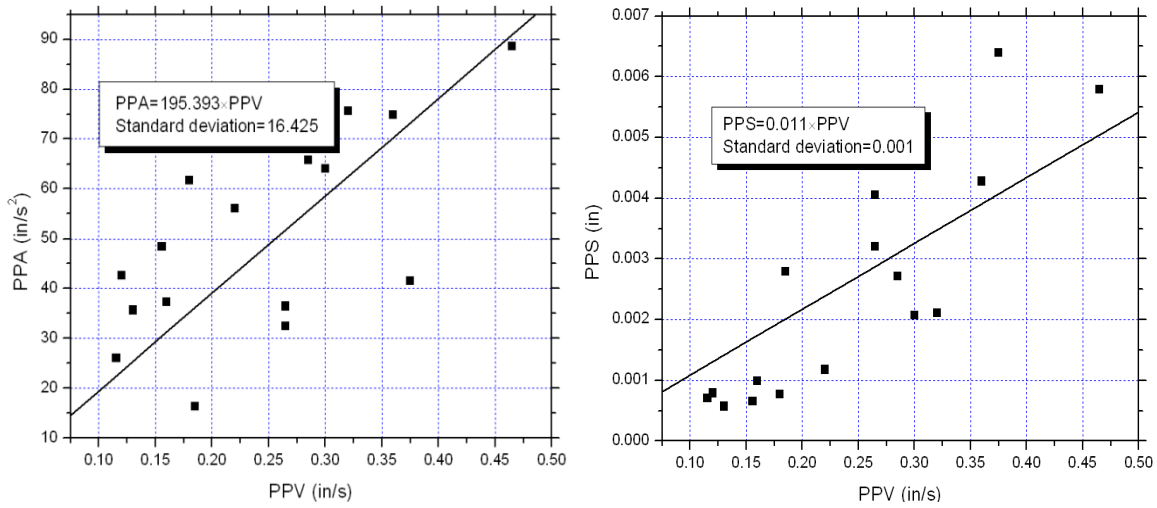

Figure 3.15: Empirical relations between PPV, PPA and PPS

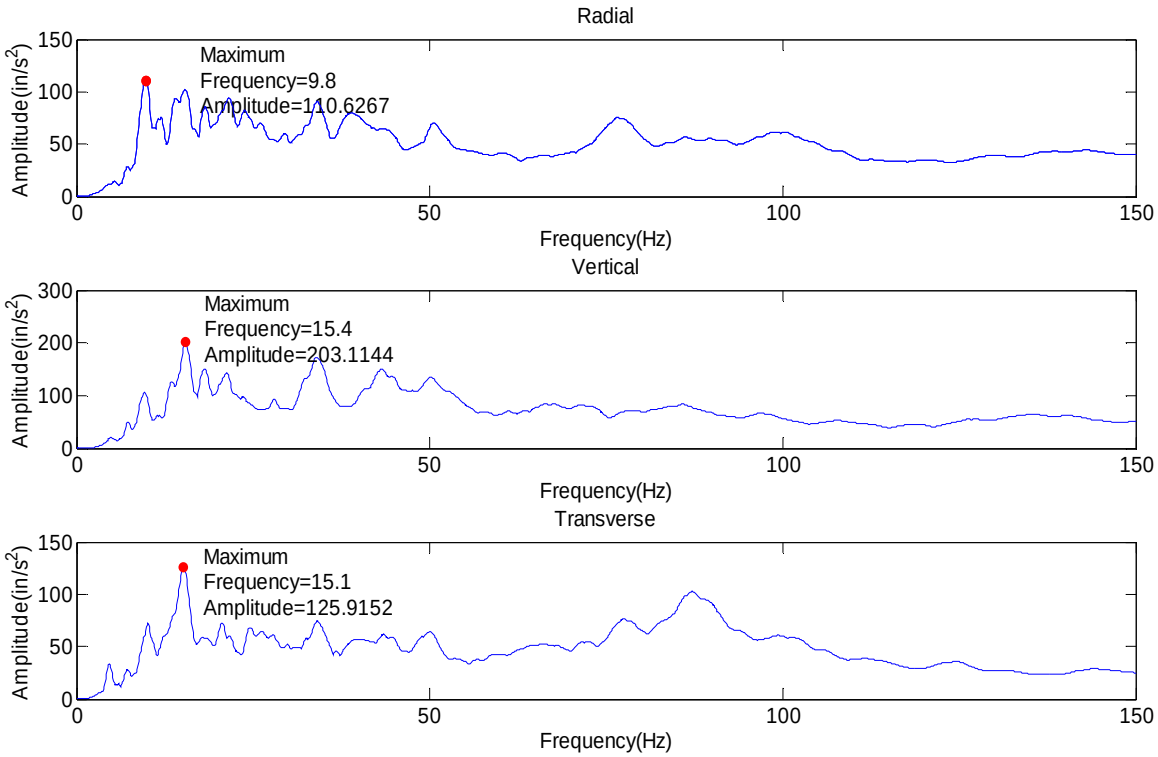

Figure 3.16: Response spectrum for R5 acceleration

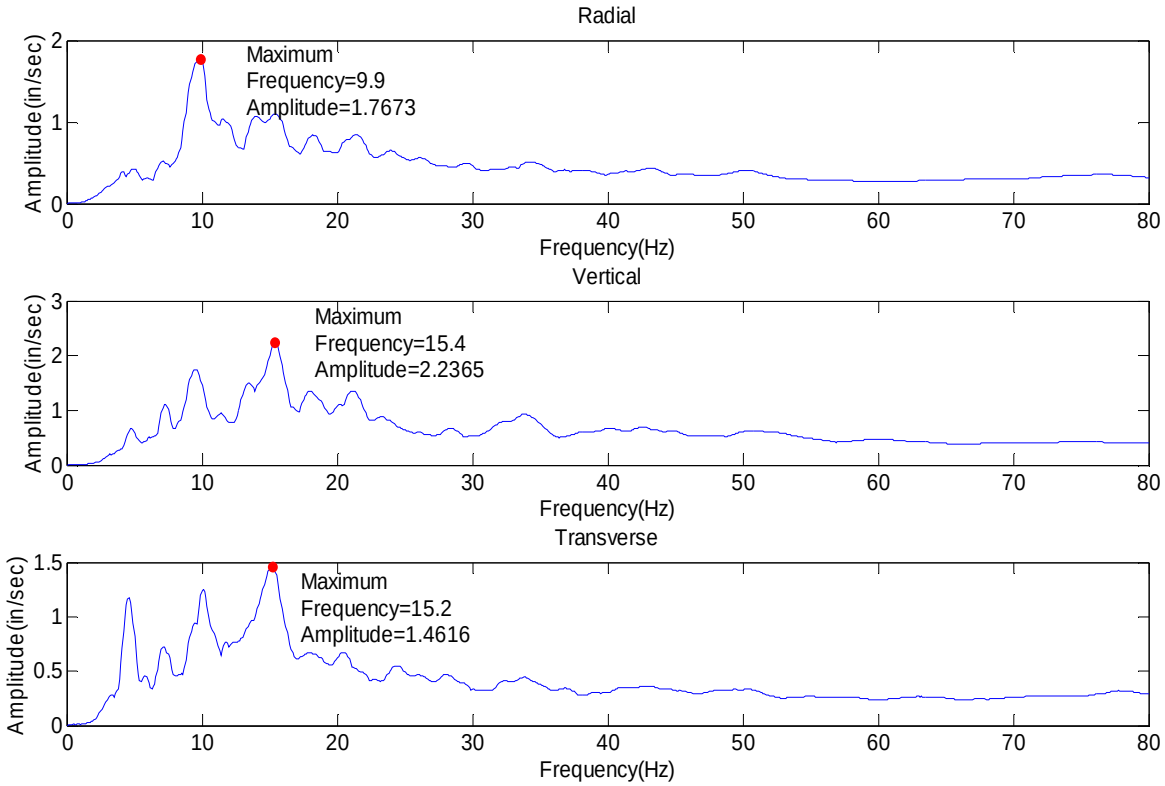

Figure 3.17: Response spectrum for R5 velocity

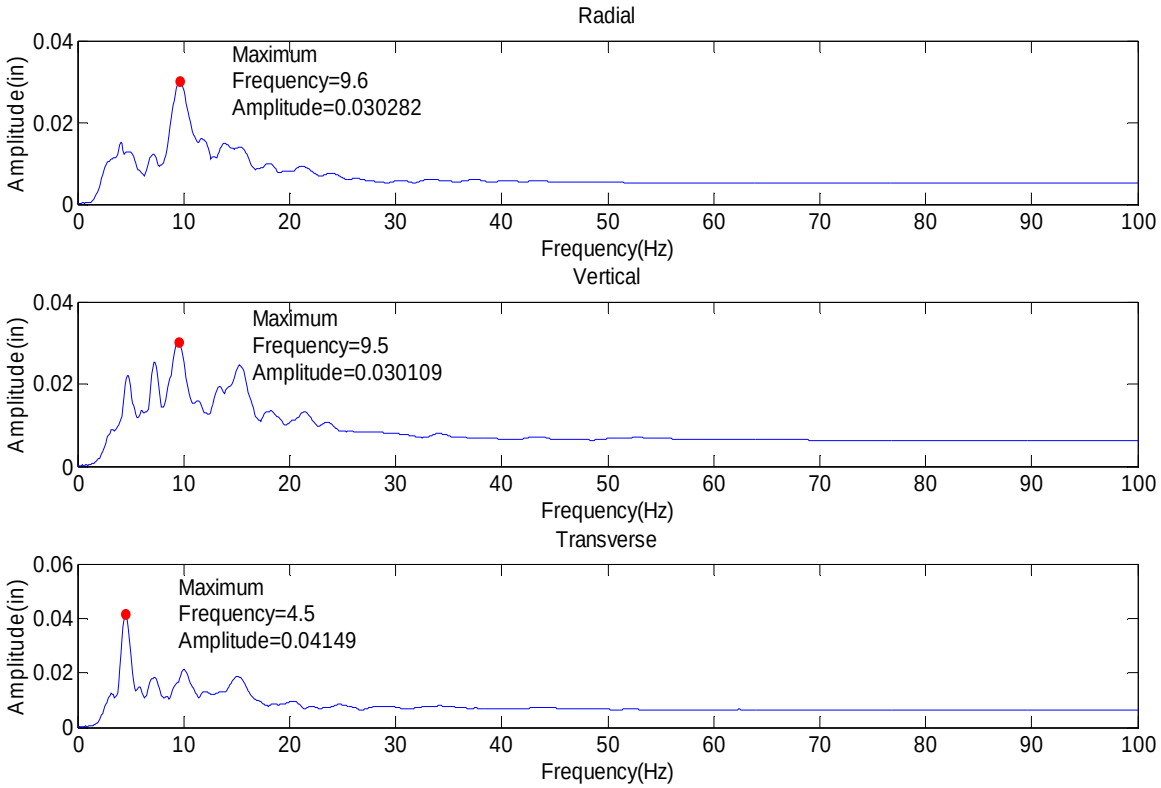

Figure 3.18: Response spectrum for R5 displacement

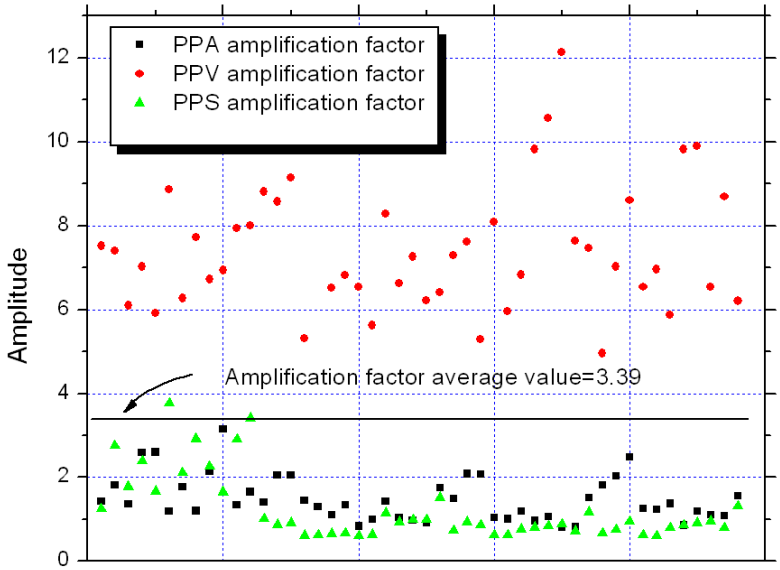

Figure 3.19: The average value of amplification factors

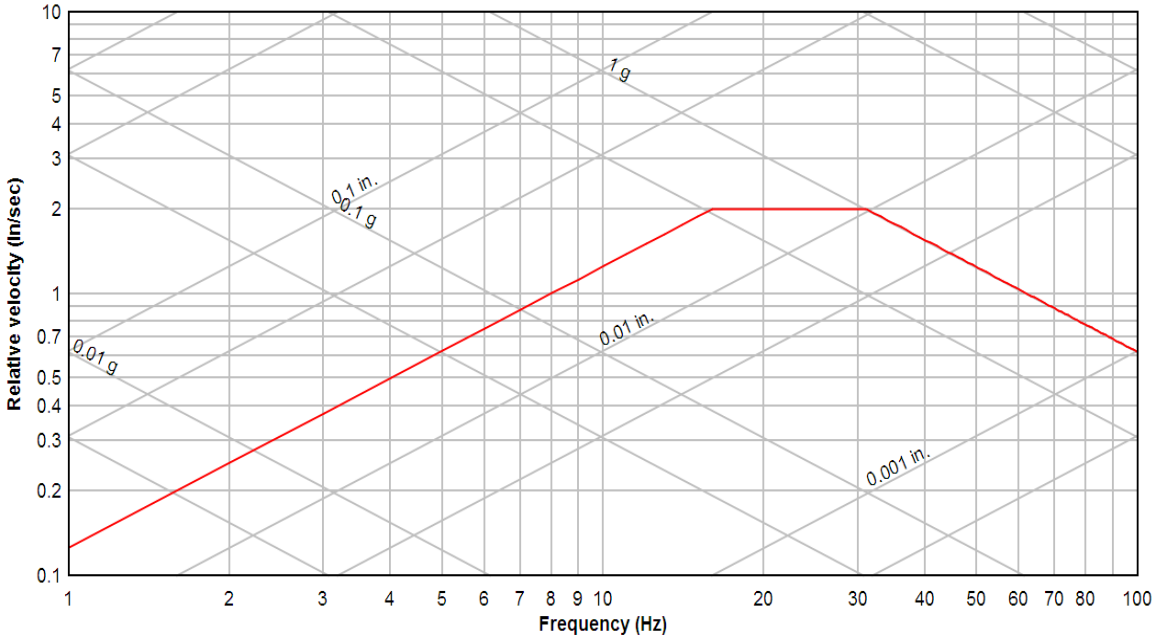

Figure 3.20: Predicted ground motions based on 2 in/s PPV criterion

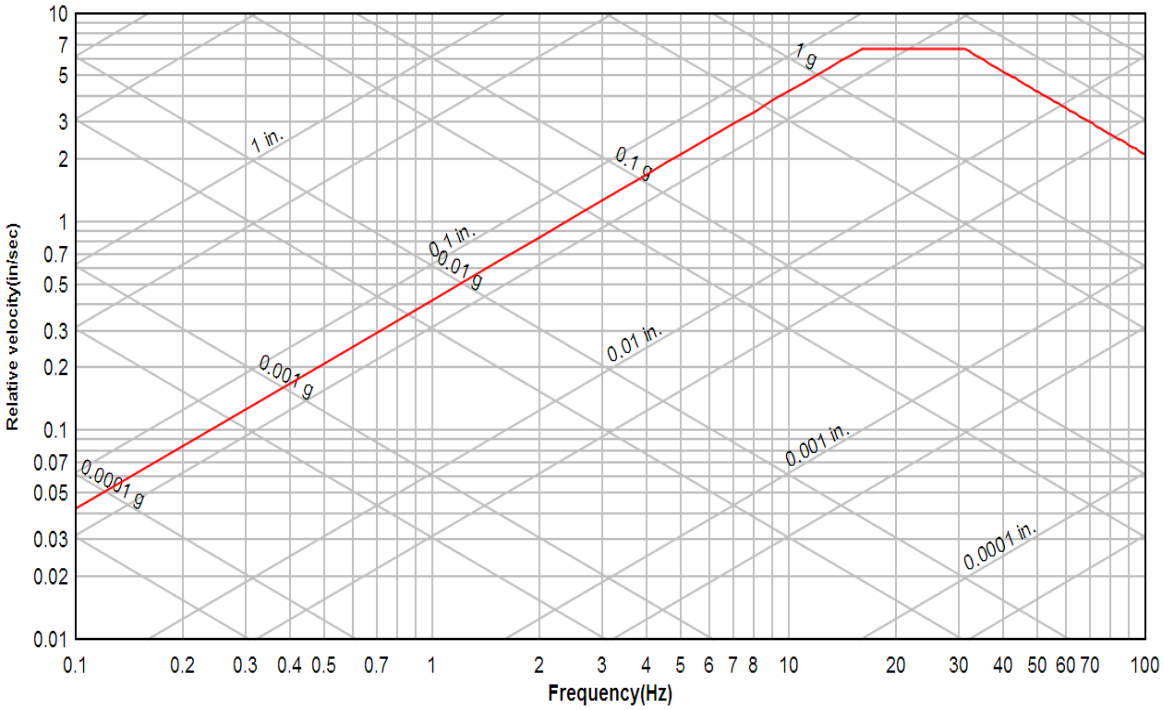

Figure 3.21: Design response spectrum based on 2 in/s PPV criterion

Table 3.1: Summary of selected blast records

Record	*Data type*	*Site*
U1	Acceleration time history	A
U2	Acceleration time history	B
U3	Acceleration time history	B
U4	Acceleration time history	B
U5	Acceleration time history	B
R1	Velocity time history	A
R2	Velocity time history	A
R3	Velocity time history	A
R4	Velocity time history	A
R5	Velocity time history	A
R6	Velocity time history	A
R7	Velocity time history	B
R8	Velocity time history	B
R9	Velocity time history	B
R10	Velocity time history	B
R11	Velocity time history	B

Table 3.2: Peak values of signals recorded with wireless accelerometers

Record	*channel 1*			*channel 2*			*channel 3*		
	PPA (in/s^2)	PPV (in/s)	PPS (in)	PPA (in/s^2)	PPV (in/s)	PPS (in)	PPA (in/s^2)	PPV (in/s)	PPS (in)
U1	16.3623	0.1848	0.0028	13.3692	0.1086	0.0014	9.5732	0.1073	0.0014
U2	22.4293	0.0995	0.0005	26.1046	0.1155	0.0007	18.0242	0.0710	0.0004
U3	37.3167	0.1600	0.0010	32.0862	0.1297	0.0009	28.8242	0.1574	0.0010
U4	26.0213	0.0893	0.0003	35.2167	0.1074	0.0004	35.6900	0.1303	0.0006
U5	48.3594	0.1214	0.0005	34.7805	0.1279	0.0004	45.8623	0.1557	0.0007

Table 3.3: Peak values of signals recorded with geophones

File name	*Radial*			*Vertical*			*Transverse*		
	PPA (in/s^2)	PPV (in/s)	PPS (in)	PPA (in/s^2)	PPV (in/s)	PPS (in)	PPA (in/s^2)	PPV (in/s)	PPS (in)
R1	42.4742	0.3200	0.0058	88.5661	0.4650	0.0049	55.9770	0.2900	0.0042
R2	30.4873	0.2150	0.0043	74.8431	0.3600	0.0028	40.1113	0.1800	0.0021
R3	41.0648	0.2000	0.0027	57.8273	0.2850	0.0024	65.8390	0.2400	0.0022
R4	19.6262	0.1600	0.0023	32.4483	0.2650	0.0030	19.8486	0.1650	0.0032
R5	33.0622	0.2700	0.0051	41.6164	0.3750	0.0064	26.3073	0.2100	0.0062
R6	29.3380	0.2500	0.0041	36.4633	0.2650	0.0025	23.2745	0.2050	0.0020
R7	67.5367	0.2800	0.0016	75.5914	0.3200	0.0021	70.0913	0.2600	0.0017
R8	52.7385	0.2200	0.0011	54.4310	0.2000	0.0012	56.0255	0.1800	0.0011
R9	39.6927	0.1200	0.0007	42.6915	0.1200	0.0008	38.0564	0.1000	0.0007
R10	64.0132	0.2000	0.0012	60.4789	0.3000	0.0021	47.9476	0.1600	0.0013
R11	61.6753	0.1600	0.0007	57.8441	0.1800	0.0008	51.6437	0.1600	0.0007

CHPATER 4: FREE VIBRATION CHARACTERISTICS OF THE TRANSMISSION POLE STRUCTURE

4.1 Introduction

Free vibrations of a structure, also known as modal behaviors, yield valuable information about the inherent dynamic characteristics of the system in the formats of natural frequencies, mode shapes and damping. Studies on free vibration of transmission poles are limited: Lantrip (1995) and Chen et al. (2006) reported modal tests as well as FE analysis on concrete poles; Polyzois et al. (1998) studied composite poles by using the finite element method to obtain natural frequencies. All of the above studies are based on free-free or cantilevered beam models. In reality, however, depending on the rigidity of the direct embedment foundation, the boundary condition may or may not be assumed to be fixed.

This chapter reports research results from a series of tests on modal behaviors of a tubular steel pole structure and three prestressed concrete poles. Modal testing was conducted by impact excitation to seek eigensolutions of the pole vibration. Modal analysis was also executed through finite element modeling. The influences of some physically significant parameters on modal characteristics of concrete poles were numerically investigated. Investigative modeling work was also performed on two operational transmission lines. Simplified computational models were developed for the coupled transmission system based on the method proposed by Li et al. (2005).

The results of this work pave the way for the study of dynamic responses of transmission structures under blast induced ground vibration.

4.2 Modal testing of transmission pole structures

4.2.1 Testing program I

Modal testing is an experimental technique that involves measuring frequency response functions (FRF) of a structure. Modal testing using impact excitation can obtain FRFs that contain necessary information about a system in forms of natural frequencies, mode shapes and damping factors. In this study, impact modal testing was conducted on two prestressed concrete poles (Table 4.1). The tests were performed by fixing response location (output from the sensor) and roving force excitation points (input from the hammer). Testing configurations include suspended, simple-supported, and direct-embedded poles (Figures 4.1, 4.2). The equipments consist of accelerometers, a data acquisition system, and an instrumented hammer. The FRFs were then processed to extract modal parameters such as natural frequencies and corresponding mode shapes (Figure 4.3). The identified eigen-frequencies of the pole vibration are listed in Table 4.2. Figure 4.4 gives the representative mode shapes of two different test configurations. Mode shapes from CP1 and CP4 are not shown here since they are similar to those of CP2 and CP3.

4.2.2 Testing program II

Two in-operation pole supported transmission lines were experimentally studied (Figure 4.5). The steel pole (OSP) is used in a 115 kV double-circuit transmission line section. The concrete pole (OCP) is the support structure in a 46 kV power line. These

two lines are in close distance to each other. Both poles are directly embedded. The steel pole is also guyed with four cables.

Full-scale impact modal testing was conducted on both these poles. The experimental design and equipments used in the testing are similar to those conducted on concrete poles in test program I. Since ground movements are transmitted through the buried end of the pole, unlike wind loads, which stimulate any part of the electric power grid, more interests were devoted to measure the pole structural responses. With one accelerator attached on the pole, multi-point impacts were applied along the pole with an instrumented hammer. The free vibration behaviors of these two poles were extracted from their FRFs. Identified natural frequencies are listed in Table 4.3. Due to strong coupling phenomena in the steel pole, especially guy wire effects, its modal behaviors are not very well derived.

4.3 Modal sensitive parameter study of transmission concrete poles

The finite element modeling technique has been proven to be an effective tool to study vibration behaviors of transmission structures. The influences of physically significant parameters on modal characteristics of transmission poles were numerically examined by studying a 95 feet pole (CP1) and the concrete pole in the operation power line (OCP).

4.3.1 Numerical study of a 95 feet concrete pole

The 95 feet concrete pole in test CP1 was numerically analyzed. Material properties and geometry information for the original model are listed in Tables 4.4 and 4.5. Concrete and prestress strands were respectively modeled with solid elements (SOLID65) and truss elements (LINK8) provided in ANSYS, whereas the spiral wires were smeared

into concrete by their volume ratio along the pole length (Figure 4.6). Nonlinear static analysis and modal analysis were conducted sequentially so as to include prestress effects into eigen-solutions of the pole vibration (ANSYS 2005).

Modal analysis was conducted with varied prestressing forces in order to investigate sensitivity of frequency to prestress level. The resulting correlation between prestress force change and corresponding natural frequencies is shown in Figure 4.7, which indicates that prestress is not a very sensitive parameter for frequency shifts. Previous studies (Dallasta and Dezi 1996; Deak 1996; Hamed and Frostig 2006; Jain and Goel 1996) explained the prestress effect on the natural frequency; Generally speaking, prestress effects can be neglected during numerical elastic modal analysis of prestressed concrete structures for practical purposes.

Concrete strength sensitivity was then studied by adjusting the concrete modulus of elasticity, which was obtained through Equation (4.1) (PCI 2004). The correlation between change of concrete strength and natural frequencies of pole vibration is shown in Figure 4.8. It was found that eigenfrequencies of the pole vibration deviate within 13% range when concrete strength varies from -40% to 30% of its original value (11000 psi).

$$E_c = \left(40000\sqrt{f_c'} + 1.0 \times 10^6\right)\left({}^{w_c}/_{145}\right)^{1.5} \quad (psi) \tag{4.1}$$

where: E_c (psi) is concrete modulus of elasticity; f_c' (psi) is concrete compressive strength, and w_c (lb/ft^3) is concrete density.

To study effects of boundary conditions, linear springs (COMBIN14) were added to the original FE model at the location of the supports. It was found that, for similar mode shapes, natural frequencies increased with an increase of spring stiffness (k) (Figure 4.9). For example, the fundamental frequency at k=10000.00 lb/in is 5.60 Hz while at

k=1000.00 is 3.10 Hz. Different spring stiffness brought changes in the boundary condition, which to some degree introduced changes to mode shapes.

4.3.2 Numerical study of a 35 feet concrete pole

Most pole structures are directly embedded. Special attention is given to the study of soil-structure interaction effects on dynamic behaviors of the prestressed concrete pole.

Transmission poles can be generalized as tapered-end, round beams made of steel or concrete with prestressed and normal reinforcements. Thus far, modal studies on transmission poles have been mostly conducted on suspended poles (Lantrip 1995) or simple supported poles (Chen et al. 2006). Although Chen et al. (2006) also performed experimental modal analysis on an embedded concrete pole, the testing was restricted to only single-point impact and mode shapes were not obtained. Also, fixed end boundary was assumed in their numerical models. However, the cantilever-beam assumption may not always be representative of the true boundary conditions which is typically a function of the stiffness of surrounding soil (Bhattacharya and Dutta 2004; Sanayei et al. 1999).

The direct embedment foundation used for transmission poles is somewhat similar to that of drilled shaft foundation. Loading conditions may include high overturning moments with relatively low axial and lateral shear loads. Soil-structure interaction (SSI) effects could be considered as soil springs, which represent the stiffness of annular material. Rojas-Gonzalez et al. (1991), for example, utilized the four-spring nonlinear subgrade modulus model to predict the load-deformation of direct embedded poles.

With linear elastic assumption, soil-structure interaction can be modeled as a set of linear translational and rotational springs and dampers, which represent surrounding annular material (backfill materials and soil). Assuming [K] is the system stiffness

matrix, which is composed of pole structure stiffness matrix ($[K_p]$) and linear soil spring stiffness matrix ($[K_s]$). The governing equation for basic structural dynamic behaviors of the pole can be expressed as Equation (4.2), in the form of mass and stiffness matrices:

$$[M_p]\{\ddot{x}\} + [K_p]\{x\} = \{R\} \tag{4.2}$$

where $[M_p]$ is the mass matrix of the pole; and $\{R\}$ is the boundary reaction.

Eigensolutions to the pole system can then be obtained by solving:

$$([K] - \omega^2[M_p])\{\varphi\} = \{0\} \tag{4.3}$$

where ω is natural frequency of the pole with soil-spring boundary conditions, and $\{\varphi\}$ is the corresponding mode shape vector. The matrix calculation can be performed through numerical methods, such as FE modeling.

Modal behaviors of the embedded concrete pole were simulated using the finite element modeling technique. Eigenvalue analysis was performed using commercial software - ANSYS (2005). The pole structure was modeled using tapered beam elements (BEAM189). The input information, including geometry of the pole, Young's modulus (E) and mass density (ρ) are listed in Table 4.6.

SSI effects were studied by adding a series of liner elastic massless springs (COMBIN14). Assuming small deformation and linear elasticity, a four-spring Winkler model (Figure 4.10) was used to define these springs. The influence of backfill-material in combination of surrounding soil was considered by the approximate relations in Equations (4.4) and (4.5) (Gerolymos and Gazetas 2006). The base springs in the model were further simplified as vertical restraints-this is because directly embedded poles usually have very small base areas, thus, providing very little rotational resistance. For

the modal testing procedure described earlier, there is no excitation in the torsional direction, hence rotational behavior is assumed as non-existent.

$$k_h^s \approx 1.75 \left(\frac{H_B}{D_B}\right)^{-0.13} E_S \tag{4.4}$$

$$k_\theta^s \approx 0.85 \left(\frac{H_B}{D_B}\right)^{-1.71} E_S H_B^2 \tag{4.5}$$

where k_h^s (lb/in^2) and k_θ^s (lb) are spring constants for translational and rotational springs along the buried pole, respectively; E_S (psi) is modulus of elasticity of the backfill-material/soil; H_B (in) is buried depth; and D_B (in) is the average diameter of buried portion of the pole.

Through adjusting soil spring stiffness; more specifically, modifying soil modulus of elasticity (E_S) in Equations (4.4) and (4.5), modal characteristics of the pole with different embedment conditions were obtained by using finite element analysis.

Figure 4.11 shows changes in the eigenfrequencies for first three bending modes with different soil springs. Natural frequencies are shown to increase as soil springs stiffens. This is obvious especially when elastic moduli of soil springs (E_S) are small. Higher modes are shown to be more sensitive to the boundary fixity. The result also indicates that the cantilevered beam ($E_S \rightarrow \infty$) assumption is not always valid for the pole, especially for higher frequency modes, which can be observed by comparing the test results with numerical solutions of different soil spring stiffness (Figure 4.11).

Stiffness variance of the directly embedded foundations also has influence on mode shapes for the vibrating poles (Figure 4.12). When there is a big discrepancy in soil spring stiffness, such as $E_S = 0.5$ (ksi) and $E_S = 15$ (ksi), normalized displacements of

the same modes do not have same shape functions. This is especially true for higher modes that are sensitive to boundary conditions.

4.4 Development of simplified FE models for transmission pole structures

4.4.1 Coupled system of the transmission structure

The interaction between support structures and cables in transmission grids is very complicated. Measurements from a full-scale transmission tower have indicated that conductors affect vibration of the towers (Momomura 1997). The long spanning feature of transmission lines makes it difficult for physical experimentations. Due to cost and safety associated with large scale testing, numerical analysis is widely used by researchers to study dynamic characteristics of transmission structures. Detailed modeling, can also be time consuming and computationally expensive, hence, researchers have proposed various methods to study the coupled system of transmission lines, which consist of support structures (towers or poles) and cables. Ozono et al. suggested simplified models for in-plane vibration of transmission systems (Ozono et al. 1992; Ozono et al. 1988), where conductors were modeled as massless springs. Based on structural characteristics of the transmission line, Li et al. (2005) proposed simplified models for in-plane and out-of-plane vibration of the transmission tower-line system. The coupling effects for the out-of-plane model are mainly reflected by rigidity matrix while mass matrix is main modification for the in-plane model when considering conductor influence (Li et al. 2005):

out-of-plane vibration:

$$[M] = \begin{bmatrix} [M]_{line} & [M]_{tower} \end{bmatrix}^T$$

$$[K] = \begin{bmatrix} [K]_{line} & [K]_{coupling} \\ [K]_{coupling}^T & [K]_{tower} \end{bmatrix} \tag{4.6}$$

in-plane vibration:
$$[M] = \begin{bmatrix} [M]_{line} & [M]_{coupling} \\ [M]_{coupling}^{T} & [M]_{tower} \end{bmatrix}$$
$$[K] = \begin{bmatrix} [K]_{line} & [0] \\ [0]^{T} & [K]_{tower} \end{bmatrix} \quad (4.7)$$

where $[M]$ and $[K]$ are mass and stiffness matrices of the coupled system; $[M]_{tower}$ and $[K]_{tower}$ are mass and stiffness matrices of the tower, respectively; $[M]_{line}$ and $[K]_{line}$ are mass and stiffness matrices of cables; and $[M]_{coupling}$ and $[K]_{coupling}$ are mass and stiffness matrices generated by tower-line interactions.

For the purpose of structural dynamic analysis under earthquakes, Li et al. (2005) further simplified conductor effects by adding mass Δm. The comparison study performed on this approach demonstrated acceptable accuracy for seismic response computation.

Considering the fact that both blasting and earthquakes introduce threats to power grids through exciting support structures (towers or poles), the simplified models put forward by Li et al. (2005) have promising application in pole dynamic response analysis under blasting induced ground motions. Their models were tailored by adding soil springs to investigate boundary effects.

4.4.2 Characterization of pole direct embedment foundations

The Spectral Analysis of Surface Waves (SASW) technique was developed as an in-situ seismic testing method. Applications of this nondestructive testing technique have been found in various fields, such as pavement (Nazarian et al. 1988) and concrete (Cho 2003). Chen et al. introduced the SASW technique into the transmission line survey and design (Chen et al. 2004; Ong et al. 2006). Their research indicated the potential of applying such a methodology for the power industry.

The SASW method depends on the measurement of Rayleigh wave propagation over a wide range of frequencies. Schematic figure (Figure 4.13) shows a typical field test setup. A vertical excitation at the ground surface generates transient surface waves. Two receivers are placed on the ground surface to record these excited waves. The spacing of these two sensors (L) is equal to the distance between the impact source to the nearest receiver. Each recorded time series signal from the receivers is transformed into frequency domain by Fourier transformation. The phase difference between two signals is then determined and travel time (t) between the two receivers at each frequency can be obtained as (Ong et al. 2006):

$$t = \frac{\emptyset}{2\pi f} \tag{4.8}$$

where $\emptyset$ is phase difference at a given frequency f.

The surface wave velocity (V_s) can be obtained from Equation (4.9), where L is distance between the two receivers.

$$V_s = \frac{L}{t} \tag{4.9}$$

The corresponding wavelength (λ) is determined by:

$$\lambda = \frac{V_s}{f} \tag{4.10}$$

Calculations are performed at each applied frequency and result in dispersion curves. These dispersion curves are then used to determine the theoretical shear wave velocity profiles through an iterative process of fitting the experimental dispersion curve to the assumed theoretical shear wave velocity curve. The theoretical shear wave velocity profile corresponds to the maximum shear modulus at small strains of the test site (Kim et al. 2001).

When the SASW testing is performed at the vicinity of the embedded pole, the resultant shear wave velocity is assumed to approximately indicate the quality of embedment foundations. The mean shear wave velocity (V_s) from SASW testing was calculated using:

$$\overline{V_s} = \frac{\sum_{i=1}^{n} d_i}{\sum_{i=1}^{n} \frac{d_i}{V_{si}}} \tag{4.11}$$

where d_i and V_{si} are thickness and shear wave velocity for each layer, respectively; n is the number of layers.

Although the testing depth did not reach 100 ft, NEHRP site classification (BSSC 2004) was referred to define soil property of the testing location. The resultant $\overline{V_s}$ is 1480.55 fps and the site is classified as very dense soil. Elastic constant (E_s) of the soil springs along embedded pole was estimated as 160 ksi.

4.4.3 Numerical analysis of the coupled transmission pole-line systems

Modal analysis of the tested operational transmission lines was conducted using the finite element method. Eighteen different models with varied degree of details were created (Table 4.7). The coupled transmission line sections with two spans of conductors in the models were created either through detailed modeling (poles, all cables, insulators, and arms) or using simplified models proposed by Li et al. (2005), which count conductor effects into the models by adding mass calculated from:

$$\Delta m = f(l) \times l \times q \tag{4.12}$$

where Δm is the additional mass of the pole when considering conductor effects; l is the horizontal distance between two poles; q denotes the conductor mass of a unit length; and $f(l)$ is a factor determined from Equation 4.13:

out-of-plane:

$$f(l)=\begin{cases}0.17+{}^{3l}/_{200l_0} & soft\\ 0.21+{}^{l}/_{100l_0} & mid-hard\\ 0.35+{}^{l}/_{20l_0} & hard\end{cases}\quad(\text{if } f(l)>0.7,\text{ then } f(l)=0.7)\qquad(4.13)$$

in-plane:

$$f(l)=0.5+\frac{l}{200l_0}\quad\text{at all sites}\qquad(\text{if } f(l)>1.0,\text{ then } f(l)=1.0)\qquad(4.14)$$

in which l_0 is the limit span; when the span exceed this value, cable effects need to be considered. For example, l_0=656.00 feet for the mid-hard site.

Using ANSYS (2007), the pole structures were modeled with tapered beam elements (BEAM189) for all the models. For the coupled pole-line systems: the cables, including conductors, shield wires, and guy wires, were modeled with tension-only truss element (LINK10); insulators were generated with uniaxial spar element (LINK8); and arms that connect insulators and pole structures were modeled with elastic beam elements (BEAM4) or spar element (LINK8), depending on the joint type. When SSI is considered, no-mass spring elements (COMBIN14) were added to the tampered beams' nodes along the pole burial length. Geometric and material information for these two poles either provided by the industry partner or through available documentation (Bansal et al. 1995; Kálmám et al. 2007; Kumosa et al. 2002; McClure and Lapointe 2003; Shehata et al. 2005) were referred to. These properties were listed in Tables 4.8 and 4.9. From SASW results, the testing site was determined to be stiff soil. Therefore, in the models of CPE, CPF, SPG, SPH, SPI, SPJ, SPK and SPL, additional mass factor was calculated from Equation (4.13). Soil elastic constant (E_S) was estimated as 160 ksi for the soil springs in the models that considered SSI (CPB, CPD, CPF; SPB, SPD, SPF, SPH, SPJ, SPL).

Pole-line system models were shown in Figure 4.14. Modal analysis was directly conducted for the isolated pole models (CPA, SPB; SPA, SPB, SPG and SPH) and simplified pole-line system models (CPE, CPF, SPG, and SPH). For detailed pole-line system models (CPC, CPD, SPE, and SPF) and the guyed steel pole structure (SPC, SPD, SPI and SPJ), nonlinear static analyses were first conducted to sag the cables (conductors, shield wires, and guy cables of the steel pole) (Figure 4.14). The sag-to-span ratio was estimated from maximum sag divided by span of the cable. The sag ratio values for conductors were approximately 0.04 and 0.03 for shield wires in CPC/CPD models. In SPE/SPF models, the sag ratio values were 0.05 for conductors and 0.02 for shield wires. Mass elements (MASS21) were added at the nodes where cables connect the main structure in the simplified models (CPE, CPF; SPG, SPH, SPI, SPJ, SPK and SPL). The guy cables in models SPK and SPL were further simplified as single tension-only truss elements (LINK10). The Block Lanczos eigenvalue solver, using the Lanczos algorithm in which the Lanczos recursion is performed with a block of vectors, was then used in afterward modal analysis (ANSYS 2005).

Numerical analysis results show strong coupling phenomena for both studied structures. Cable vibration dominated in lower modes, which can be called “cable leading modes” (Figure 4.15). The cable components (shield wires, conductors and guy cables) of the coupled system vibrated locally and their dynamic effects transmitted to the pole structure. The main structure (pole) vibration at lower modes was not easily identified due to significant cable deformation. These “cable leading modes” played important role in dynamic analysis of electric transmission structures under wind loads. At higher modes, however, local vibration of the pole structure dominated, which can be termed as

"pole leading modes" (Figures 4.16-4.17). An interesting observation was that at certain modes whose frequency was close to the frequency of uncoupled pole structure models (without considering cables), cables almost kept stationary when they were away from the main structure (Figures 4.16-4.17). The eigenfrequencies of the in-plane vibration were usually smaller than the out-of-plane counterparts at the same mode shapes, which agreed well with the theory proposed by Li et al (2005). These "pole leading modes" are expected to be interested in the study of dynamic responses of the coupled transmission structure under ground movements, such as earthquakes and blast induced ground motions.

The coupling issues make free vibration of transmission lines a complex problem. Around eigensolutions of the isolated pole vibration, there were usually a cluster of dominant frequencies. Various possibilities of the cable vibration offered different coupling scenarios with designated main structure vibration modes. This increased the difficulty in identifying vibration mode, especially in lower modes. Figure 4.18 shows the first bending mode of pole structures coupled with cable vibration. Different cable vibration coupled with the pole cantilever deformation at several eigenfrequencies for both in-plane and out-of-plane vibrations. This phenomenon offered an explanation to the question of why the first bending mode could not be easily identified in the full-scale modal testing. The coupled steel pole-line system demonstrated more complicated dynamic behaviors because the steel pole-line has more components (more shield wires, more conductors, more insulators, and additional guy cables) involved in vibration. Figure 4.19 compares vibration modes in which the pole structure has similar bending shapes while natural frequencies vary due to shield wire/conductor coupling. The

frequency for the steel pole-line system included in the figure cannot be claimed as the only eigenvalue of that particular mode. This coupling is also reflected in the modal experiment conducted on the steel pole: it is of little confidence to determine eigensolution from the simple peak picking method in analyzing system FRFs.

Simplified models were generated by following the approach proposed by Li et al (2005): Table 4.10 lists the additional mass calculated from Equations (4.13) and (4.14). These models can greatly reduce computation time and afterward analysis efforts. Figure 4.20 shows the first four modes of simplified concrete pole model. Figure 4.21 gives the second to the fourth modes of the simplified steel pole with guy wires. Because of the coupling effect between the main structure (steel pole) and the guy cables, some lower bending modes have multi-eigenfrequencies, as shown in Figure 4.22. Again, this coupling issue makes it difficult to claim a sole eigen-frequency for certain vibration mode. When the guy cables were simplified into one-tension-only-truss models (SPK, SPL), all the modes are pole leading modes; so the steel pole bending modes were easily identified. Figure 4.23 shows the first in-plan vibration results from SPK. Out-of-plan vibration mode shapes were similar to the in-plan for the same mode, but the eigenfrequencies were different due to different additional masses at these two directions.

For models with soil springs, natural frequencies at the same vibration modes decreased a little compared to those models in which soil effects were not considered. Mode shapes, however, did not change much at the same mode. The soil was very stiff where the poles were embedded; so coupling effects demonstrated greater influence than the fix-end assumption for eigensolution variation for the studied transmission lines. The method developed by Li et al. (2005) have included the soil effects by site classification,

simplified models established by following this approach seemed to be able to yield relatively accurate results without adding soil springs at the embedded portion of the pole.

Table 4.11 sums up the frequencies obtained from both modal testing and numerical analysis of different FE models. The first bending modes were not detected because the coupling made it difficult to claim a sole frequency solution for a certain mode shape. Numerical solutions for the concrete pole system correlated well with experimental results. When the concrete pole was modeled as an isolated structure (CPA and CPB), frequency values were larger than the corresponding experimentally identified frequencies. When cable effects were included in the models (CPC and CPD), calculated frequencies became closer to testing results. This improvement indicates that if more accurate solutions are expected, modeling the pole structure itself is not adequate. Simplified pole system models (CPE and CPF) built following Li et al. (2005) showed better results than the isolated pole models (CPA and CPB). The eigenfrequencies computed from CPE were close to both experimental results and solutions from the detailed coupled system model (CPC), which suggested potential use of this model for future structural dynamic response analysis. These conclusions were not obvious for the steel pole system. Based on available observations, simplified models with guy included (SPI) seemed to be able to provide relatively accurate results with less computation efforts.

4.5 Discussions

Impact modal testing was performed in this study on both the isolated pole and the pole-line system. It was found that the coupling between the pole and the cable increased

difficulties in deriving modal behaviors of the main structure in the pole-line system. For simplicity, only a part of the power grid (two line spans with a single pole) was modeled. The boundary conditions of the conductors in the detailed pole-line system models were assumed to be fix-supported in this study. Optimizing the boundary conditions to include influence from neighboring structures in the grids may increase the accuracy of numerical results, which needs further investigation. FE modeling offers a cost effective way to study large scale structures. But modeling uncertainties are problems faced by most researchers. For in-situ structures, although most of the input information can be obtained from design documentations, they may not exactly reflect actual situations. Modulus of elasticity in the concrete pole model, for example, may vary from its design value because of the prestress effects. Damping was not considered in the modeling due to difficulties of determining its value. But it is a significant factor in structural dynamic response analysis and should be included in future studies.

4.6 Summary

In this chapter, modal behaviors of the transmission structures were studied both experimentally and numerically. According to research results, the following conclusions can be drawn:

(1) Soil-structure interaction needs to be considered in dynamic analysis of the isolated direct embedded pole structure. The embedded single pole can be treated as a cantilever beam, but the fix-end assumption may not always provide sound solutions.

(2) SASW is a NDT technique that can be easily employed in site investigation. It can supply necessary information to quantify the soil property to a reasonable degree.

(3) Transmission structures have a strong coupling issue between main structures and cables. FE models only considering the pole itself yield natural frequencies that differ from the physical testing results. For example, the 2nd bending mode in-plane frequency of CPA is 11.31% difference from modal testing results (Table 4.11).

(4) Detailed FE models of the coupled pole-line system yield insights to coupling phenomena. Both the “cable leading mode” and the “pole leading mode” were observed in the analysis. The coupling issue made it difficult in specifying natural frequencies for certain modes.

(5) Simplified models proposed by Li et al. (2005) are good candidates for modeling the coupled pole-line system. The lower mode natural frequencies calculated from the simplified models of the studied pole-line system were close to experimental data and detailed modeling results.

(6) The simplified analytical method suggested by Li et al. (2005) is a semi-empirical model. It has included the soil effects by site classification, hence does not need additional soil springs. Since blast induced ground vibration usually has the same excitation mechanism with earthquakes, the simplified model has the potential in dynamic response calculations of transmission structures under the blast loading.

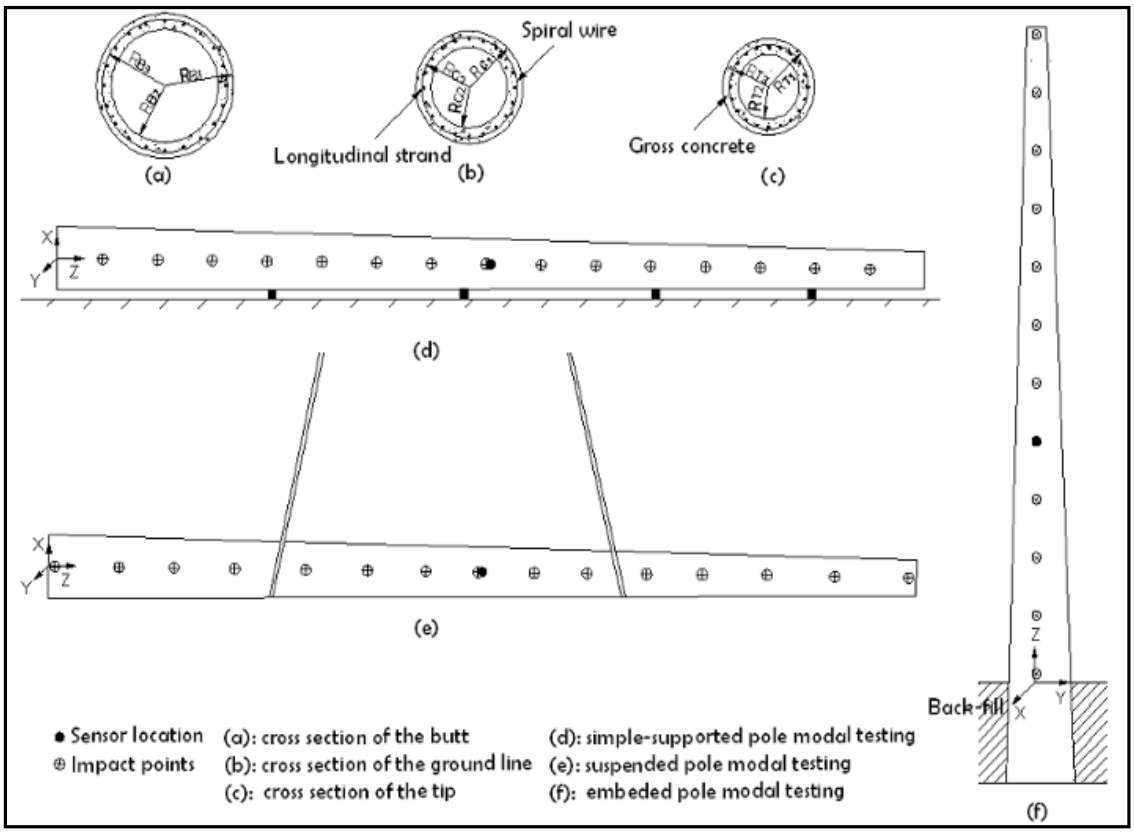

Figure 4.1: Modal testing set-up

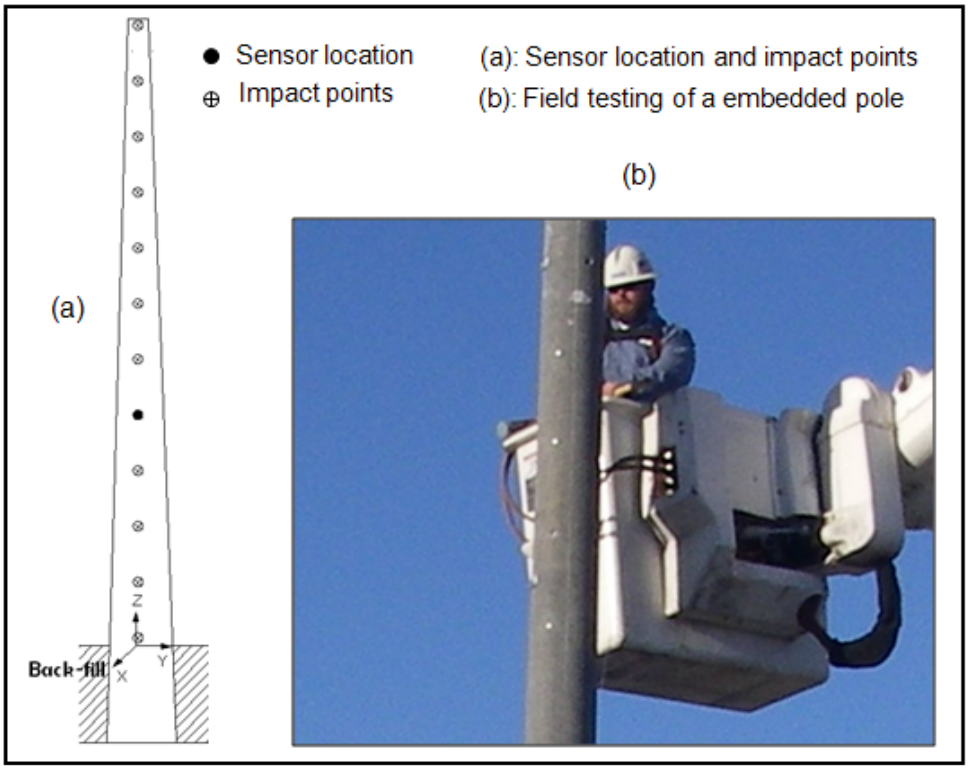

Figure 4.2: Field testing of an embedded concrete pole

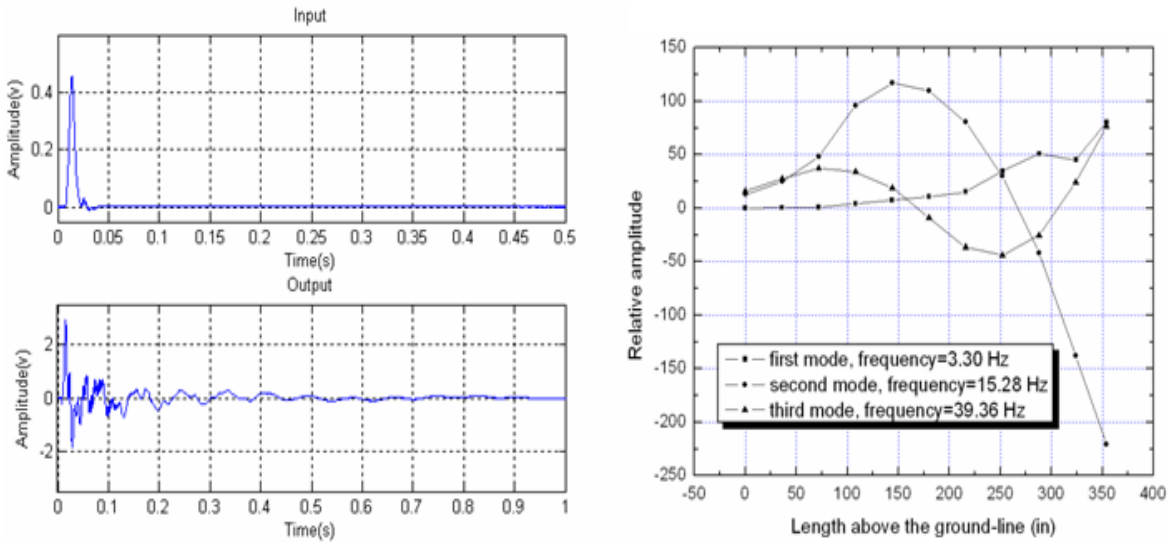

Figure 4.3: Modal testing results analysis: (a) typical input-output signals from the impact modal testing; (b) identified mode shapes and frequencies

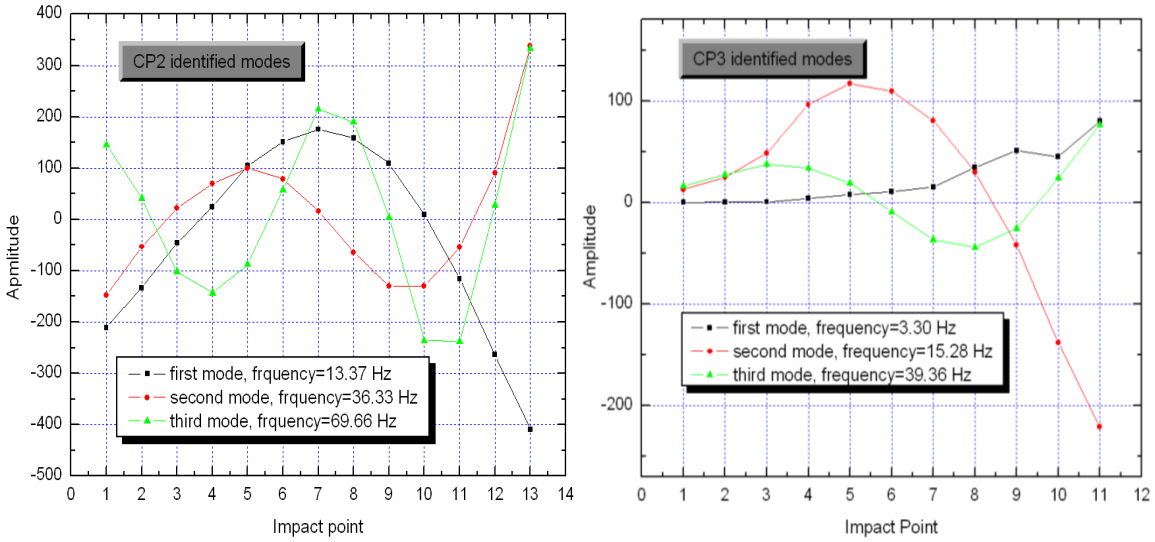

Figure 4.4: Representative vibration mode shapes

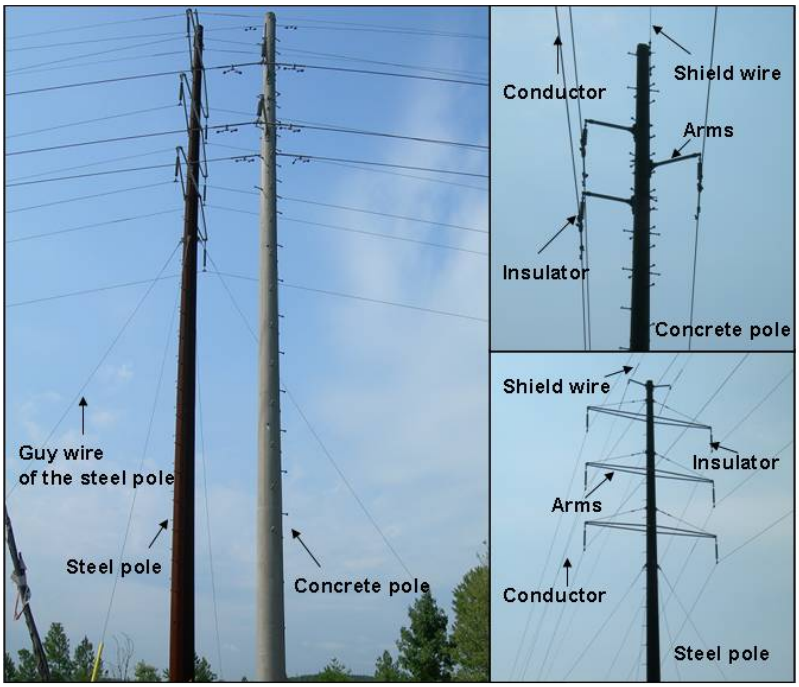

Figure 4.5: Development of simplified FE models for transmission pole structures

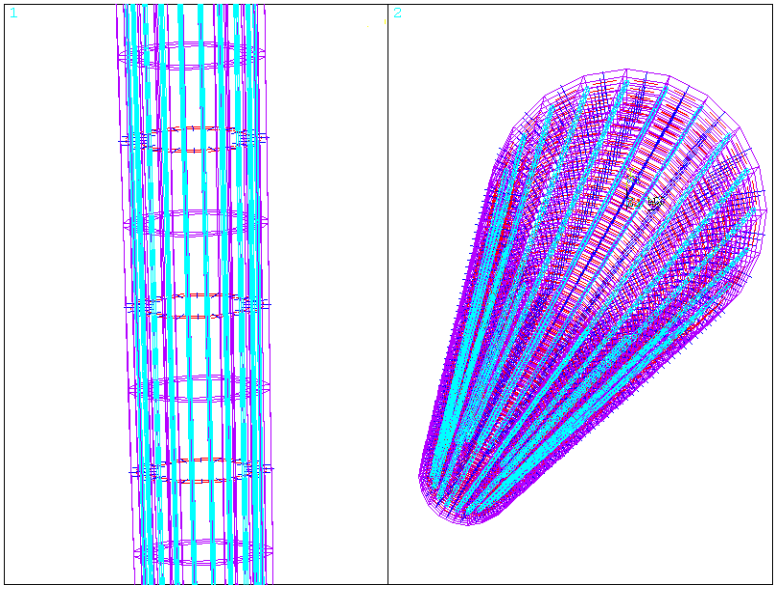

Figure 4.6: Detailed FE model of the 95 feet concrete pole

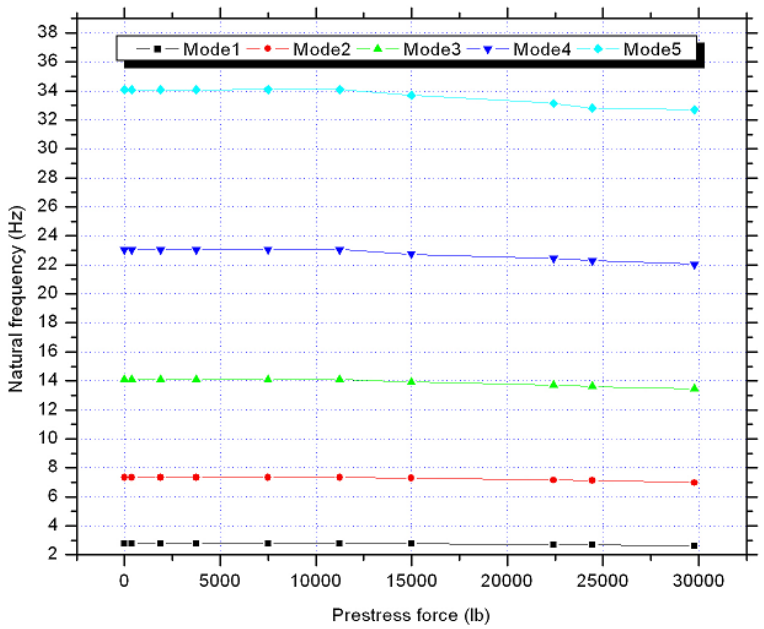

Figure 4.7: Prestress effects on natural frequencies

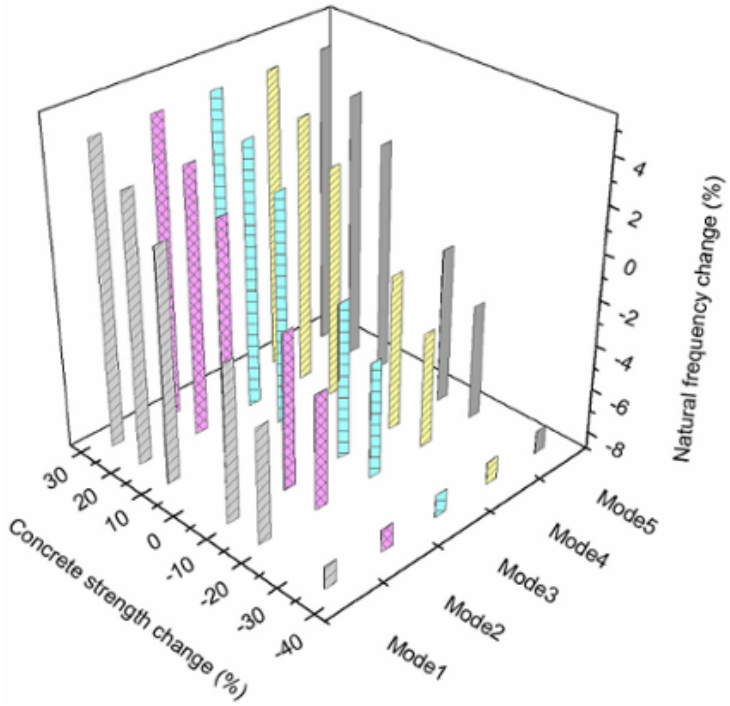

Figure 4.8: Influence of concrete strength on natural frequencies

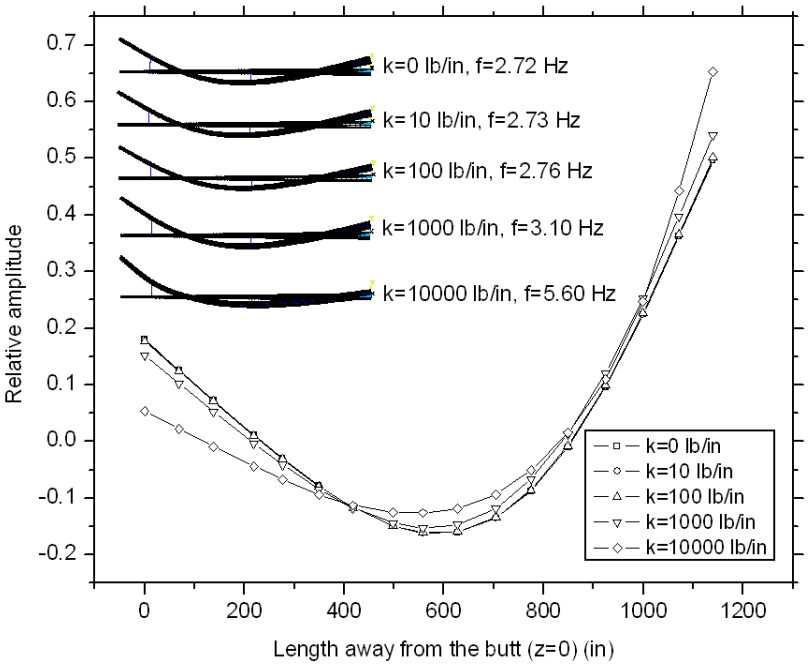

Figure 4.9: Eigensolutions under different boundary stiffness

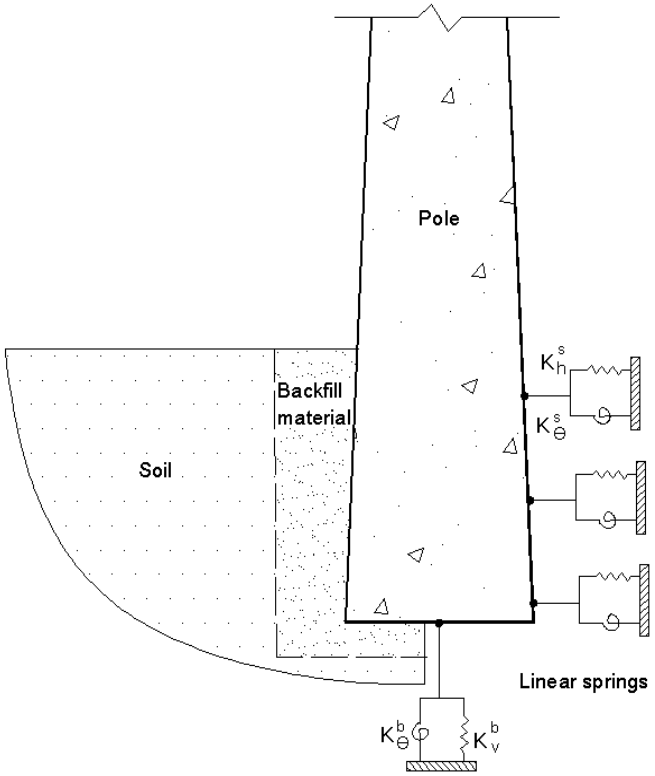

Figure 4.10: Soil spring models for the direct embedded pole

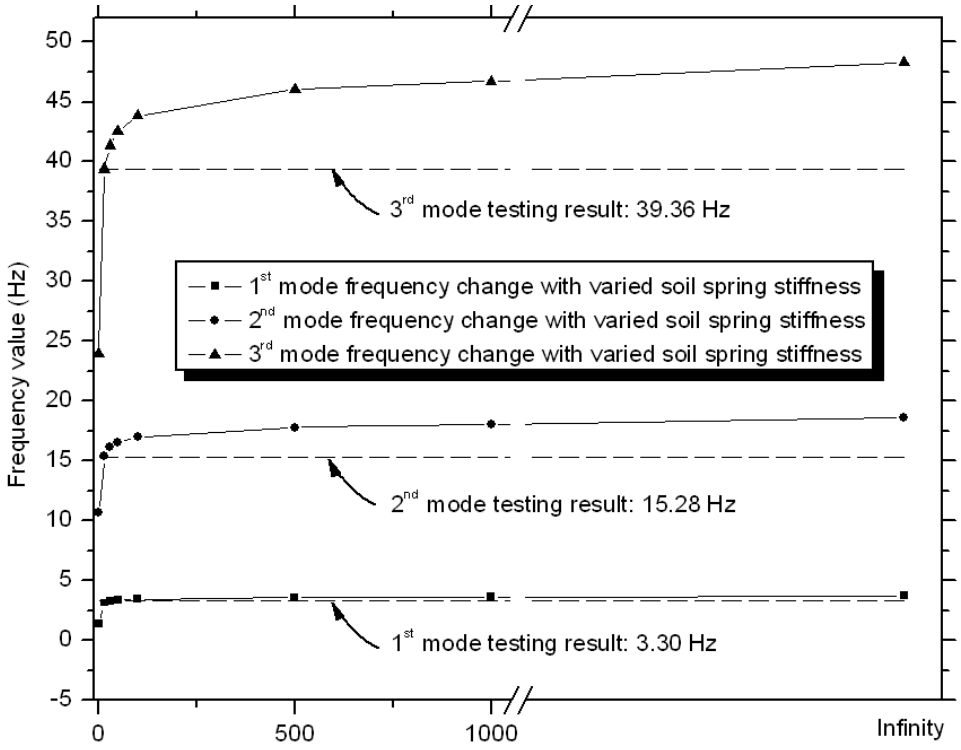

Figure 4.11: Frequency change due to different soil stiffness

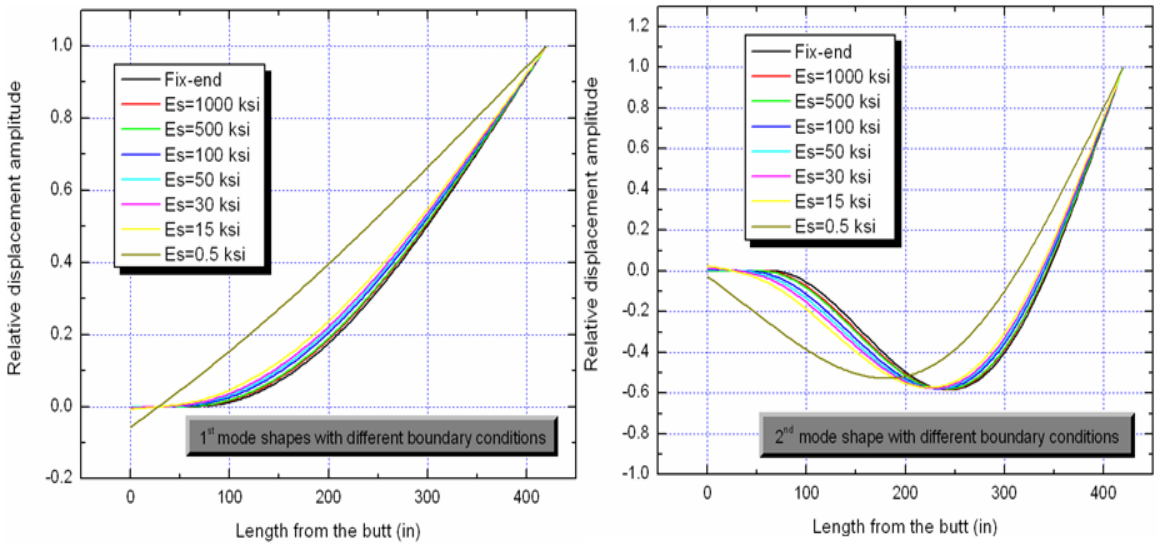

Figure 4.12: Mode shape change considering soil spring effects

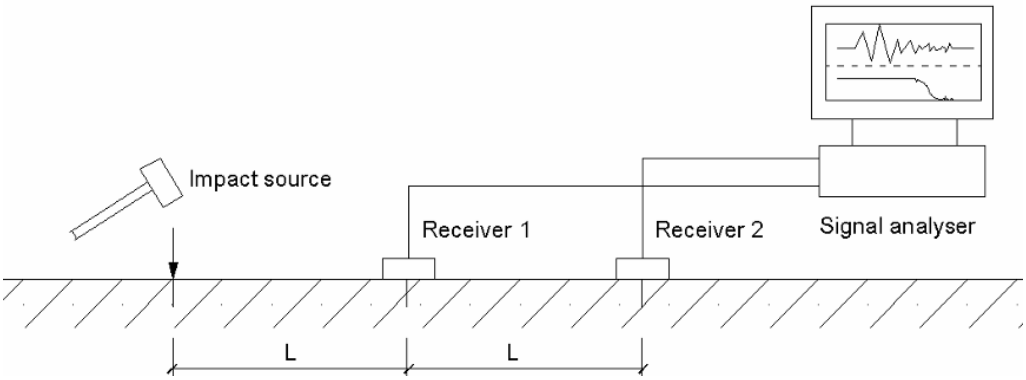

Figure 4.13: Field setup for the SASW testing

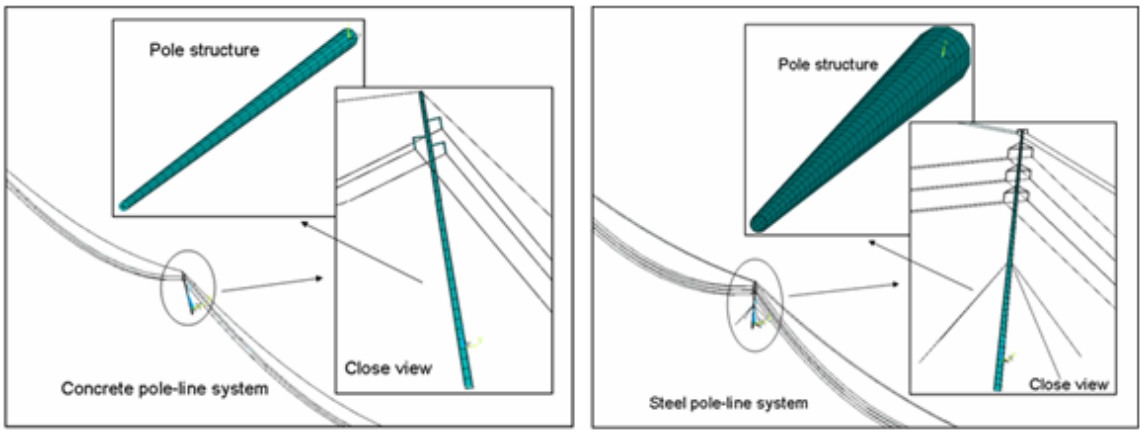

Figure 4.14: FE models for numerical study

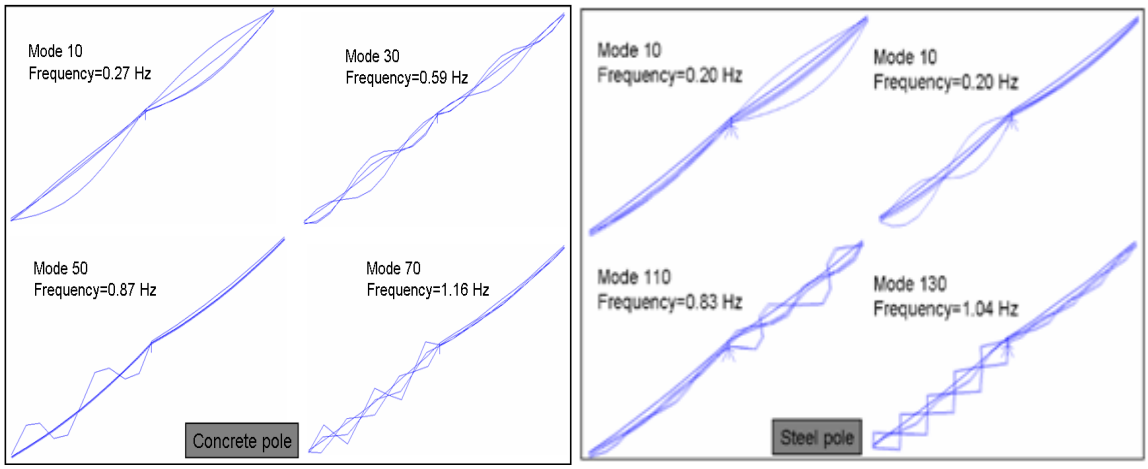

Figure 4.15: Representative cable leading modes of the coupled system

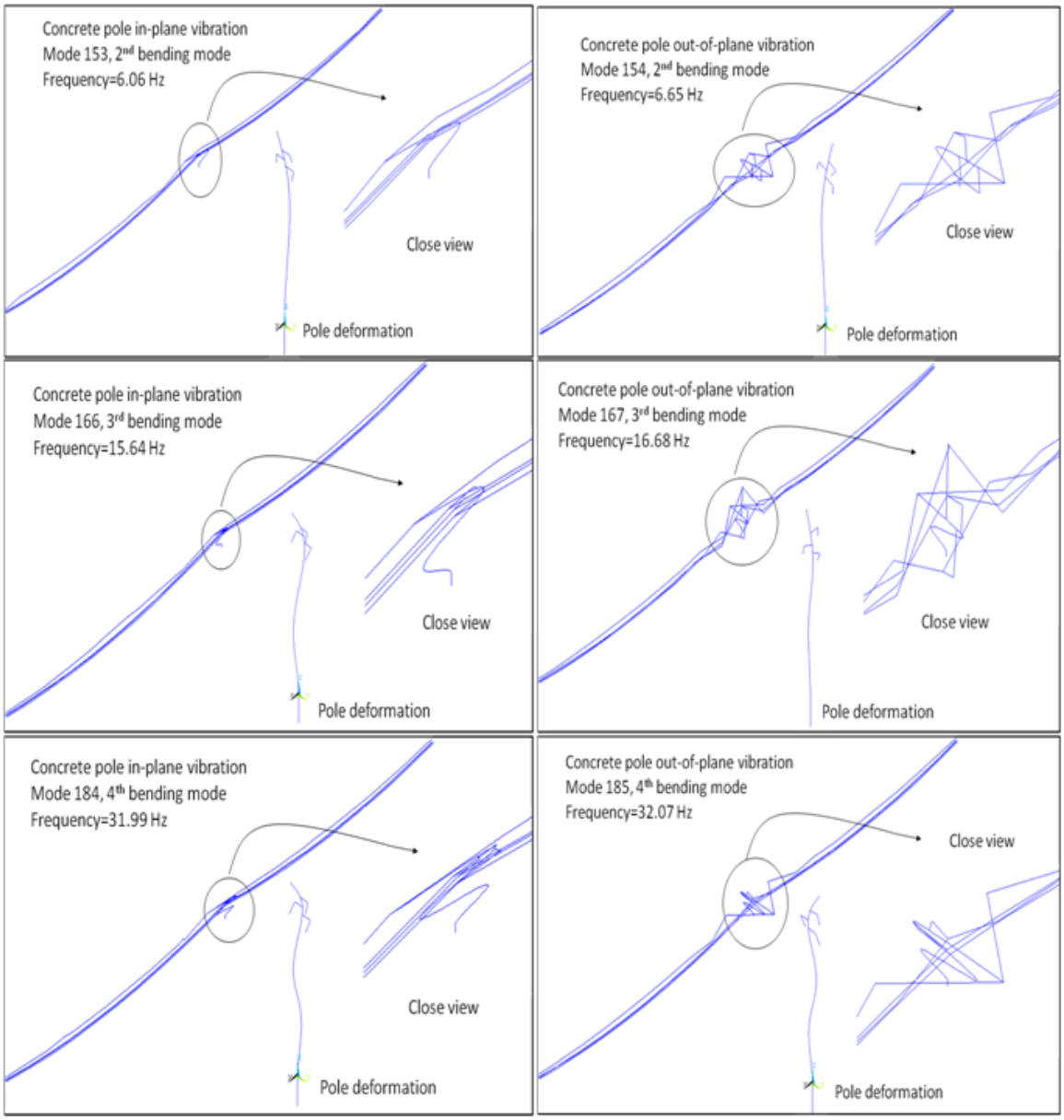

Figure 4.16: Representative pole leading modes of the coupled concrete pole-line system

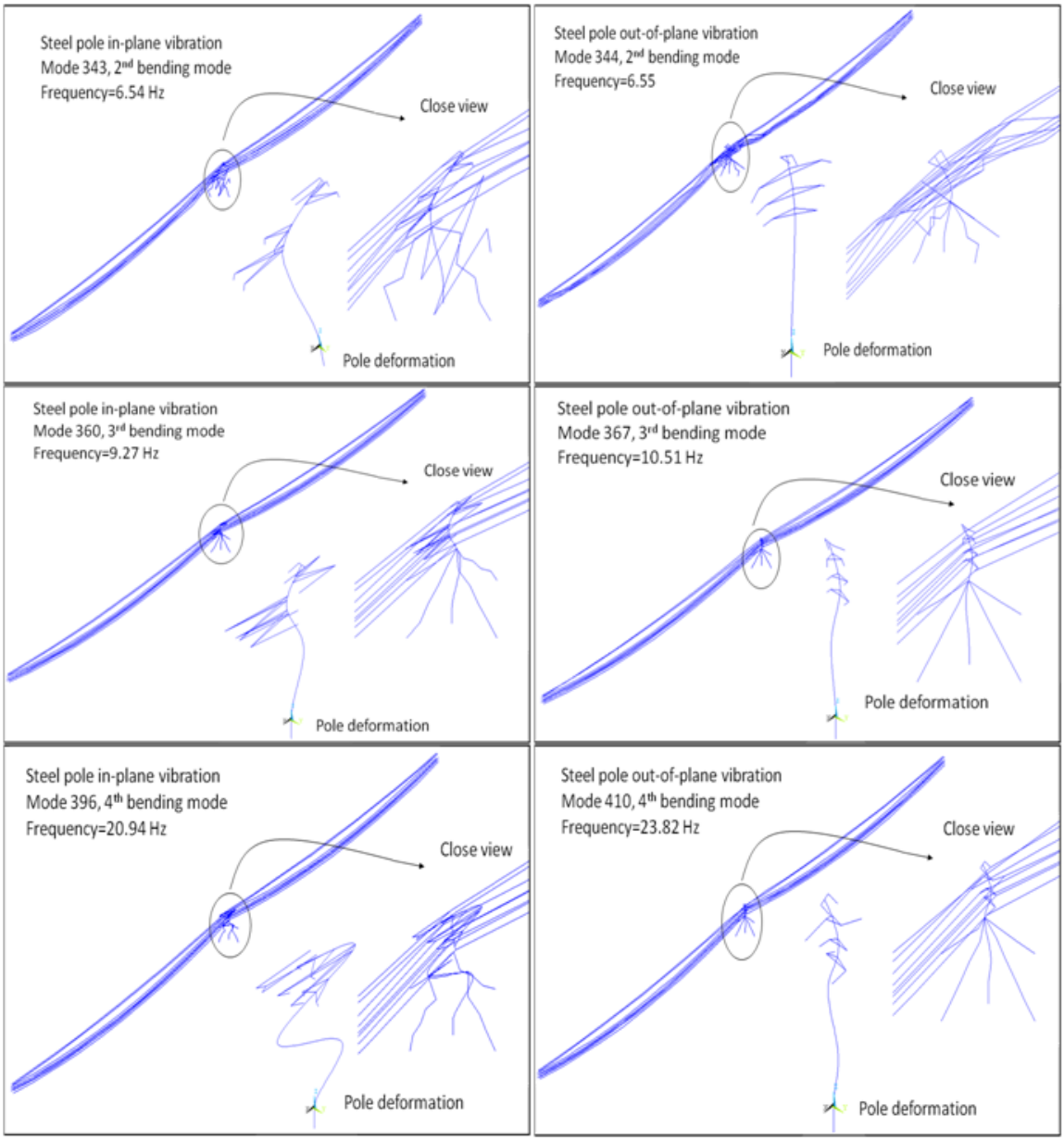

Figure 4.17: Representative pole leading modes of the coupled steel pole-line system

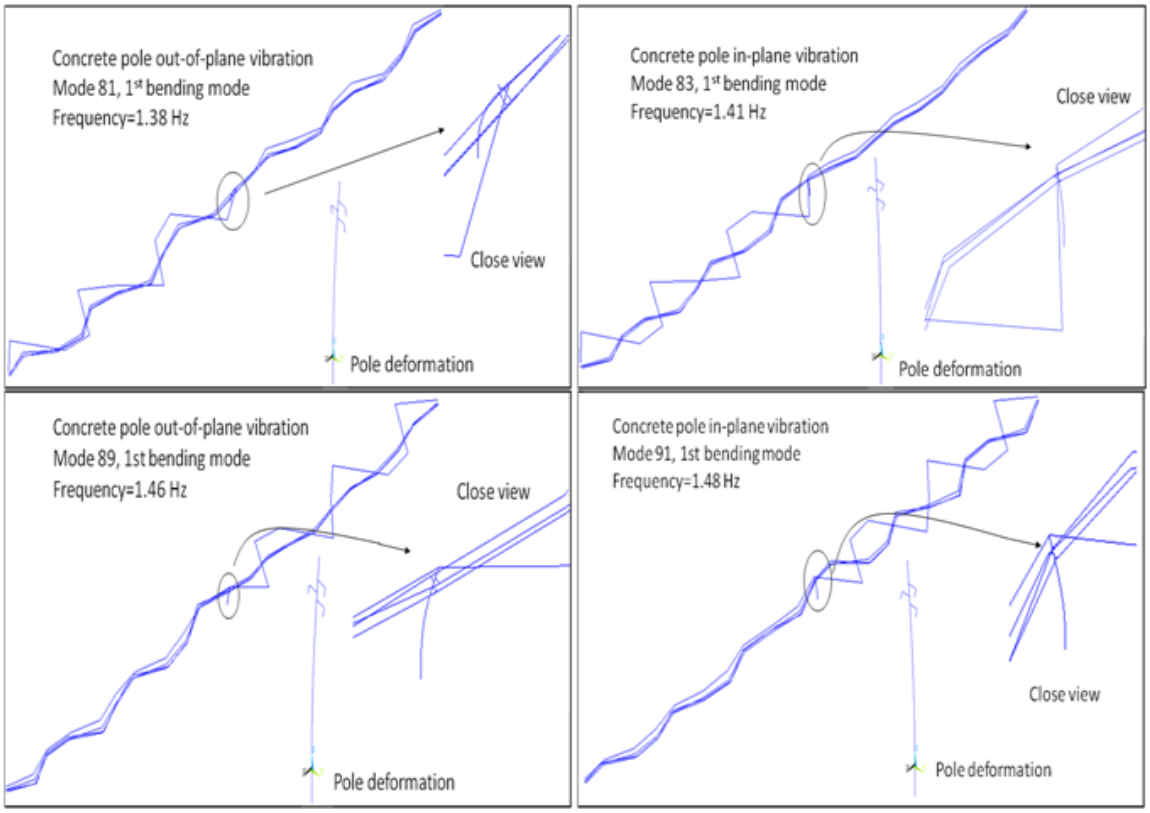

Figure 4.18: Various 1st bending mode of the coupled concrete pole-line system

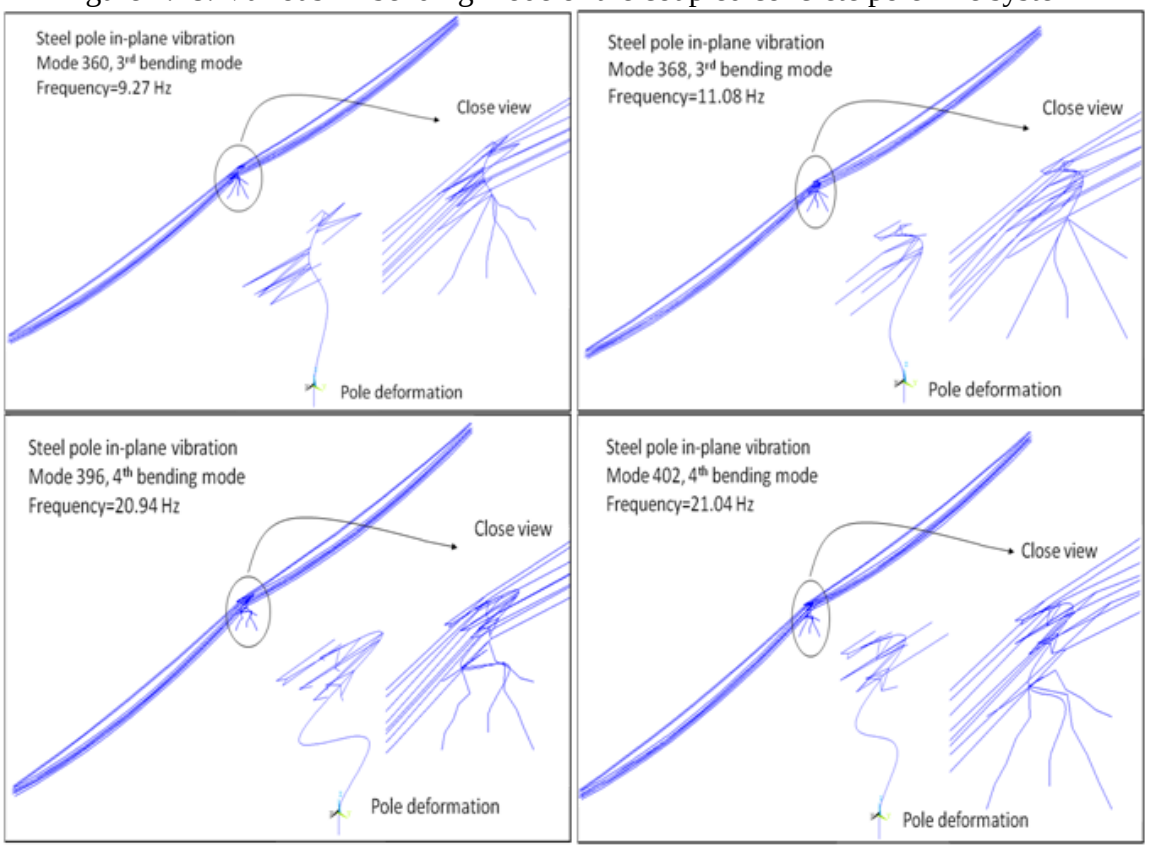

Figure 4.19: Varied eigenfrequencies at the similar vibration mode

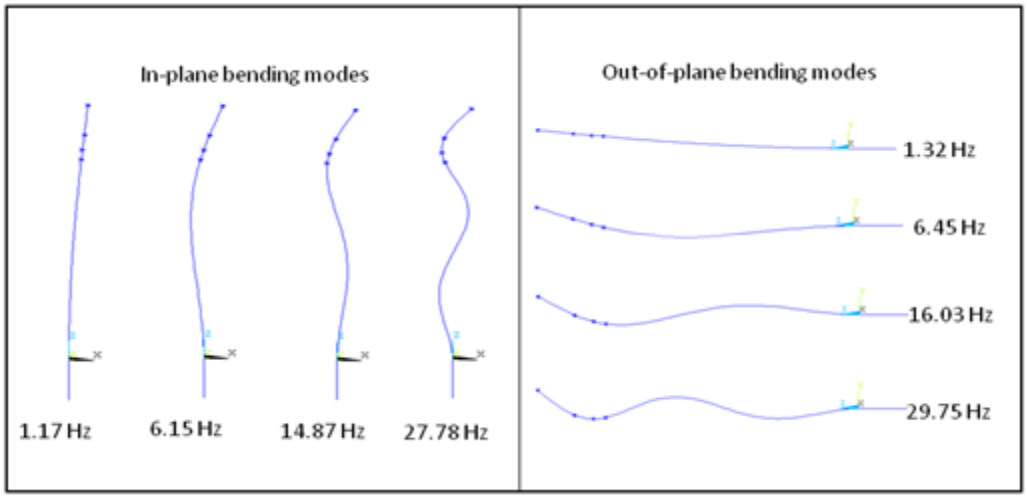

Figure 4.20: The first four vibration modes of the simplified concrete pole

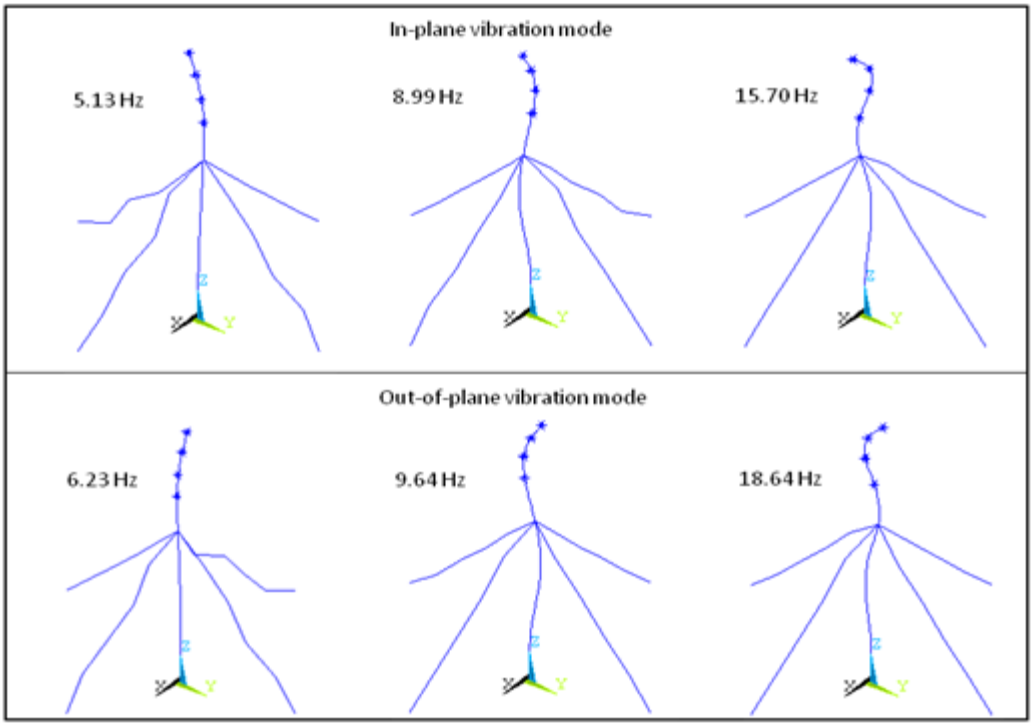

Figure 4.21: The pole-leading vibration modes of the simplified steel pole

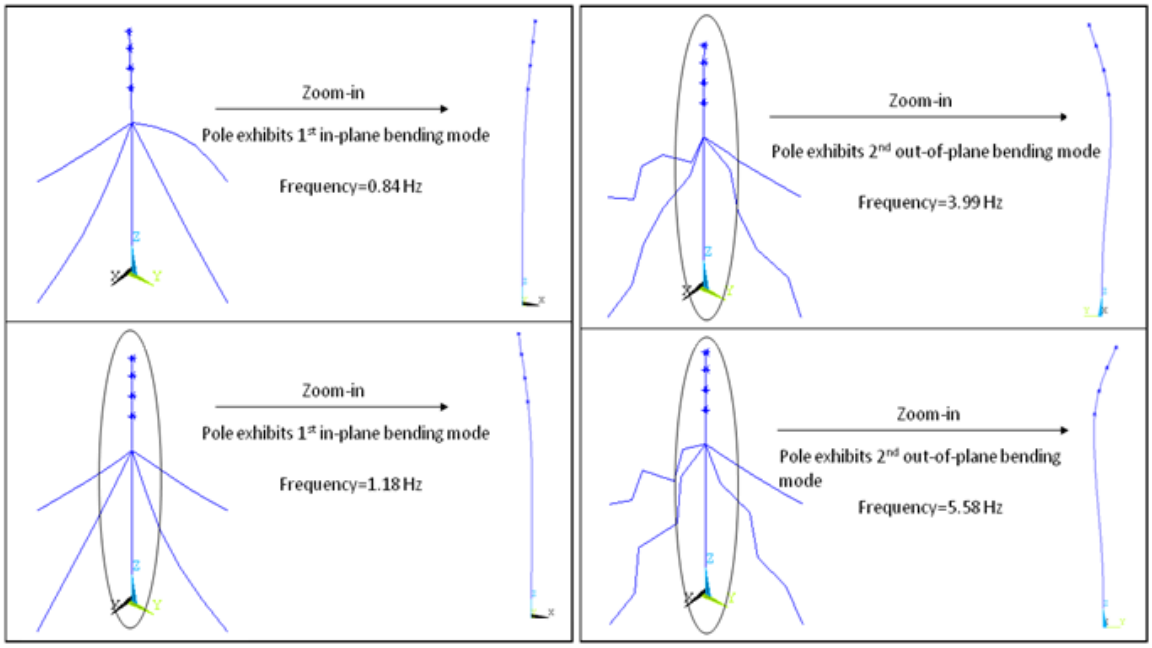

Figure 4.22: Typical guy wire dominating modes of the simplified guyed steel pole

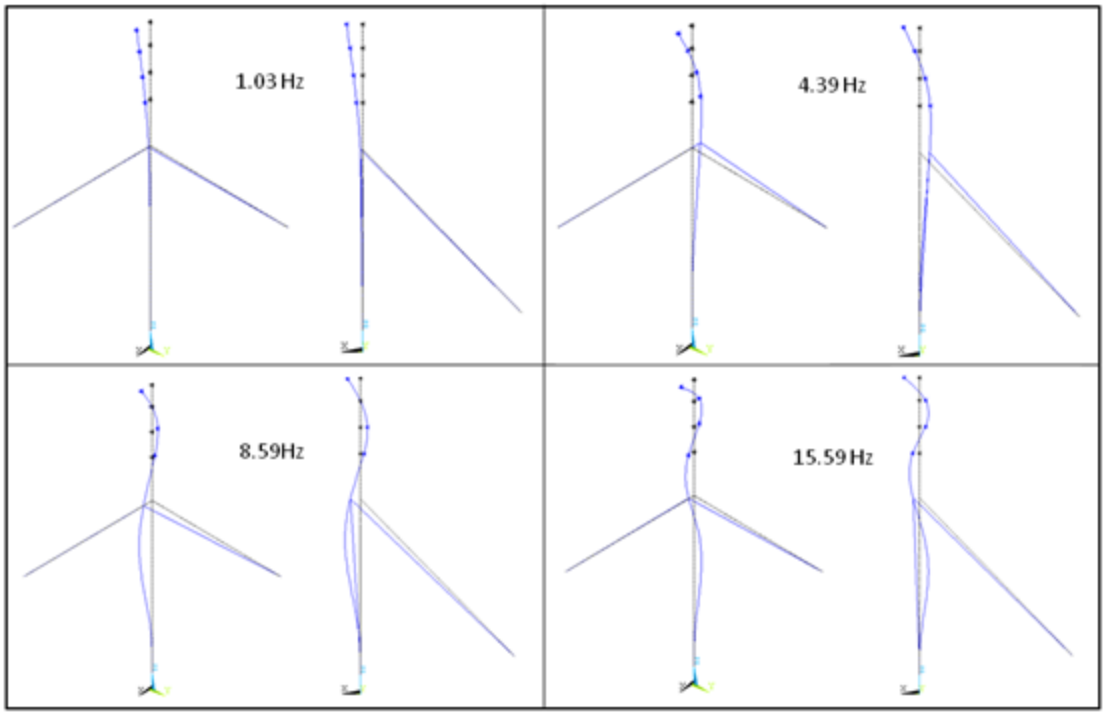

Figure 4.23: First four in-plane bending modes of SPK

Table 4.1: Tested prestressed concrete poles

Name	*Tested pole*	*Boundary condition*
CP1	A 95 feet height isolated concrete pole	Simple-supported
CP2	A 35 feet height isolated concrete pole	Suspended
CP3	The same 35 feet pole used above	Embedded with soil as back-fill
CP4	The same 35 feet pole used above	Embedded with gravel as back-fill

Table 4.2: Identified natural frequencies

Test	*Frequency*	*Description*
CP1	2.51 (Hz)	1st bending mode of the simple-supported 95 feet pole
	8.13 (Hz)	2nd bending mode of the simple-supported 95 feet pole
	13.87 (Hz)	3rd bending mode of the simple-supported 95 feet pole
CP2	13.37 (Hz)	1st bending mode of the suspended 35 feet pole
	36.33 (Hz)	2nd bending mode of the suspended 35 feet pole
	69.66 (Hz)	3rd bending mode of the suspended 35 feet pole
CP3	3.30 (Hz)	1st bending mode of the soil back-filled embedded 35 feet pole
	15.28 (Hz)	2nd bending mode of the soil back-filled embedded 35 feet pole
	39.36 (Hz)	3rd bending mode of the soil back-filled embedded 35 feet pole
CP4	3.30 (Hz)	1st bending mode of the gravel back-filled embedded 35 feet pole
	15.18 (Hz)	2nd bending mode of the gravel back-filled embedded 35 feet pole
	39.46 (Hz)	3rd bending mode of the gravel back-filled embedded 35 feet pole

Table 4.3: Eigenvalues identified from modal testing

Testing results or models	*1st bending*		*2nd bending*		*3rd bending*		*4th bending*	
	In*	Out*	In*	Out*	In*	Out*	In*	Out*
Concrete pole (OCP)	-	-	6.10	6.71	15.26	17.09	30.52	31.74
Steel pole (OSP)	-	-	-	-	8.54	-	-	-

* In— in-plane-vibration; Out— out-of-plane vibration; unit: Hz.

Table 4.4: Material property

Material	*Young's Modulus*	*Density*	*Poisson's ratio*	*Constitutive law and failure criterion*
Concrete	5466.30 (ksi)	0.000225 ($lb \cdot s^2/in^4$)	ν_c=0.20	Multi-linear σ-ε; considering cracks f'_c=11000.00 (psi)
Prestress strand	29000.00 (ksi)	0.000734 ($lb \cdot s^2/in^4$)	ν_s=0.27	Bilinear σ-ε f_{pu}=250000.00 (psi)
Spiral wire	29000 .00 (ksi)	0.000732 ($lb \cdot s^2/in^4$)	ν_w=0.27	Bilinear σ-ε f_y= 65000.00 (psi)

Table 4.5: Geometry input information

Portion	*Length (in)*	*Cross section diameter (in)*			*Wire volume ratio (%)*
1	H1=138	DB1=31.59	DB2=23.81	DB3=28.59	u1=0.594
2	H2=966	DG1=29.11	DG2=21.60	DG3=26.11	u2=0.280
3	H3=36	DT1=11.07	DT2=5.57	DT3=8.07	u3=0.781

Table 4.6: Input information for the isolated concrete pole FE model

Length (in)		*Butt cross section diameter (in)*		*Tip cross section diameter (in)*		*Material properties*	
Buried portion	Above ground	Inside	Outside	Inside	Outside	E (ksi)	ρ (lbm/in3)
66.00	354.00	10.35	15.85	4.05	9.55	7000.00	0.00023

Table 4.7: FE models used in numerical analysis

Model	*Structural configuration*
CPA	FE model of the isolated concrete pole
CPB	FE model of the isolated concrete pole considering SSI
CPC	FE model of the concrete pole-line system
CPD	FE model of the concrete pole-line system considering SSI
CPE	FE model of the isolated concrete pole with added conductor mass
CPF	FE model of the isolated concrete pole with added conductor mass and SSI
SPA	FE model of the isolated steel pole
SPB	FE model of the isolated steel pole considering SSI
SPC	FE model of the guyed steel pole
SPD	FE model of the guyed steel pole considering SSI
SPE	FE model of the steel pole-line system
SPF	FE model of the steel pole-line system considering SSI
SPG	FE model of the isolated steel pole with added conductor mass
SPH	FE model of the isolated steel pole with added conductor mass considering SSI
SPI	FE model of the guyed steel pole with added conductor mass
SPJ	FE model of the guyed steel pole with added conductor mass considering SSI
SPK	FE model of the steel pole with added conductor mass and 4 simplified guy-lines
SPL	FE model of the steel pole with added conductor mass and 4 simplified guy-lines considering SSI

Table 4.8: Parameters of the concrete pole-line system

Items	*Values*
Overall length (ft)	60.00
Embedment depth (ft)	8.00
Density (lb/ft^3)	160.00
Modulus of elasticity (ksi)	6021.90
Line parameters	
Left span length (ft)	1059.00
Difference in elevation at the left span (ft)	22.00
Right span length (ft)	1119.00
Difference in elevation at the right span (ft)	52.00
Conductor parameters	
Nominal cross-section diameter (in)	0.74
Weight per unit length (lb/ft)	0.43
Modulus of elasticity (ksi)	8700.00
Shield wire parameters	
Nominal cross-section diameter (in)	0.38
Weight per unit length (lb/ft)	0.27
Modulus of elasticity (ksi)	25800.00
Insulator parameters	
Overall weight (lb)	4.00
Estimated modulus of elasticity (ksi)	6525.00
Arm parameters	
Overall weight per arm combination connection (lb)	1.20
Modulus of elasticity (lb)	6525.00

Table 4.9: Parameters of the steel pole-line system

Steel pole parameters	
Overall length (ft)	105.00
Embedment depth (ft)	12.50
Density (lb/ft^3)	490.00
Modulus of elasticity (ksi)	29000.00
Line parameters	
Left span length (ft)	1093.00
Difference in elevation at the left span (ft)	23.12
Right span length (ft)	1139.00
Difference in elevation at the right span (ft)	62.67
Conductor parameters	
Nominal cross-section diameter (in)	0.57
Weight per unit length (lb/ft)	0.77
Modulus of elasticity (ksi)	8700.00
Shield wire parameters	
Nominal cross-section diameter (in)	0.46
Weight per unit length (lb/ft)	0.25
Modulus of elasticity (ksi)	25800.00
Guy wire parameters	
Nominal cross-section diameter (in)	0.50
Weight per unit length (lb/ft)	0.66
Modulus of elasticity (ksi)	25686.00
Insulator parameters	
Overall weight (lb)	10.00
Estimated modulus of elasticity (ksi)	6525.00
Arm parameters	
Overall weight per arm combination connection (lb)	65.00
Modulus of elasticity (lb)	6525.00

Table 4.10: Additional mass in the simplified FE models

Shield wire additional mass (lb-m)			*Conductor additional mass (lb-m)*		
Concrete pole	In-plane	0.39	Concrete pole	In-plane	0.62
	Out-of-plane	0.17		Out-of-plane	0.28
Steel pole	In-plane	0.75	Steel pole	In-plane	2.27
	Out-of-plane	0.33		Out-of-plane	1.01

Table 4.11: Eigenvalue comparison between different models

Testing results or models	*1st bending*		*2nd bending*		*3rd bending*		*4th bending*	
	In*	Out*	In*	Out*	In*	Out*	In*	Out*
Concrete pole modal testing	-	-	6.10	6.71	15.26	17.09	30.52	31.74
CPA	1.49	1.49	6.79	6.79	17.18	17.18	32.46	32.46
CPB	1.45	1.45	6.58	6.58	16.60	16.60	31.33	31.33
CPC	-	-	6.06	6.65	15.64	16.68	31.99	32.07
CPD	-	-	5.92	6.45	15.35	16.28	31.18	30.97
CPE	1.17	1.32	6.15	6.45	14.87	16.03	27.78	29.75
CPF	1.14	1.28	5.97	6.25	14.45	15.54	26.84	28.76
Steel pole modal testing	-	-	-	-	8.54	-	-	-
SPA	1.20	1.20	4.92	4.92	11.99	11.99	22.36	22.36
SPB	1.18	1.18	4.84	4.84	11.79	11.79	21.97	21.97
SPC	-	-	7.41	7.41	12.01	12.01	22.83	22.83
SPD	-	-	7.32	7.32	11.83	11.83	22.45	22.45
SPE	-	-	6.54	6.55	9.27	10.51	20.94	23.82
SPF	-	-	6.53	6.63	9.18	9.79	20.63	21.22
SPG	0.60	0.78	3.37	3.97	8.26	9.38	15.51	18.20
SPH	0.59	0.77	3.33	3.91	8.12	9.24	15.34	17.94
SPI	-	-	5.13	6.23	8.99	9.64	15.70	18.64
SPJ	-	-	5.12	6.20	8.81	9.45	15.57	18.41
SPK	1.10	1.47	5.02	6.12	8.96	9.64	15.68	18.53
SPL	1.10	1.47	5.02	6.10	8.78	9.45	15.54	18.30

* In— in-plane-vibration; Out— out-of-plane vibration; unit: Hz.

CHAPTER 5: SPECTRUM ANALYSIS OF TRANSMISSION POLES

5.1 Introduction

Spectrum analysis is to calculate maximum structural responses based on design spectrum and structure modal characteristics. For example, maximum displacement response ($|\{x(t)\}|_{max}$) for the *r*th mode can be calculated as (Tedesco et al. 1999):

$$|\{x(t)\}|_{max} = |\{\Phi\}_r \Gamma_r|(S_d)_r \tag{5.1}$$

where $\{\Phi\}_r$ is mode shape of the *r*th mode; $(S_d)_r$ is spectral displacement for the *r*th mode, which can be determined from response spectrum; and Γ_r is the earthquake participation factor and is determined as (Tedesco et al. 1999):

$$\Gamma_r = \frac{\{\Phi\}_r^T [m]\{I\}}{\{\Phi\}_r^T [m]\{\Phi\}_r} \tag{5.2}$$

in which $\{m\}$ is mass matrix and $\{I\}$ is unit vector. Contributions from each mode are determined directly from maximum responses at a particular frequency. The total structural response is then obtained from a combination of modal maxima with the square-root-of-the-sum-of-the-square (SRSS) method or the complete-quadratic-combination (CQC) method. SRSS renders accurate approximations for structural systems, exhibiting well-separated vibration frequencies, and is given as:

$$R_{max} = \sqrt{\sum_{r=1}^{p} R_r^2} \tag{5.3}$$

where R_{max} is the maximum value of a particular response such as displacement; R_r is the peak value for the *r*th mode; and p is the number of modes involved. The CQC method is a good approach for systems with closely spaced modes and is expressed as:

$$R_{max} = \sqrt{\sum_{r=1}^{p} \sum_{s=1}^{p} R_r P_{rs} R_s} \tag{5.4}$$

where R_r and R_s are peak values of a particular response for the *r*th and *s*th mode. P_{rs} is given as:

$$P_{rs} = \frac{8\zeta^2(1+\eta)\eta}{(1+\eta^2)^2+4\zeta^2\eta(1+\eta)^2} \tag{5.5}$$

where ζ is a constant modal damping; η is the ratio of circular frequencies between *s*th mode and *r*th mode.

In this chapter, spectrum analysis of two pole structures (OCP, OSP) in operation power lines was performed using two FEM packages, ALGOR® and ANSYS®. The aim of using two FE software is to ensure that embedded numerical integration schemes provide identical and compatible results. The FE models for the poles are those simplified models discussed in Chapter 4. Response spectra designed based on measurements at Chapter 3 were used as input excitations. Structural responses of pole structures at various blast limits based on different levels of peak particle velocity criteria were quantitatively investigated. The results were then used to compare with design requirements in Chapter 7 to develop a reasonable blast limit.

5.2 Spectrum analysis of transmission poles

5.2.1 Spectrum analysis with ALGOR®

Spectrum analysis was first performed using ALGOR®. For simplicity, only pole structures were modeled and all accessories, including conductors, ground lines,

insulators, and guy wires were ignored in the ALGOR® FE models. The parameters of these two structures (OCP and OSP in Chapter 4) used in the modeling are listed in Table 5.1.

FE models of the two poles are shown in Figure 5.1, where the concrete pole was modeled by using 312 BRICK elements, while the steel pole model was created with 444 elements (ALGOR 2007).

Modal analysis was first performed to derive natural frequencies and mode shapes. Natural frequencies of the first four modes are listed in Table 5.2. Spectrum analysis is a restart-calculation in ALGOR®: The design response spectrum (Figure 3.21) based on 2 in/s PPV was imported as acceleration versus period. The resultant displacement and maximum principal stress distribution along the pole were drawn in Figures 5.2-5.9. The maximum values were identified and summarized in Table 5.2.

Natural frequencies of pole structures calculated from ALGOR® were close to experimental results (Table 4.3), especially for the concrete pole. Conductors and other accessories were not included in the ALGOR® FE models. Further analysis with ANSYS®, would take the effects of these accessories into account.

5.2.2 Spectrum analysis with ANSYS®

Based on modal behavior comparison, simplified models were proposed to compute structural responses of pole structures caused by ground vibration (see Chapter 4 for details). Conductors and other accessories were considered in the model by additional mass elements (MASS21) (Figure 5.10). Tapered beam elements (BEAM189) were used to model pole structures while guy lines were modeled by truss elements (LINK10) (ANSYS 2007).

Spectrum analysis was performed by importing design response spectra in two horizontal directions (in-plane and out-of-plane) and vertical direction. The in-plane horizontal direction is parallel with the power line whereas the out-of-plane direction is perpendicular to the power line. The mode combination method for the concrete pole was SRSS whereas the CQC method was used for the steel pole mode combination. 0.02 damping ratio was assumed in calculation for both poles. At the response spectrum designed based on 2 in/s PPV, the resultant first principal stress distributions are shown in Figures 5.11 and 5.12. Maximum displacements and reaction forces at the fix end are listed in Table 5.3.

It is found from ANSYS® that the maximum displacements for both poles (0.14 in for the concrete pole and 0.12 in for the steel pole at 2 in/s PPV criterion) are less than ALGOR® results (0.19 in for the concrete pole and 0.20 in for the steel pole); whereas maximum first principal stress values from ANSYS® are larger (331.54 psi for the concrete pole and 1445.00 psi for the steel pole at 2 in/s PPV criterion). For practical purpose, they are considered reasonably close. ANSYS® results seem to indicate more rigid structures because of considering conductor effects.

Following the same analytical procedure, different response spectra were designed based on different target PPV criteria. With these designed spectra as input excitations, spectrum analyses were performed on transmission pole structures. Figures 5.13 and 5.14 show the concrete pole first principal stress states under response spectra designed based on 4 in/s PPV or 5 in /s PPV criteria, detailed results are summarized in Tables 5.4 and 5.5.

The calculation also shows that at the material level, the concrete pole is more vulnerable than the steel pole. In order to find a uniform blast limit, more attentions were given on the analysis of the concrete pole. One of the current prestressed concrete pole classification methods is based on the standard wood pole equivalent design. The common pole height is within the range of 30 feet to 125 feet. With the increasing of its height, the pole becomes less rigid. At the same height, a label with a larger number is assigned to the pole with a greater cross dimension. For instance, for the height of 30 feet pole, H_7 has the tip outer diameter 11.35 in, which is less than H_8 class (the tip outer diameter 13.15 in). Spectrum analysis was then performed with different response spectra designed based on various PPV criteria on the most rigid concrete pole (Wood Pole Class: 30-1) and the least rigid concrete pole (Wood Pole Class: 125-H_5) and the typical first principal stress state results are shown in Figure 5.15.

5.3 Summary

Spectrum analyses of two pole structures in operation power lines (OCP, OSP) were performed using two FE software (ALGOR® and ANSYS®). Pole structural responses of at the blast limit based on current 2 in/s peak particle velocity criteria were quantitatively investigated. Through designing different target spectra with various PPV criteria, pole dynamic responses at different levels of PPV were obtained. Spectrum analysis was also extended to other commonly used prestressed concrete poles. Structural responses of the most rigid pole and the least rigid pole under target response spectra designed based on various PPV blast limits were obtained. The results from this chapter would be used to compare with design requirements in Chapter 7 to develop a reasonable blast limit.

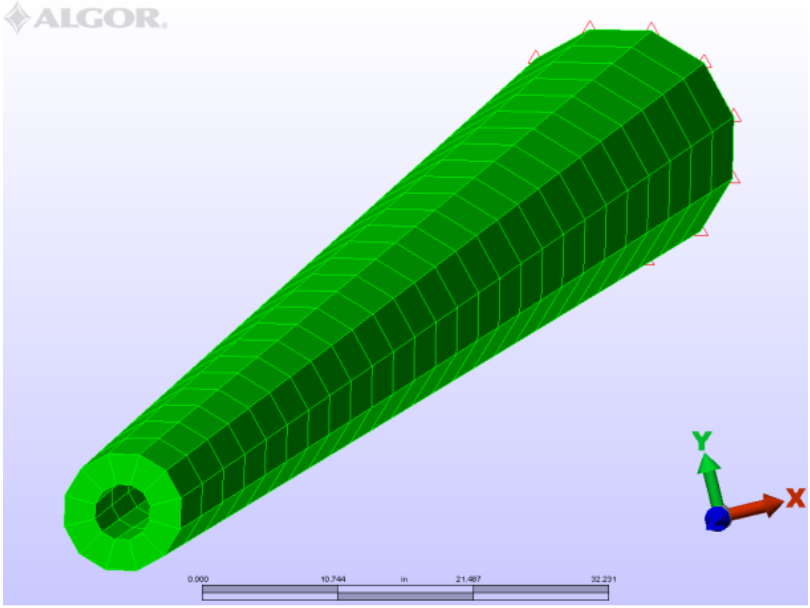

(a)

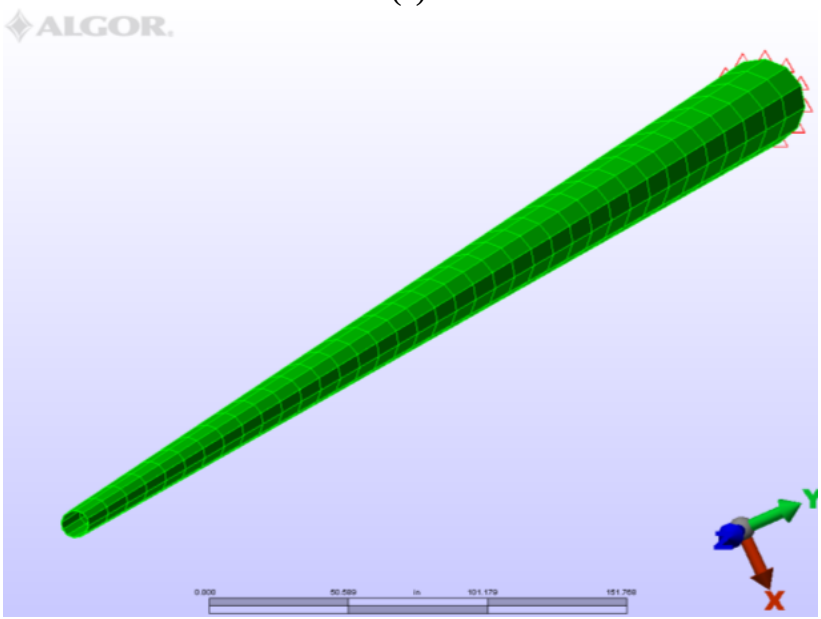

(b)

Figure 5.1: Pole models generated in ALGOR®: (a) concrete pole (OCP); (b) steel pole (OSP)

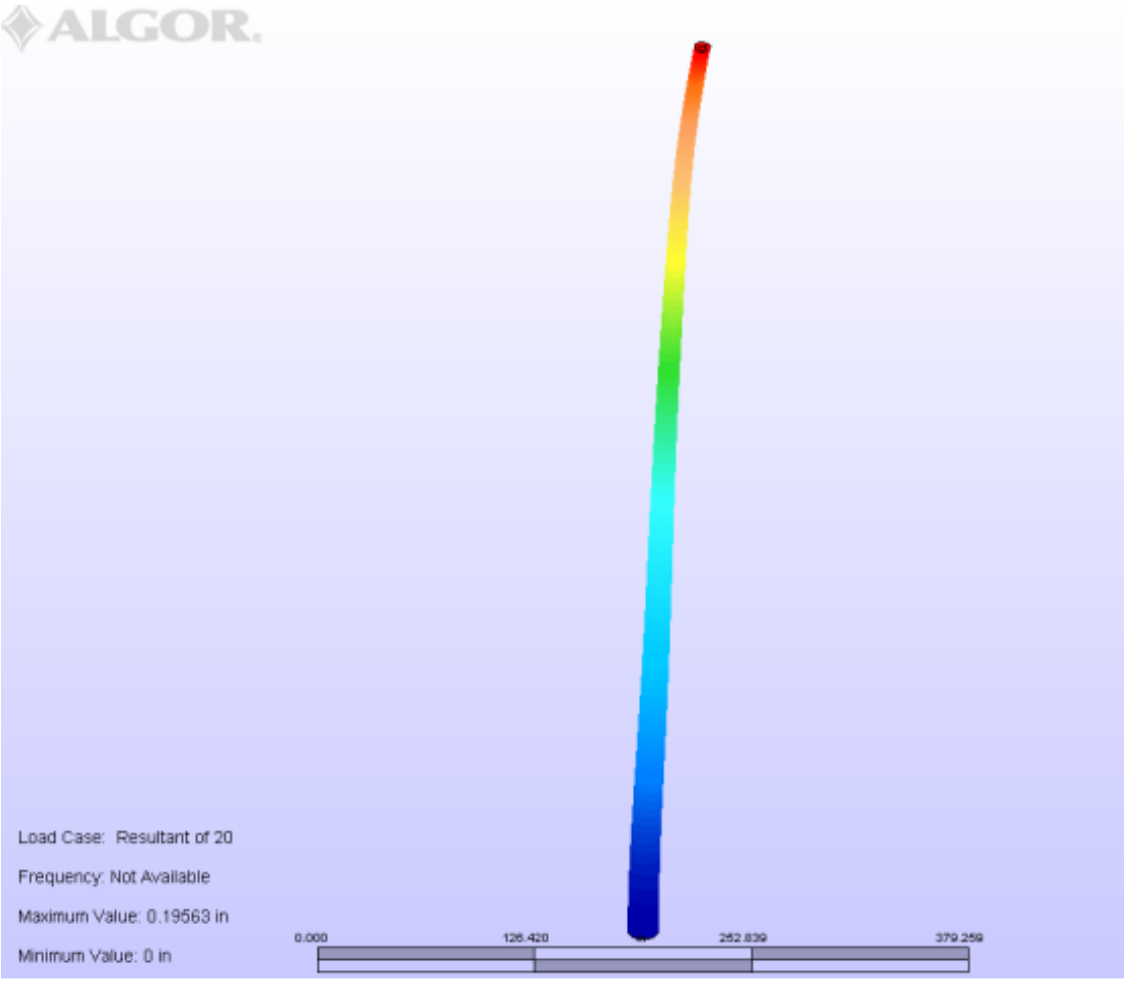

Figure 5.2: Concrete pole (OCP) spectrum analysis results at 2 in/s PPV criterion: displacement under the horizontal excitation (Maximum Value=0.196 in)

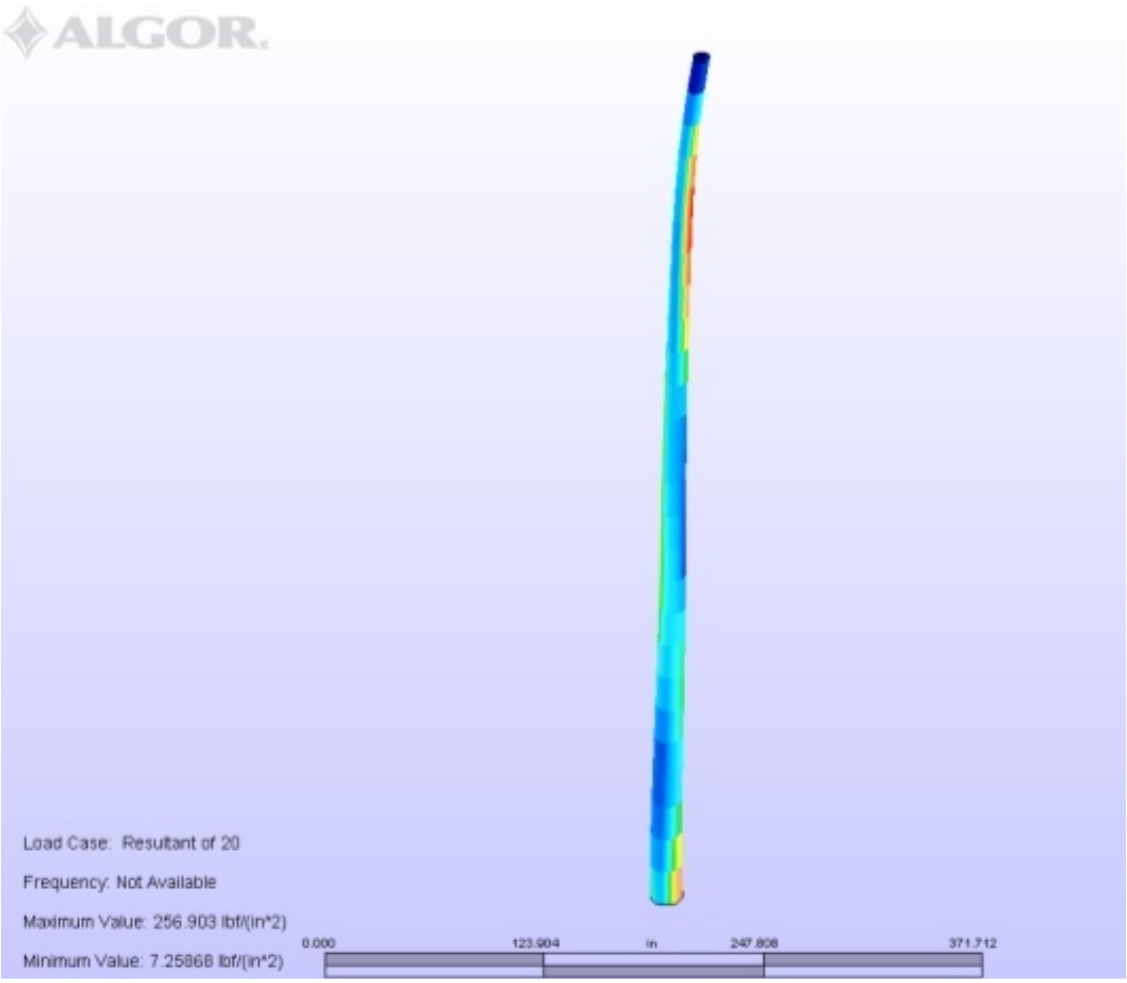

Figure 5.3: Concrete pole (OCP) spectrum analysis results at 2 in/s PPV criterion: first principal stress under the horizontal excitation (Maximum value=256.903 lbf/(in^2); Minimum value=7.259 lbf/(in^2))

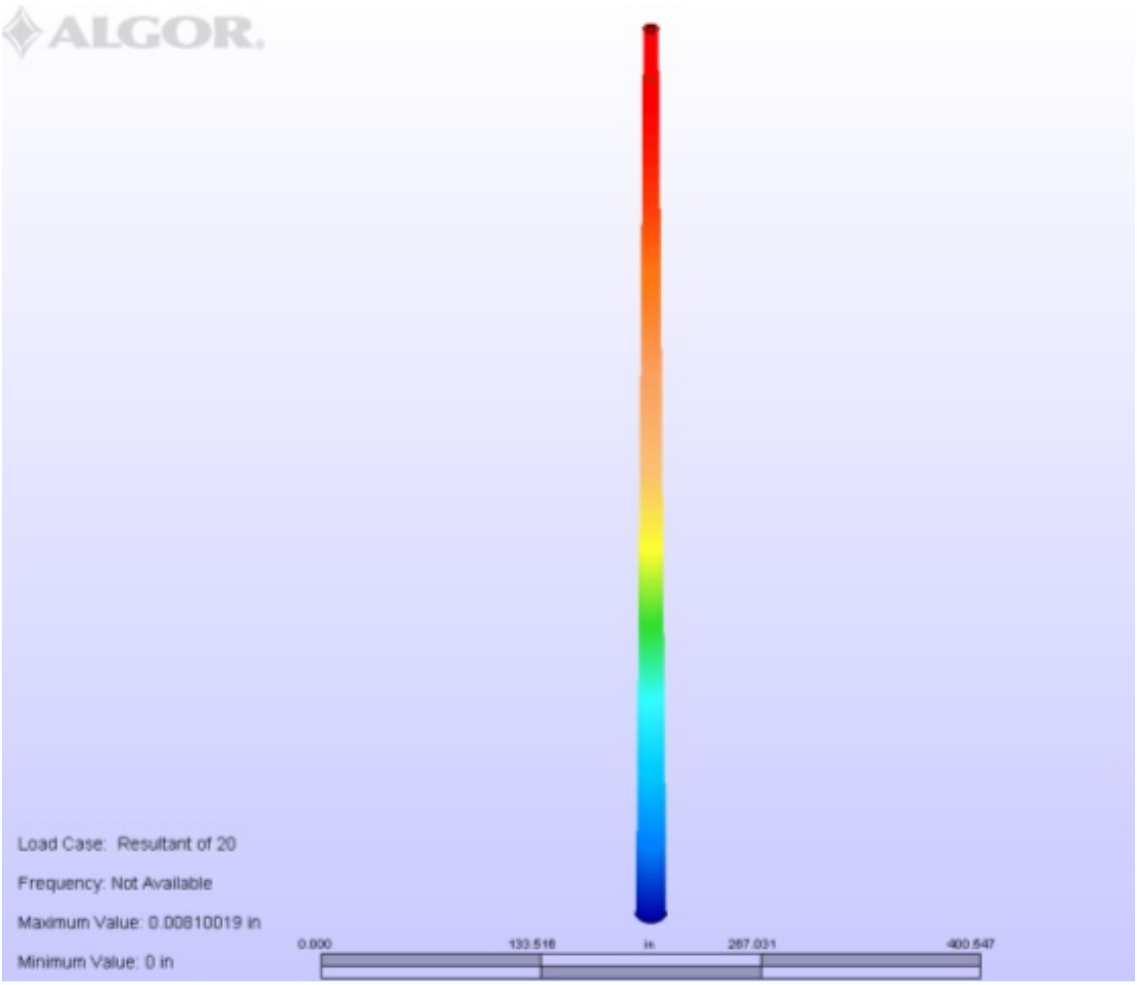

Figure 5.4: Concrete pole (OCP) spectrum analysis results at 2 in/s PPV criterion: displacement under the vertical excitation (Maximum Value=0.008 in)

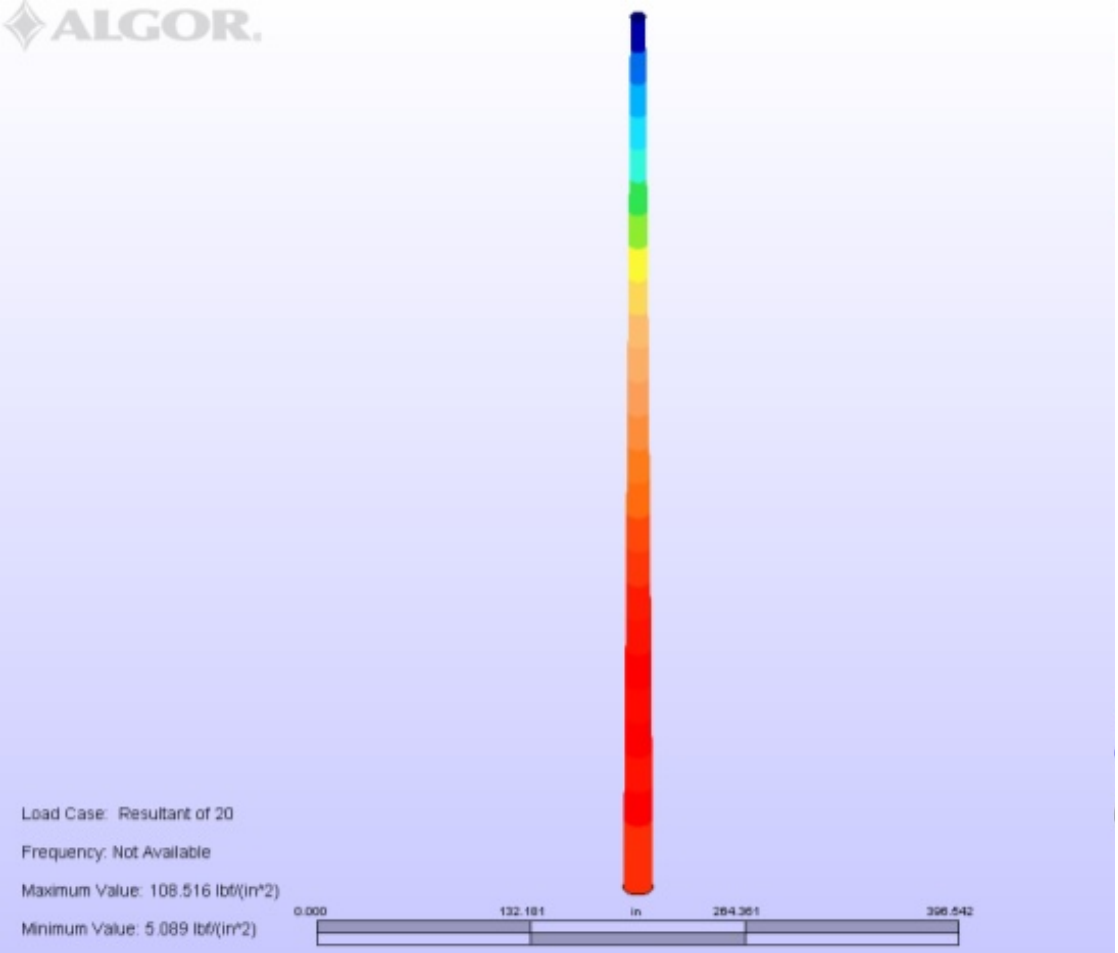

Figure 5.5: Concrete pole (OCP) spectrum analysis results at 2 in/s PPV criterion: first principal stress under the vertical excitation (Maximum value=108.516 lbf/(in^2); Minimum value=5.089 lbf(in^2))

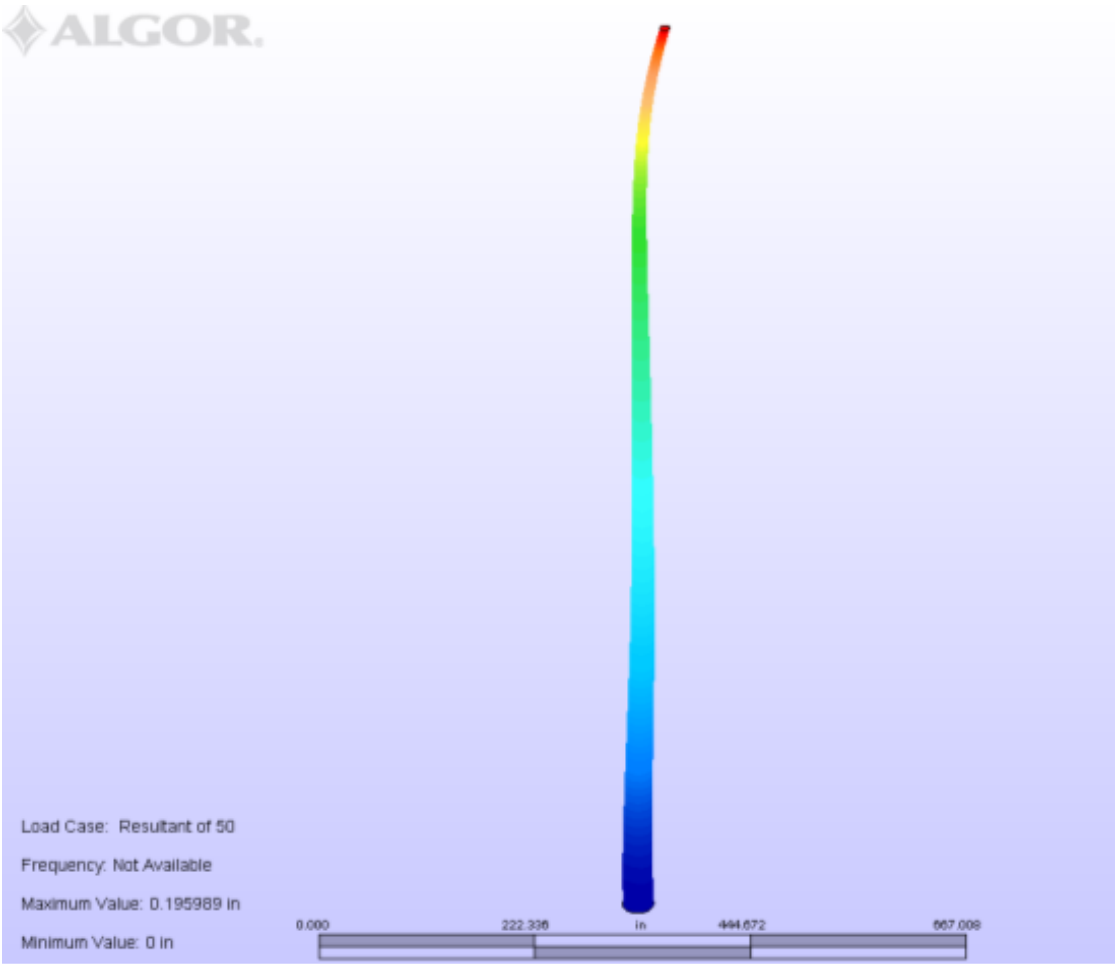

Figure 5.6: Steel pole (OSP) spectrum analysis results at 2 in/s PPV criterion: displacement under the horizontal excitation (Maximum value=0.196 in)

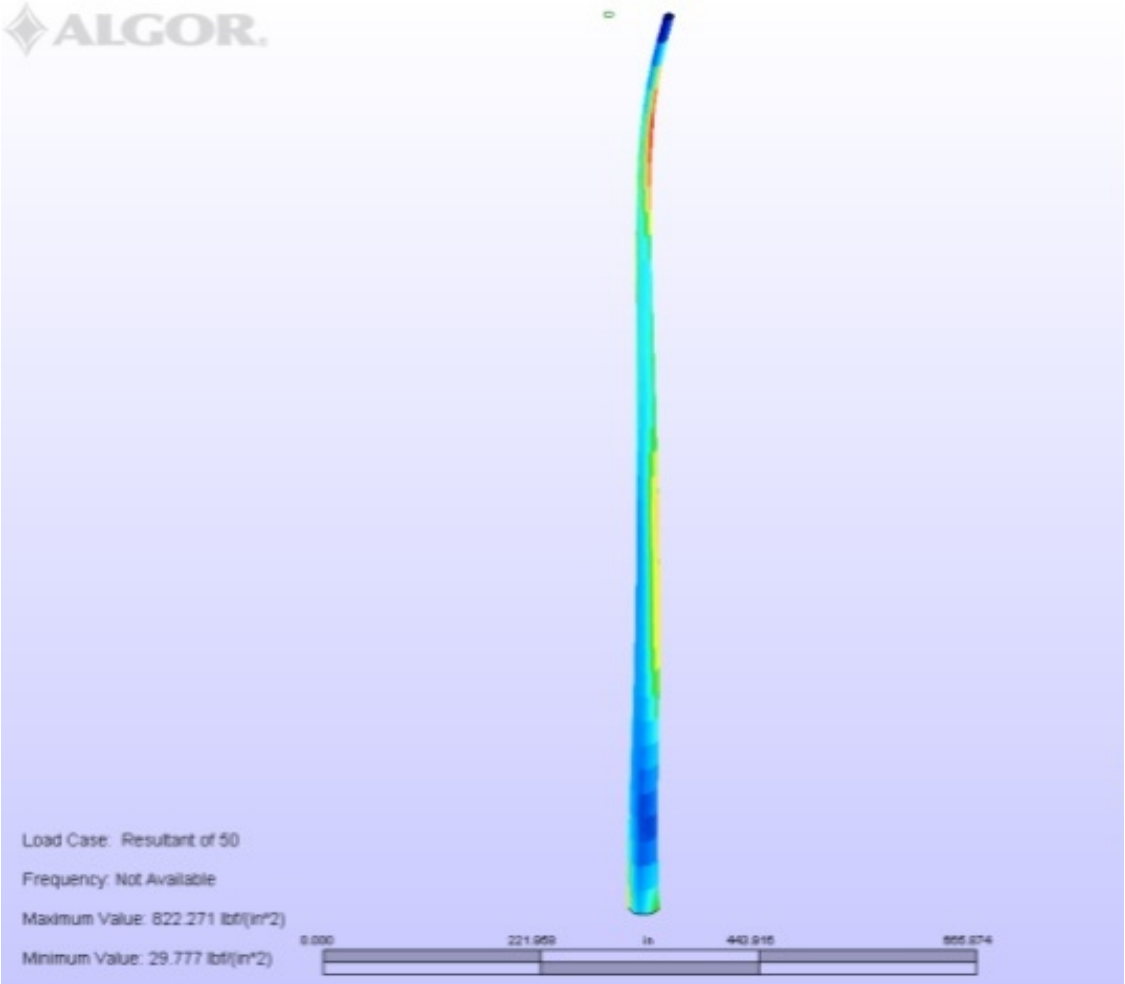

Figure 5.7: Steel pole (OSP) spectrum analysis results at 2 in/s PPV criterion: first principal stress under the horizontal excitation (Maximum value=822.271 lbf/(in^2); Minimum value=29.777 lbf/(in^2))

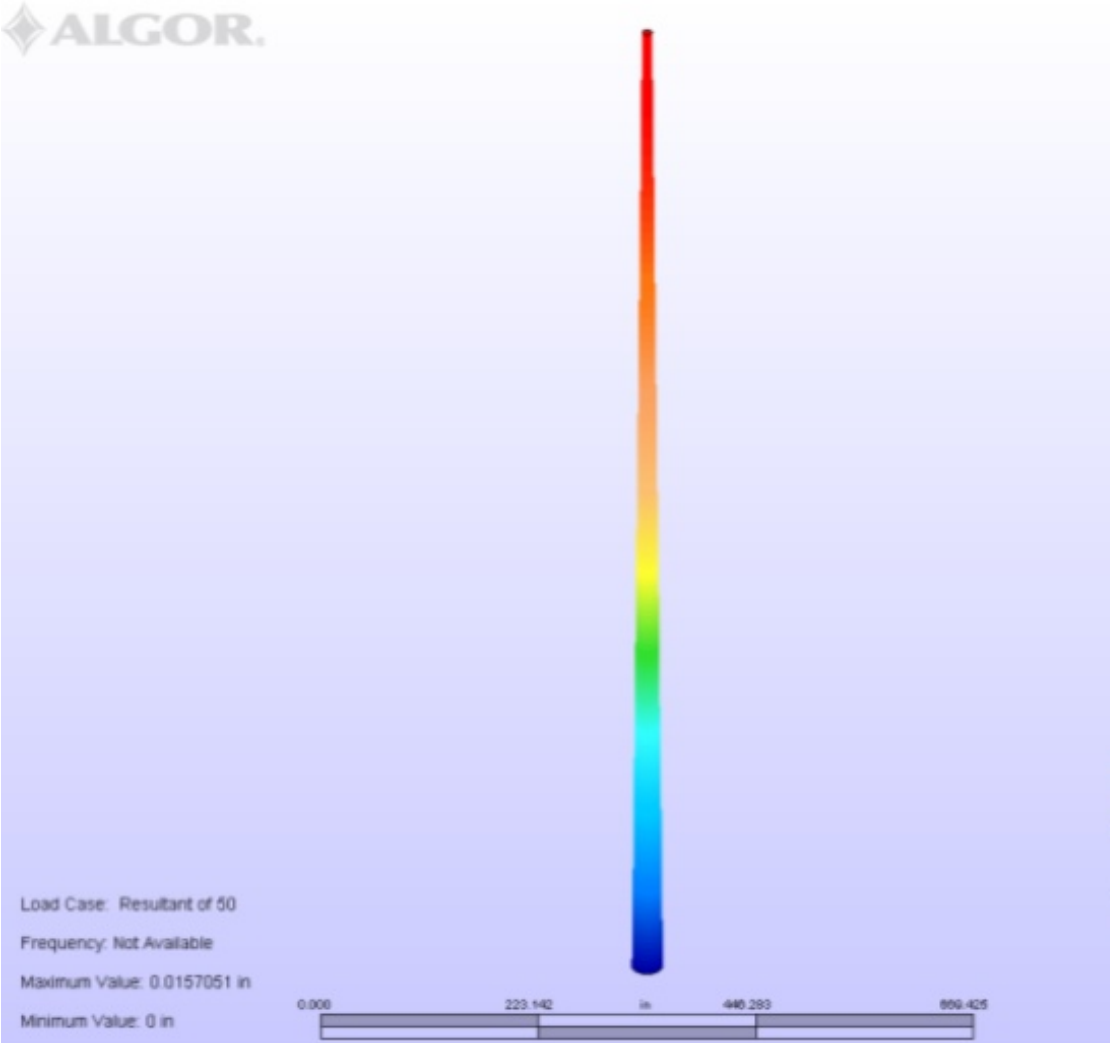

Figure 5.8: Steel pole (OSP) spectrum analysis results at 2 in/s PPV criterion: displacement under the vertical excitation (Maximum value=0.016 in)

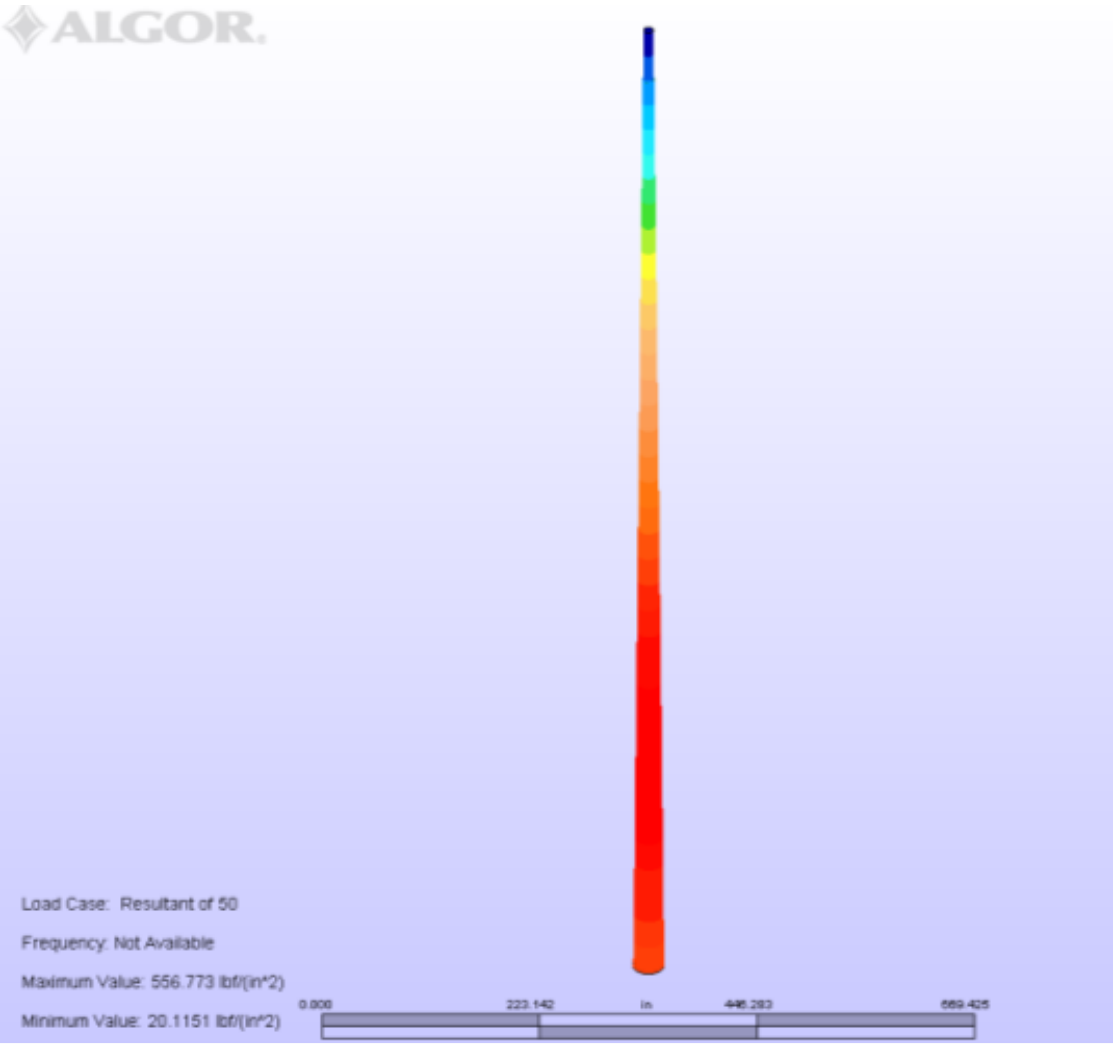

Figure 5.9: Steel pole (OSP) spectrum analysis results at 2 in/s PPV criterion: first principal stress under the vertical excitation (Maximum value=556.773 lbf/(in^2); Minimum value=20.115 lbf/(in^2))

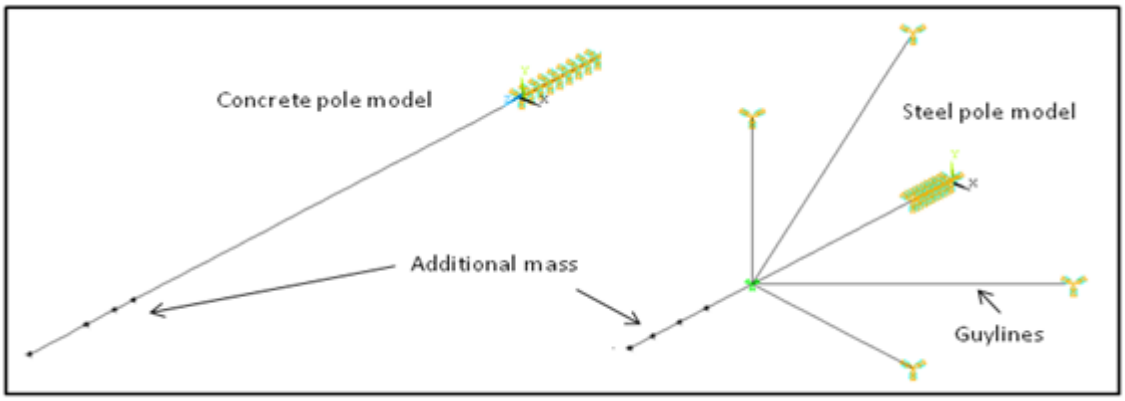

Figure 5.10: Pole FE models in ANASYS®

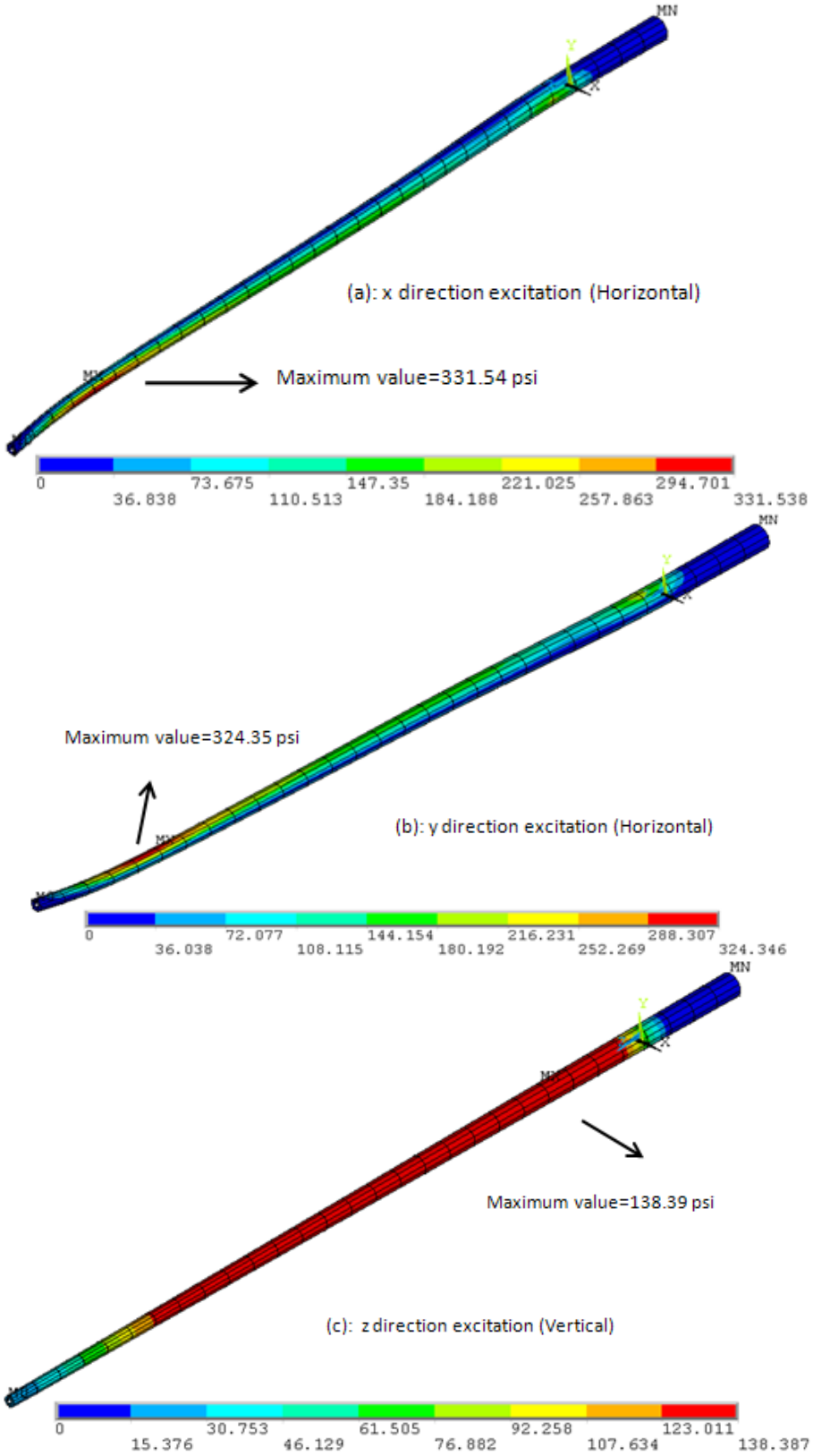

Figure 5.11: ANSYS results of first principal stress at 2 in/s PPV criterion for the concrete pole (OCP)

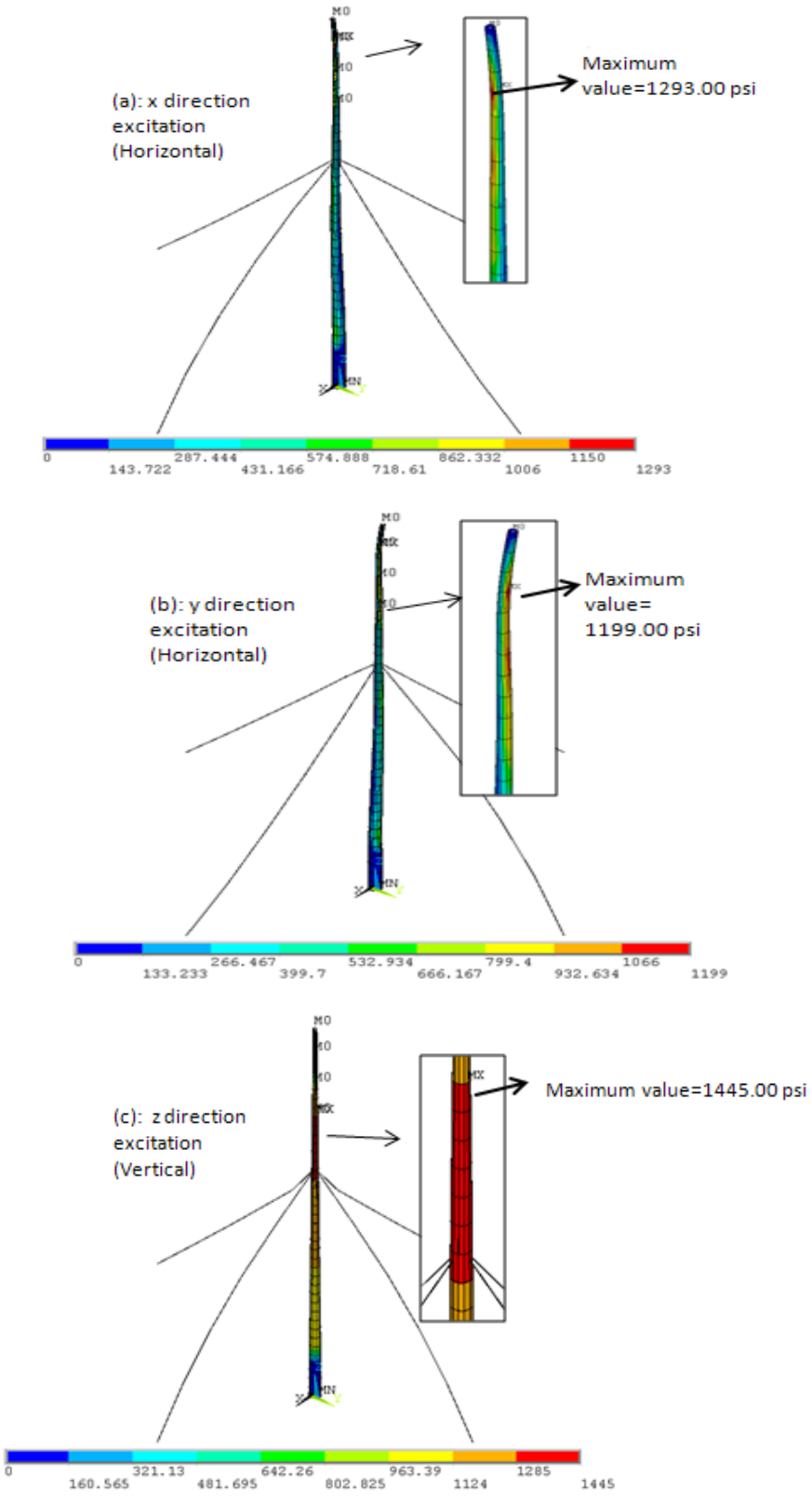

Figure 5.12: ANSYS results of first principal stress at 2 in/s PPV criterion for the steel pole (OSP)

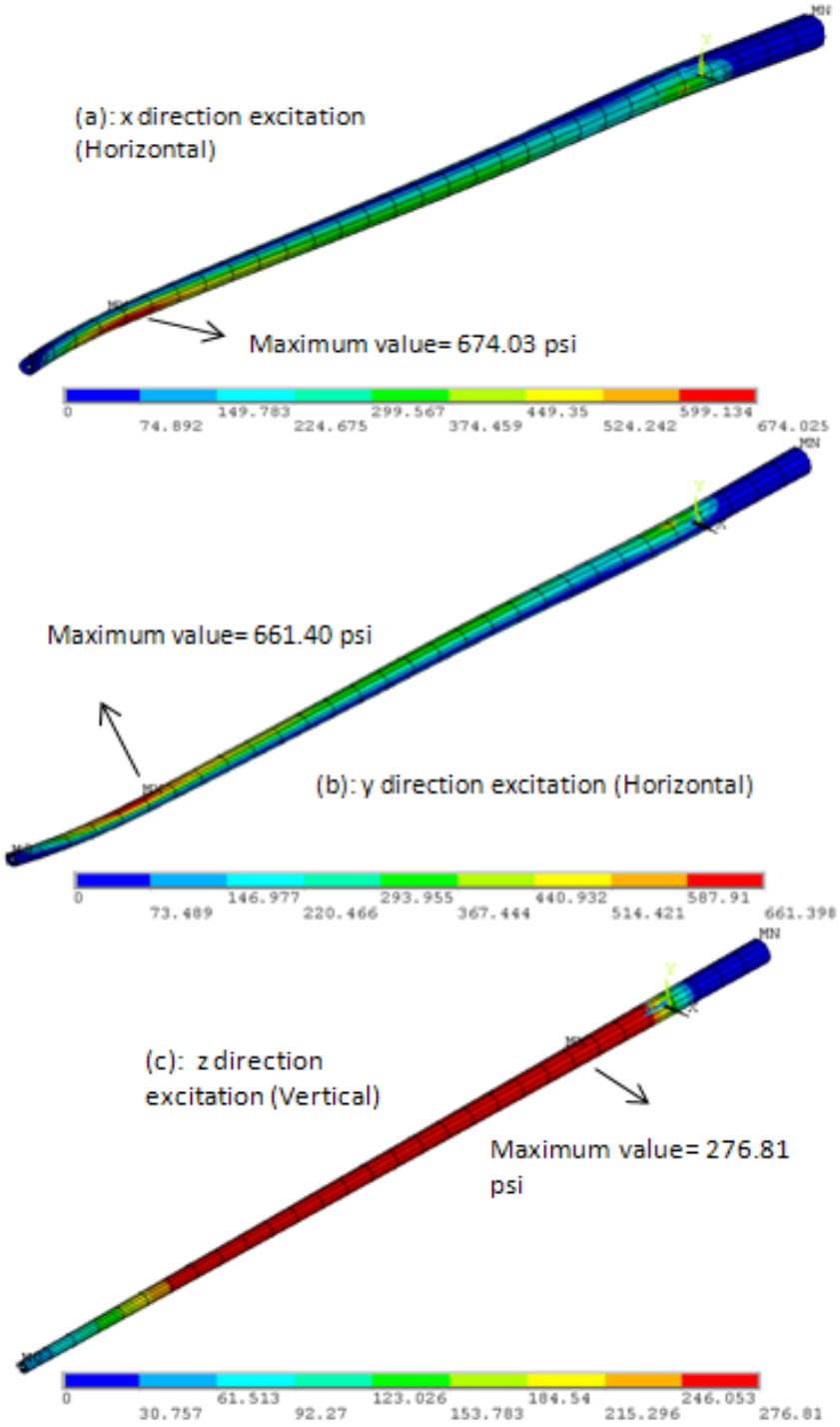

Figure 5.13: ANSYS® results of the concrete pole (OCP) first principal stress at 4 in/s PPV criterion

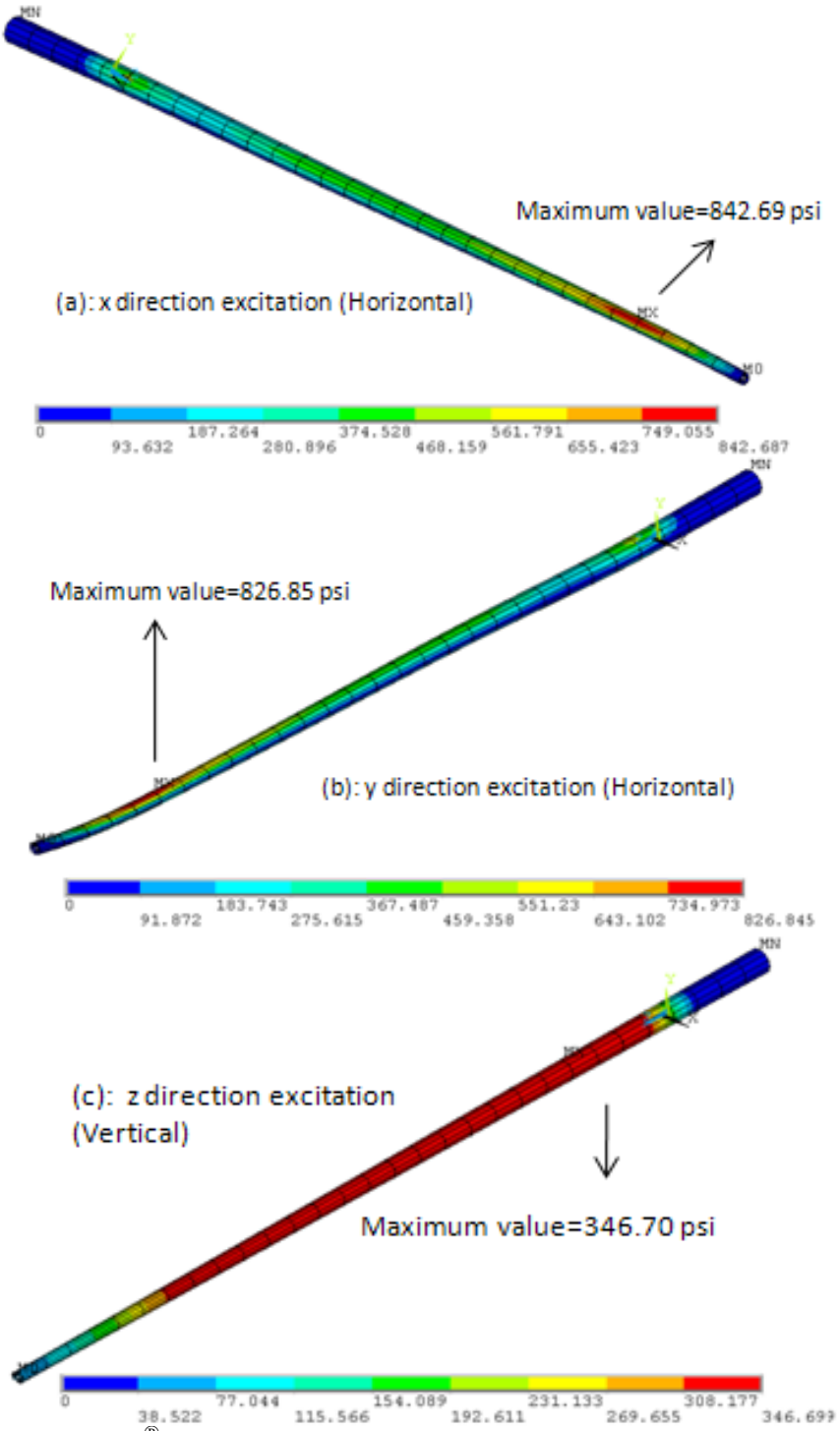

Figure 5.14: ANSYS® results of the concrete pole (OCP) first principal stress at 5 in/s PPV criterion

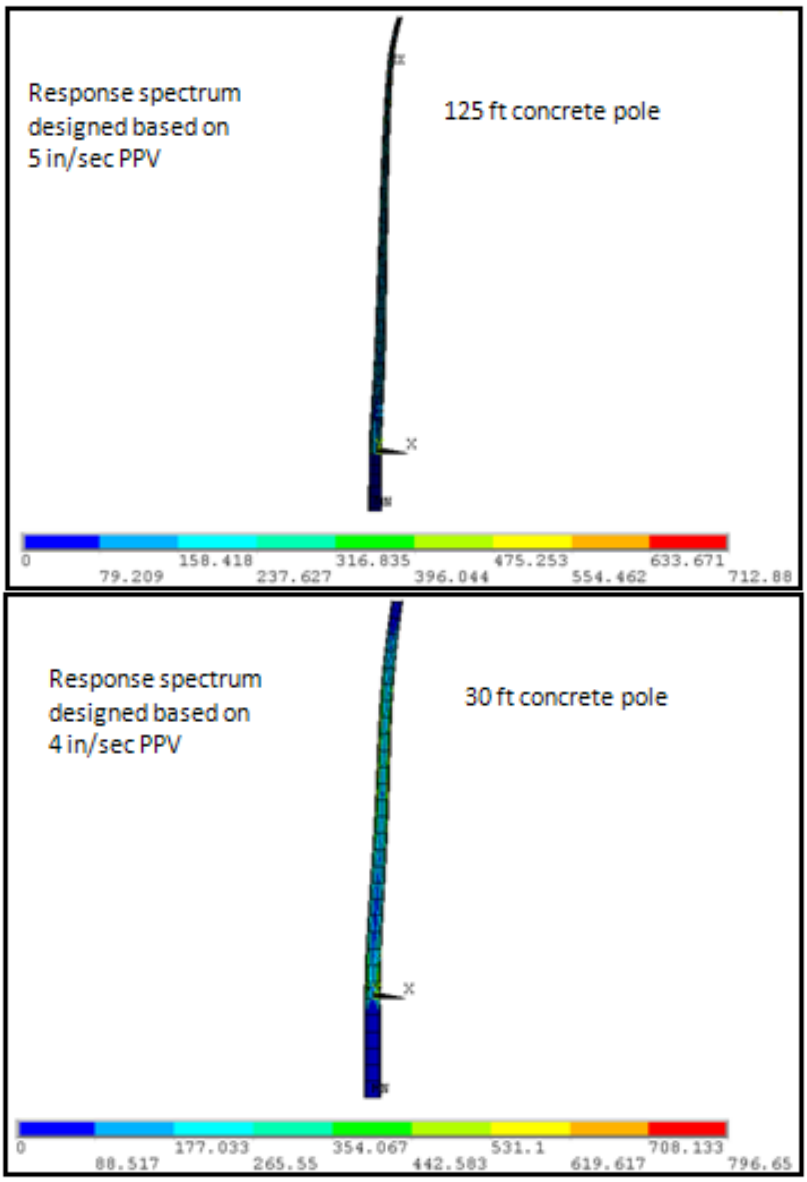

Figure 5.15: Typical spectrum analysis results of different types of concrete poles

Table 5.1: Model parameters for the pole structures

Parameters	*Concrete pole (OCP)*	*Steel pole (OSP)*
Overall length (ft)	60.00	105.00
Embedment depth (ft)	8.00	12.50
Density (lb/ft^3)	160.00	490.00
Modulus of elasticity (ksi)	6021.90	29000.00
Tip outer diameter (in)	9.55	10.13
Tip inner diameter (in)	4.55	10.06
Butt outer diameter (in)	20.35	35.69
Butt inner diameter (in)	15.35	35.32

Table 5.2: Modal analysis and spectrum analysis results from ALGOR® at 2 in/s PPV criterion

Concrete pole (OCP)			*Steel pole (OSP)*		
Natural frequency (Hz)*	1st	1.46	Natural frequency (Hz)*	1st	1.17
	2nd	6.64		2nd	4.82
	3rd	16.82		3rd	11.77
	4th	31.86		4th	21.99
Maximum displacement (in)	X	0.19	Maximum displacement (in)	X	0.20
	Z	0.008		Z	0.016
Maximum 1st principal stress (psi)	X	256.90	Maximum 1st principal stress (psi)	X	822.27
	Z	108.52		Z	566.78

*All modes here are bending modes.

Table 5.3: Spectrum analysis results from ANSYS® at 2 in/s PPV criterion

Concrete pole (OCP)			*Steel pole (OSP)*		
Maximum displacement	X	0.13 in	Maximum displacement	X	0.11 in
	Y	0.14 in		Y	0.12 in
	Z	0.01 in		Z	0.04 in
Fix-end reaction	Fx	1392.10 lb	Fix-end reaction	Fx	922.34 lb
	My	120520.00 lb-in		My	134830.00 lb-in
	Fy	1447.70 lb		Fy	879.68 lb
	Mx	124990.00 lb-in		Mx	127490.00 lb-in
	Fz	17158.00 lb		Fz	18630.00 lb
Maximum 1st principal stress	X	331.54 psi	Maximum 1st principal stress	X	1293.00 psi
	Y	324.35 psi		Y	1119.00 psi
	Z	138.39 psi		Z	1445.00 psi

Note: (1) X ,Y and Z are excitation directions; (2) Fix-end reactions are the maximum reaction force.

Table 5.4: Spectrum analysis results at 4 in/s PPV criterion

Concrete pole (OCP) structural response under 4 in/s PPV criterion		
Maximum displacement	X	0.27 in
	Y	0.29 in
	Z	0.02 in
Fix-end reaction	Fx	3164.90 lb
	My	246080.00 lb-in
	Fy	3254.60 lb
	Mx	254390.00 lb-in
	Fz	34319.00 lb
Maximum 1st principal stress	X	674.03 psi
	Y	661.40 psi
	Z	276.81 psi

Table 5.5: Spectrum analysis results at 5 in/s PPV criterion

Concrete pole (OCP) structural response under 5 in/s PPV criterion		
Maximum displacement	X	0.33 in
	Y	0.36 in
Fix-end reaction	Fx	3959.50 lb
	My	307690.00 lb-in
	Fy	4071.50 lb
	Mx	318070.00 lb-in
Maximum 1st principal stress	X	842.69 psi
	Y	826.85 psi

CHPATER 6: TIME HISTORY ANALYSIS OF TRANSMISSION POLES

6.1 Introduction

To study transmission structure responses under strong ground vibration, dynamic analysis can be performed using the finite element (FE) method. Spectrum and time history analyses are two typical approaches to obtain structural behaviors under dynamic loads. Spectrum analysis, discussed in Chapter 5, is usually included in dynamic design of a system. Time history analysis, or transient dynamic analysis, a technique used to obtain time-varying displacements, stresses, forces etc. of a structure excited by time-dependent loads is an uncommon design practice due to its time consuming computation. Most design codes suggest that for an important structure or unusual loading conditions, time history analysis needs to be conducted to supply necessary information for a safe design.

Spectrum analysis of transmission pole structures was performed in Chapter 5. The objective of this chapter is to provide supplement information for blast limit development and at the same time, to verify the results from spectrum analysis. Since from Chapter 5 the concrete pole is more vulnerable during blasting induced ground vibration, in Chapter 6, time history analysis was implemented only to the prestressed concrete pole (OCP). The results from this chapter provide valuable information about the concrete pole structural response time history.

The simplified pole FE models were first established based on modal analysis results (Chapter 4). The input excitations are the blast induced ground vibration record from field monitoring work (Chapter 3) as well as the artificially modified ground motions, which was realized by amplifying the amplitude of the signal for simplicity. Structural responses of the concrete pole (OCP) under various target spectra were obtained. Through comparing analysis results with the design capacity of these poles, a reasonable blast limit would be proposed, which is summarized in Chapter 7.

6.2 Blast records

An extensive blast monitoring was carried out at coal mines and a rock quarry in southeastern U.S. (Alabama and Georgia states) (Chapter 3). A typical time history of ground movement velocity (Figure 6.1, R5 record: PPV=0.375 in/s for vertical direction; PPV=0.21 in/s for the transverse direction) was selected and numerically integrated into acceleration time history, which was taken as the basic excitation in the finite element analysis. Its corresponding acceleration time history is shown in Figure 6.2. The modified ground excitations were obtained by amplifying original signals (Figure 6.1). These modified ground motion accelerations, if being integrated into velocities, maximum amplitudes are the target PPV values, i.e., 2 in/s as in Figure 6.3 or 4 in/s as in Figure 6.4.

6.3. Time history analysis

Strong interaction phenomena between support structures and cables were observed in transmission grids, which made it difficult to exactly model the electric transmission line system (Ozono et al. 1988; Ozono et al. 1992). Different FE models were generated to study dynamic behaviors of the two poles. The details of FE modeling of these two transmission pole structures can be referred to in Chapter 4. Simplified FE models,

established following the method proposed by Li et al. (2005) were chosen for performing time history analysis in this chapter.

Implicit time history analysis was performed numerically using ANSYS (2007). The transient dynamic equilibrium equation (Equation (6.1)) of the pole was directly solved by the Newmark time integration method. The time step is $\Delta t = 0.001(\mathrm{s})$ and hence, there are a total of 6656 steps of iterations involved.

$$[M]\{\ddot{x}\} + [C]\{\dot{x}\} + [K]\{x\} = \{F\} \tag{6.1}$$

where $[M]$ is mass matrix; $[C]$ is damping matrix; $[K]$ is structural stiffness matrix; $[\ddot{x}]$ is acceleration vector; $[\dot{x}]$ is velocity vector; $[x]$ is displacement vector; and $\{F\}$ is excitation vector.

Damping $[C]$ is Rayleigh damping in the form of (Tedesco et al. 1999):

$$[C] = \alpha[M] + \beta[K] \tag{6.2}$$

α and β were calculated from:

$$\zeta_r = \frac{1}{2}\left(\frac{\alpha}{\omega_r} + \beta\omega_r\right) \tag{6.3}$$

where ζ_r is damping ratio and it was assumed to be 0.02 for the pole structure (ASCE 1991); ω_r is the natural frequency and could be obtained from the field modal testing or from the FE modal analysis. In this reseach, $\omega_1 = 38.33\, rad/s$ and $\omega_2 = 95.88\, rad/s$ for the concrete pole (OCP). Therefore, $\alpha = 1.0948$ and $\beta = 0.0003$ were calculated.

The input excitations included original blast records (Figure 6.1) as well as artificially modified ground vibration time histories based on the original blast measurements. This modification work was simply realized by amplifying the acceleration amplitude with certain factors. The transverse acceleration time histories were input at the pole base as horizontal excitation from both in-plane (parallel with the power lines) and out-of-plane

(perpendicular to the power lines) directions; while the vertical acceleration record and its modifications were taken as vertical input excitations.

Three main structural responses were investigated: (1) tip displacement of the pole; (2) maximum moment at the ground line; and (3) maximum first principal stress.

Figure 6.5 shows tip displacements of the concrete pole (OCP) under the original ground motion record (Figure 6.2), including both horizontal and vertical excitations. Figure 6.6 shows moment time histories when the concrete pole (OCP) was excited with original ground vibration records (Figure 6.2). Maximum values of both tip displacements and ground line moments are identified and listed in Table 6.1.

A modified ground vibration velocity was obtained by amplifying the original ground motion record to ensure its velocity time history satisfied specified PPV (i.e. 2 in/s). After that, it was differentiated into acceleration time history. Structural responses of the concrete pole were obtained by inputting modified ground movements as an exterior excitation. Tip displacements of the pole (OCP) and ground line moments are shown in Figures 6.7 and 6.8. Maximum values of these variables are also summarized in Table 6.1.

The concrete pole (OCP) maximum first principal stresses under different ground excitations were obtained by identifying stress states at corresponding peak structural responses. Figure 6.9 and Figure 6.10 shows the first principal stress diagram. Maximum values are summarized in Table 6.1.

Compared with spectrum analysis results from Chapter 5, structural responses of the concrete pole (OCP) using time history analysis are slightly larger than those from Chapter 5. But they are in the same order of magnitudes. This increases the confidence

about the results from both analyses. Table 6.2 lists main parameters obtained from both methods.

Computation work was further performed with input excitations designed based on other different peak particle velocity criteria. Figure 6.11 shows results of the concrete pole (OCP) structural responses under modified ground vibrations based on 3 in/s PPV, which has a peak displacement of 0.3 in, maximum moment of around 250 in-kip, and maximum first principal stress of 858.64 psi.

6.4 Summary

Time history dynamic analyses were performed on the prestressed concrete pole (OCP) excited by selected original ground motion records from blast monitoring and their modified ground vibrations based on different peak particle velocity criteria. The results from these transient analyses are close to spectrum analysis results from Chapter 5. They provide supplement information useful for the later blast limit establishment in Chapter 7.

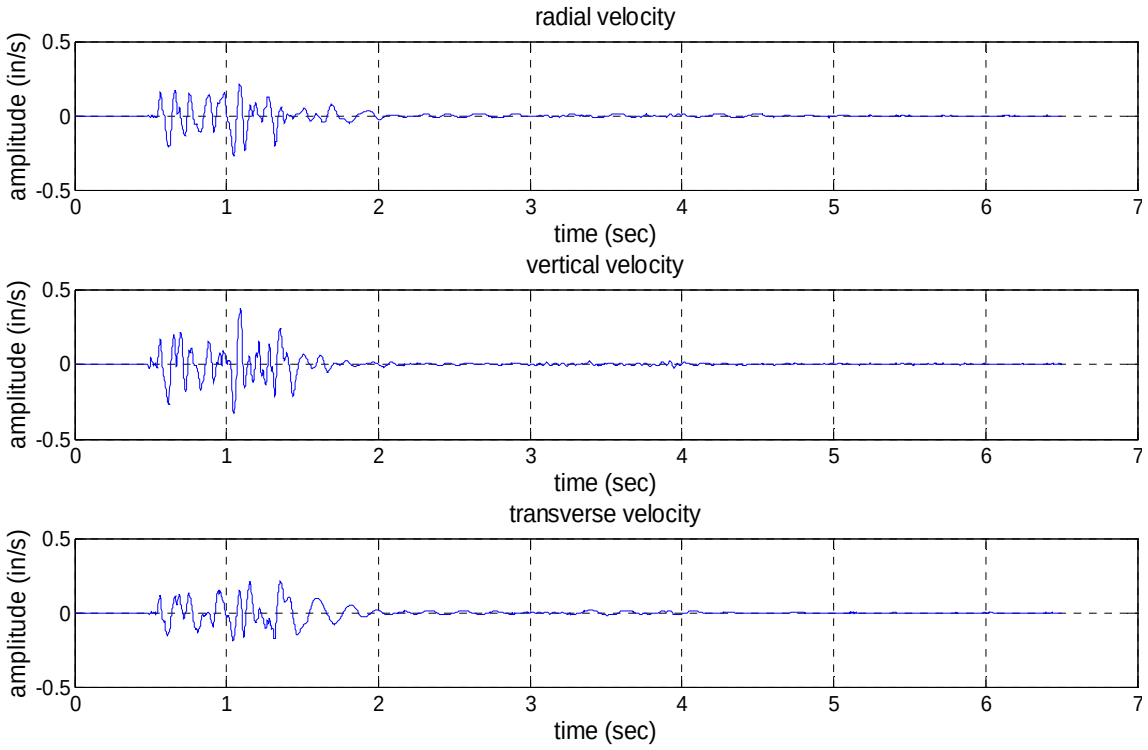

Figure 6.1: A typical velocity time history of ground vibration

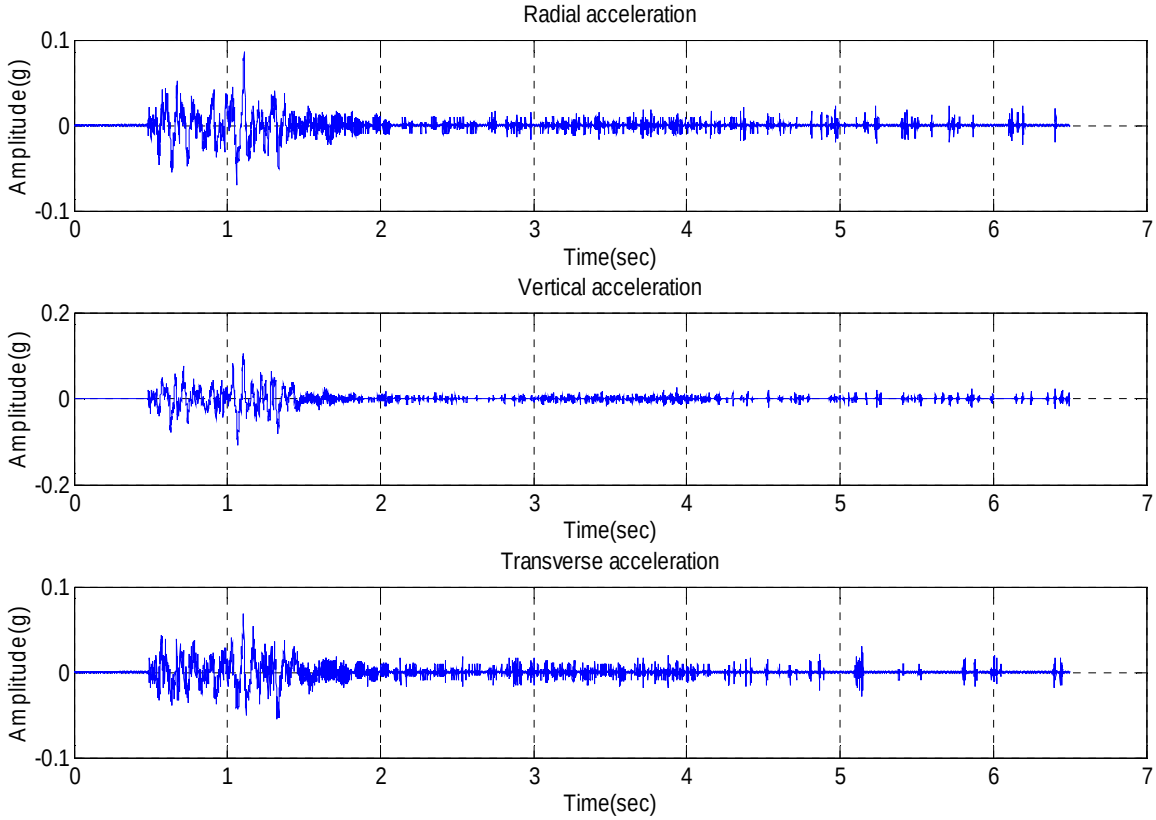

Figure 6.2: Acceleration time history of ground movements used as input excitations

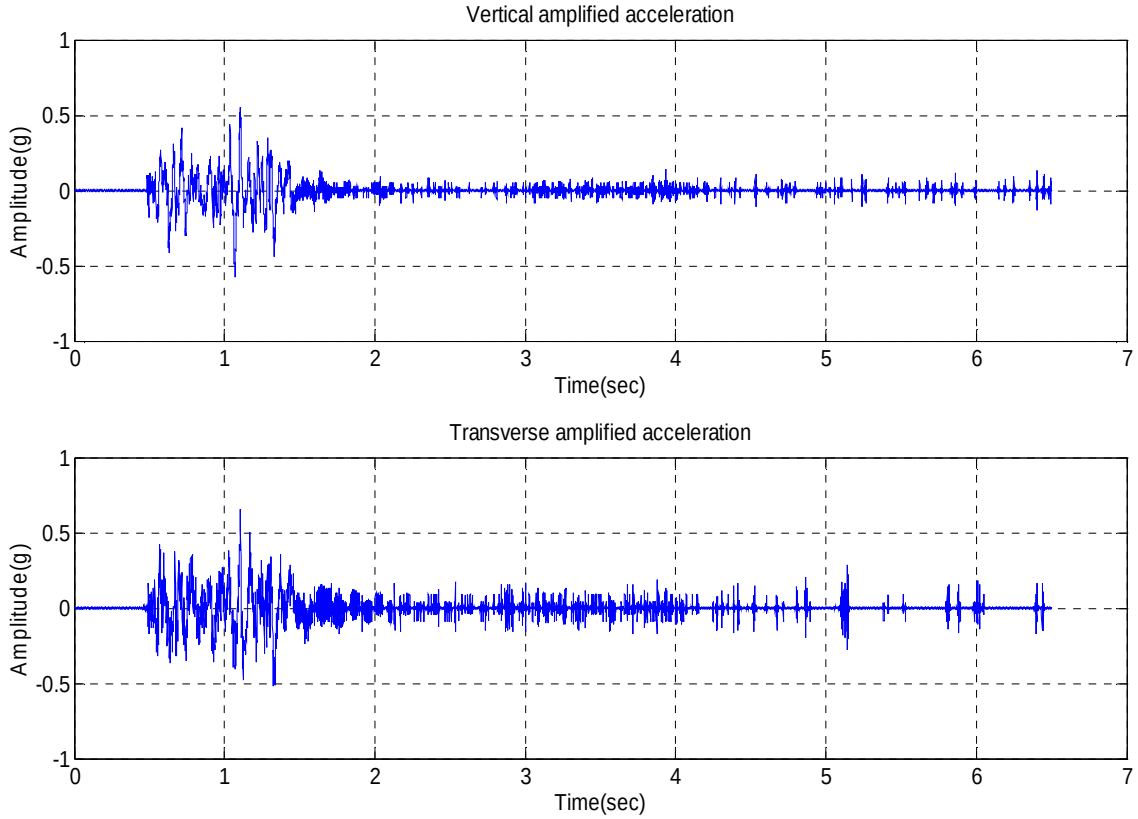

Figure 6.3: Modified acceleration time histories of ground movements based on 2 in/s PPV

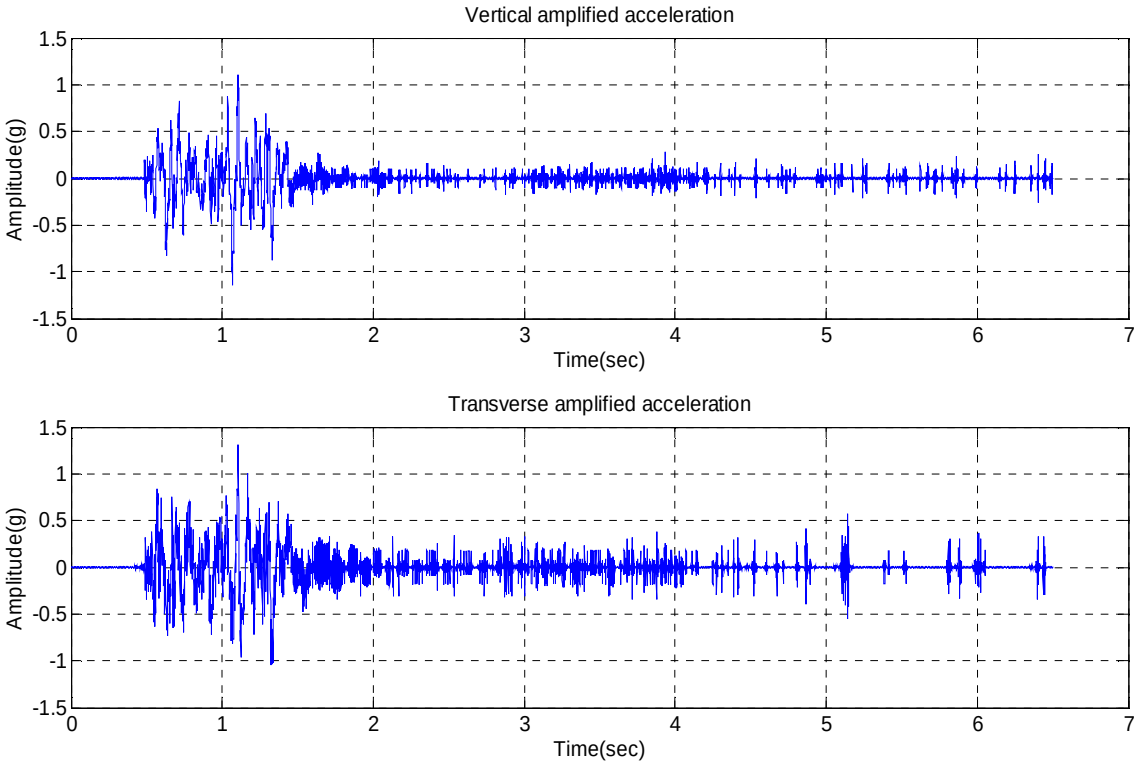

Figure 6.4: Modified acceleration time histories of ground movements based on 4 in/s PPV

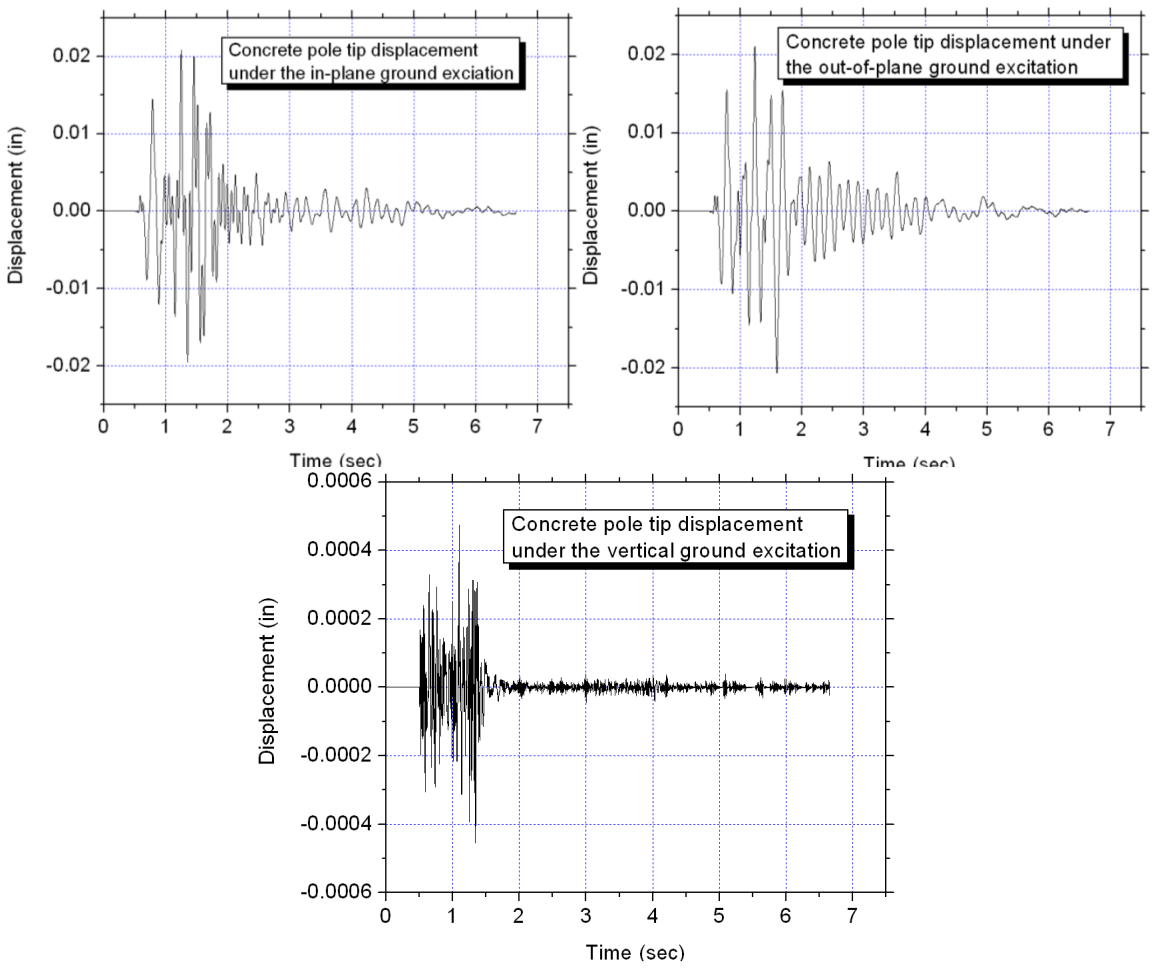

Figure 6.5: The concrete pole (OCP) tip vibration under the original ground movement record

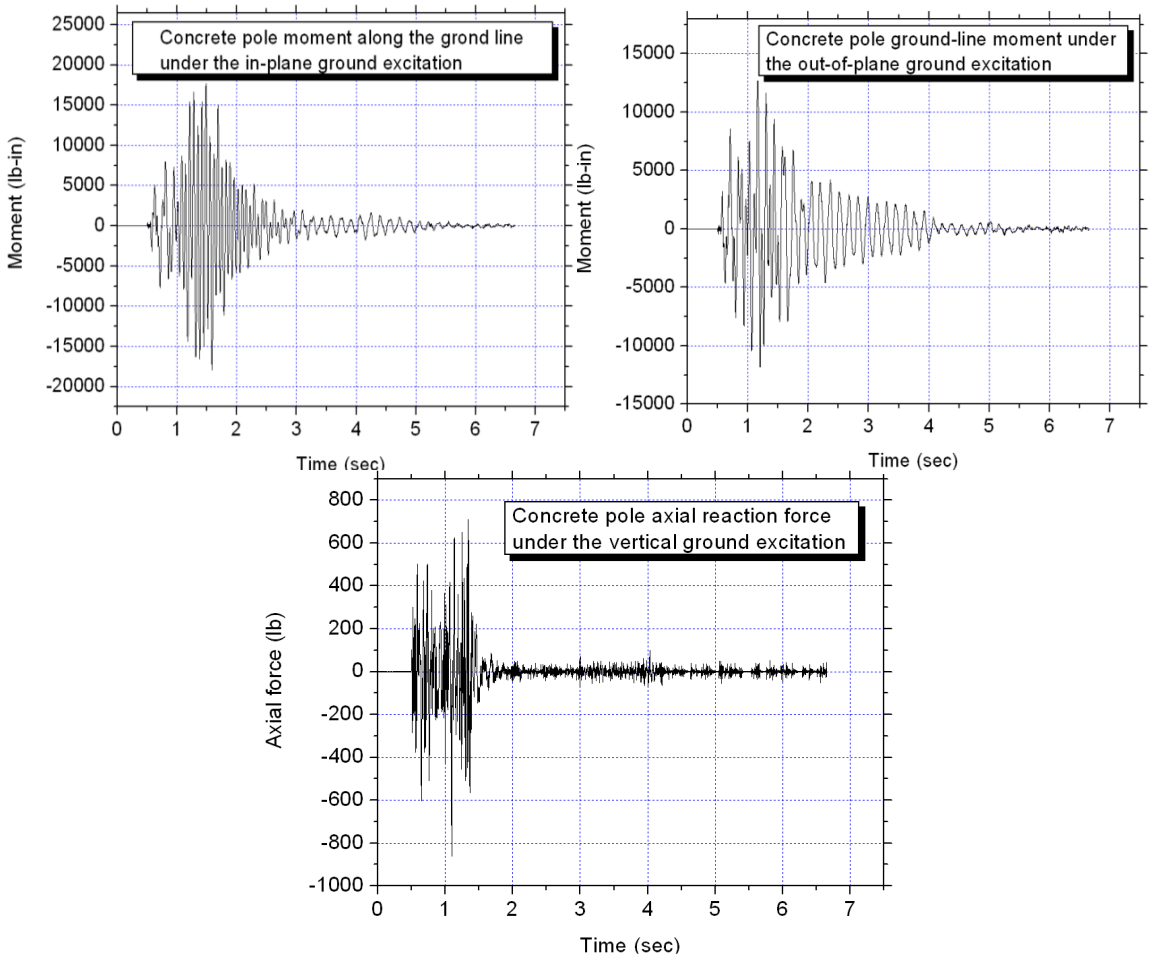

Figure 6.6: The concrete pole (OCP) reactions under the original ground movement record

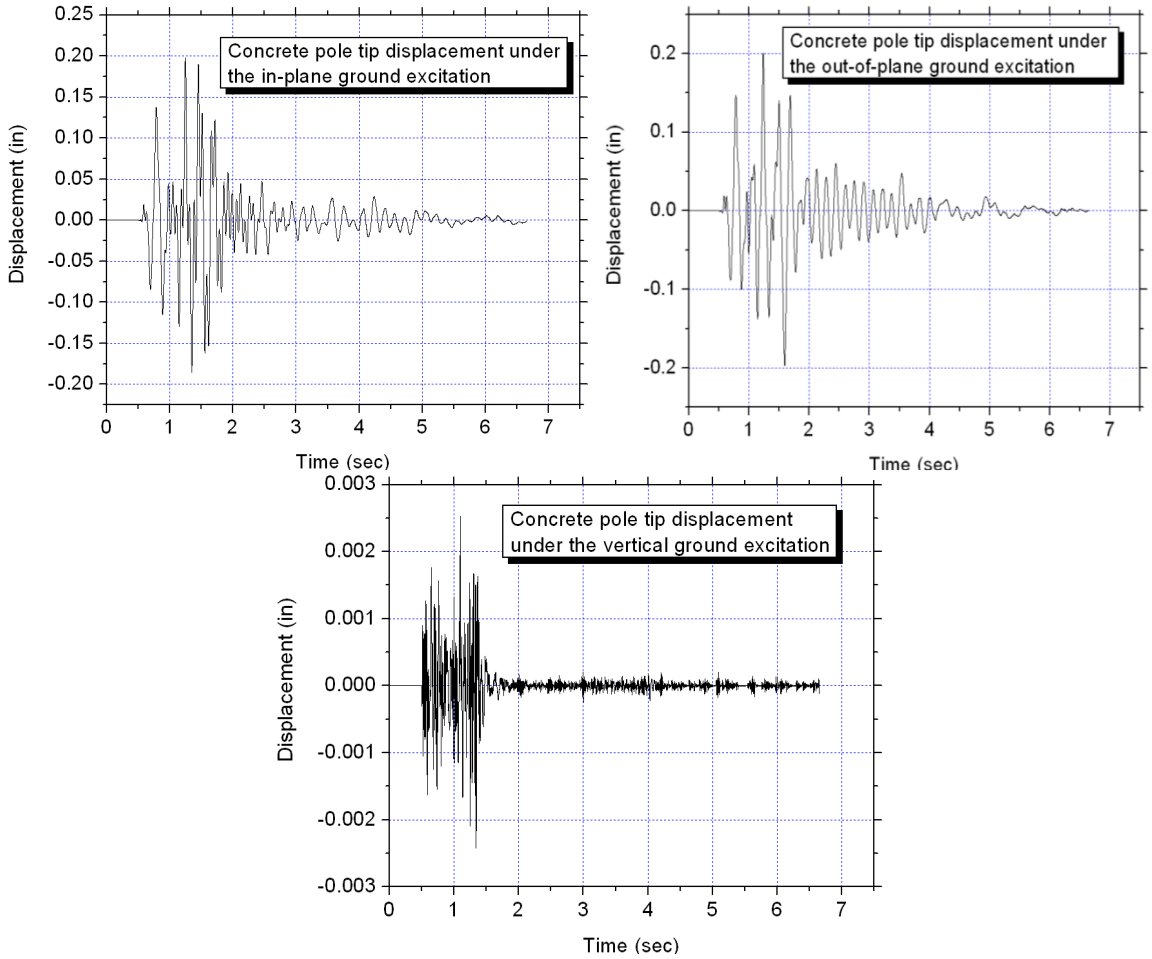

Figure 6.7: The concrete pole (OCP) tip vibration under the modified ground movement based on 2 in/s PPV

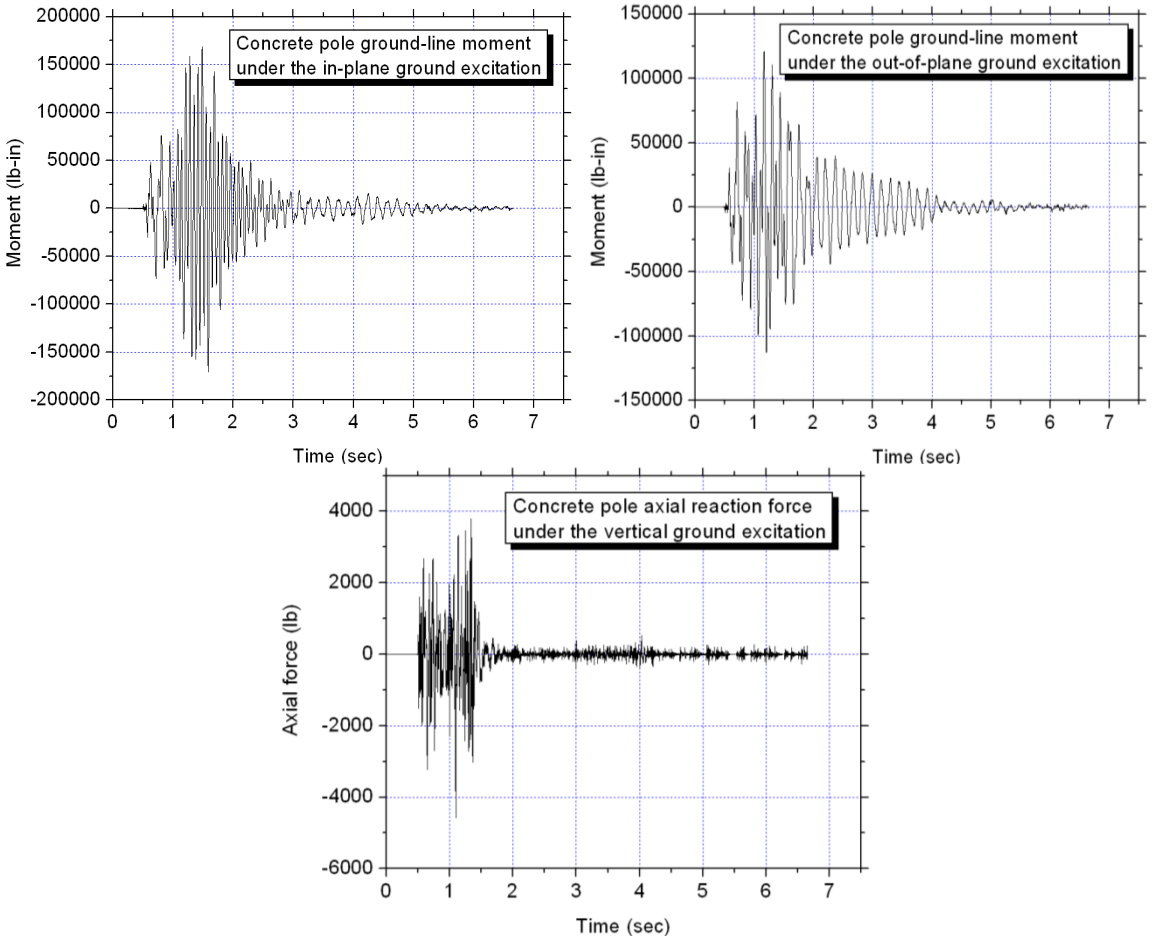

Figure 6.8: The concrete pole (OCP) ground line reactions under the modified ground vibration based on 2 in/s PPV

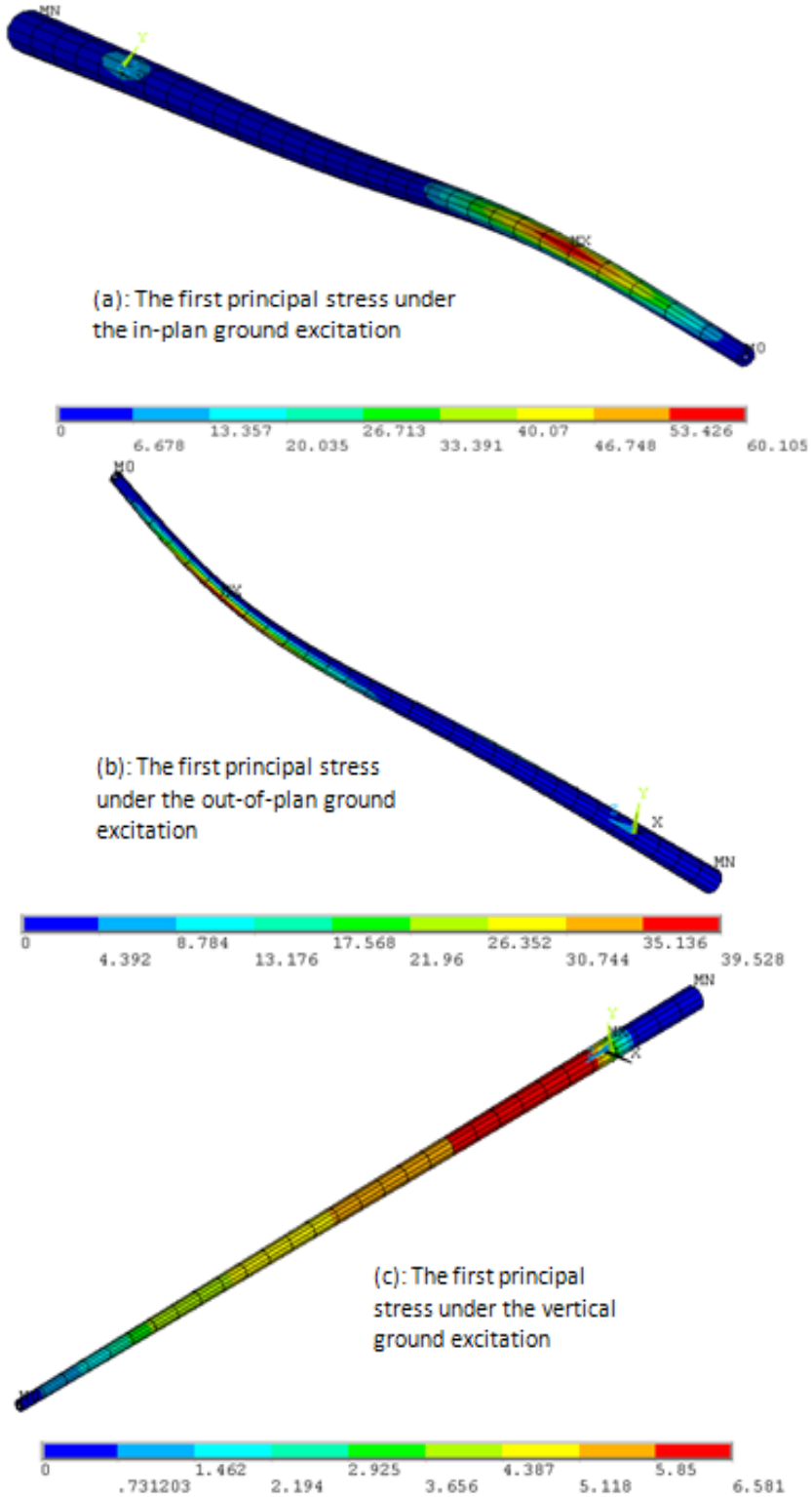

Figure 6.9: The concrete pole (OCP) first principal stress under the original ground excitation record

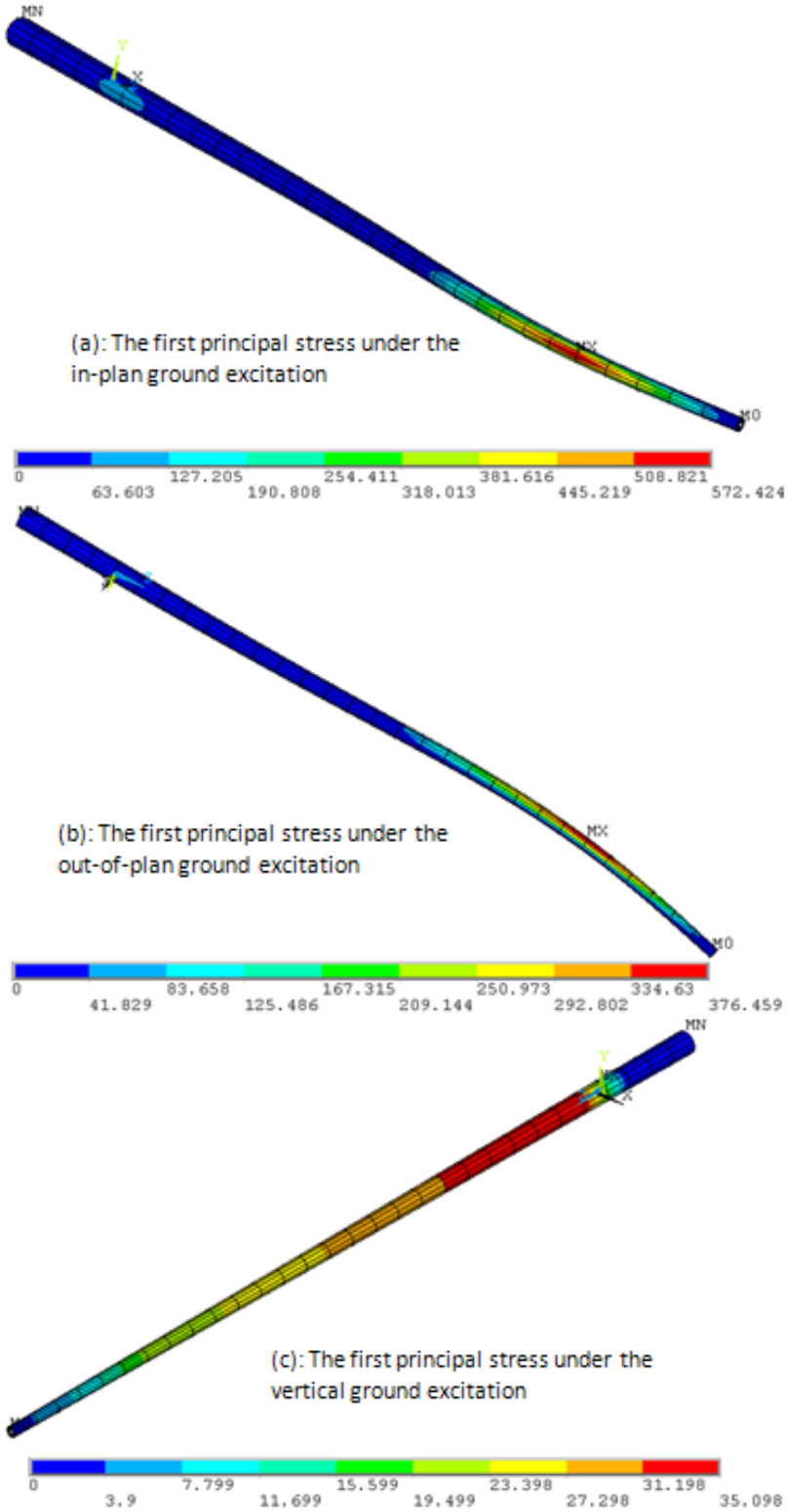

Figure 6.10: The concrete pole (OCP) maximum first principal stress under the modified ground excitation based on 2 in/s PPV

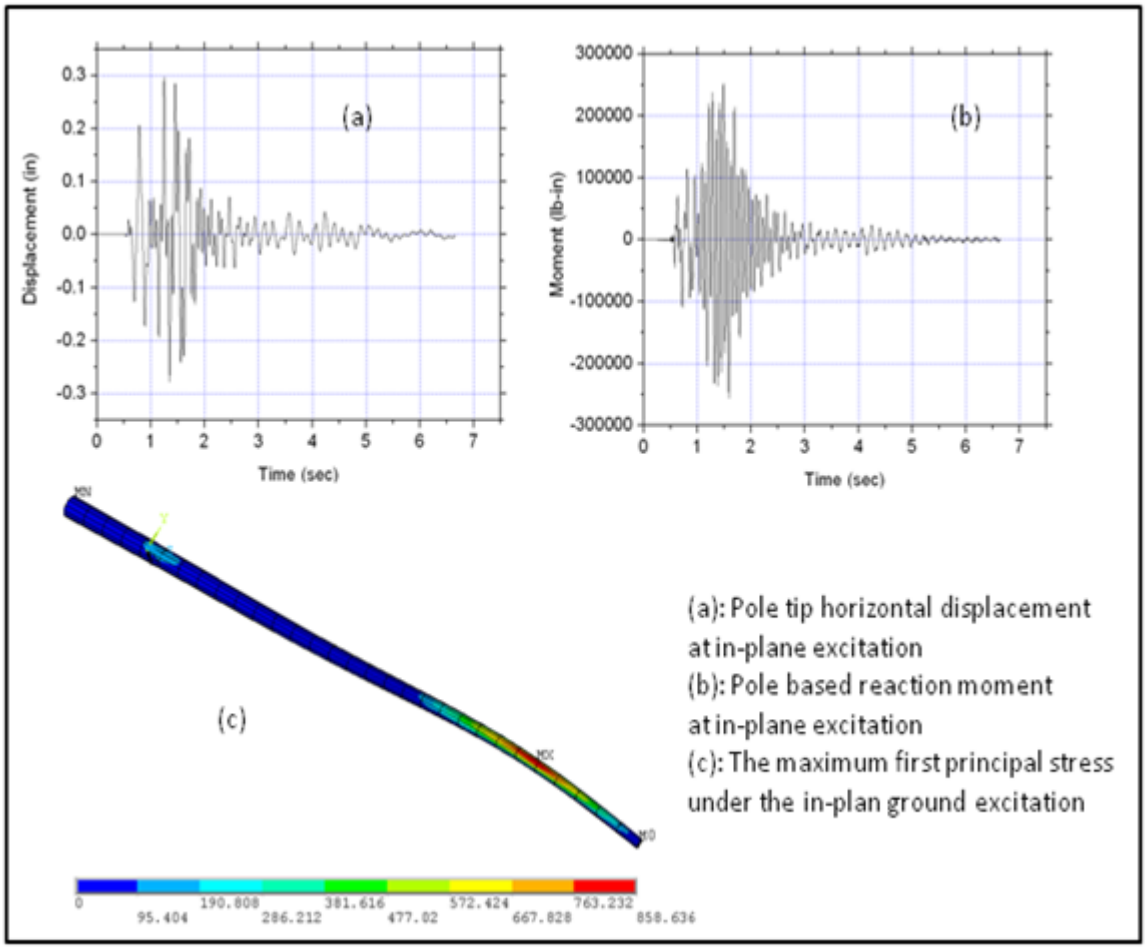

Figure 6.11: The concrete pole (OCP) structural response under the modified ground excitation based on 3 in/s PPV

Table 6.1: Maximum values of the concrete pole (OCP) dynamic responses

Original blast induced ground vibration		*Modified ground vibration based on 2 in/s PPV*	
Maximum tip displacement under the horizontal excitation	0.0211 in	Maximum tip displacement under the horizontal excitation	0.2011 in
Maximum tip displacement under the vertical excitation	0.0005 in	Maximum tip displacement under the vertical excitation	0.0025 in
Maximum moment under the horizontal excitation	17949.50 lb-in	Maximum moment under the horizontal excitation	170948.00 lb-in
Maximum force under the vertical excitation (lb)	858.90 lb	Maximum force under the vertical excitation	4580.70 lb
Maximum first principal stress under the horizontal excitation	60.11 lb/in^2	Maximum first principal stress under the horizontal excitation	572.42 lb/in^2
Maximum first principal stress under the vertical excitation	6.58 lb/in^2	Maximum first principal stress under the vertical excitation	35.10 lb/in^2

Table 6.2: Maximum values of the pole (OCP) dynamic responses at 2 in/s PPV blast criterion

Spectrum analysis		*Time history analysis*	
Maximum tip displacement under the horizontal excitation	0.14 in	Maximum tip displacement under the horizontal excitation	0.2011 in
Maximum moment under the horizontal excitation	124990.00 lb-in	Maximum moment under the horizontal excitation	170948.00 lb-in
Maximum first principal stress under the horizontal excitation	331.54 lb/in^2	Maximum first principal stress under the horizontal excitation	572.42 lb/in^2

CHAPTER 7: STRUCTURAL INTEGRITY ANALYSIS OF TRANSMISSION POLES UNDER BLAST INDUCED GROUND MOVEMENTS

7.1 Design of transmission pole structures

The design of prestressed concrete poles is mainly concerned with strength and serviceability under various loading conditions (ASCE/PCI 1997). Four distinct conditions (ultimate flexural strength, cracking strength, zero tension strength and deflection) are considered in a typical design process. For example, cracking moment can be calculated from:

$$M_{cr} = \frac{f_r I_g}{y_t} + \frac{P I_g}{A_g y_t} \tag{7.1}$$

where f_r is modulus of rupture of concrete, I_g is gross moment inertia of the pole section, $A_g$is the gross area of the cross section, and P is the prestress force.

The design of the transmission steel pole structure is also based on ultimate strength method (ASCE/SEI 2006). The stresses calculated using factored design loads should not exceed capacities of the member for tension, compression, shear, bending and combined stresses. For instance, the compression stress needs to meet:

$$\frac{P}{A} + \frac{Mc}{I} \leq F_a \tag{7.2}$$

in which:

$$F_a = F_y \text{ when } \frac{w}{t} \leq \frac{240\Omega}{\sqrt{F_y}} \tag{7.3}$$

$$F_a = 1.45F_y(1.0 - 0.00129\frac{1}{\Omega}\sqrt{F_y}\frac{w}{t}) \text{ when } \frac{240\Omega}{\sqrt{F_y}} \leq \frac{w}{t} \leq \frac{374\Omega}{\sqrt{F_y}} \tag{7.4}$$

$$F_a = \frac{104980\Phi}{\left(\frac{w}{t}\right)^2} \text{ when } \frac{w}{t} \geq \frac{374\Omega}{\sqrt{F_y}} \tag{7.5}$$

where P is axial force, A is cross-sectional area, I is moment of inertia cross section, M_c is bending moment, F_y is yield stress, w is flat width of a side, t is wall thickness, Ω = 1.0, and Φ = 1.0.

It is not unusual for engineers in the power industry to design transmission poles following the wood pole equivalent method, because it is simple and easy for hand calculations. The specification lays out requirements of ultimate moment capacity, crack loading (concrete pole), and maximum deflection based on the pole class. Generally, pole design should meet requirements of (Southern Company 1992; Southern Company 2006):

(1) Minimum ultimate moment capacity at certain locations under the design loads;

(2) Maximum horizontal deflection at the pole tip with the 36% design load applied at 2 feet from the pole tip;

(3) Not to crack under a load equivalent to 40% of design load applied at two feet from the concrete pole tip.

7.2 Structural integrity of transmission poles under blast loads

7.2.1 The concrete pole (OCP)

(1) Concrete cracking

Concrete pole cracking is investigated by comparing the maximum first principal stress with concrete tensile strength or modulus of rupture calculated as follows (Nawy 2003):

$$f_{ct} = 0.10 f_c' = 1100.00\ psi \quad (7.6)$$

$$f_{cr} = 7.5\sqrt{f_c'} = 786.61\ psi \quad (7.7)$$

where f_c' is compressive strength of concrete.

Comparison was made between the maximum first principal stress results (σ_1) from ANSYS with material allowable stress ($[\sigma_1]$) for the concrete pole (OCP) (Table 7.1).

From Table 7.1, it is shown that 2 in/s PPV criterion always gives a safe blast design. If economic reasons are taken into account, peak particle velocity limit may be able to be relaxed to 3 in/s. Although the maximum first principal result from time history analysis at 3 in/s PPV is greater than concrete modulus of rupture, the concrete pole may not crack since other factors such as soil structure interaction effects may take place. However, blast designers should be careful because 3 in/s blast limit might not be safe for a concrete pole that is more rigid than the one in this study (OCP). To be conservative, a blast limit described as the peak particle velocity of explosion induced ground vibration not exceeding 2 in/s at the pole foundation location is suggested.

In the following, emphasis will be put to verify the validity of this 2 in/s PPV criterion.

(2) Ultimate moment capacity

The design specification requires a concrete pole of Class H3 at the given design load of 4688 lbs has minimum ultimate moment capacity of (Southern Company 1992):

a) 70 ft-kips or 840000 lb-in (10 ft from the tip);

b) 93 ft-kips or 1116000 lb-in (18 ft from the tip);

c) 119 ft-kips or 1428000 lb-in (26 ft from the tip).

To compare with the allowable moment [M], Table 7.2 lists maximum moment values (M_{max}) from spectrum analysis and time history analysis. Table 7.2 indicates that effects (170948 lb-in) generated from 2 in/s PPV blast events do not exceed the design requirement (minimum value of 840000 lb-in) in the ultimate moment capacity aspect.

(3) Maximum deflection

Absolute deflection can affect the pole serviceability due to special considerations of power transmission grids, such as the conductor swing-out problem. It is obvious from both spectrum and time history analyses that pole maximum deformations under blast induced ground vibration are very small (Table 7.3: less than 0.2 in). Considering the benefits of insulator mobility, the maximum pole tip deflection is not a control factor in transmission pole dynamic responses under blast induced ground vibration.

From the above analyses, the concrete pole ultimate capacity is controlled at material level by the first principal stress. Transient analysis of the 60-ft concrete pole (OCP) under the modified ground excitation based on 3 in/s PPV yields the maximum first principal stress (858.64 psi) exceeding the allowable stress (786.61 psi). Hence, 2 in/s PPV is designated to be a blast limit. Although it may be conservative considering the simplicity of FE models, such as ignoring soil-structure interaction and material nonlinearity, this 2 in/s PPV criterion is believed to provide sufficient safety margin.

7.2.2 The steel pole (OSP)

Through the above concrete pole analyses, 2 in/s PPV criterion is determined to be a reasonable blast limit for concrete poles. Steel pole structures usually have better anti-seismic performances than concrete poles. The following is just to verify that 2 in/s PPV criterion is also adequate for steel poles based on spectrum analysis results.

(1) Stress analysis

Base on yielding strength requirements, steel pole strengths are assumed to be (ASCE/SEI 2006):

$$F_t = F_y = 65000.00\ psi \tag{7.8}$$

Since $\frac{240\Omega}{\sqrt{F_y}} = 29.77 \geq \frac{w}{t} = \frac{2.83}{0.19} = 15.07$

$$F_a = F_y = 65000.00\ psi \tag{7.9}$$

$$F_v = 0.58F_y = 37700.00\ psi \tag{7.10}$$

where F_t is tensile stress permitted, F_y is specified minimum yield stress, F_a is compressive stress permitted, and F_v is shear stress permitted.

Stress distributions of the steel pole (OSP) from spectrum analyses were shown in Figures 7.1 and 7.2. Design values of the normal stress and shear stress were calculated using the following equation and compared with the corresponding strengths in Table 7.4.

$$\sigma_{combined} = \sqrt{\sigma_x^2 + \sigma_y^2 + \sigma_z^2} \tag{7.11}$$

It is concluded that the steel pole stress state is within a safe range from this comparing work: for tension/compression stress, the calculated maximum first principal stress is 1445.00 psi, which is less than the steel pole tension/compression strength of 65000.00 psi; maximum shear stress of 106.70 psi is also less than shear strength of 37700.00 psi.

(2) Ultimate moment capacity

The design specification requires the steel pole (OSP) in this study (Pole Class: H_7) at the given design load (8063 lbs) has a minimum ultimate moment capacity of 128 ft-kips (10 feet from the tip), 164 ft-kips (18 ft from the tip) and 209 ft-kips (26 ft from the tip). The maximum moment value from the spectrum analysis is 134830.00 psi ≤ 1536000.00

psi (128 ft-kips), which indicates that blast effects do not exceed the design requirement in the ultimate moment capacity.

(3) Maximum deflection and guy wire stress

The deflection results from spectrum analyses are very small, usually less than 0.5 in, hence, the deflection limit is not a problem for the guyed steel pole structure. Guy wires carry tension force during spectrum analysis whereas they slag under compression. Hence, guy wires cannot carry compression forces. The forces in tensioned wires were derived and averaged. The average tension forces for guy lines are 1119.22 lbs, 1156.72 lbs and 519.04 lbs for X, Y, Z directions of ground excitations, respectively, which were calculated based on the 2 in/s PPV criterion. Based on design information, guy wires in the steel pole (OSP) are ½'' E.H.S. steel guys and have the ultimate strength of 26900 lbs. It is obvious that the tension level of guy wires are within the capacity.

7.3 Blast limit design

From the above studies, 2 in/s PPV criterion is determined to be a reasonable blast limit. This criterion can be relaxed if the structure is less rigid than the prestressed concrete pole (OCP) in this study. Steel poles usually have better performances under ground vibration. But this 2 in/s PPV criterion is determined by limited studies on allowable material stresses. There are other factors that may need to be taken into account, such as soil-structure interaction and material nonlinearity. Also, for other types of transmission structures, like self-supported lattice towers, this criterion might be conservative. But for the guyed tower structures, engineers should design blasts with cautions when using this 2 in/s blast limit, especially when explosions can cause very strong vertical direction ground motions. There have been observations of local buckling

of the guyed lattice tower caused by vertical ground vibration. Because this study is only limited to transmission pole structures, how transmission towers perform under this 2 in/s blast limit has not been quantified.

To provide a comprehensive blast plan, the blast limit is not the only factor in blast design although it is a critical one. Other considerations include flyrock issue, site geology, airblast are also necessary for a reasonable blast design. For these conceptual blast design aspects, the readers can refer to Conner (2007). An example of a blast design is shown in Figure 7.3.

7.4 Summary

Base on structural responses obtained from spectrum analysis (Chapter 5) and time history analysis (Chapter 6), 2 in/s PPV blast limit is established for transmission pole structures. Performances of both the concrete pole (OCP) and the steel pole (OSP) in this study are within guideline requirements under blast induced ground vibrations with 2 in/s peak particle velocity. Although this criterion may be conservative for some less rigid structures, it is taken as a general requirement to simplify blast design. To develop a more comprehensive blast limit, complement research needs to be conducted for other types of transmission structures and in other geological sites.

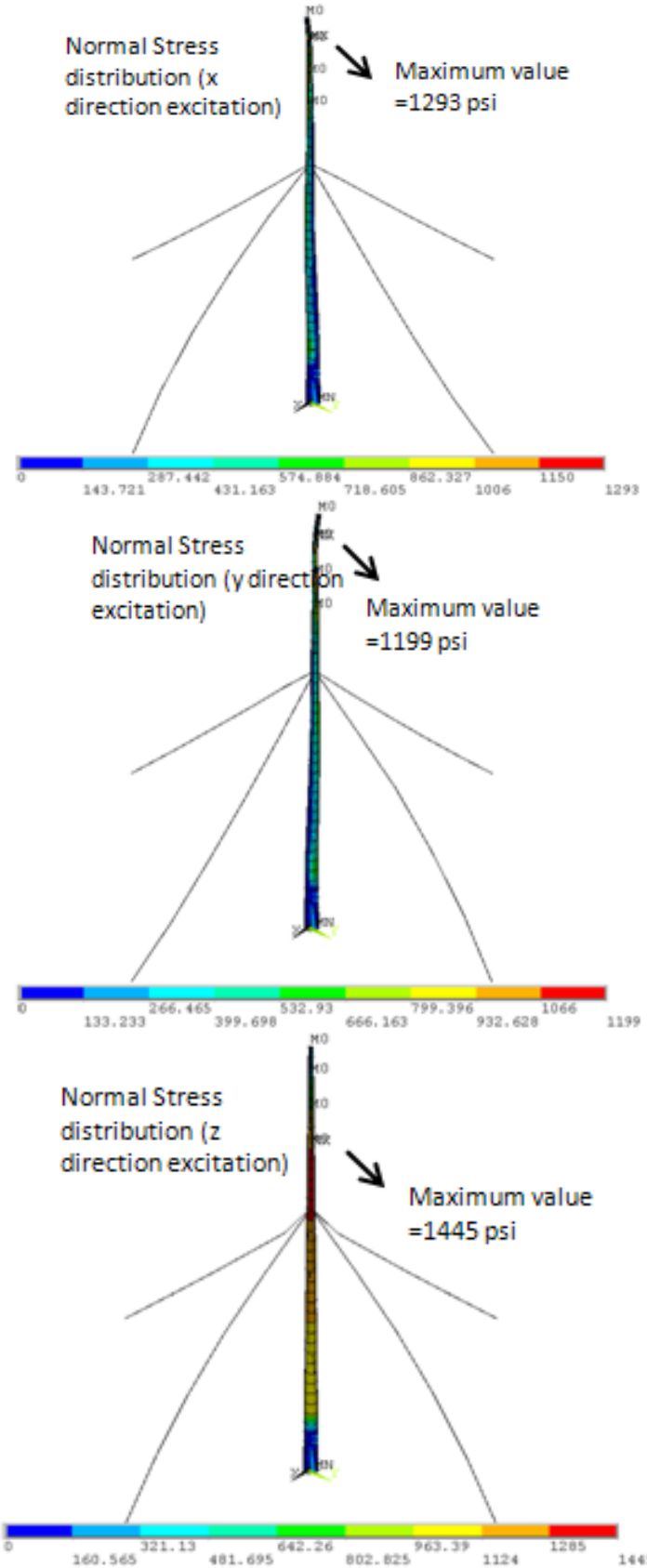

Figure 7.1: Normal stress distributions of the steel pole under 2 in/s PPV criterion

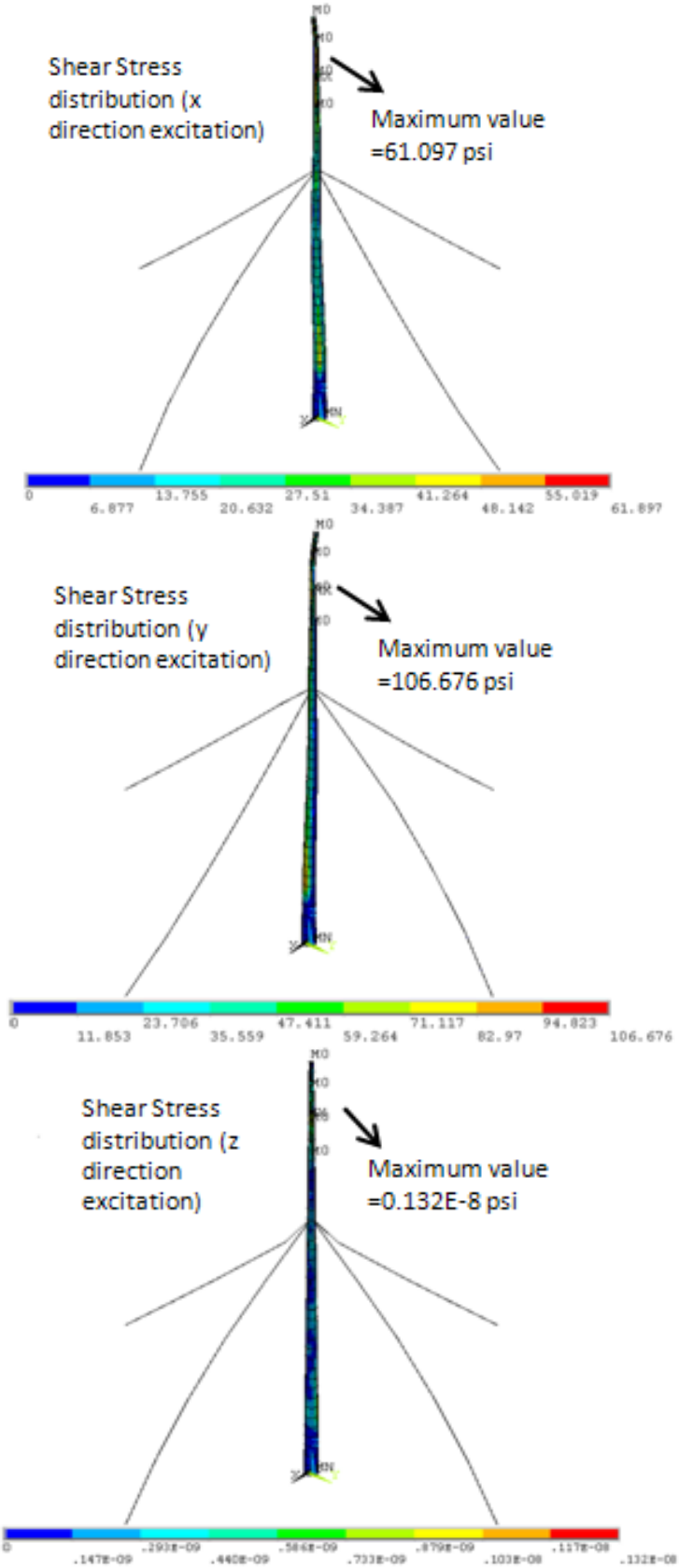

Figure 7.2: Shear stress distributions of the steel pole under 2 in/s PPV criterion

The blast plan calls for:

1) The maximum ground vibration limit of 2 inches per second (PPV), and an airblast level of 130 decibels.

2) Geological profiling shall be conducted for site characterization. It will be used to compare with the site where this research conducted to estimate the feasibility of applying 2 in/s conclusion. Also it may be used to identify fractures/mudseams. Establishment of valid FE models also needs this information.

3) A pre-blast survey on structures within 1500 ft of the excavation area will be performed to make note of existing structural conditions (i.e. cracks, deformations, etc.).

4) Each critical blast will be monitored by vibration and air pressure measurement equipments placed close to the foundation of the structure.

5) To prevent resonance, the blast design should try to avoid creating dominant blast frequencies that coincide the pole's natural frequencies.

6) Any landowner within ½ mile radius of the blast will be notified of the date and approximate time of blasts, it they request it. In addition, blasts will be warned with an audible horn immediately prior, as per Mining Safety and Health Administration (MSHA) regulations.

7) A "safe zone" perimeter of 550 feet shall be applied.

8) The use of blasting mats shall be implemented to control flyrock debris when necessary.

9) Post-blast inspection will be conducted to detail any changes from the initial pre-blast survey.

10) All relevant blast procedures and monitoring results shall be recorded for retention by the facility.

11) All relevant blast procedures and monitoring results shall be recorded for retention by the facility.

Figure 7.3: An example of blast plan (modified after Conner 2007)

Table 7.1: Stress state comparison

Case	σ_1 *(psi)*	$[\sigma_1]$ *(psi)*	*Compare*
Spectrum analysis at 2 in/s PPV criterion	331.54	786.61	$\sigma_1<[\sigma_1]$
Spectrum analysis at 4 in/s PPV criterion	674.03	786.61	$\sigma_1<[\sigma_1]$
Spectrum analysis at 5 in/s PPV criterion	842.69	786.61	$\sigma_1>[\sigma_1]$
Time history analysis at 2 in/s PPV criterion	572.42	786.61	$\sigma_1<[\sigma_1]$
Time history analysis at 3 in/s PPV criterion	858.64	786.61	$\sigma_1>[\sigma_1]$

Note: The 2 in/s PPV criterion means that the response spectrum or modified acceleration time history is developed based on the 2 in/s peak particle velocity target. Other PPV criteria follow the same idea.

Table 7.2: Maximum moment comparison

Case	M_{max} *(lb-in)*	*[M] (lb-in)*	*Compare*
Spectrum analysis at 2 in/s PPV criterion	124990.00	840000.00	$M_{max}<[M]$
Time history analysis at 2 in/s PPV criterion	170948.00	840000.00	$M_{max}<[M]$

Table 7.3: Maximum deflection

Case	D_{max} *(in)*
Spectrum analysis at 2 in/s PPV criterion	0.14
Time history analysis at 2 in/s PPV criterion	0.20

Table 7.4: Steel pole stress analysis

Items	*Strength* $[\sigma_1]$ *(psi)*	*Stress* σ_1 *(psi)*	*Comparison*
Tension	65000.00	1445.00	$\sigma_1<[\sigma_1]$
Compression	65000.00	1445.00	$\sigma_1<[\sigma_1]$
Shear	37700.00	106.70	$\sigma_1<[\sigma_1]$
Combination	65000.00	2277.70	$\sigma_1<[\sigma_1]$

CHAPTER 8: DEVELOPMENT OF HEALTH MONITORING STRATEGIES OF TRANSMISSION STRUCTURES

8.1 Introduction

The concept of structural health monitoring is put forth based on the idea that civil infrastructures go through aging process as we human beings do. Vibration-based structural damage detection technique is a promising approach for developing health monitoring of electric power transmission lines. Application of structural health monitoring strategy for electric power transmission lines has not been in practice yet. Although there is a long history of monitoring application for power transmission, in which case, focus is placed in voltage, current or power measurements. Typical maintenance practices in the power industry are still to periodically conduct inspection along power grids. Considering the geographically dispersed nature of electric power lines, this kind of inspection is expensive and time consuming. In this chapter, two Nondestructive Testing (NDT) techniques were proposed for assessment of transmission pole direct embedment foundations. A pilot work was performed to explore a potential design of the health monitoring system for the electric power lines.

8.2 NDT techniques for assessment of direct embedment foundations

Two dynamic impact tests, Modal Testing (MT) and Spectral Analysis of Surface Waves (SASW), were proposed as non-intrusive investigation techniques for directly-

embedded poles. MT is an established dynamic structural testing technique and was used in this case through tailoring of pole boundary conditions based on global dynamic behaviors of the embedded pole. The surface wave testing technique for soil relies on field measurements of surface wave velocities at various frequencies as well as an inversion process to determine soil stiffness profiles (Ong et al. 2006). It is proven to be a cost-effective method to supply reliable foundation capacity for transmission line design (Chen et al. 2004).

The research results and basic theoretical principles of two nondestructive techniques, MT and SASW, were described herein. Feasibility study was performed through determining dynamic characteristics of a full-scale 35 feet long concrete pole with two different embedment conditions: loosely backfilled soil and densely backfilled soil. Study shows that both methods are able to yield indicative information for possible issues during pole erection. It is proposed that these two NDT techniques can be developed into quality control strategies during transmission line structure stability inspections.

8.2.1 Fundamentals of the two proposed NDT techniques

Modal testing is used for determining the inherent dynamic characteristics of a structural system. This technique has successful applications in various civil engineering problems, such as FE model verification (Živanović et al. 2006) and damage detection (Teughels and DE Roeck 2004). The basic concept of this method is based on the understanding that structural dynamic behaviors (natural frequencies and mode shapes) are directly related to stiffness properties of a system. Hence, any change in stiffness matrix due to structural modification, such as boundary condition changes, can be reflected by corresponding changes in dynamic behaviors of the system. In this study, the

embedded pole mass and stiffness matrices were assembled using the finite element method. The direct embedment foundation was simplified as the elastic boundary condition. Through the process of updating the FE model to match correlated modal parameters obtained from modal testing, boundary stiffness could be quantified. The boundary stiffness was then used as an indicator of soil and backfill-material properties around the embedded pole.

Considering the embedded pole structure in Figure 4.10, when damping is ignored, with assumption of linear elasticity and small deformation, surrounding soil and backfill materials can be simplified into a set of linear translational and rotational springs (refer to as "soil springs" hereafter) (Figure 4.10). The stiffness matrix of these springs represents the interaction mechanism between the embedded pole and combination effects of annulus backfill-material and surrounding soil along the buried portion of the pole.

Assuming $[K_p]$ is stiffness matrix of the pole structure and $[K_s]$ is soil spring stiffness matrix, governing equations to free vibration of the suspended pole and the embedded pole are expressed as Equations (8.1) and (8.2), respectively. Solutions to these equations, natural frequencies (ω) and mode shapes ($\{\varphi\}$), can be derived through modal testing. $[K_p]$ and $[K_s]$ can therefore be back-calculated from these structural dynamic equations.

$$[M_p]\{\ddot{x}_p\} + [K_p]\{x_p\} = \{0\} \tag{8.1}$$

$$[M_p]\{\ddot{x}\} + [K]\{x\} = \{0\} \tag{8.2}$$

where $[M_p]$ is pole structure mass matrix, $[K]$ is stiffness matrix of the embedded pole system, which is a combination of pole stiffness matrix ($[K_p]$) and soil spring matrix ($[K_s]$).

With the design data, FE modeling is an explicit approach to establish and solve governing Equations (8.1) and (8.2). Parameters in these FE models, however, have inherent input uncertainties. Modal testing can be conducted to derive the exact modal model (frequencies and mode shapes). While these modal models are correlated with FE models, the latter can be updated. When preset minimum discrepancies of solutions to Equations (8.1) and (8.2) (both ω and $\{\varphi\}$) between FE models and modal models are met, the resultant FE models are believed to truly represent actual dynamic behaviors of the system. The spring stiffness matrix ($[K_s]$) back-calculated from these models therefore provides information of geotechnical conditions of embedment foundations.

The Spectral Analysis of Surface Waves (SASW) technique was developed as an in-situ seismic testing method. This method depends on measurement of Rayleigh wave propagation over a wide range of frequencies. The general theory of SASW testing was introduced in 4.4.2.

When SASW testing is performed at the vicinity of the embedded pole, the resultant shear wave velocity is assumed to approximately indicate the quality of embedment foundations. This method was implemented without causing any disturbance to the embedded foundation after the pole is installed. It showed both technical and economic advantages to contemporary soil property exploration practices.

8.2.2 Case study of a transmission concrete pole

In this study, two NDT techniques developed based on hammer impact were performed on a 35 feet long concrete pole. Table 1 lists the scope of studies, including both experimental and numerical works conducted.

(1) MT method

The impact modal testing was carried out on the 35 feet long prestressed concrete pole. Testing was conducted with an accelerometer placed at a fixed position on the pole to record structural responses caused by hammer impacts at different target points (Figure 8.1).

Testing was performed on suspended condition first, and then on the same pole after it was directly embedded in different soil conditions. In this manner, the modal models of both freely suspended pole structures and embedded poles can be derived. Embedment conditions included two scenarios (loosely backfilled soil and densely backfilled soil), which were realized through soil tamping. Thus, three sets of modal tests (MT_1, MT_2, and MT_3) were conducted on the same concrete pole (Table 8.1). Dynamic behaviors (natural frequencies and corresponding mode shapes) of both the suspended pole and the embedded pole were obtained through post-processing of recorded input-output data. These modal models represented actual dynamic characteristics of the pole structure and were then used to further update the FE models.

To derive mass and stiffness matrices of the pole and soil springs, FE models of both the directly embedded pole and the suspended pole were established. Geometry input information is listed in Table 8.2. Young's modulus and mass density of the pole were estimated as 5466 ksi and 150 lb/ft^3 of concrete material for the original FE model.

The pole structure was modeled using tampered beam elements (BEAM189) under ANSYS (2007). The embedment foundation was modeled as a series of linear elastic massless springs (COMBIN14). Based on the assumption of small deformation in a homogeneous and elastic material, a soil spring model in Figure 4.10 was used.

Modal analysis was performed on FE models to solve eigen-problems defined by Equations (8.1) and (8.2). Model updating was then implemented to identify boundary stiffness of the embedded pole through the following procedure: (1) The concrete property in the original FE model was updated based on MT_1 results. The FE model after this verification process was assumed to accurately represent the concrete pole itself. (2) This valid FE model was then modified by adding soil springs and was further updated for convergence to MT_2 or MT_3 data. The second updating was achieved by tuning stiffness of soil springs. Models after step (2) yielded accurate information about boundary conditions of the embedment foundation.

Measurements from modal testing were processed. The identified natural frequencies of the pole vibration are listed in Table 8.3. It should be noted that the first bending mode identified from testing on embedded poles is a cantilevered mode, which does not exist in the suspended pole case. Corresponding mode shapes identified from modal testing are shown in Figures 8.2, 8.3 and 8.4 with numerical results drawn together for comparison.

The iterative updating of the FE model was performed to make FE results converge to experimental data by minimizing discrepancies in both natural frequencies and mode shapes. The later was achieved by observing the Modal Assurance Criterion (MAC) values, which were obtained from (Ewins 2000):

$$MAC(\varphi_{a,}\varphi_e) = \frac{|\varphi_a^T \varphi_e|}{(\varphi_a^T \varphi_a)(\varphi_e^T \varphi_e)} \tag{8.3}$$

where φ_a and φ_e are the FE and experimental mode shape vectors, respectively.

The final comparison between experimental and numerical results is shown in Table 8.4 and Figures 8.2, 8.3 and 8.4, which indicate that there is no much discrepancies for both natural frequencies (ω) and mode shapes ($\{\varphi\}$) between the two models; thus, the

resultant FE models are believed to well-represent dynamic behaviors of both the suspended pole and the embedded pole.

It is clearly shown from the results that with the increasing stiffness of embedment foundations, natural frequencies also increased simultaneously. Hence, the natural frequency can be used as an indicator of foundation stiffness change. Furthermore, through quantitative inverse analysis, the final derived soil modulus (E_s) is 1230 (*psi*) for MT_2 and is and 10800 (*psi*) for MT_3. These values are assumed to reflect the physical properties of foundation stiffness and are consistent with the observation that tamped soil has a higher E_s value than the loosely backfilled soil.

(2) SASW method

SASW testing was first conducted at the marked site where the pole was going to be embedded. After the pole was erected, SASW testing was performed in the vicinity of the embedded concrete pole (Figure 8.5). A sledge hammer was used to generate excitations on ground surface by vertical impacts. Time histories of ground vibrations in the form of particle velocity were recorded by a linear array of two geophones, which were attached to ground surface with the spacing equal to the distance between the excitation source and the nearest receiver. Signals were collected by a portable computer acquisition system. At each line, tests were conducted by changing the spacing of two receivers and the source-to-receiver distance. WinSASW (Joh 1996) was used to construct experimental dispersion curves. By further processing the results through inverse modeling, theoretical shear wave velocity profiles were obtained and used for quality investigation of the tested embedment foundations based on the assumption that shear wave velocity is directly correlated to elastic constants (shear modulus) of the tested soil.

SASW testing data from the two receivers were captured. The cross power spectrum (Figure 8.6 (a)) between two receivers was obtained and is shown in frequency domain. The phase shift ($\emptyset$) (Figure 8.6 (a)) of signals from the two receivers was also computed. The travel time (t) between two receivers was obtained from Equation (3). The surface wave velocity (V_s) and wavelength (λ) were determined by Equations (4) and (5), respectively. The plot of surface wave velocity (V_s) versus wavelength (λ) is a dispersion curve. A typical compact dispersion curve is shown in Figure 8.6 (b).

The resultant theoretical shear wave velocities obtained through inverse process were averaged along pole embedment depth and are shown in Table 8.5. Based on the theory that the shear wave velocity corresponds well to elastic modulus of the test site at small strains, the test results in Table 8.5 clearly indicate that: tamped soil is the stiffest with its largest average shear velocity ($SASW_3$); when backfilled soils are not tamped, stiffness is represented by the smallest average shear velocity ($SASW_2$).

8.2.3 Conclusions

A case study was conducted on a concrete pole with two different embedment conditions: tamped backfill soil and soil backfill without tamping. From research results, it is observed that: (1) Modal testing combined with the FE model updating technique is capable of quantifying boundary conditions by identifying stiffness matrix of soil springs that represent annulus materials around the embedded pole. (2) SASW testing offers an easy approach to evaluate direct embedment foundation quality through comparing the average shear wave velocity obtained from the testing. The study reported here indicates a potential of using nondestructive testing methods to solve engineering problems for the power industry.

8.3 Pilot exploration of the health monitoring system for transmission structures

8.3.1 Components of the transmission line

The overhead power line (Figure 8.7) is usually composed of four individual components: foundations, support structures, interfaces and conductors. The failure of any component may lead to collapse of entire transmission facilities. This kind of failure could be sudden, occurring in very short time with instability, rupture or complete separation; or it could be progressive, which means damage after long periods of time. Support structures in transmission lines can be divided into two main types: strain and suspension supports. Strain supports carry conductor tensile forces and serve as rigid points in the entire transmission line. They are designed not only based on vertical forces, but also conductor tensile forces differing in both sides in order to prevent cascading structural failures. Strain support structures usually are placed every 3 to 6 miles for long straight line sections. Structures in turn-over locations or somewhere there are extreme changes, strain supports are also designed and constructed. As for suspension supports, conductors transfer vertical forces to the supports by swinging at insulator connections. In this case, in theory, no tensile forces are transferred to the support because longitudinal forces are cancelled each other from both directions (León 2007).

Mechanical loads on the transmission line include wind, ice, snow, earthquakes, flooding and human related hazard such as blasting induced ground vibration. Wind, ice and snow are main loading considerations for transmission line design; while earthquakes, flooding and blast effects mainly affect support structure safety. The power current flow can cause the rise of temperature in conductors. The hot spot phenomenon

appears in coupling between energized conductors and interfaces. It needs to be considered in the health monitoring system.

8.3.2 Sensor selection for the health monitoring system

Typical sensors available that can be used in the health monitoring system of civil structures include: acceleration, strain and displacement sensors, thermocouples, fiber optic sensors, etc. Considering the geographically remote nature of power lines, means for data communication is one of the critical factors in the design of a valid health monitoring system. The remote sensing technology can provide a broad coverage of multiple structures. Depending on the measurement distance, satellite, airborne or flyover based aerial photography imaging (Figure 8.8), LIDAR remote sensing systems, and infrared spectrometry, etc. are remote sensing techniques that have application potentials for electric power transmission systems.

In the proposed health monitoring system here, wireless sensors are selected for practical purpose. The placement of the sensors could be described as the following: Strain sensors need to be mounted at interfaces of critical strained supports. The measurement provides information of normal tensile force changes of conductors, resulting from winds, ice accretion or neighboring structure effects. Strain sensors may also need to be placed at both sides of some critical suspension supports to detect an isolated failure of the structure. It is useful to develop a technique to integrate temperature sensors with these strain sensors. The readings from these sensors yield not only axial forces but also over-heating of the conductors, because hot spots usually highly localized close to the points of conductor attachments. Accelerometers are proposed to install on supports (poles, towers) to monitor vibration and tilt of the structures, which

can be caused by winds, earthquakes or blast induced ground movements. Tilt of the structure can be an indicator of foundation stability, which may be endangered by flooding or ground movements. Conductor vibration can be monitored by attaching acceleration sensor units to conductors (León 2007).

8.3.3 The architecture of the health monitoring system

The integrated health monitoring system usually include sensing agents, data communication agents, data interpretation as well as damage diagnostic algorithms, information fusion and user interface agents (Zhao et al. 2008). Due to widely geographically dispersed characteristics of transmission lines, sensing agents and data communication agents need to be deployed strategically. It is common to divide the large structure into different subsystems so that measurement and data communication can be easily realized with current technology. The characteristics of the power grid offer a natural way to design this architecture. With various sensing units installed at each critical support structure (Figure 8.9), measurement is made and data can be stored temporarily at memory chips of sensor units. Considering the typical practice of placing strain supports every 3 to 6 miles (Kiessling 2003), it is proposed to mount inter-support data communication and transmission devices on these strain supports. Records from each individual support are harvested by these devices. After signal aggregating, they are broadcasted to nearest processing units, which can be installed at each substation. Data from processing units can be sent to the processing and collaboration center, which can be located at control centers in a power transmission company. Data analysis, interpretation and damage diagnosis are executed in the centers. The schematic drawing of the system deployment is shown in Figure 8.10.

After signals are transmitted to a control center, sensitive parameters of structural health need to be extracted. The extracted data, when processed using certain methodology such as FFT, can sometimes be directly used as damage indicators. When these data combine with other theoretical analysis, more sophisticated damage algorithms can be developed. In this research, a damage diagnosis algorithm was proposed based on the fact that changes in structural dynamic properties can be used as damage indicators in a global scale. The main idea is to explore observable variations in modal parameters (natural frequencies, mode shapes, etc.) using accelerometers installed on the structure.

The framework of this algorithm is shown in Figure 8.11. Taking advantage of the wind-sensitive characteristic of electric grids, ambient loads can be treated as excitations to monitored structures. Structural vibration signals are delivered to the control center following the way described in Figure 8.10. Suitable modal identification techniques will be utilized to analyze measured data. Baseline FE models of the power line are established and tuned into target models for possible damaged structures by the FE model updating technique. Damage assessment can be conducted by comparing the baseline model with the target FE model through physical-meaning-bearing parameters.

This proposed damage detection method is only a part of damage evaluation management system, which should also include algorithms for evaluating displacement, temperature (hot spot) and other critical parameters. This management system needs to have a friendly user interface. The structural health status can be defined as (León 2007): normal, suspicious, imminent, and fault. For suspicious status, investigation may be required as a double-check; while for imminent damage or fault status, certain retrofits should be implemented to ensure the power transmission safety.

8.4 Summary

Two NDT techniques are developed in this chapter to exam the quality of direct embedment foundations of transmission pole structures. A case study verified the effectiveness of these two methods. An idea of health monitoring strategy for electric transmission lines is schematically described. This chapter enlightens further work with the objective of developing a health monitoring system for power transmission lines.

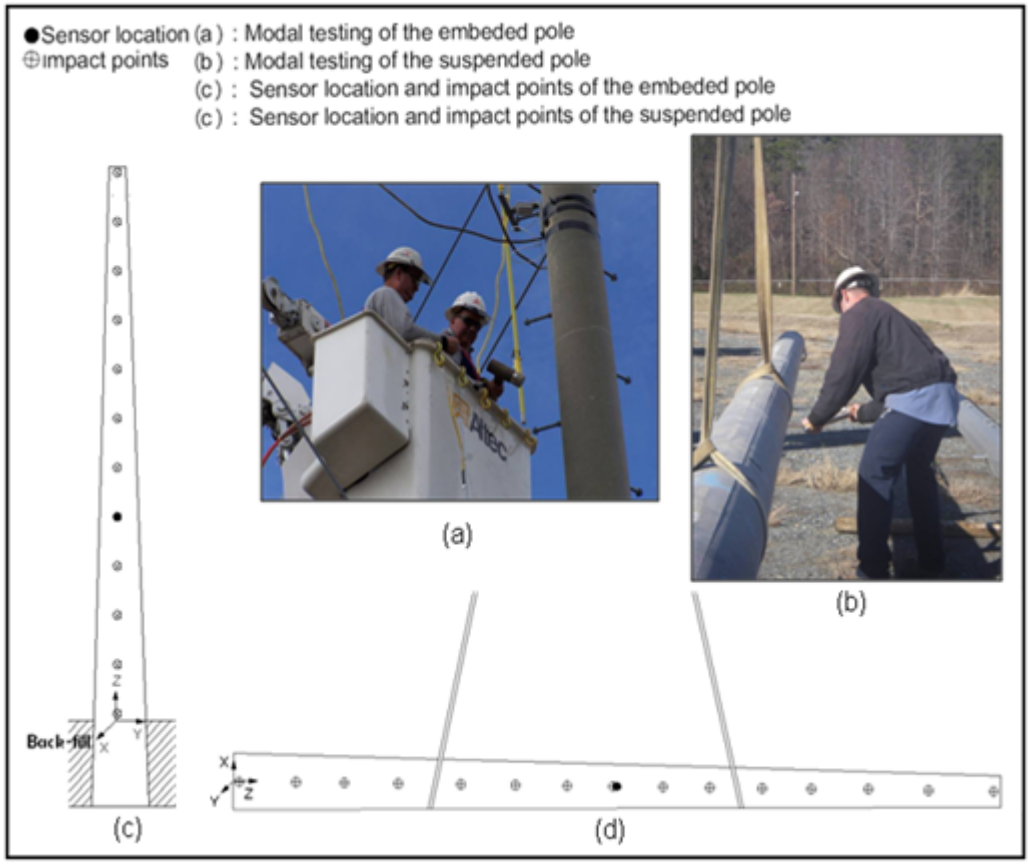

Figure 8.1: Modal testing of a concrete pole

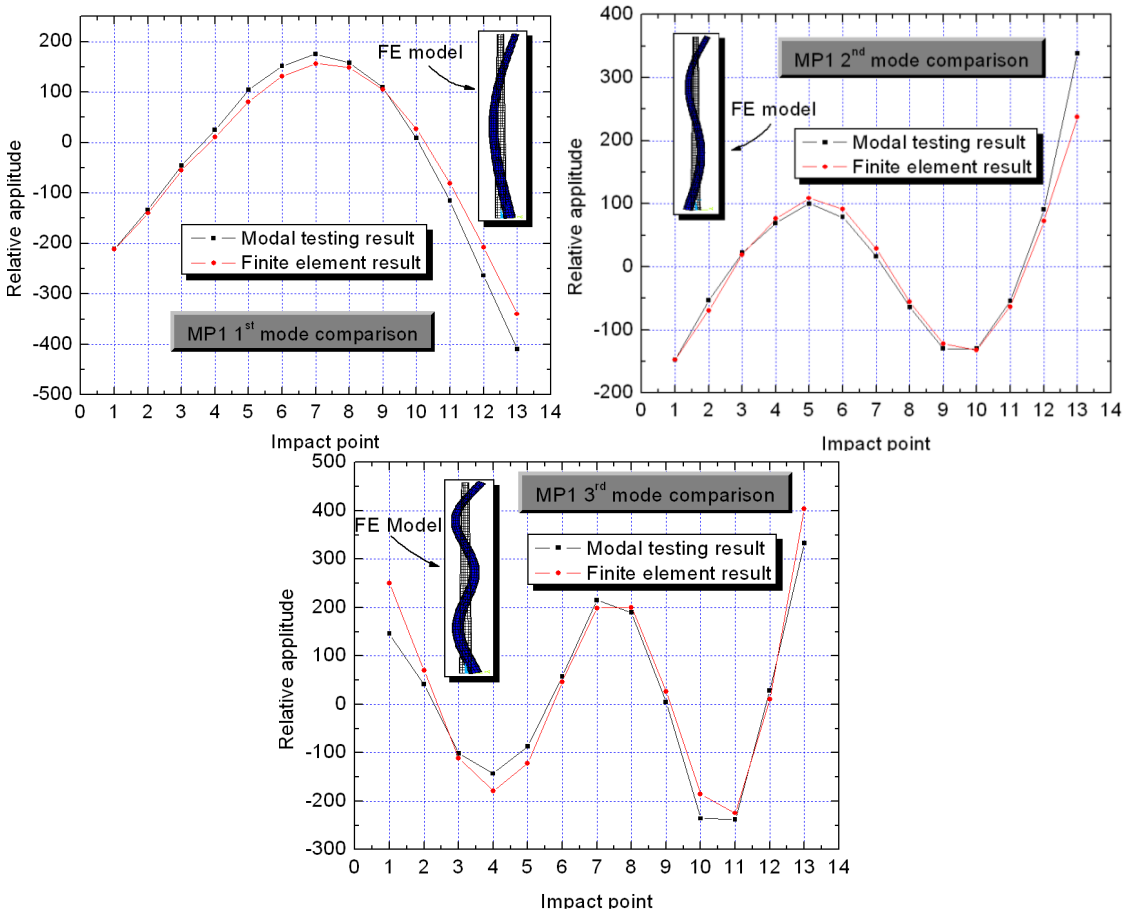

Figure 8.2: Mode shape comparison between the test result and the updating FE model for MT_1

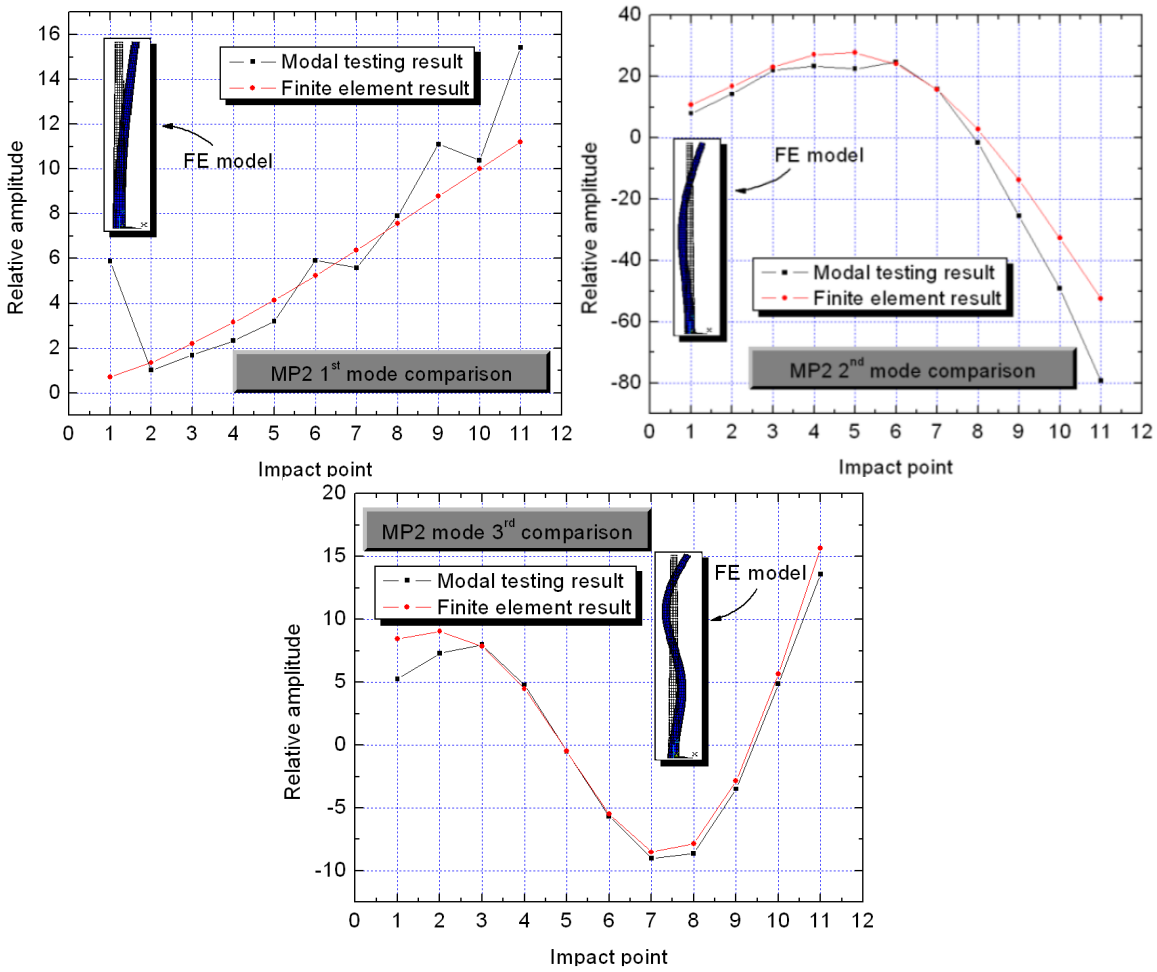

Figure 8.3: Mode shape comparison between the test result and the updating FE model for MT_2

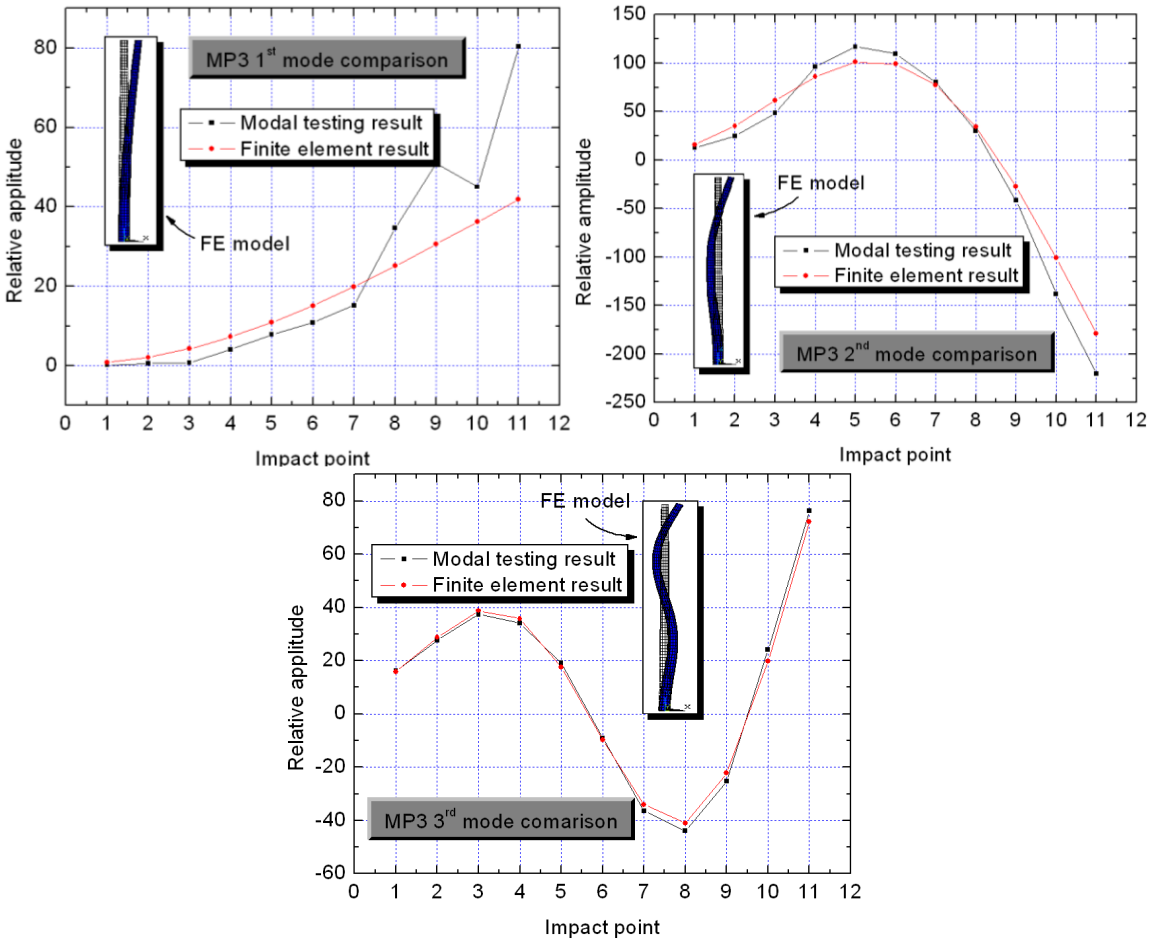

Figure 8.4: Mode shape comparison between the modal test and the updating FE model for MT_3

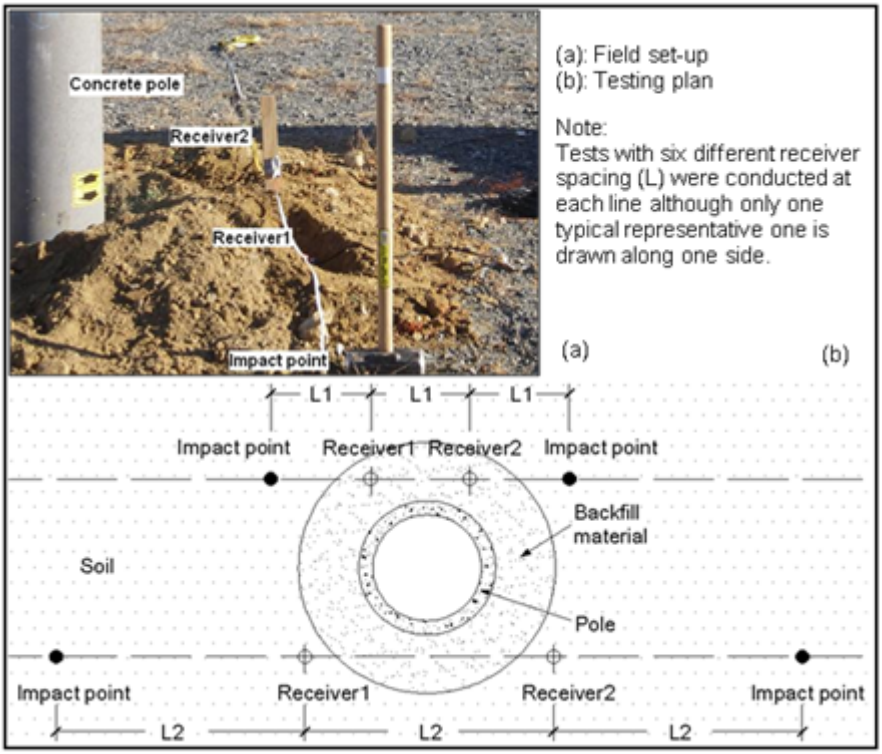

Figure 8.5: SASW testing at one side of the concrete pole

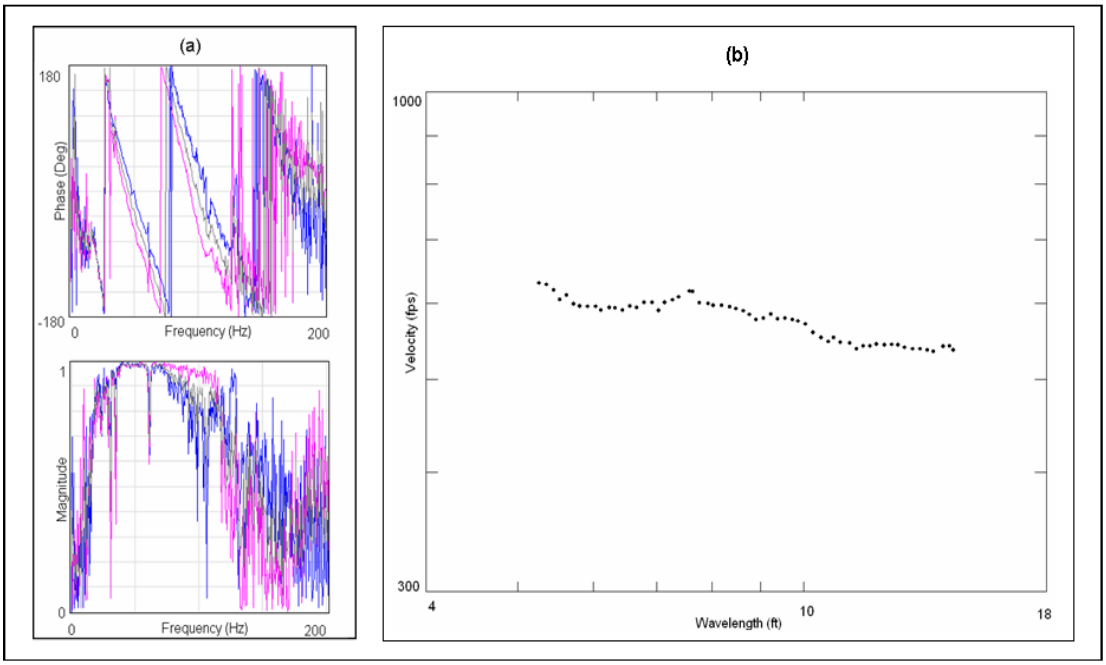

Figure 8.6: Typical SASW testing results: (a) cross power spectrum and coherence function; (b) compact dispersion curve

Figure 8.7: Typical power grids

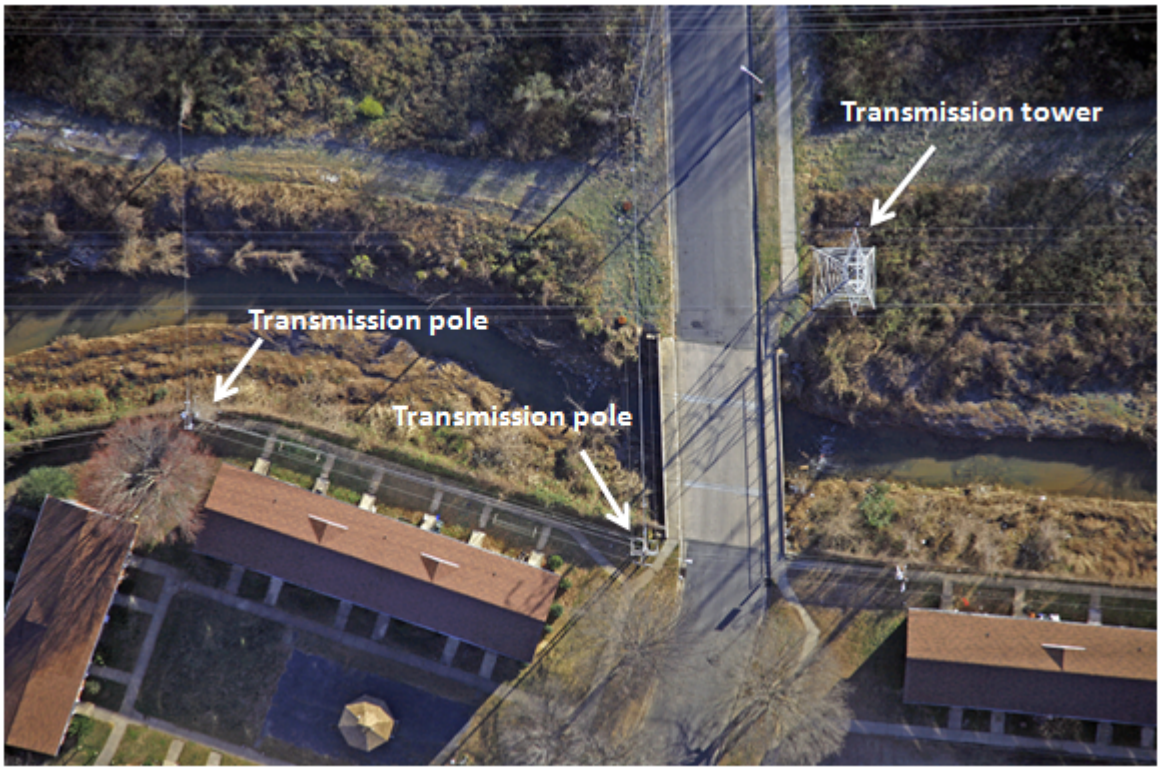

Figure 8.8: Sub-inch flyover photograph of transmission structures

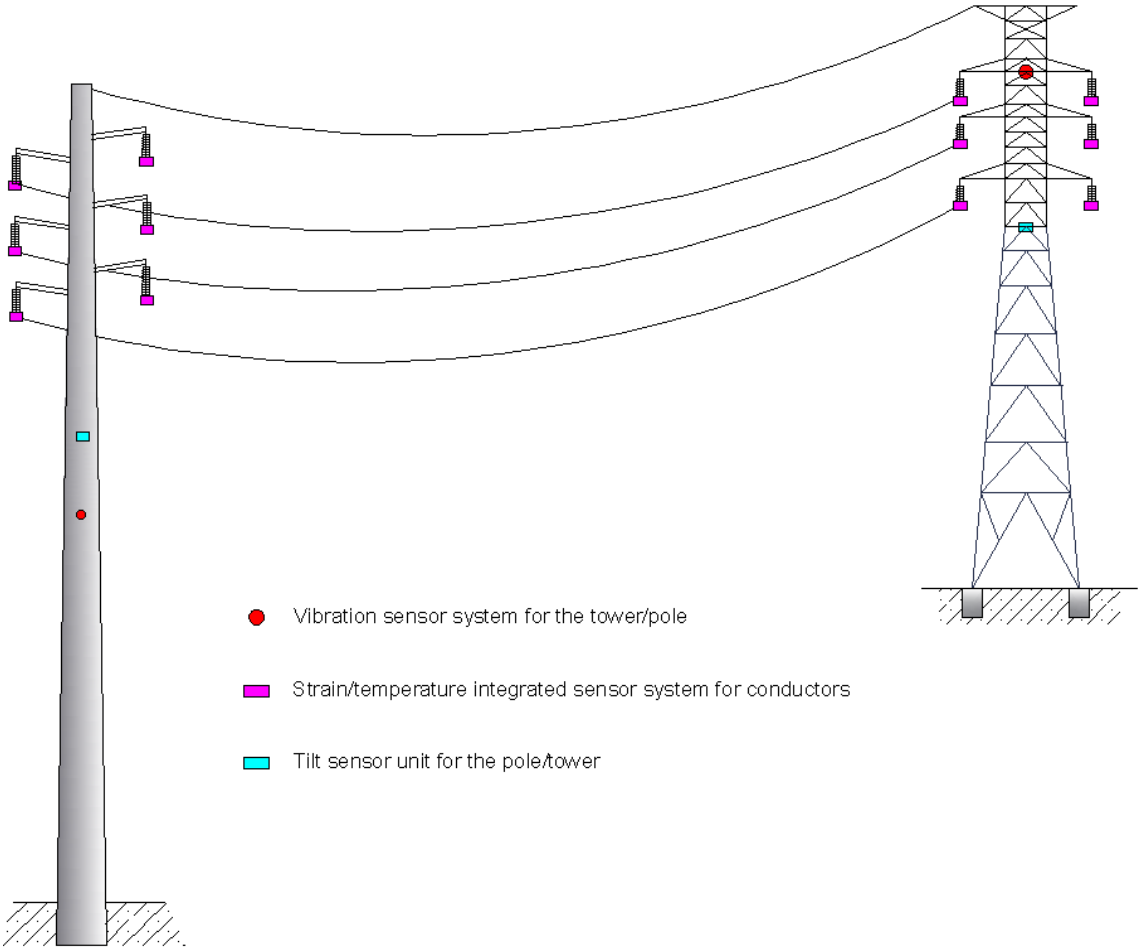

Figure 8.9: Sensing agent deployment

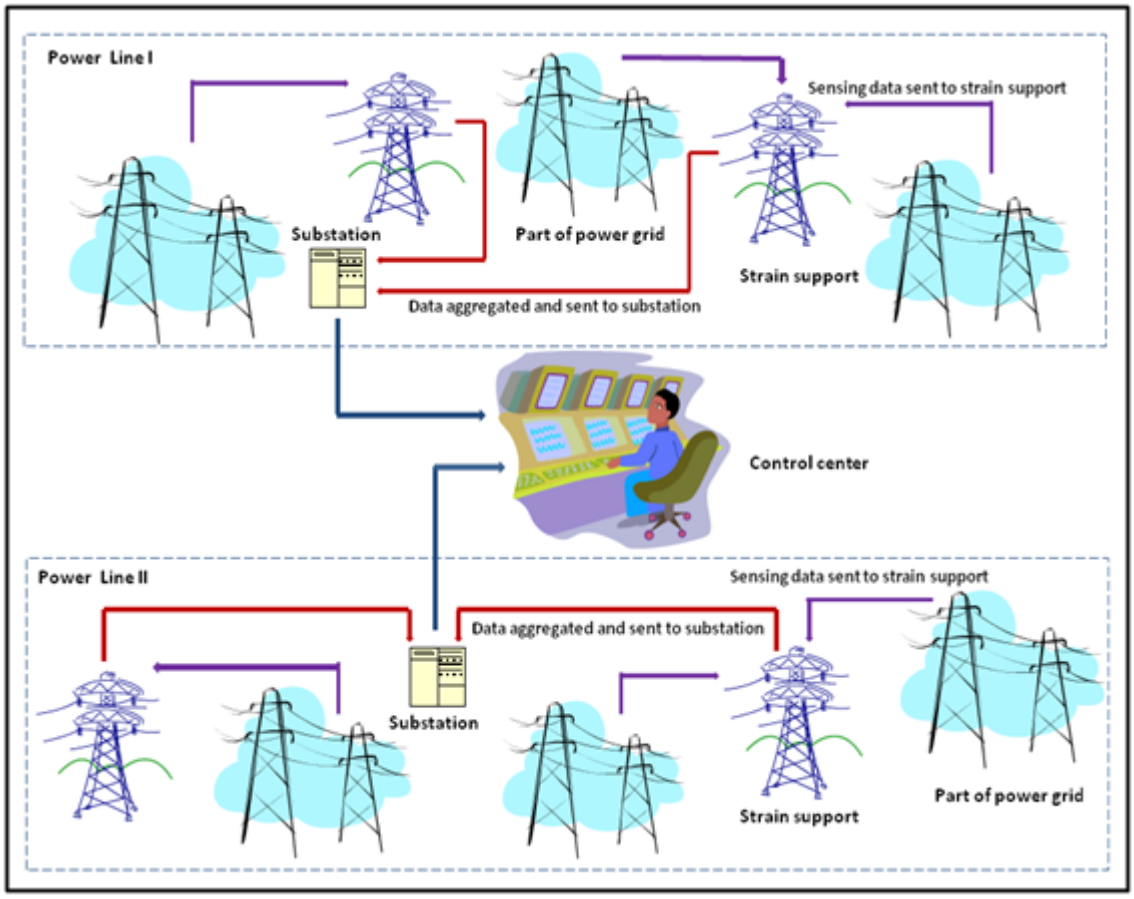

Figure 8.10: Schematic drawing of the health monitoring system

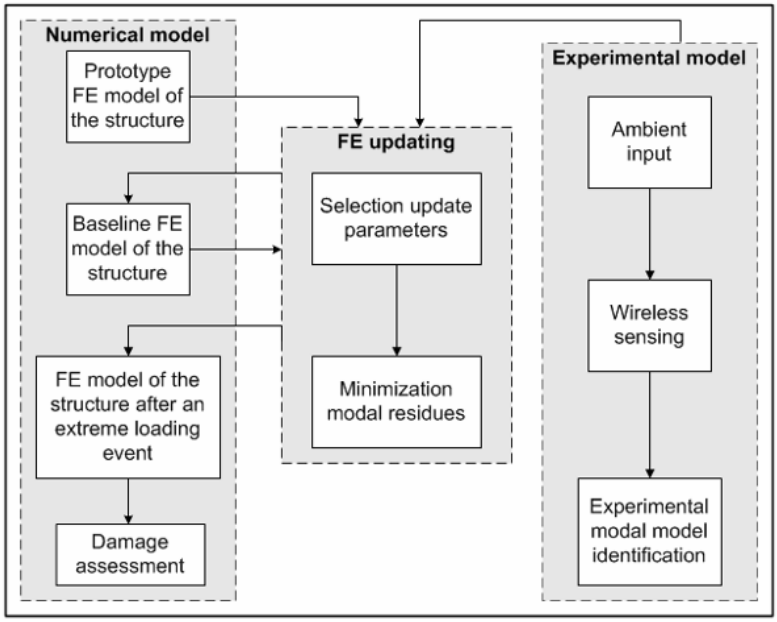

Figure 8.11: Framework of the health monitoring algorithm

Table 8.1: Comprehensive outline of the conducted studies

Subjects	*Conducted studies*
The marked site for embedding the pole	$SASW_{1*}$
The suspended concrete pole	MT_{1**}
The pole embedded with loose soil backfill	MT_2; $SASW_2$
The pole embedded with dense soil backfill	MT_3; $SASW_3$

*SASW: The Spectral Analysis of Surface Waves test.
**MT: impact Modal Testing combined with FE modal analysis work.

Table 8.2: Geometry input information

Length (in)		*Cross section diameter (in)*		
Buried portion	H1=66.00	The butt cross-section	D_{B1}=15.85	D_{B2}=10.35
Pole about the ground	H2=354.00	The tip cross-section	D_{T1}=9.55	D_{T2}=4.05

Table 8.3: Identified natural frequencies from the modal testing

Frequencies (Hz)* / *Mode*	*MT_1*	*MT_2*	*MT_3*	*Difference (%)***
1st mode	-	1.90	3.30	73.7
2nd mode	13.37	11.39	15.28	34.2
3rd mode	36.33	31.17	39.36	26.3
4th mode	69.66	-	-	-

* The values were natural frequencies of the bending modes;
MT_1 has no cantilevered mode (1st mode) while MT_2 and MT_3 4th modes were not identified.
** Difference = $(MT_3-MT_2)/MT_2\times100$.

Table 8.4: Comparison between test results and updated FE analysis

Test	*Mode*	*Measured frequency*	*FEM Results*	*Difference*	*MAC*
	1st bending	13.37 (Hz)	13.38 (Hz)	0.02%	0.99
MT_1	2nd bending	36.33 (Hz)	36.22 (Hz)	0.28%	0.96
	3rd bending	69.66 (Hz)	69.96 (Hz)	0.43%	0.96
	1st bending	1.90 (Hz)	1.96 (Hz)	3.02%	0.93
MT_2	2nd bending	11.39 (Hz)	12.02 (Hz)	5.52%	0.94
	3rd bending	31.17 (Hz)	31.02 (Hz)	0.49%	0.98
	1st bending	3.30(Hz)	3.14 (Hz)	4.85%	0.93
MT_3	2nd bending	15.28 (Hz)	15.36 (Hz)	0.51%	0.99
	3rd bending	39.36 (Hz)	39.37 (Hz)	0.02%	1.00

Table 8.5: Average shear wave velocity from SASW testing

Test #	*Average V_s (fps)*	*Explanation*
SASWT1	552	Original soil property at the testing site.
SASWT2	455	The combined material property after backfilled with untamped soil: less stiff than the original soil.
SASWT3	560	The combined material property after backfilled with tamped soil: stiffer than the original soil.

CHAPTER 9: CONCLUSIONS AND RECOMMENDATIONS

9.1 Conclusions

Through field monitoring and numerical analysis, this study addressed the issues of assessing blast effects on transmission structures. A reasonable blast limit is determined for power transmission pole structures. To ensure long term stability and safety of transmission structures, research is extended to some pilot works in developing health monitoring strategies for the electric power transmission lines. The research findings can be summarized as follows:

(1) Tri-axial wireless sensing units were used to record blast induced ground movements at two sites located in southeastern United States with reasonable successes. Data from both wireless sensors and traditional geophones show comparable frequency contents as well as amplitudes for the recorded blast induced ground motions: Most events last around one second and frequencies of peak amplitudes are mainly between 10 to 50 Hz.

(2) Site-specific empirical relations were established between peak particle acceleration (PPA), peak particle velocity (PPV), and peak particle displacement (PPS) based on analyses of blast monitoring records from two sites in southeastern US. Response spectrum amplification factors were also obtained through blast data analysis: An average value of 3.39 amplification factor can be assumed for simplicity.

(3) Site specific spectra of blast induced ground vibration were developed based on field measurement data, which were used as input ground excitations in numerical analysis. Design spectra were established based on target ground vibrations, which were defined by different PPVs.

(4) Modal behaviors of transmission pole structures were systematically studied. Full-scale impact modal tests were performed on both prestressed concrete poles and tubular steel poles. Natural frequencies below 100 Hz and corresponding mode shapes of pole vibration were identified. Results indicated that fundamental frequencies are beyond 1 Hz for the studied single pole structures.

(5) Modal sensitive parameters were numerically studied. It is concluded that boundary conditions need to be considered for pole structures with less rigid embedment foundations. Under the elastic assumption, prestress does not have effects on eigensolutions of prestressed spun-cast concrete poles.

(6) FE modeling of transmission pole structures was optimized based on free dynamic behaviors of these poles. Simplified but relatively accurate FE models that take the structure-cable coupling issue into account were proposed. Eigensolutions from the simplified pole FE models are close to modal behaviors of real pole structures obtained from field impact modal testing with the maximum natural frequency difference of 8.98%.

(7) Dynamic responses of transmission pole structures under blast caused ground vibration were obtained both by spectrum analysis and by time-history analysis. These analytical works yielded structural performances of both concrete and steel poles under blast induced ground motions. Within linear elastic range, the concrete

pole is more vulnerable than the steel pole structure at material level. Concrete cracks at the acceleration time history based on 3 in/s PPV criterion in transient analysis.

(8) 2 in/s PPV blast limit for transmission pole structures was established based on site-specific blast records and analysis work on limited structure types. Some other factors such as flyrock issues, mudseam fracture, and airblast should also be included in a comprehensive blast design.

(9) Two NDT techniques (modal testing and SASW testing) were proposed to exam the quality of direct embedment foundations of transmission pole structures. Results from modal testing and SASW testing were successfully used as indictors for stiffness of direct embedment foundations. The former gives information about embedment foundation quality through back-calculating stiffness of soil springs and SASW method directly yields different average surface wave velocity values at foundations with different stiffness.

(10) An idea of vibration-based health monitoring strategy for the electric transmission structure was schematically described. Structural health information can be obtained by deploying sufficient sensors on the power line system. Abnormal scenarios can be diagnosed with developed algorithms based on collected data.

9.2 Recommendations

The research of blast effects on transmission structures is to protect power transmission lines under severe events. Although a blast limit is established through extensive field monitoring work and numerical analysis, conclusions are not complete due to limited ground vibration records and limited structure types studied. Therefore, the following recommendations are proposed for future considerations and studies:

(1) The wireless technology is a cost effective solution to long or short term monitoring, but its performance and reliability need to be further studied. Noise should be reduced at hardware level. Causes of frequency distribution difference between wireless sensors and geophones need further study. Development of a reliable wireless technology for the transmission structure health monitoring is an interesting research topic.

(2) Supplementary field monitoring is needed to enhance precision and confidence of design response spectra. Improvements can especially be made with the amplification factor value. Furthermore, results from additional tests at sites with different geological properties would provide more universally applicable blast limits.

(3) Similar dynamic analyses need to be conducted to other types of transmission structures so that a more inclusive guideline can be established. Modal behaviors of most pole structures as well as steel towers can be studied. Difference of the fundamental frequencies between this research results and those from the ASCE guideline, which suggests 0.5-1.0 Hz fundamental frequencies for pole structures (ASCE 1991), needs to be re-solved. Special attentions should be paid to the guyed tower under strong vertical ground vibration.

(4) Besides study on structural damage of the poles, which is the main topic of this dissertation, foundation stability is the very next concern considering the possibility of foundation failure occurs ahead of structural damage under some extreme loading conditions.

(5) A more comprehensive blast guideline based on the blast limit established in this research and other considerations suggested by Conner (2007) needs to be developed.

Besides the blast limit proposed in this dissertation, other factors such as flyrock and airblast also need to be quantitatively studied.

(6) More works are needed in order to develop a practical structural health monitoring system for power transmission lines. Although the vibration-based structural health monitoring is proven to be a promising approach, studies related to this method, such as sensor development and damage detection algorithm design, are needed. Physical case study need to be supported in order to verify the feasibility of proposed conceptual health monitoring design.

REFERENCES

Aktan, A. E., Catbas, F. N., Grimmelsman, K. A., and Pervizpour, M. 2003. Development of a model health monitoring guide for major bridges. Report submitted to: Federal Highway Administration Research and Development. Dexel Intelligent Infrastructure and Transportation Safety Institute, Philadelphia, PA.

ALGOR. 2007. ALGOR user's guide, V20. ALGOR®, Inc. Pittsburgh, PA.

Aldas, G. U. 2005. Application of the Stockwell transform to blasting-induced ground vibration. International Journal of Surface Mining, Reclamation and Environment, 19(2): 100-107.

ANSI. 1979. Specification and dimensions for wood poles. ANSI 05.1, American National Standard Institute, New York.

ANSI/ASCE. 1991. Design of steel latticed transmission structure. ASCE/ANSI 10-90, American Standards committee for Design of Steel Transmission Towers, American Society of Civil Engineers, New York.

ANSYS. 2005. Release 10.0 documentation for ANSYS®. SAS IP, Inc. Canonsburg, PA.

ANSYS. 2007. Release 11.0 documentation for ANSYS®. SAS IP, Inc. Canonsburg, PA.

ASCE. 1987. Guide for the design and use of concrete pole. American Society of Civil Engineers, New York.

ASCE. 1990. Design of steel transmission pole structure. American Society of Civil Engineers, New York.

ASCE. 1991. Guideline for transmission line structural loading. Task Committee on Structural Loadings of the Committee on Electrical Transmission Structures, Structural Division, American Society of Civil Engineers, New York.

ASCE/PCI. 1997. Guide for the design of prestressed concrete poles. PCI Journal, 42(6), 94-134.

ASCE/SEI. 2006. Design of steel transmission pole structures. ASCE/SEI 48-05, American Society of Civil Engineers, Reston, Virginia.

Bai, Y. and Keller, T. 2008. Modal parameter identification for a GFRP pedestrian bridge. Composite Structures, 82(1): 90-100.

Bansal, A., Schubert, A., Balakrishnan, M. V., and Kumosa, M. 1995. Finite element analysis of substation composite insulators. Composites Science and Technology, 55(4), 375-389.

Battista, R. C., S.Rodrigues, R.S., and Pfeil, M. S. 2003. Dynamic behavior and stability of transmission line towers under wind forces. Journal of wind engineering and industrial aerodynamics, 91(8), 1051-1067.

Bhattacharya, K. and Dutta, S. C. 2004. Assessing lateral period of building frames incorporating soil-flexibility. Journal of Sound and Vibration, 269(3-5), 795-821.

Brownjohn, J. M. W., Xia, P. Q., Hao, H., Xia, Y. 2001. Civil structure condition assessment by FE model updating: methodology and case studies. Finite Elements in Analysis and Design, 37(10): 761-775.

BSSC 2004. NEHRP recommended provision for seismic regulations for new buildings and other structures. 2003 ed. Washington, DC: Building Seismic Safety Council, 47-48.

Chang, C. N. 1985. Study of the axial-torsional coupling effect on a sagged transmission line. Ph.D dissertation, Iowa State University, Ames, Iowa.

Chen, S. E., Dai, K. S., and Conner, E. G. 2007. Study of blast-loading effects on transmission structures. Interim Phase Report, Department of Civil and Environmental Engineering, University of North Carolina at Charlotte, Charlotte, NC.

Chen, S. E., Ong, C. K., and Delatte, N. 2004. SASW soil profiling and anchor holding capacity prediction for transmission structures-pilot study. Project report, Department of Civil and Environmental Engineering, University of Alabama at Birmingham, Birmingham, AL.

Chen, S. E., Ong, C. K., and Antonsson, K. 2006. Modal behaviors of spun-cast prestressed concrete pole structures. Proceeding of IMAC-XXIV, Society of Experimental Mechanics, Saint Louis, Missouri.

Cho, Y. S. 2003. Non-destructive testing of high strength concrete using spectral analysis of surface waves. NDT & E International, 36(4): 229-235.

Conner, C. G., Dai, K. S., and Chen, S. E. 2007. A comprehensive blast plan for transmission structures due to mining induced blasts. Proceeding of IMAC-XXV, Society for Experimental Mechanics, Orlando, FL.

Conner, E. G. 2007. Design of a qualitative blast plan for transmission structures. M. S. thesis, University of North Carolina at Charlotte, Charlotte, NC.

Cunha, J., and Piranda, J. 1999. Application of model updating techniques in dynamics for the identification of elastic constants of composite materials. Composites: Part B Engineering, 30(1): 79-85.

Dallasta, A. and Dezi, L. 1996. Prestress force effect on vibration frequency of concrete bridges—discussion. Journal of Structural Engineering, 122(4): 458-458.

Deak, G. 1996. Prestress force effect on vibration frequency of concrete bridges—discussion. Journal of Structural Engineering, 122(4): 458-459.

Dowding, C. H. 1985. Blasting vibration monitoring and control, Prentice-Hall, Inc., Englewood Cliffs, NJ.

Duvall, W. I., and Fogelson, D. E. 1962. Review of criteria for estimating damage to residences from blasting vibrations. Report of Investigations 5968, U. S. Bureau of Mines, Pittsburgh, PA.

El-Attar, M. M. 1997. Nonlinear dynamics and seismic response of power transmission lines. Ph.D dissertation. McMaster Univertiy, Hamilton, Ontario, Canada.

Ewins, D. J. 2000. Modal testing: theory, practice and application, Research Studies Press Ltd, Baldock, UK.

Fang, S. J., Roy, S., and Kramer, J. 1999. Transmission structures. Structural Engineering Handbook, W. F. Chen, ed., CRC Press LLC., Boca Raton, FL.

Farrar, C.R. and James III, G. H. 1997. System identification from ambient vibration measurements on a bridge. Journal of Sound and Vibration, 205(1): 1-18.

FLHP. 2008. Vibration recommendations. Federal Lands Highway Program, Federal Highway Administration. <http://www.cflhd.gov/agm/engApplications/VibratonMeasurements/714VibrationRecom.htm>

Gerolymos, N. and Gazetas, G. 2006. Winkler model for lateral reponse of rigid caission foundations in linear soil. Soil Dynamics and Earthquake Engineering, 26: p. 347-361.

Ghobarah, A., Aziz, T. S., and El-Attar, M. 1996. Response of transmission lines to multiple support excitation. Engineering Structures, 18(12): 936-946.

Hamed, E., and Frostig, Y. 2006. Natural frequencies of bonded and unbonded prestressed beams–prestress force effects. Journal of Sound and Vibration, 295(1-2): 28-39.

Hao, H., Ma, G. W., and Lu, Y. 2002. Damage assessment of masonry infilled RC frames subjected to blasting induced ground excitations. Engineering Structures, 24(6):799-809.

Hao, H., and Wu, C. 2005. Numerical study of characteristics of underground blast induced surface ground motion and their effect on above-ground structures. Part II. Effects on structural responses. Soil Dynamics and Earthquake Engineering, 25(1): 39-53.

Hao, H., Wu, Y., Ma, G., and Zhou, Y. 2001. Characteristics of surface ground motions induced by blasts in jointed rock mass. Soil Dynamics and Earthquake Engineering, 21(2): 85-98.

He, J., and Fu, Z. F. 2001. Modal analysis, Butterworth-Heinemann, Boston, Massachusetts.

Hensley, G. M. 2005. Finite element analysis of the seismic behavior of guyed masts. M. S. Thesis, Virginia Polytechnic Institute and State University, Blacksburg, VA.

Herrell, J. P. 1996. Surface mine blast vibration transmission over deep mines. M.S. thesis, University of Louisville, Louisville, KY.

Horr, A.M., Yibulayin, A., and Disney, P. 2004. Nonlinear spectral dynamic analysis of guyed towers. Part II: Manitoba towers case study. Canada Journal of Civil Engineering, 31(6): 1061-1076.

IEEE. 1991. IEEE trial-use design guide for wood transmission structures. IEEE Standard 751, Institute of Electrical and Electronics Engineers, New York.

Ivanovic, S. S., Trifunac, M. D., Novikova, E. I., Gladov, A. A., and Todorovska, M. I. 2000. Ambient vibration tests of a seven-story reinforced concrete building in Van Nuys, California, damaged by the 1994 Northridge earthquake. Soil Dynamics and Earthquake Engineering, 19(6): 391-411.

Jain, S. K. and Goel, S.C. 1996. Prestress force effect on vibration frequency of concrete bridges—discussion. Journal of Structural Engineering, 122(4): 459-460.

Jenkins, W. K., Poularikas, A. D., Bomar, B. W., Smith, L. M. and Cadzow, J. A. 2000. Digital signal processing. The electrical engineering handbook, Chapter 14, Richard C. Dorf, eds., CRC, Boca Raton, F.L.

Joh, S. H. 1996. Advances in the interpretation technique for spectral-analysis-of-surface-waves (SASW) measurements. Ph. D dissertation, University of Texas at Austin, Austin, Texas.

Kahriman, A. 2004. Analysis of parameters of ground vibration produced from bench blasting at a limestone quarry. Soil Dynamics and Earthquake Engineering. 24(11): 887-892.

Kálmám, T., Farzaneh, M., and McClure G. 2007. Numerical analysis of the dynamic effects of shock-load-induced ice shedding on overhead ground wires. Computers and Structures 85: 375-384.

Karam, L. J., McClellan, J. H., Selesnick, I. W., and Burrus, C. S. 1999. Digital filtering. Digital signal processing handbook, Chapter 11. V. K. Madisetti and D. B. Williams, eds., CRC Press, Boca Raton, FL.

Khandelwal, M., and Singh, T. N. 2005. Prediction of blast induced ground vibrations and frequency in opencast mine: A neural network approach. Journal of Sound and Vibration, 289(4-5): 711-725.

Khedr, M. A. H. 1998. Seismic analysis of lattice towers. Ph.D dissertation, McGill University, Montreal, Canada.

Kiessling, F., Nefzger, P., Nolasco, J. F., and Kaintzyk, U. 2003. Overhead power lines—planting, designing, construction. Berlin, Germany: Springer-Verlag, 2003.

Kim, D. S., Shin, M.-K. and Park, H. C. 2001. Evaluation of density in layer compaction using SASW method. Soil Dynamics and Earthquake Engineering, 21(1): 39-46.

Kocer, F. Y., and Arora, J. S. 1996. Design of prestressed concrete transmission poles: optimization approach. Journal of Structural Engineering, 122(7): 804-814.

Kudzys, A. 2006. Safety of power transmission line structures under wind and ice storms. Engineering Structures, 28(5): 682-689.

Koh, B. H. and Dyke, S. J. 2007. Structural health monitoring for flexible bridge structures using correlation and sensitivity of modal data. Computers and Structures, 85(3-4): 117-130.

Kumar, B. P. 2005. Digital signal processing laboratory, Taylor & Francis, Sacramento, CA.

Kumosa, M., Han, Y., and Kumosa, L. 2002. Analyses of composite insulators with crimped end-fittings: Part I-non linear finite element computations. Composite Science and Technology, 62(9): 1191-1207.

Lantrip, T. B. 1995. Identification of structural characteristics of spun prestressed concrete poles using modal testing methods. M.S. thesis, University of Alabama at Birmingham, Birmingham, Alabama.

León, R. A., Vittal, V., and Manimaran, G. 2007. Application of sensor network for secure electric energy infrastructure. IEEE Transactions on Power Delivery, 22(1-2): 1021-1028.

Li, H. N., Shi, W. L., Wang, G. X., and Jia, L. G. 2005. Simplified models and experimental verification for coupled transmission tower-line system to seismic excitations. Journal of Sound and Vibration, 286(3): 569-585.

Loh, C. H., and Wu, T. C. 2000. System identification of FEI-TSUI arch dam from forced vibration and seismic response data. Journal of Earthquake Engineering, 4(4): 511-537.

Loredo-Souza, A. M. 1996. The behavior of transmission lines under high winds. Ph. D. dissertation, The University of Western Ontario, London, Ontario, Canada.

Loredo-Souza, A. M. and Davenport, A. G. 2003. The influence of the design methodology in the response of transmission towers to wind loading. Journal of wind engineering and industrial aerodynamics, 91(8): 995-1005.

Lu, Y., Hao, H., and Ma, G. 2002a. Experimental investigation of structural response to generalized ground shock excitations. Experimental Mechanics, 42(3): 261-271.

Lu, Y., Hao, H., Ma, G., and Zhou, Y. 2002b. Local-mode response and its structural effects under horizontal ground shock excitations. Journal of Sound and Vibration, 254(1): 51-68.

Lu, Y., Wang, Z., and Chong, K. 2005. A comparative study of buried structure in soil subjected to blast load using 2D and 3D numerical simulations. Soil Dynamics and Earthquake Engineering, 25(4), 275-288.

Ma, H. J., Quek, S. T., Ang, K. K. 2004. Soil-structure interaction effect from blast-induced horizontal and vertical ground vibration. Engineering Structures, 26(12):1661-1675.

Ma, G., Hao, H., and Zhou, Y. 2000. Assessment of structure damage to blasting induced ground motions. Engineering structures, 22(10): 1378-1399.

Ma, G., Hao, H., Lu, Y., and Zhou, Y. 2002. Distributed structural damage generated by high-frequency ground motion. Journal of Structural Engineering, 128(3): 390-399.

Madugula, M. K. S., Wahba, Y. M. F., and Monforton, G. R. 1998. Dynamic response of guyed masts. Engineering Structures, 20(12): 1097-1101.

Maeck, J. 2003. Damage assessment of civil engineering structures by vibration monitoring. Ph. D dissertation, K. U. Leuven, Leuven, Belgium.

Manassah, J. T. 2001. Elementary mathematical and computational tools for electrical and computer engineers using MATLAB®. CRC, Boca Raton, F.L.

MATLAB® 2008. MATLAB® Product help document, R2008a. The Mathworks ™, Natick, MA.

McClure, G. and Lapointe, M. 2003. Modeling the structural dynamic response of overhead transmission lines. Computers and Structures, 81(8-11): 825-834.

Melhem, H. and Kim, H. 2003. Damage detection in concrete by Fourier and Wavelet analyses. Journal of Engineering Mechanics, 129(5): 571-577.

Memari, A. M., Aghakouchak, A. A., Ghafory Ashtiany M., Tiv, M. 1999. Full-scale dynamic testing of a steel frame building during construction. Engineering Structure, 21(12): 1115-1127.

Meshmesha, H. M. 2005. Dynamic analysis of guyed antenna towers for seismic loads. Ph. D dissertation, University of Windsor, Windsor, Ontario, Canada.

MicroStrain. 2007. G-Link® wireless accelerometer node, user manual, version 4.0.3. MicroStrain, Inc., Williston, VT.

Momomura, Y., Marukawa, H., Okamura, T., Hongo, E., and Ohkuma, T. 1997. Full-scale measurements of wind-induced vibration of a transmission line system in a mountainous area. Journal of Wind Engineering and Industrial Aerodynamics, 72(1): 241-252.

Murtagh, P. J., Basu, B., Broderick, B. M. 2004. Simple models for natural frequencies and mode shapes of towers supporting utilities. Computers and Structures, 82(20-21): 1745-1750.

Nafie, A. M. A. E. 1997. Development of computer software for simulation of transmission line dynamic behavior. Ph.D dissertation, Iowa State University, Ames, Iowa.

Naggar, M. H. 2003. Performance evaluation of vibration-sensitive equipment foundations under ground-transmitted excitation. Canada Geotechnology Journal, 40(3): 598-615.

Nawy, E. G. 2003. Prestressed concrete: a fundamental approach, 15th edition. Pearson Education, Inc., New Jersey.

Nazarian, S., Stokoe II, K. H., Briggs, R. C., and Rogers, R. 1988. Determination of pavement layer thickness and moduli by SASW method. Transportation Research Record, 1196: 133-150.

Nicholls, H. R., Johnson, C. F., and Duvall, W. I. 1971. Blasting vibrations and their effects on structures. Bulletin 656, U. S. Bureau of Mines, Denver, CO.

Nomis. 2003. WinNomis 2003 for Windows 32 bit operating systems. Nomis Seismographs, Birmingham, AL.

Ong, C. K., Chen, S. E., Galloway, C., Munden, C., and Mize, D. 2006. Innovative application of geophysical techniques for design of direct-embedded pole structures. Proceedings of The 2006 Electrical Transmission Conference, American Society of Civil Engineers, Birmingham, AL.

Ozono, S., Maeda, J., and Makino, M. 1988. Characteristics of in-plane free vibration of transmission line systems. Engineering Structures, 10(4): 272-280.

Ozono, S., Maeda, J., and Makino, M. 1992. In-plane dynamic interaction between a tower and conductors at lower frequencies. Engineering Structures, 14(4): 210-216.

Park, J. H., Moon, B. W., Min, K. W., Lee, S. K., Kim K. 2007. Cyclic loading test of friction-type reinforcing members upgrading wind-resistant performance of transmission towers. Engineering Structures, 29(11):3185-3196.

Pavic, A., and Reynolds, P. 2003. Modal testing and dynamic FE model correlation and updating of a prototype high-strength concrete floor. Cement & Concrete Composites, 25(7): 787-799.

PCI. 2004. PCI Design Handbook, 6th edition. Precast/Prestress Concrete Institute, Chicago, IL.

Peeters, B. 2000. System identification and damage detection in civil engineering. Ph.D dissertation, K. U. Leuven, Leuven, Belgium.

Polyzois, D., Raftoyiannis, I. G., and Ibrahim, S. 1998. Finite elements method for the dynamic analysis of tapered composite poles. Composite Structures, 43(1): 25-34.

Rahman, M. M. 2003. Identification of dynamic characteristics of linear systems. M. S thesis, University of Windsor, Windsor, Ontario, Canada.

Rao, N. P., Mohan, S. J., and Lakshmanan, N. 2004. A semi empirical approach for estimating displacements and fundamental frequency of transmission line towers. International Journal of Structural Stability and Dynamics, 4(2): 181-195.

Ren, W.X., Zatar, W., and Harik, I. E. 2004. Ambient vibration-based seismic evaluation of a continuous girder bridge. Engineering Structures, 26(5): 631-640.

Rojas-Gonzalez, L. F., DiGioia, A. M., and Longo, V. J. 1991. A new design approach for direct embedment foundations. IEEE Transactions on Power Delivery, 6(3): 1336-1342.

RUS. 2005. Design manual for high voltage transmission lines. RUS Bulletin 1724E-200, Rural Utilities Service, Washington, DC.
< http://www.usda.gov/rus/electric/bulletins.htm>

Sanayei, M., McClain, J. A. S., Wadia-Fascetti, S., and Santini, E. M. 1999. Parameter estimation incorporating modal data and boundary conditions. Journal of Structural Engineering, 125(9): 1048-1055.

Savory, E., Parke, G. A. R., Disney, P. and Toy, N. 2008. Wind induced transmission tower foundation loads: A field study-design code comparison. Journal of Wind Engineering and Industrial Aerodynamics, 96(6): 1103-1110.

Shehata, A. Y., El Damatty, A. A., and Savory, E. 2005. Finite element modeling of transmission line under downburst wind loading. Finite Elements in Analysis and Design, 42(1): 71-89.

Siringoringo, D. M., and Fujino, Y. 2008. System identification of suspension bridge from ambient vibration response. Engineering Structures, 30(2), 462-477.

Siskind, D. E., Stagg, M. S., Kopp, J. W., and Dowding, C. H. 1980. Structure response and damage produced by ground vibration from surface mine blasting. Report of investigations 8507, U. S. Bureau of Mines.

Southern Company. 1992. Southen electric system standard specifications for wood pole equivalent spun prestressed concrete poles. SES-PD-024, Southern Company, Birmingham, AL.

Southern Company. 2006. southern company standard specifications for wood pole equivalent tubular steel poles. SES-PD-O28, Southern Company, Birmingham, AL.

Svinkin, M. R. 2003. Drawbacks of blast vibration regulations. vulcanhammer. net: geotechnical and marine engineering online library.
< http://www.vulcanhammer.net/svinkin/>

Tedesco, J. W., Mcdougal, W. G. and Ross, C. A. 1999. Structural dynamics: theory and application. Addison Wesley Longman, Inc., Boston, M.A.

Teughels, A. 2003. Inverse modelling of civil engineering structures based on operational modal data. Ph. D dissertation, Ph. D., K. U. Leuven.

Teughels, A., and DE Roeck, G. 2004. Structural damage identification of the highway bridge Z24 by FE model updating. Journal of Sound and Vibration, 278(3): 589-610.

Toraño J., Rodríguez, R., Diego, I., Rivas, J. M. and Casal, M. D. 2006. FEM models including randomness and its application to the blasting vibrations prediction, Computers and Geotechnics, 33 (1): 15-28.

Tucker, K. B. 2007. Validation of full-scale and small-scale transmission line test results on dynamic loads with numerical modeling. M.S. Thesis, Memorial University of Newfoundland, Newfoundland and Labrador, Canada.

Unger, J. F., Teughels, A., and Roeck, G. D. 2005. Damage detection of a prestressed concrete beam using modal strains. Journal of Structural Engineering, 131(9): 1456-1463.

Venkatasubramanian, S. H. 1992. Determination of the initiating mode for transmission line galloping. Ph.D. dissertation, Kansas State University, Manhattan, Kansas.

Wang J. and Hu X. 2006. Application of MATLAB® in vibration signal processing. China Hydropower Press, Beijing, China. (in Chinese).

Wiss, J. F. 1968. Effect of blasting vibrations on buildings and people. Civil Engineering, 7: 46-48.

Wu, C., Hao, H., Lu, Y. and Sun, S. 2004. Numerical simulation of structural responses on a sand layer to blast induced ground excitations. Computers and Structures, 83(9-10): 799-814.

Wu, C., and Hao, H. 2005. Numerical study of characteristics of underground blast induced surface ground motion and their effect on above-ground structure. Part I. Ground motion characteristics. Soil Dynamics and Earthquake Engineering, 25(1): 27-38.

Wu, C., Hao, H., and Lu, Y. 2005. Dynamic response and damage analysis of masonry structures and masonry infilled RC frames to blast ground motion. Engineering Structures, 27(3): 323-333.

Wu, C. and Hao, H. 2007. Numerical simulation of structural response and damage to simultaneous ground shock airblast loads. International Journal of Impact Engineering, 34(3): 556-572.

Yan, Y. J., Cheng, L., Wu, Z. Y., and Yam, L. H. 2007. Development in vibration-based structural damage detection technique. Mechanical Systems and Signal Processing, 21(5): 2198-2211.

Yasui, H., Marukawa, H., Momomura, Y., and Ohkuma, T. 1999. Analytical study on wind-induced vibration of power transmission towers. Journal of Wind Engineering Industrial Aerodynamics, 83(1-3): 431-441.

Zhao, X., Yuan, S., Yu, Z., Ye, W., and Cao, J. 2008. Designing strategy for multi-agent system based large structural health monitoring. Expert System with Applications: An International Journal. 34(2):1154-1168.

Živanović, S., Pavic, A., and Reynolds, P. 2006. Modal testing and FE model tuning of a lively footbridge structure. Engineering Structures, 28(6): 857-858.

APPENDIX

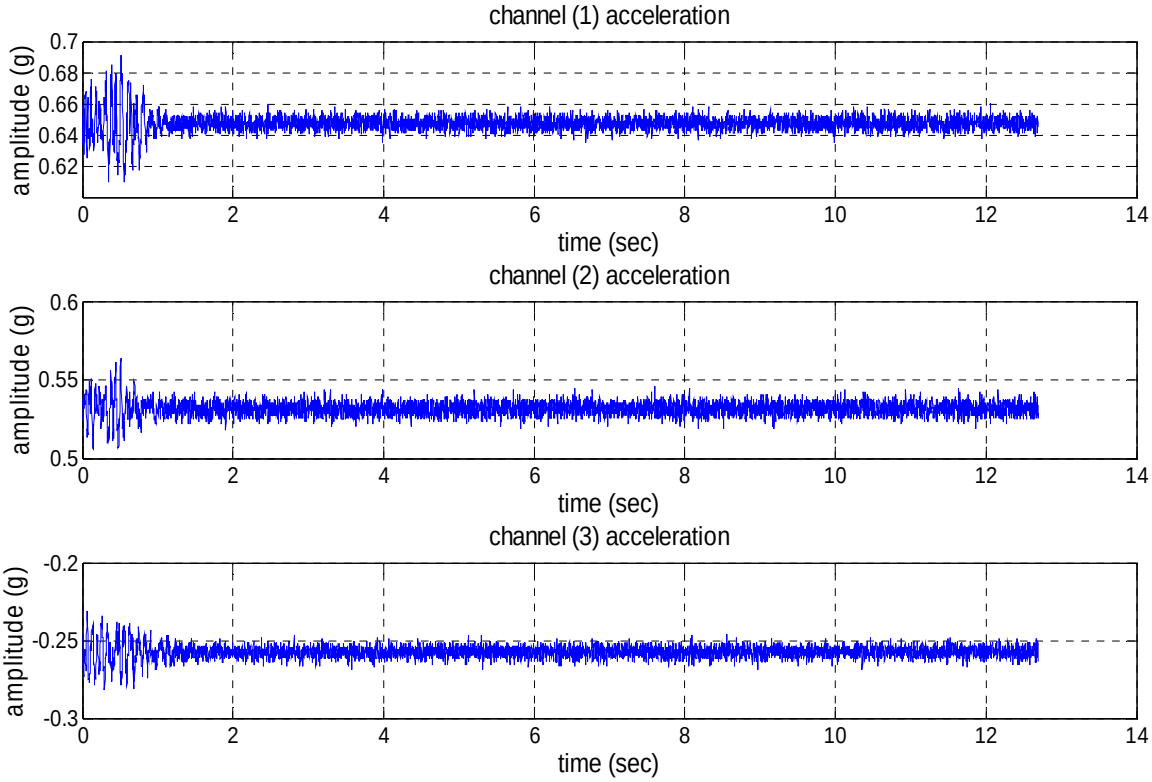

Figure A1: U1 acceleration record

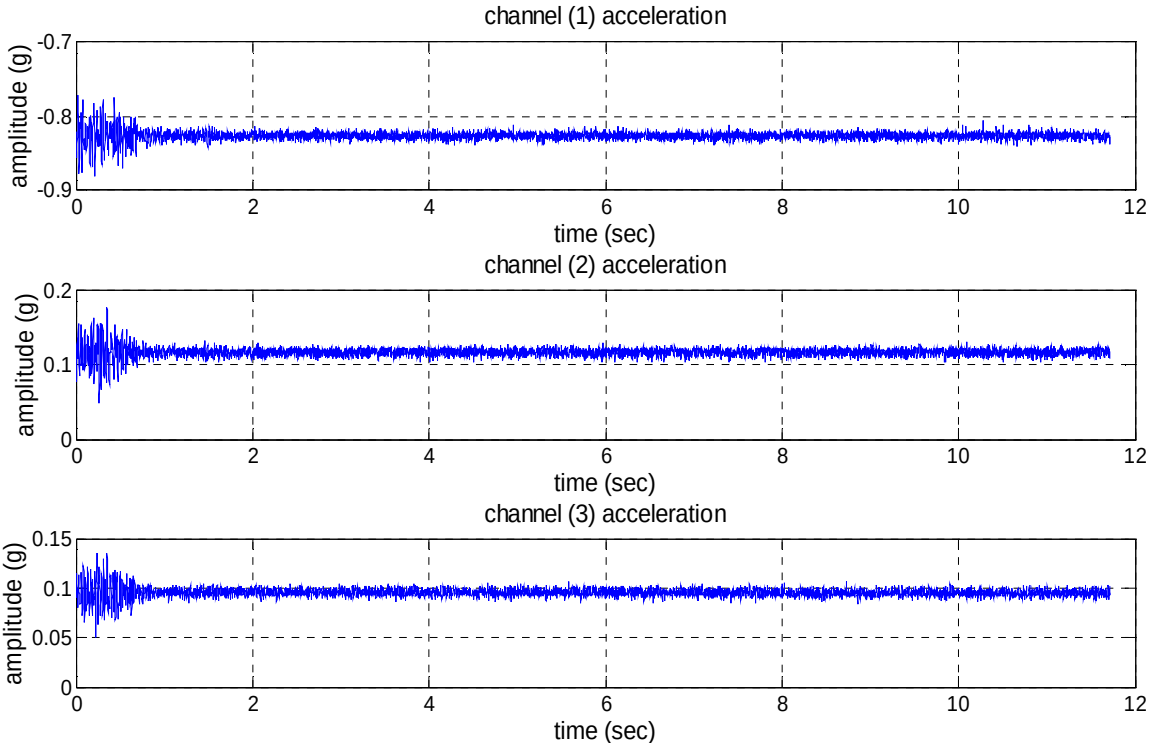

Figure A2: U2 acceleration record

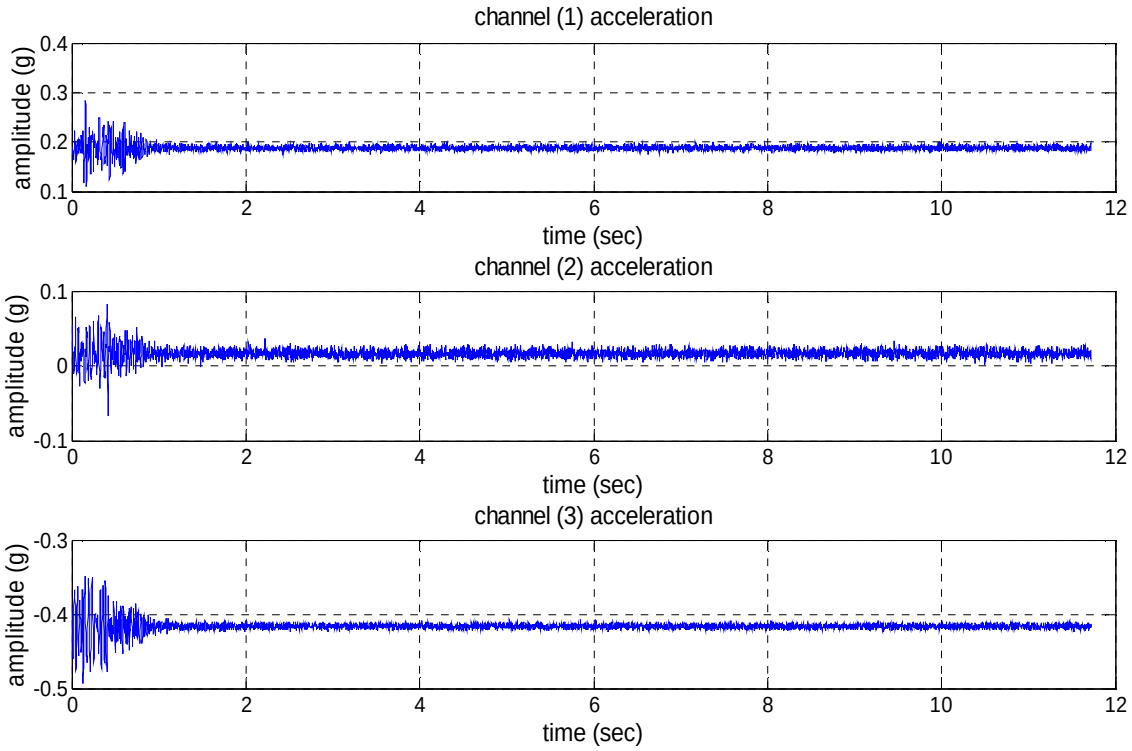

Figure A3: U3 acceleration record

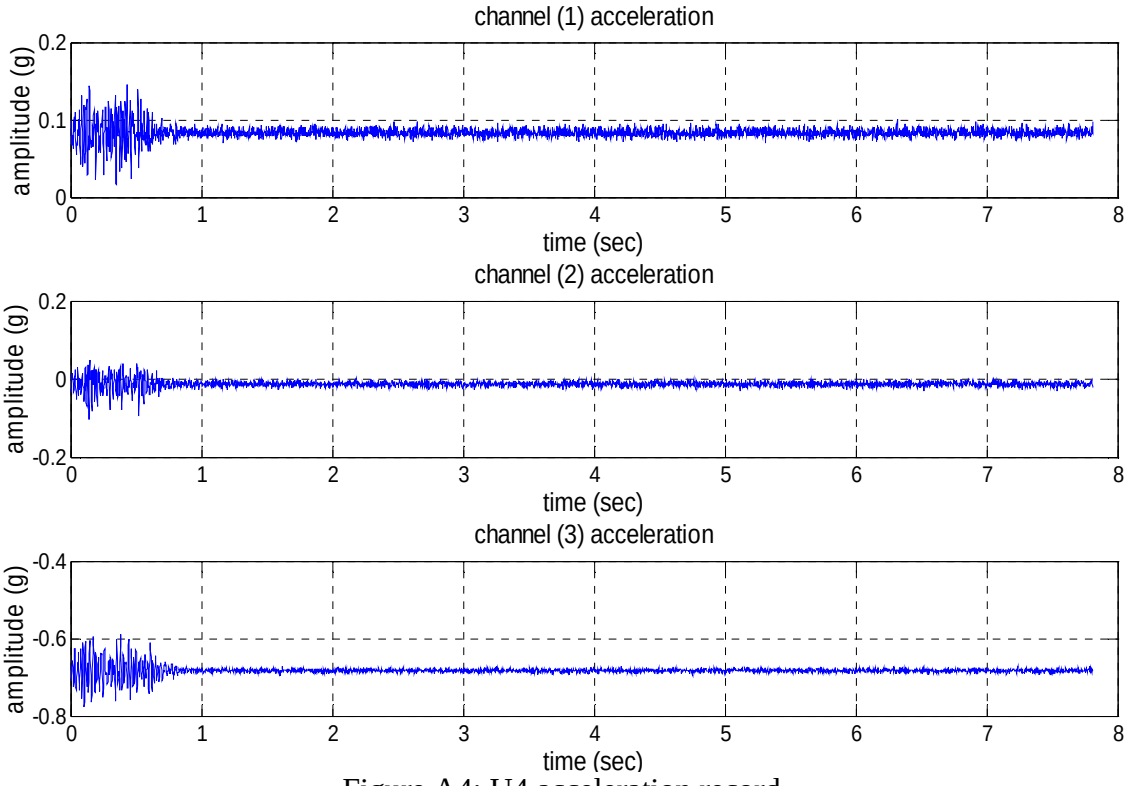

Figure A4: U4 acceleration record

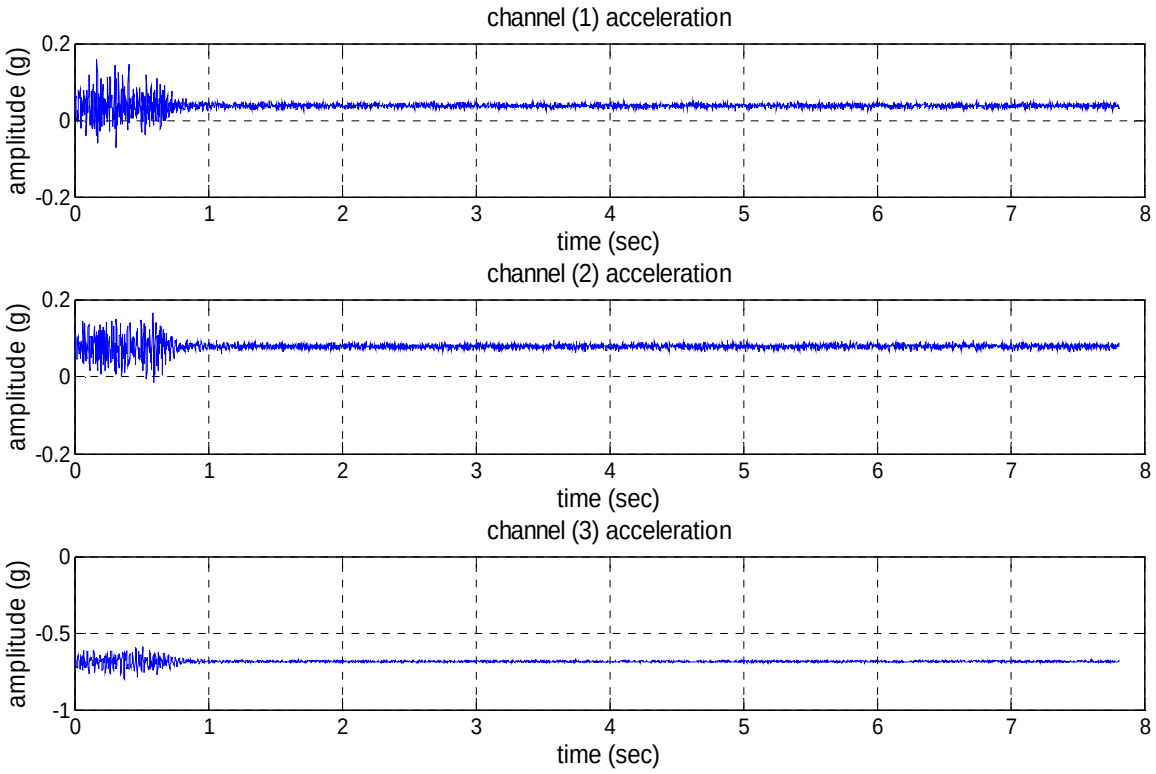

Figure A5: U5 acceleration record

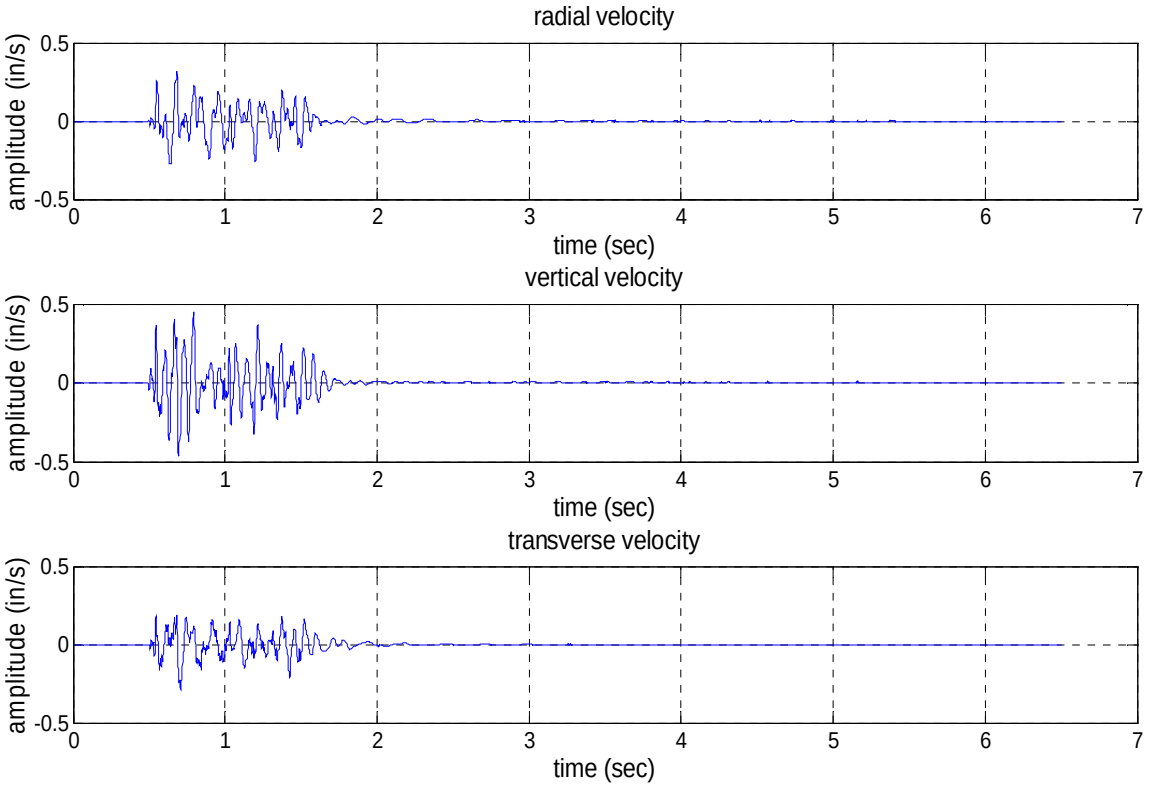

Figure A6: R1 velocity record

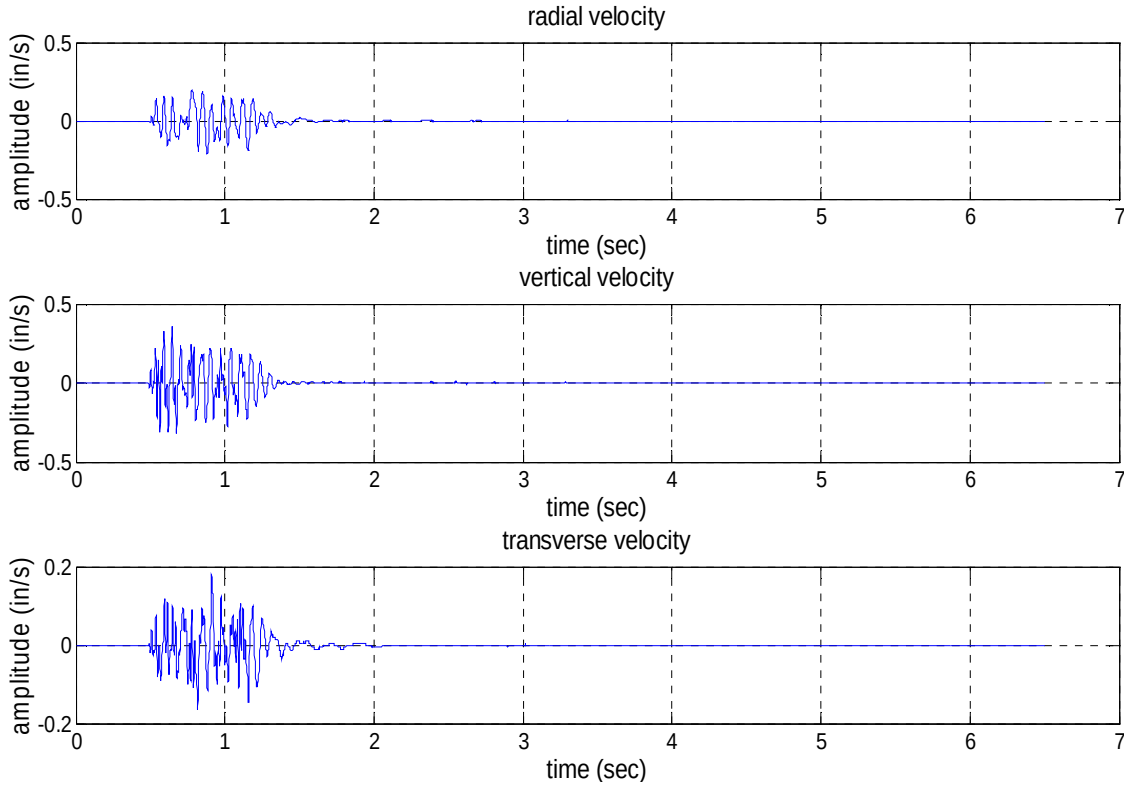

Figure A7: R2 velocity record

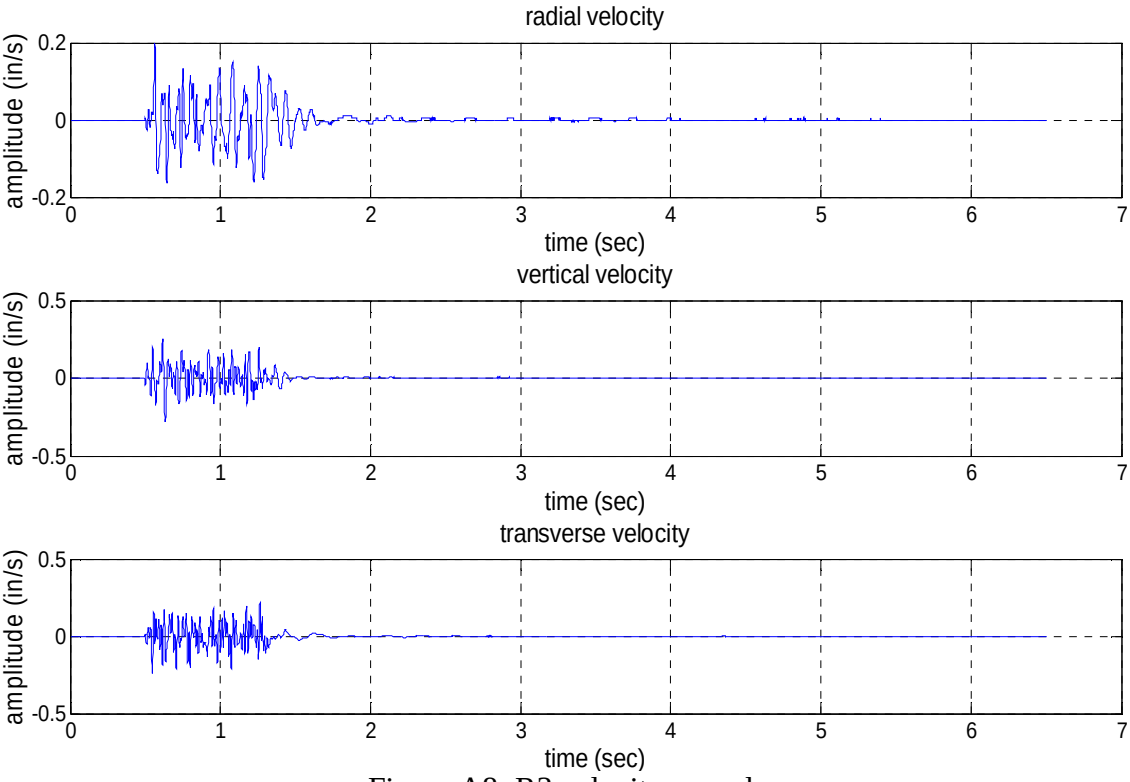

Figure A8: R3 velocity record

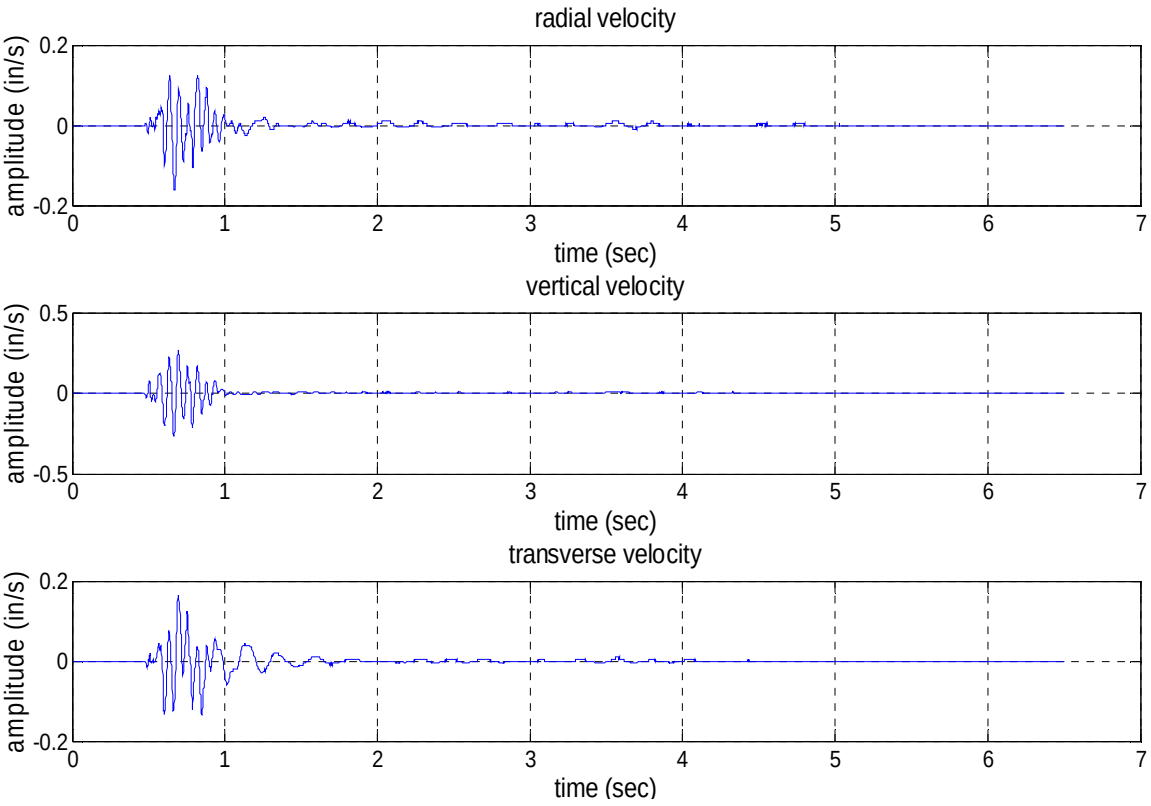

Figure A9: R4 velocity record

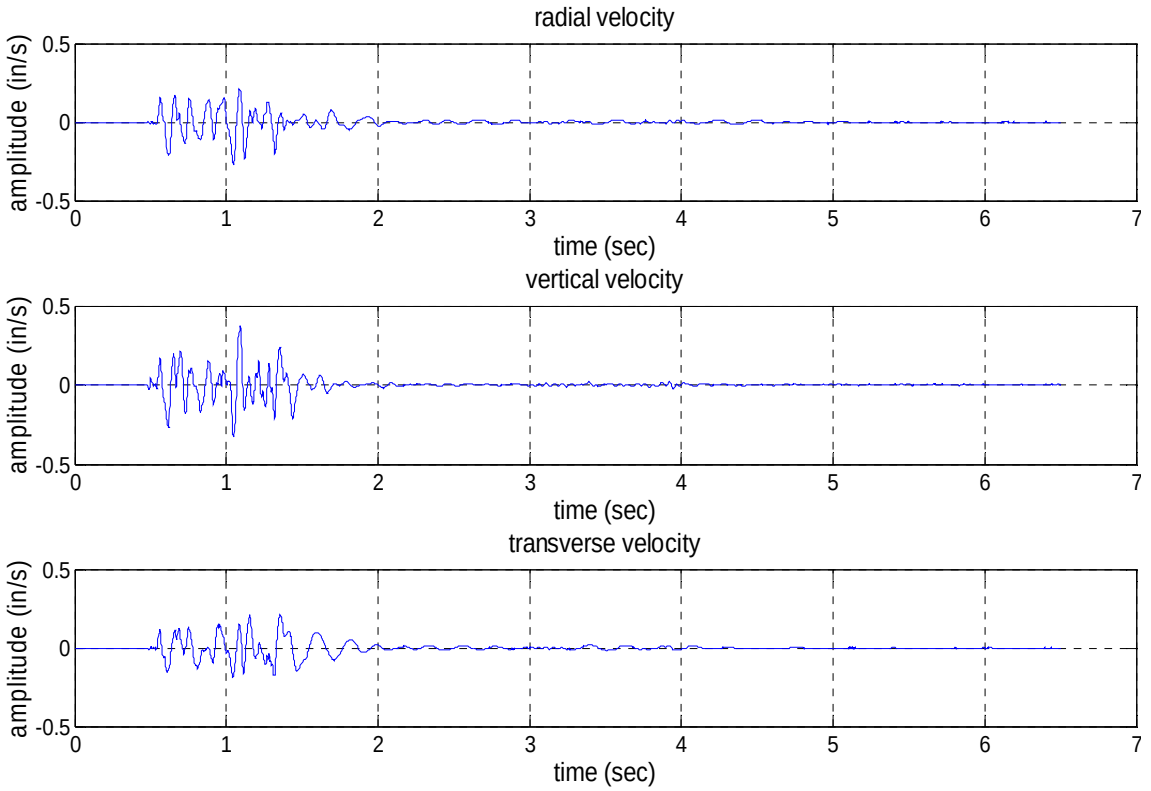

Figure A10: R5 velocity record

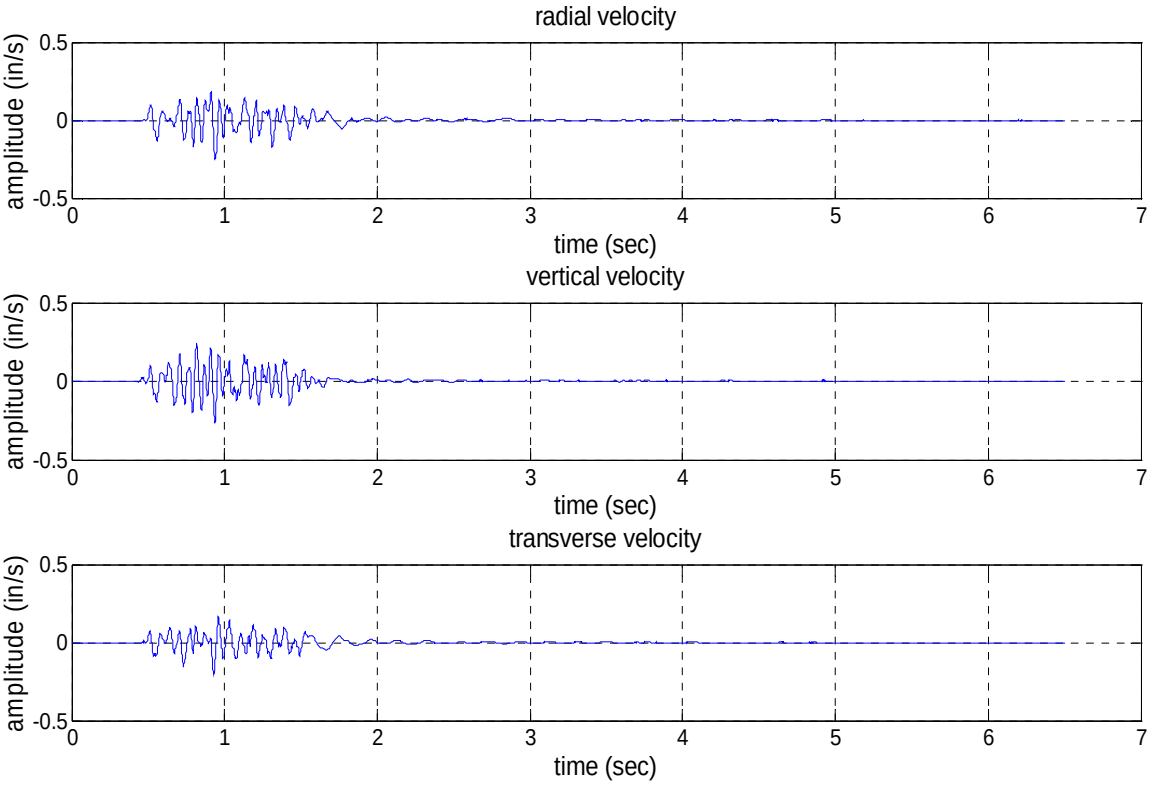

Figure A11: R6 velocity record

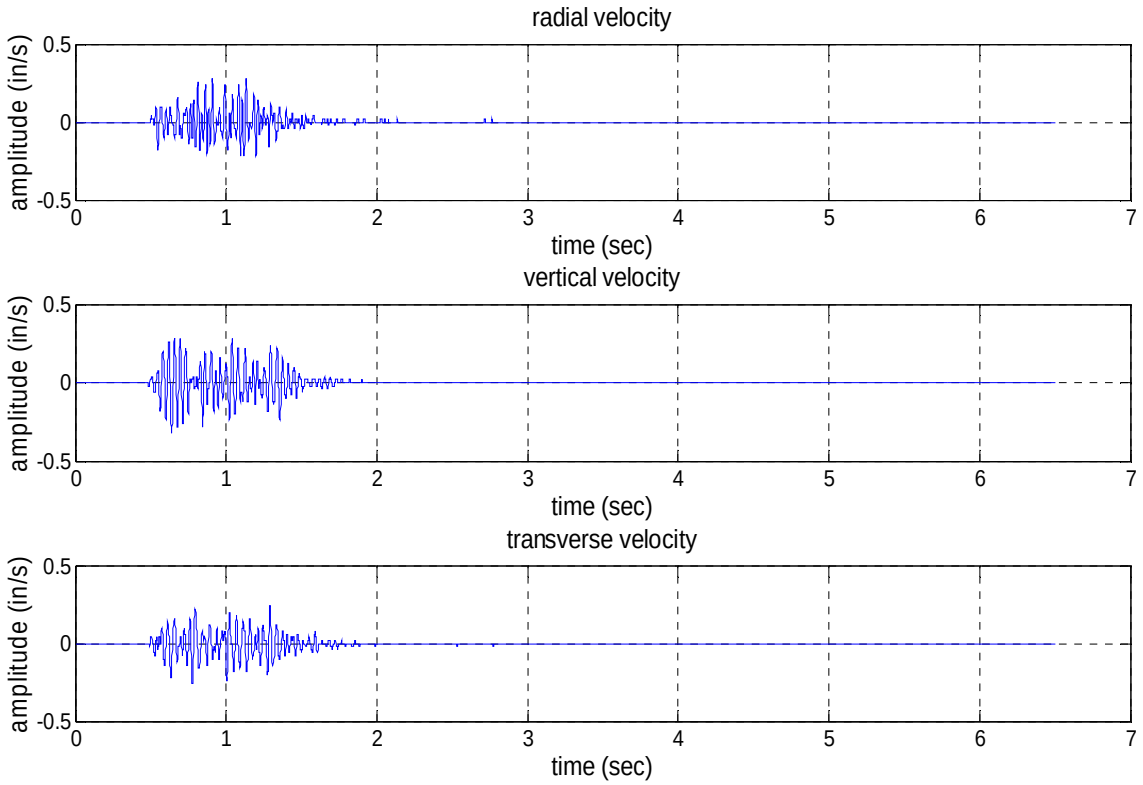

Figure A12: R7 velocity record

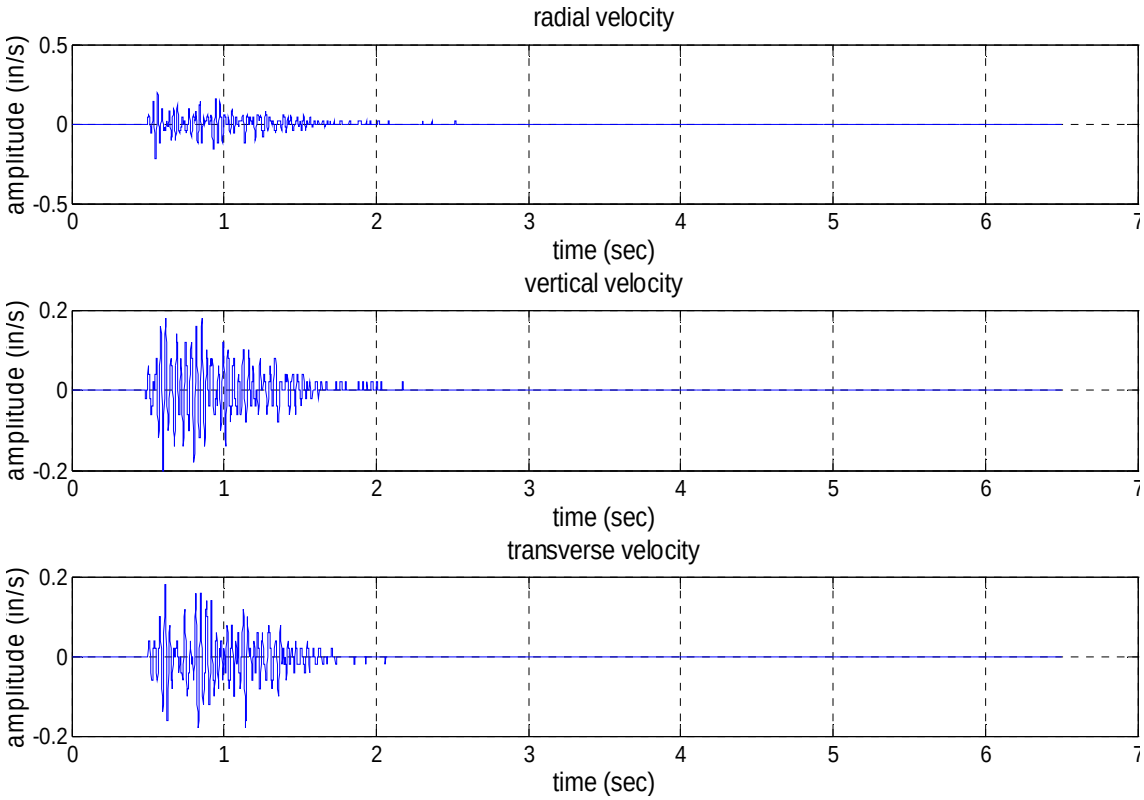

Figure A13: R8 velocity record

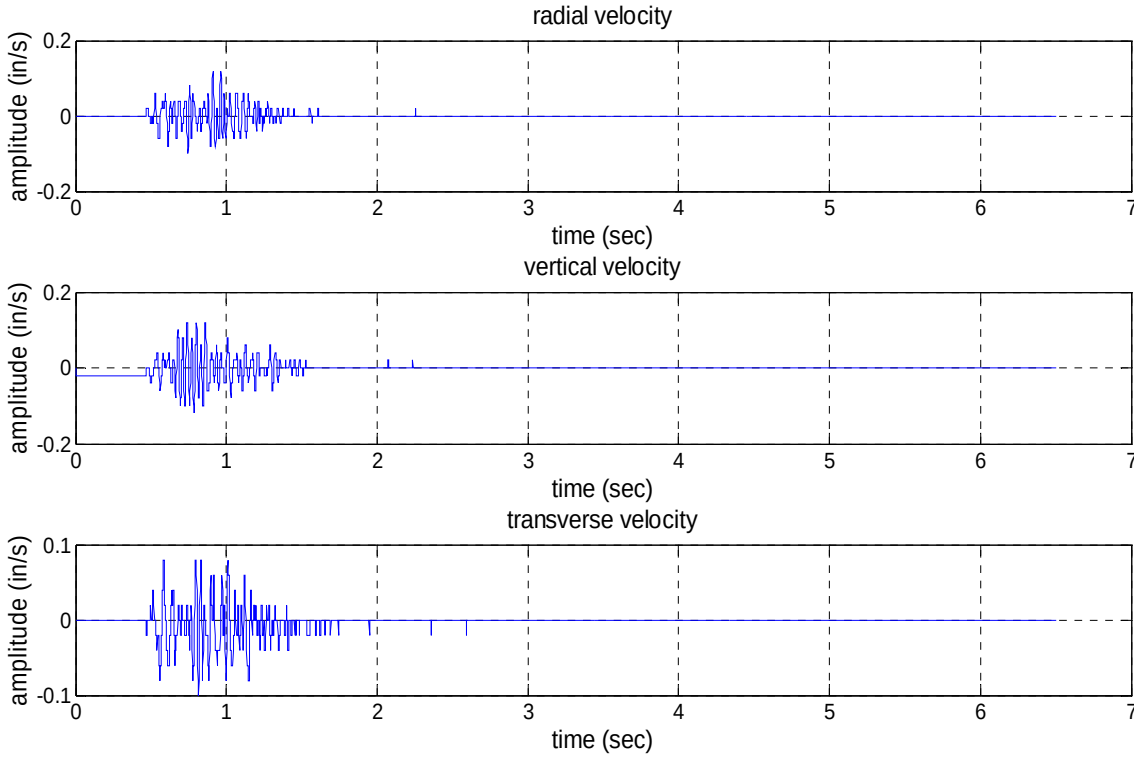

Figure A14: R9 velocity record

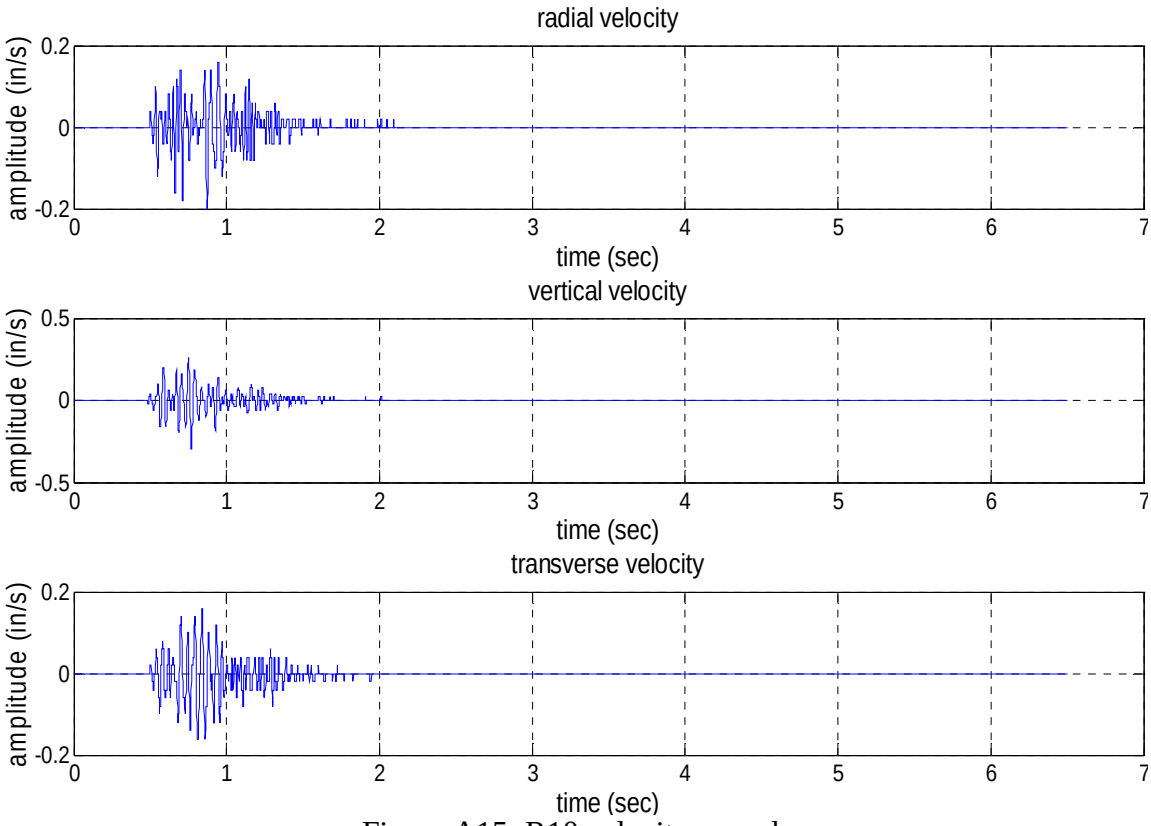

Figure A15: R10 velocity record

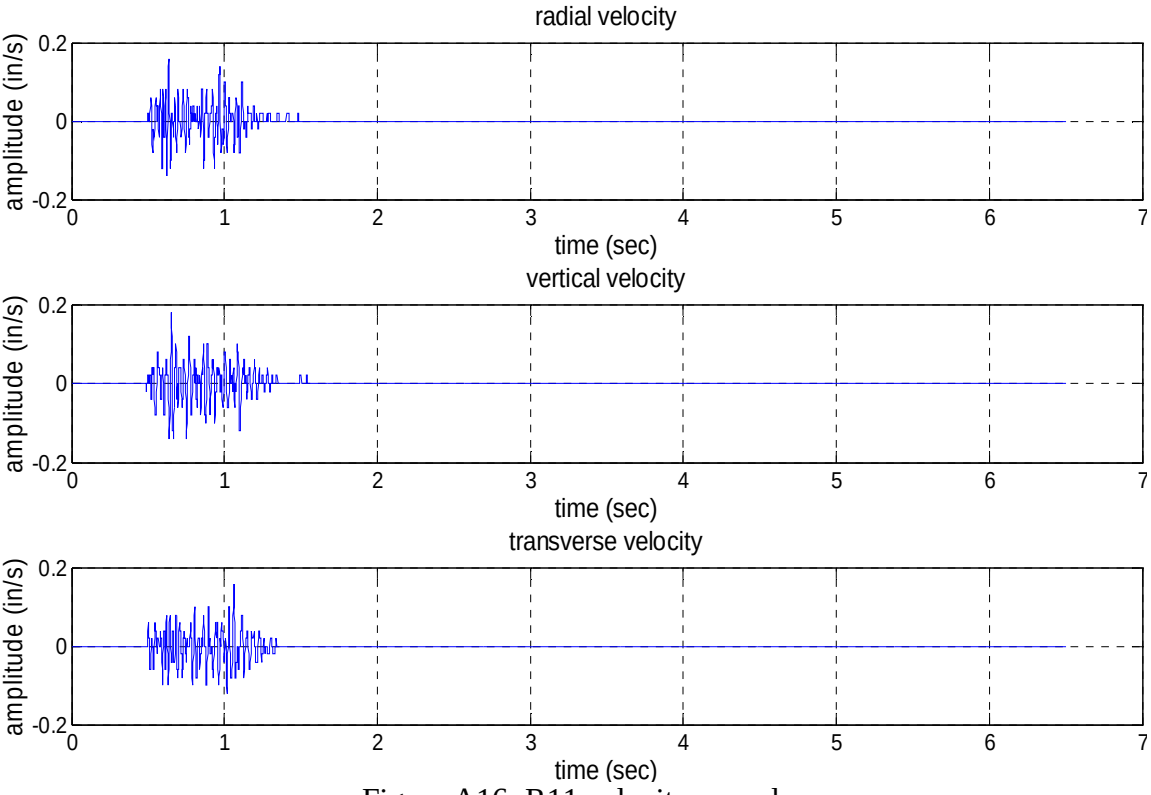

Figure A16: R11 velocity record

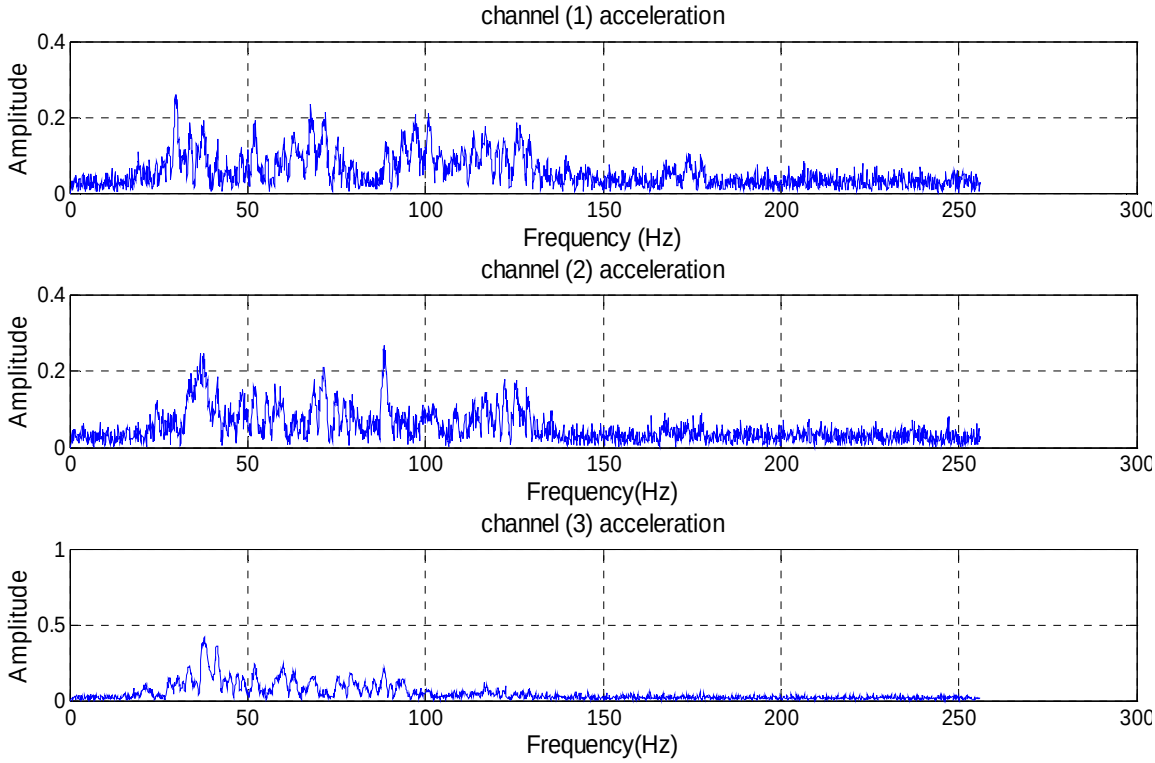

Figure A17: U1 acceleration record in frequency domain (amplitude: in/s^2)

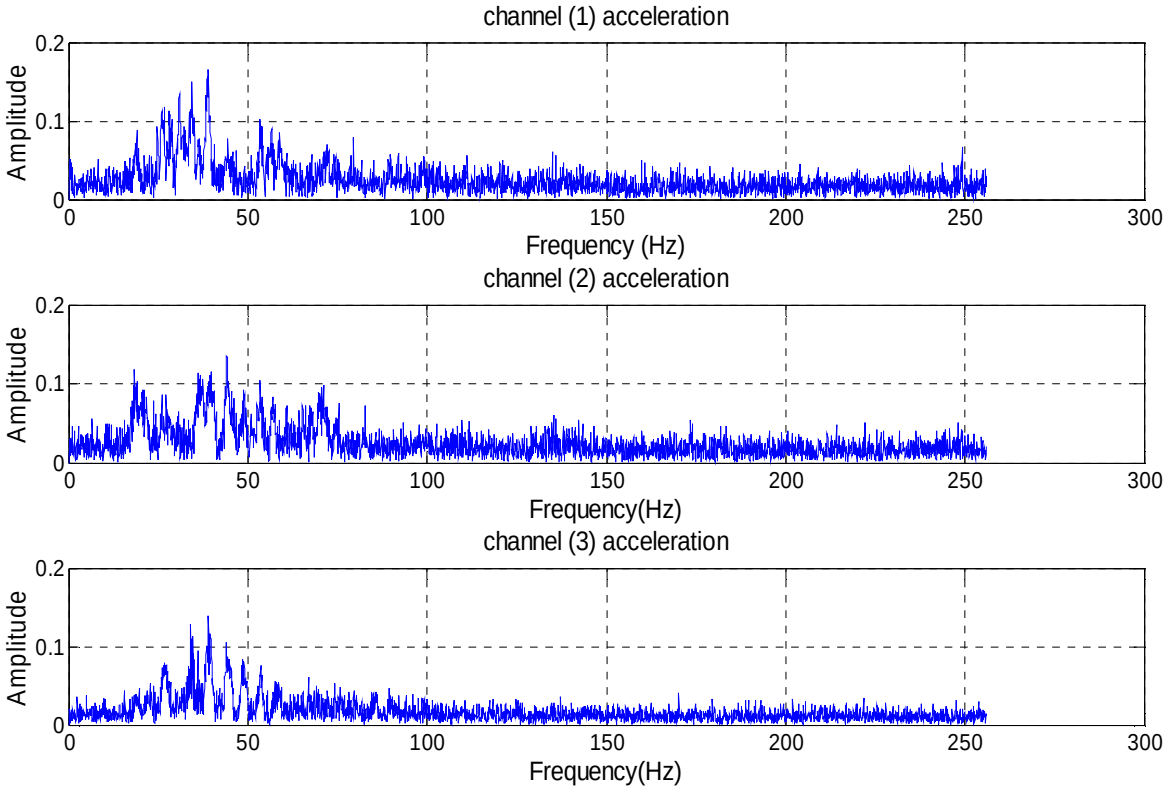

Figure A18: U2 acceleration record in frequency domain (amplitude: in/s^2)

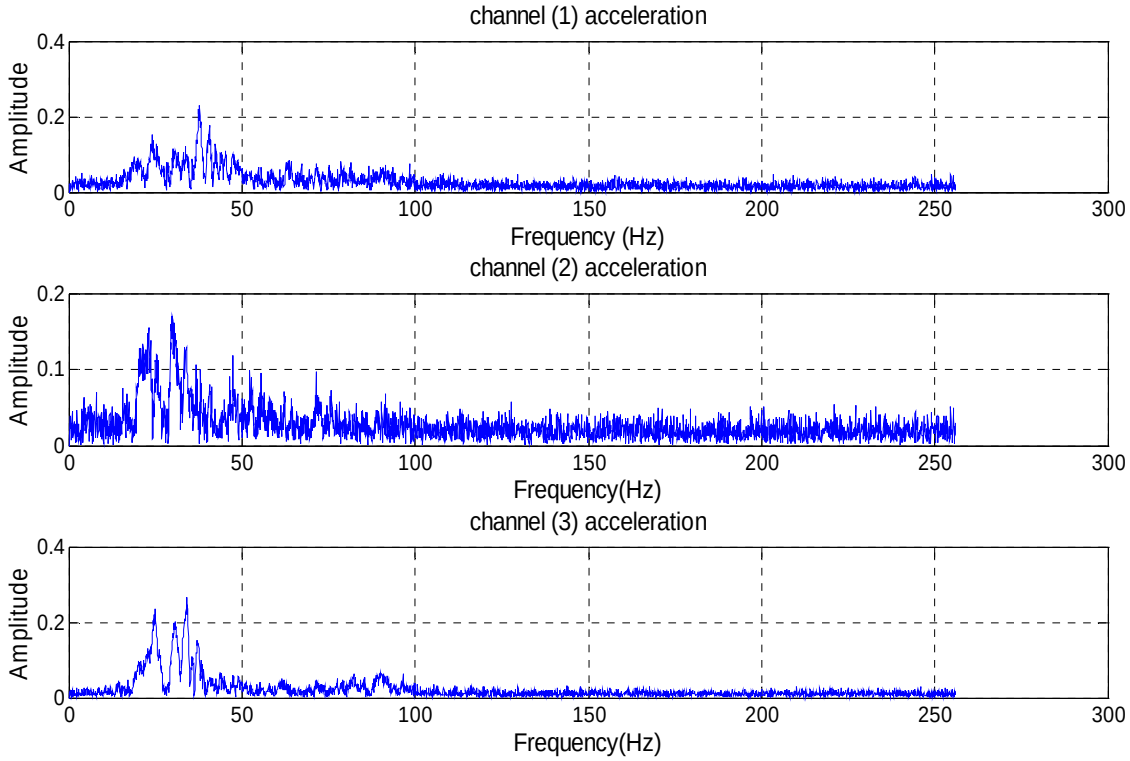

Figure A19: U3 acceleration record in frequency domain (amplitude: in/s^2)

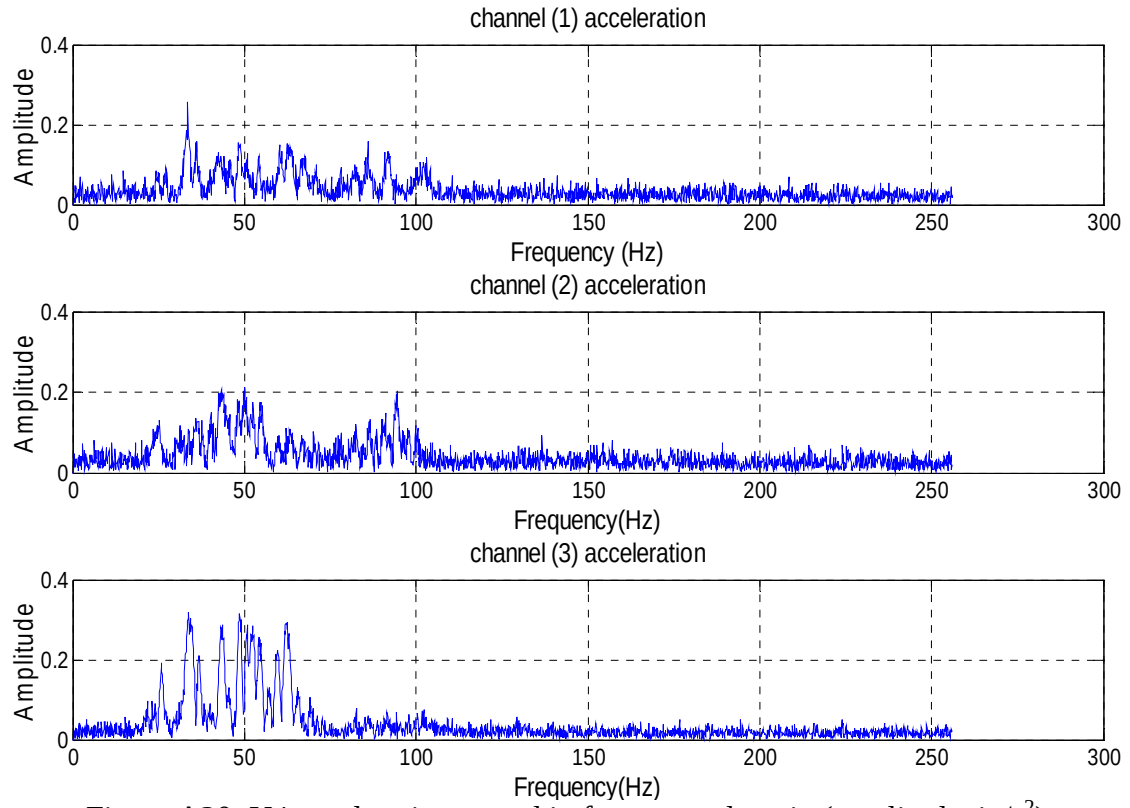

Figure A20: U4 acceleration record in frequency domain (amplitude: in/s^2)

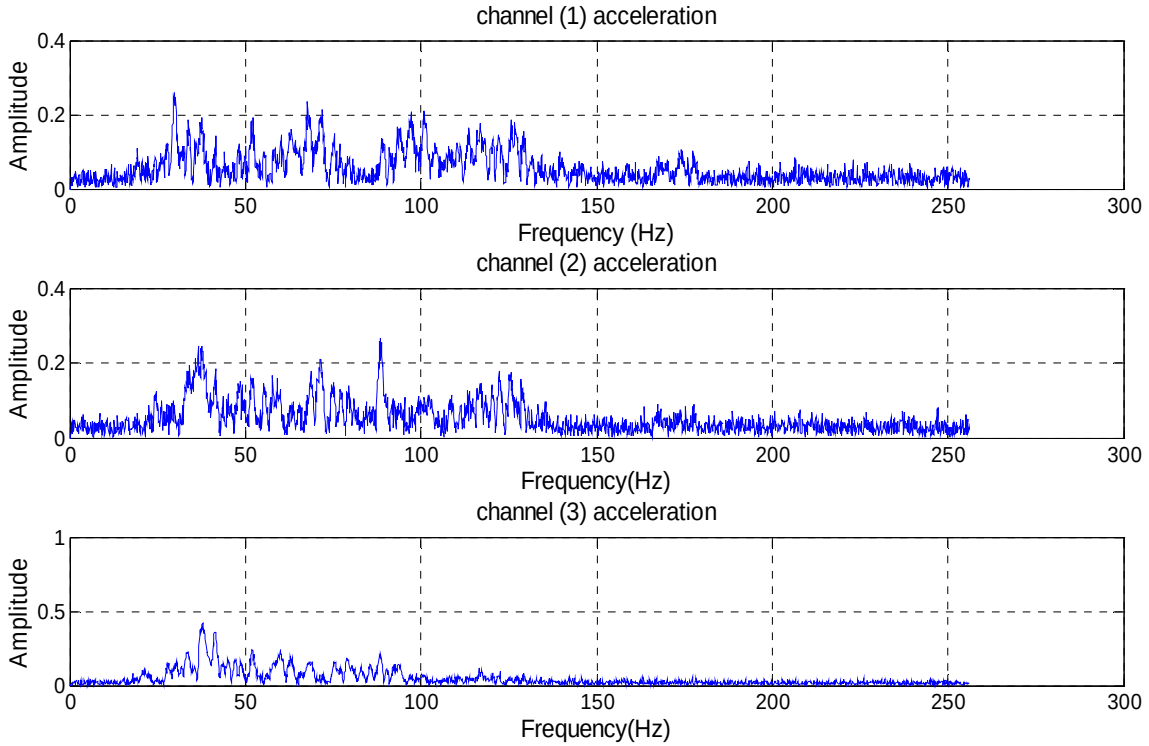

Figure A21: U5 acceleration record in frequency domain (amplitude: in/s^2)

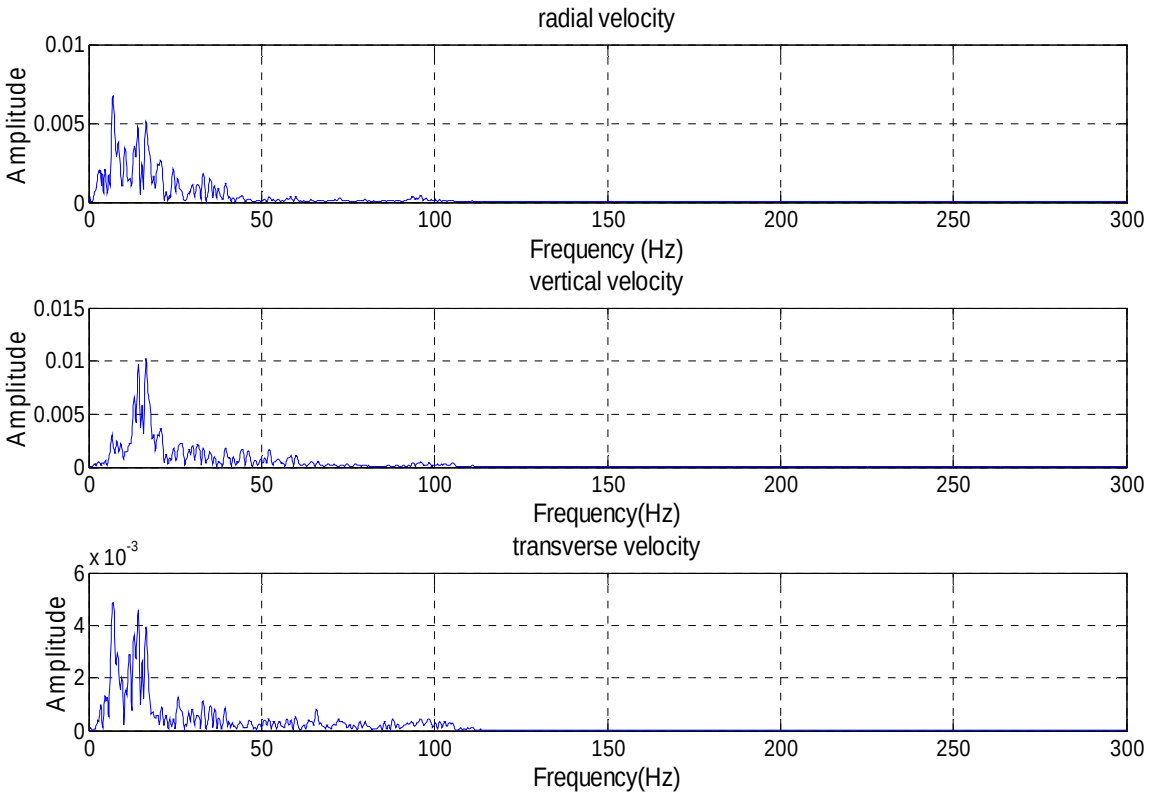

Figure A22: R1 velocity record in frequency domain (amplitude: in/s)

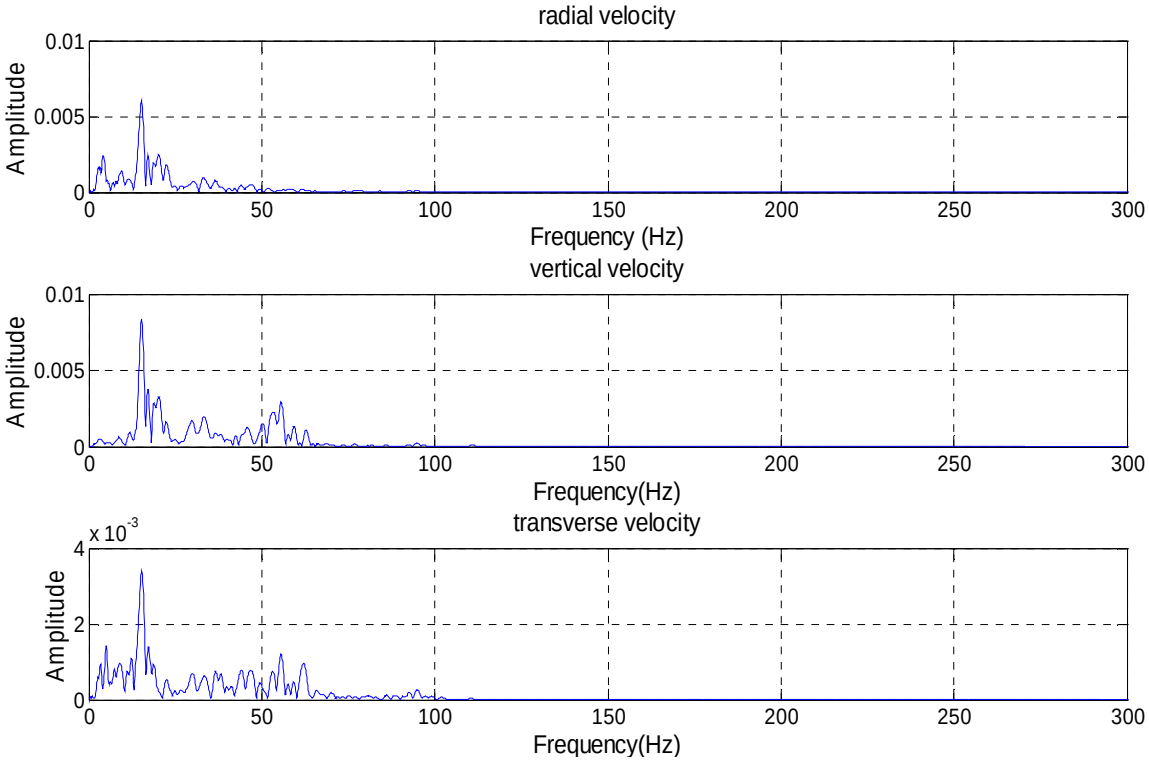

Figure A23: R2 velocity record in frequency domain (amplitude: in/s)

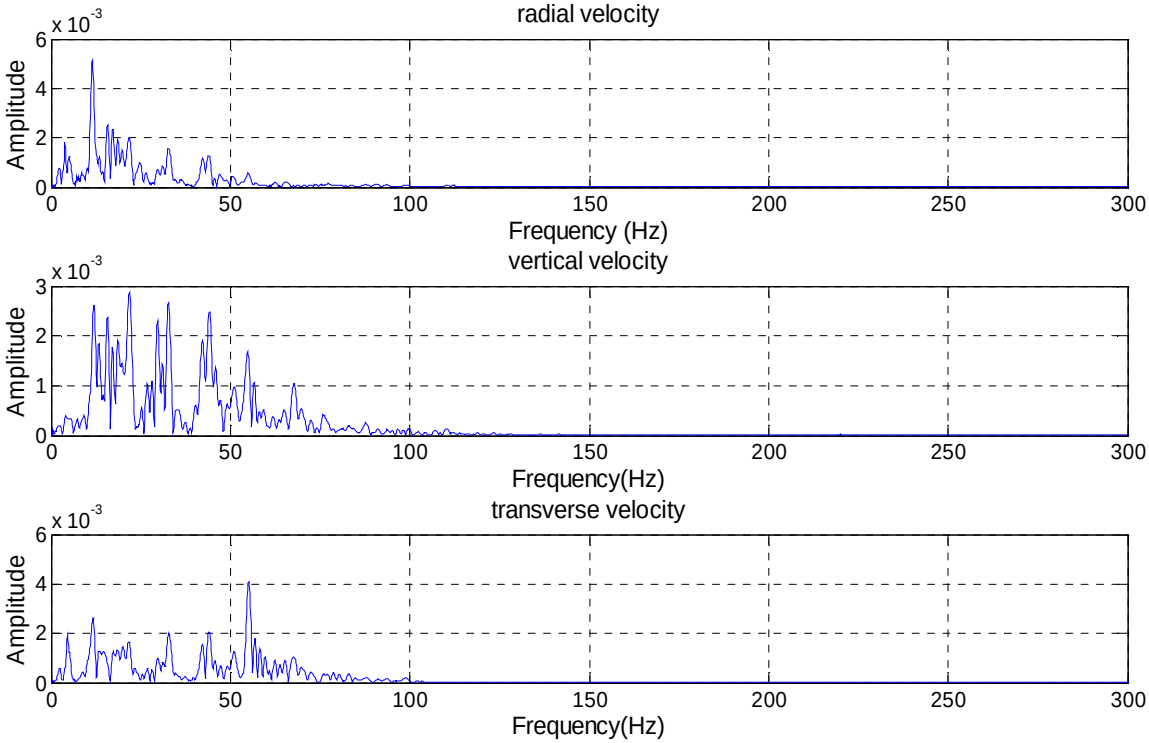

Figure A24: R3 velocity record in frequency domain (amplitude: in/s)

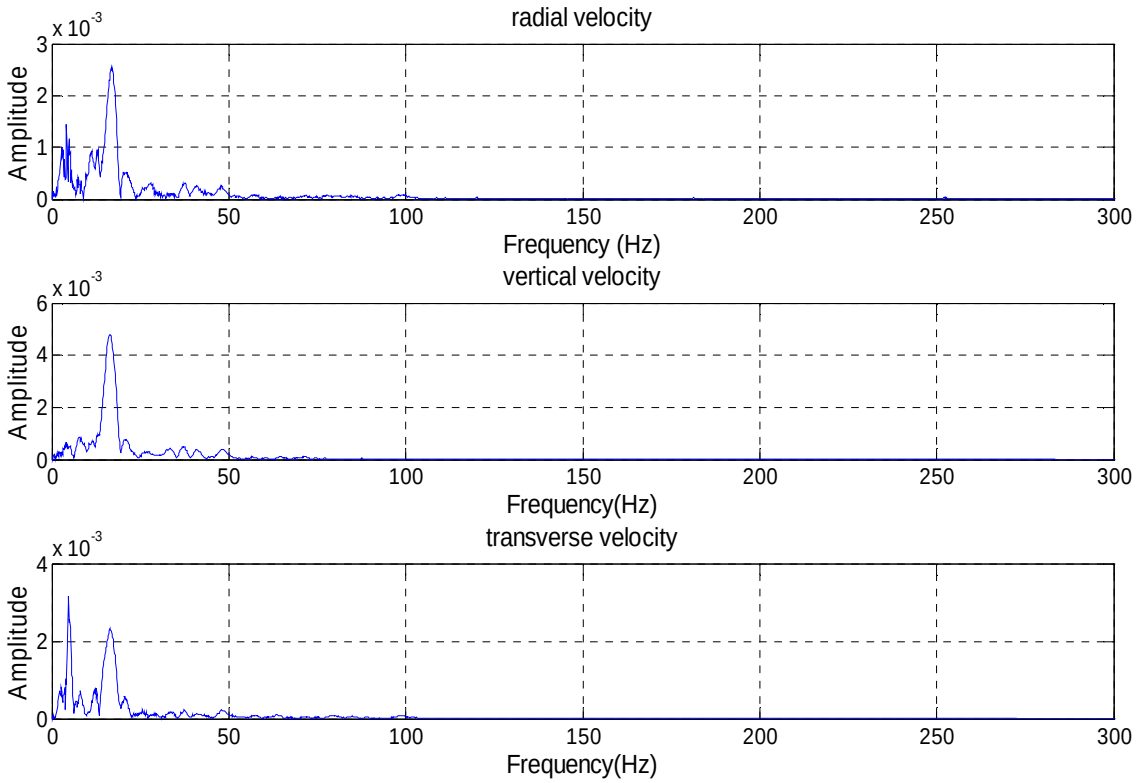

Figure A25: R4 velocity record in frequency domain (amplitude: in/s)

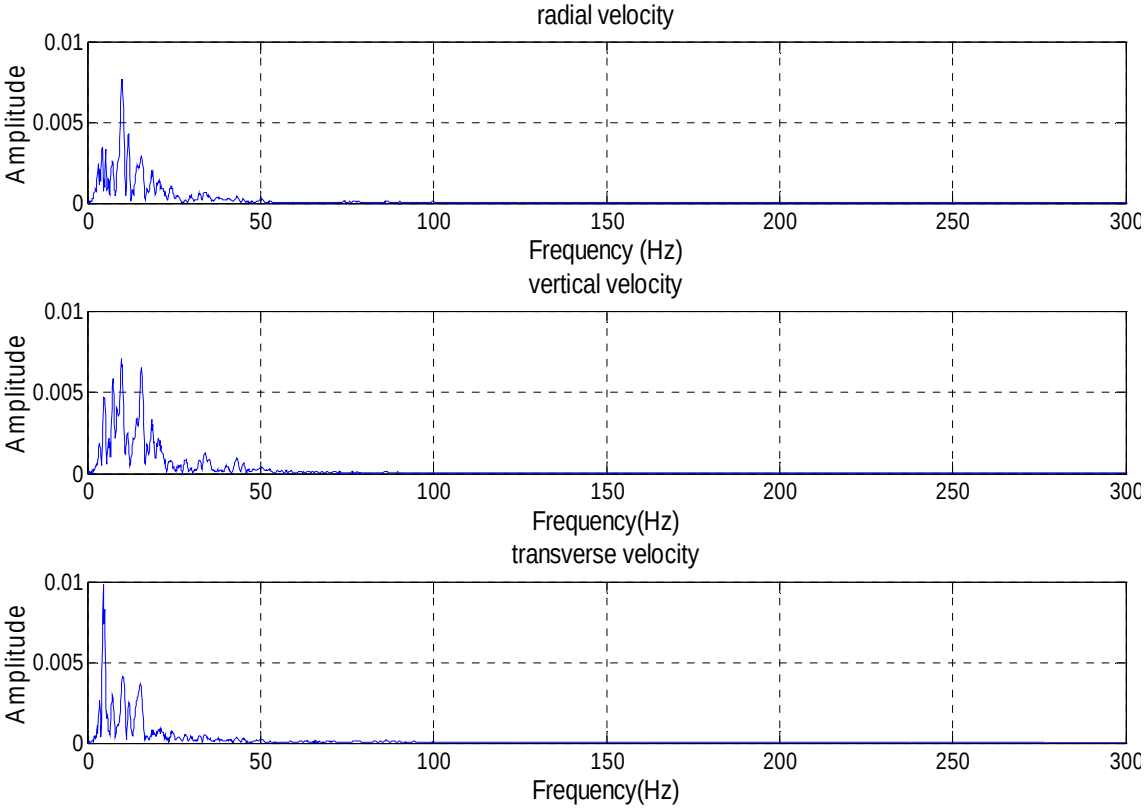

Figure A26: R5 velocity record in frequency domain (amplitude: in/s)

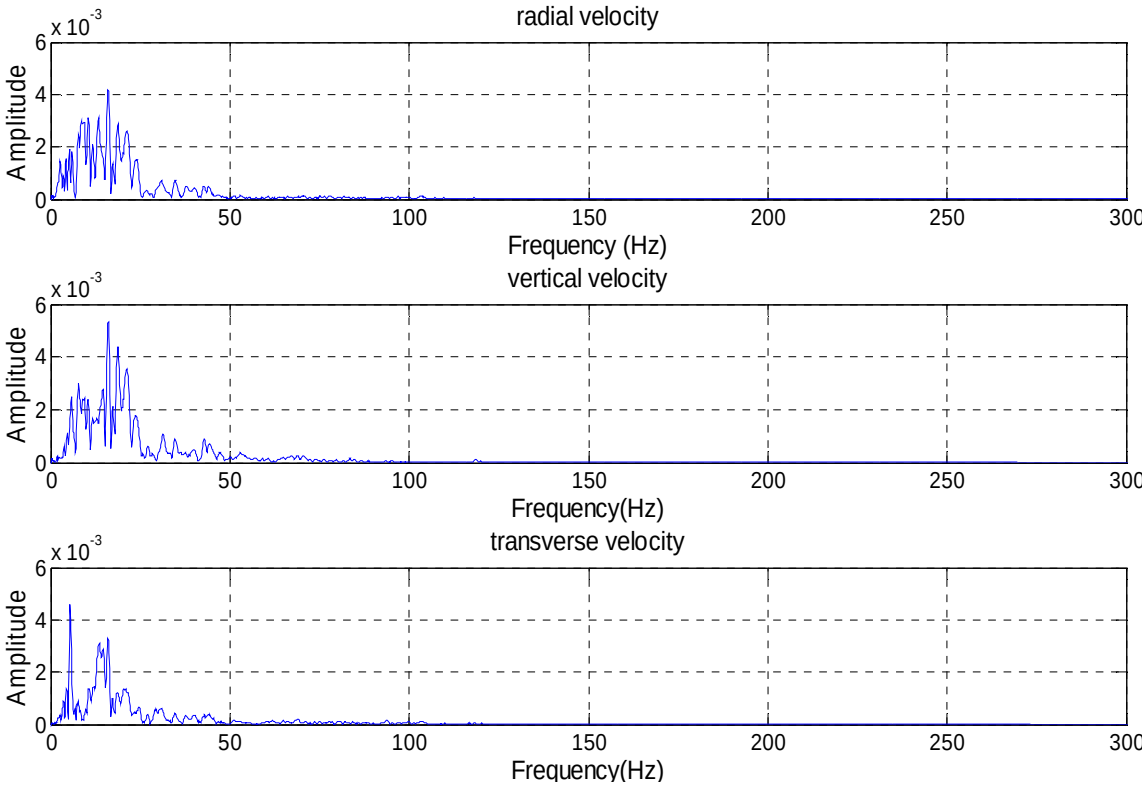

Figure A27: R6 velocity record in frequency domain (amplitude: in/s)

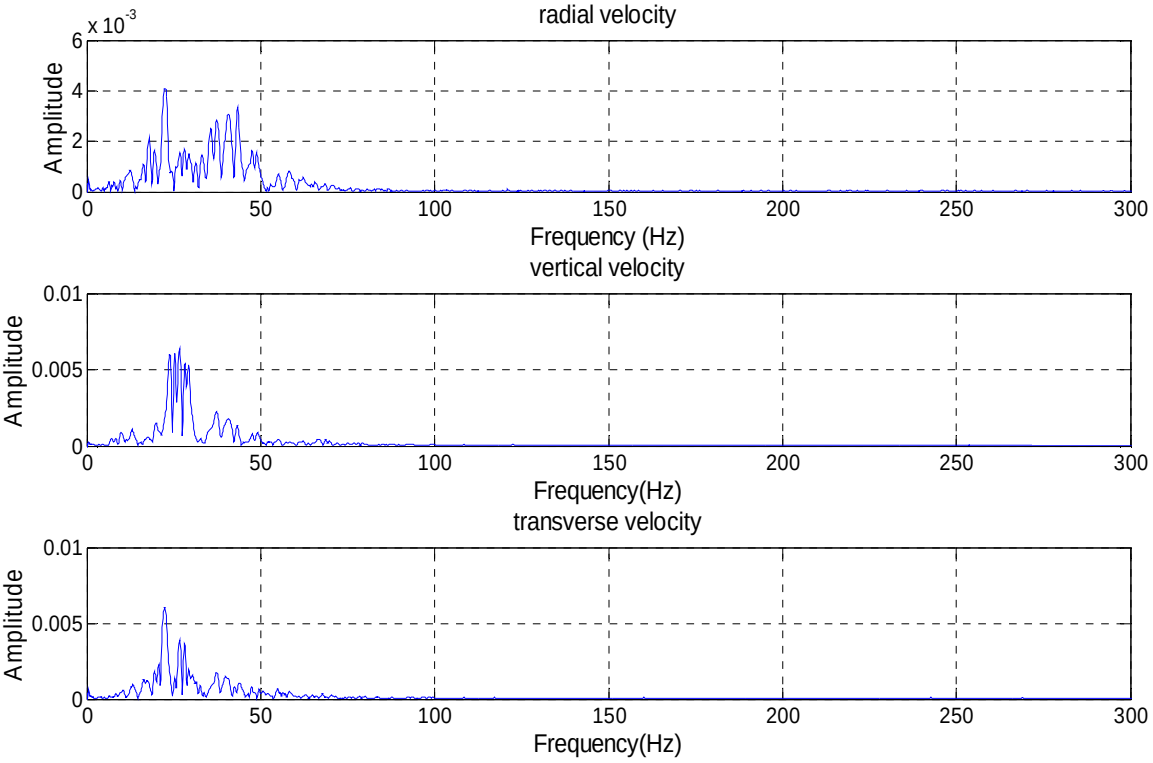

Figure A28: R7 velocity record in frequency domain (amplitude: in/s)

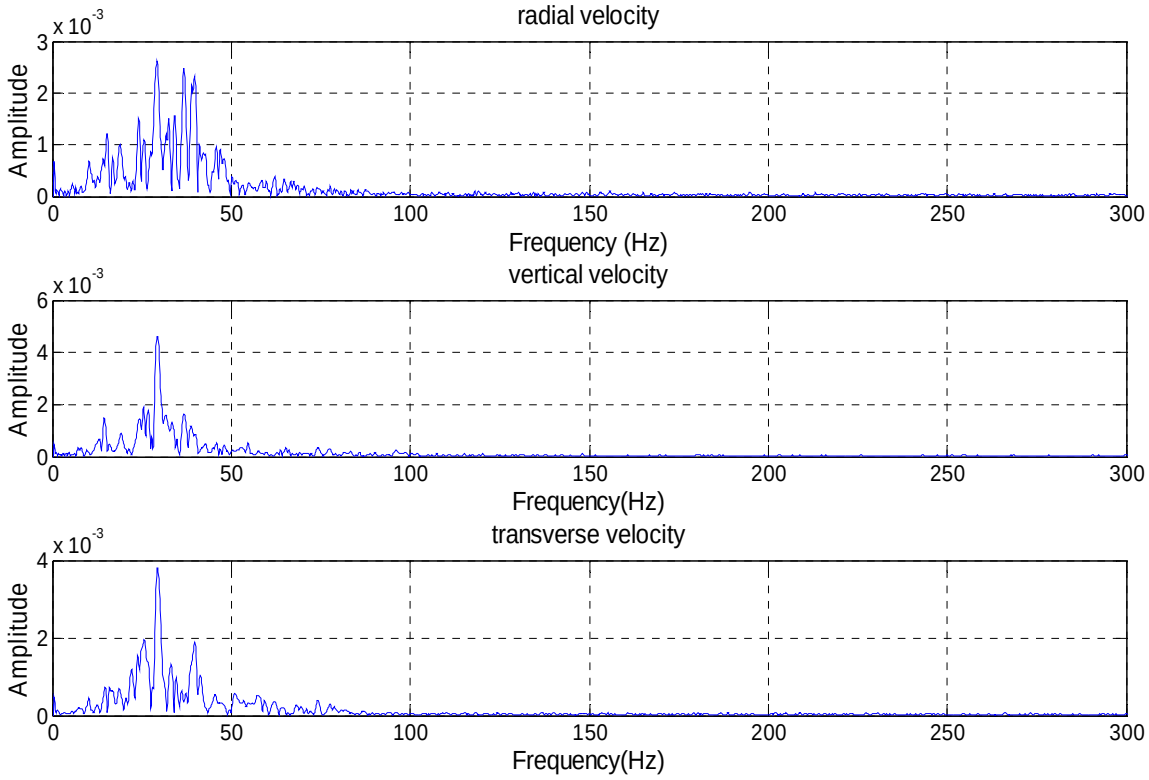

Figure A29: R8 velocity record in frequency domain (amplitude: in/s)

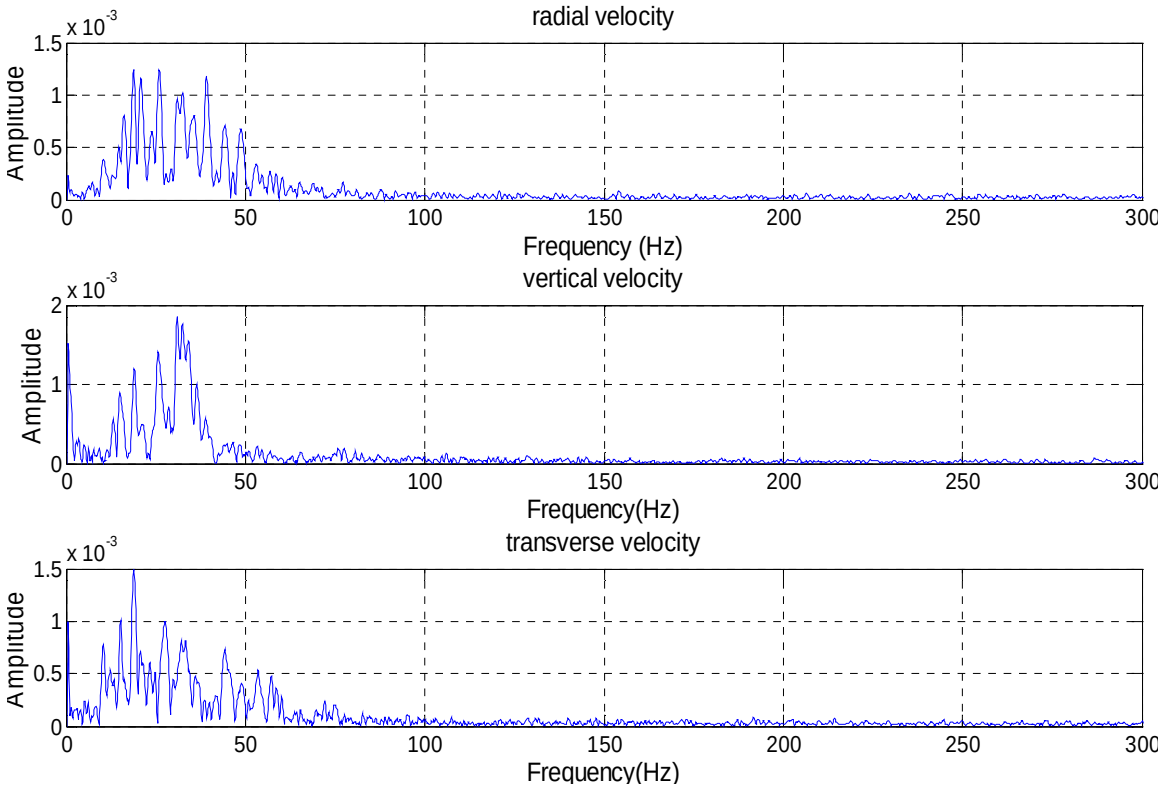

Figure A30: R9 velocity record in frequency domain (amplitude: in/s)

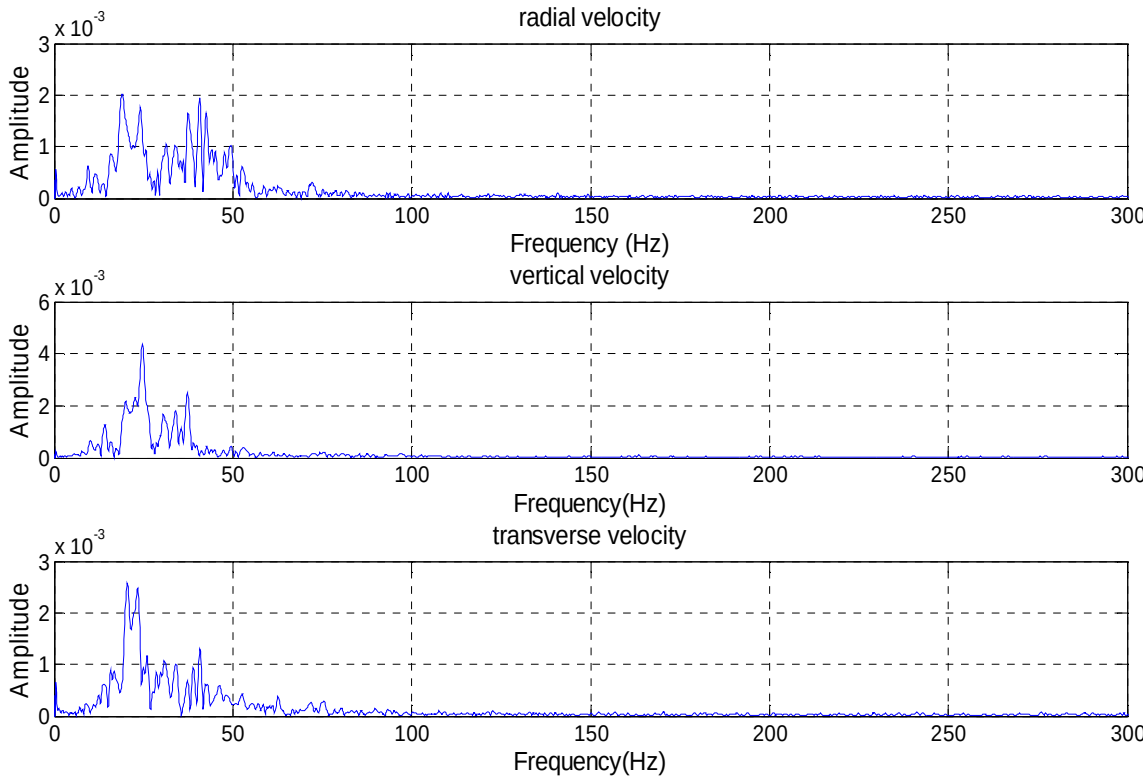

Figure A31: R10 velocity record in frequency domain (amplitude: in/s)

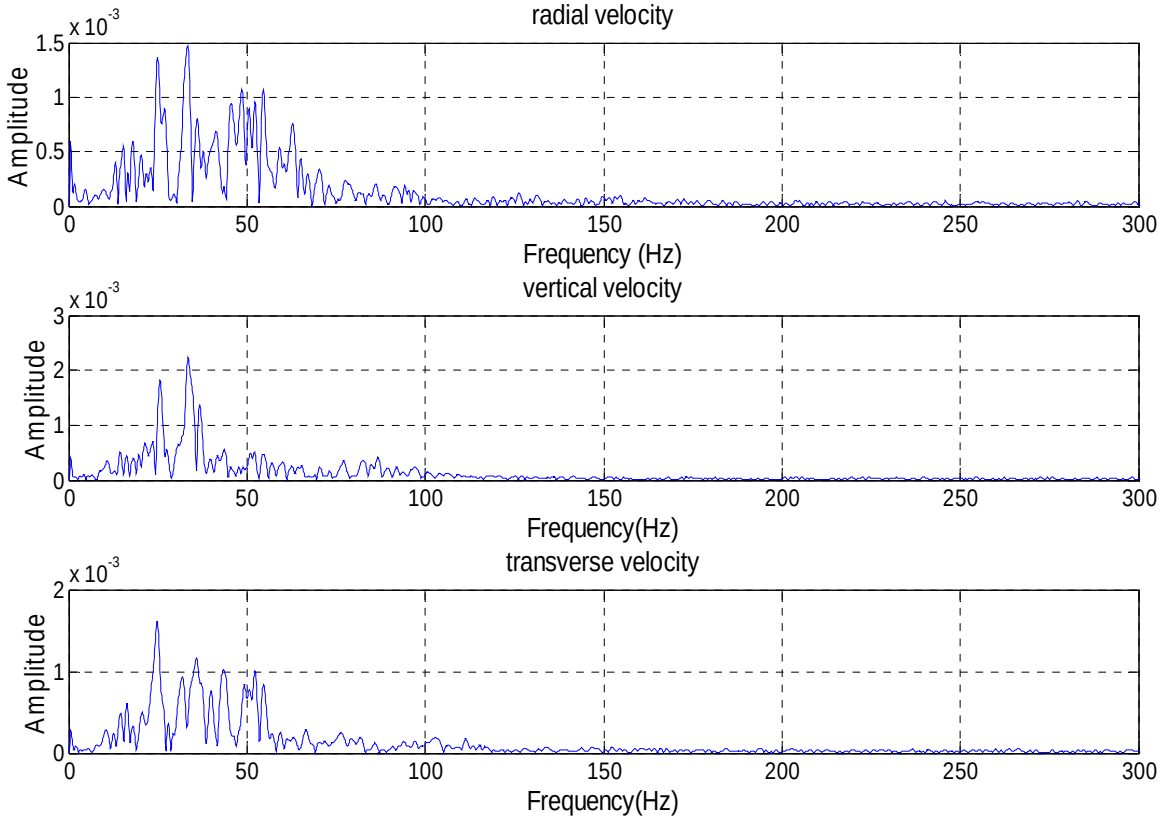

Figure A32: R11 velocity record in frequency domain (amplitude: in/s)